University of Bath

PHD

Adsorption of vapours on active carbons.

Siddiqi, Khalid Sifat

Award date:
1980

Awarding institution:
University of Bath

Link to publication

Alternative formats
If you require this document in an alternative format, please contact:
openaccess@bath.ac.uk

Copyright of this thesis rests with the author. Access is subject to the above licence, if given. If no licence is specified above, original content in this thesis is licensed under the terms of the Creative Commons Attribution-NonCommercial 4.0 International (CC BY-NC-ND 4.0) Licence (https://creativecommons.org/licenses/by-nc-nd/4.0/). Any third-party copyright material present remains the property of its respective owner(s) and is licensed under its existing terms.

Take down policy
If you consider content within Bath's Research Portal to be in breach of UK law, please contact: openaccess@bath.ac.uk with the details. Your claim will be investigated and, where appropriate, the item will be removed from public view as soon as possible.

Download date: 04. May. 2023

ADSORPTION OF VAPOURS ON ACTIVE CARBONS

Submitted by Khalid Sifat Siddiqi for the

degree of Ph.D. of the University of Bath

1980

COPYRIGHT

Attention is drawn to the fact that copyright of this thesis rests with its author. This copy of the thesis has been supplied on condition that anyone who consults it is understood to recognise that its copyright rests with its author and that no quotation from the thesis and no information derived from it may be published without the prior written consent of the author.

This thesis may be made available for consultation within the University Library and may be photocopied or lent to other libraries for the purposes of consultation.

Khalid Sifat Siddiqi

ProQuest Number: U443178

All rights reserved

INFORMATION TO ALL USERS
The quality of this reproduction is dependent upon the quality of the copy submitted.

In the unlikely event that the author did not send a complete manuscript
and there are missing pages, these will be noted. Also, if material had to be removed,
a note will indicate the deletion.

ProQuest U443178

Published by ProQuest LLC(2015). Copyright of the Dissertation is held by the Author.

All rights reserved.
This work is protected against unauthorized copying under Title 17, United States Code.
Microform Edition © ProQuest LLC.

ProQuest LLC
789 East Eisenhower Parkway
P.O. Box 1346
Ann Arbor, MI 48106-1346

UNIVERSITY OF BATH
LIBRARY
34 | 23 APR 1980
PHD

PREFACE

The author wishes to express his sincere thanks and gratitude to Professor W.J. Thomas for his keen interest, supervision and guidance during this research. He is also thankful to all the academic staff and research colleagues for their useful discussions. The help and co-operation of the technical and workshop staff in the School of Chemical Engineering were invaluable and is gratefully acknowledged.

In addition he is indebted to Miss J. Lindquist for typing this thesis.

Finally, he wishes to extend thanks to the National Coal Board for providing him with the financial help during the course of study.

SUMMARY

Experimental studies are reported on the single and binary component adsorption of various gases and organic vapours on activated carbons (Anthrasorb CC818H and CC818M) at different temperatures.

Experiments were performed for methane, ethane, methane-ethane mixtures, acetone and carbon tetra-chloride vapours. Single component isotherms were established for all the adsorbates over a range of temperatures (-6 to 50^{o}C). The empirical Langmuir and Freundlich models correlate the results well. The Polanyi adsorption potential theory depicts all of the single component data. Other empirical and theoretical isotherm equations were also tested.

Binary isotherms were obtained for methane-ethane mixtures on both Anthrasorb CC818H and CC818M. An empirical method was employed to model the binary adsorption data using single component empirical Langmuir parameters to express the binary isotherm of each component in a given mixture. The Polanyi adsorption potential theory correlates the binary adsorption data fairly well.

Breakthrough data for single and binary adsorbates (over a range of concentrations and flowrates) were obtained and mathematical models established which represents the results. A finite difference technique was used to model the fixed bed breakthrough data. Two simplified asymptotic models (linear driving force and

pore diffusion control) were also used to correlate the single component data. For the binary adsorption of methane-ethane mixtures, a linear driving force model was successfully employed to correlate the experimental breakthrough curves.

Isothermal fixed bed experiments to desorb acetone from Anthrasorb CC818H over the range of temperatures (150-250^{o}C) showed that Anthrasorb can be used to completely remove such an organic vapour and be regenerated for further use.

SUMMARY OF CONTENTS

CONTENTS

LIST OF TABLES

LIST OF PLATES

CHAPTER I

INTRODUCTION

CHAPTER 1

INTRODUCTION

With an every increasing awareness of the environmental problems created by industrial by-products and waste, coupled with the rising cost of petro-chemicals, it is now necessary to consider alternative methods for the recovery of solvents. Substantial quantities of solvents, which previously were discharged into the atomosphere as vapours, are now being reclaimed and reused. In some operations the vapours can be condensed by cooling, or by absorption into suitable liquids; but the most frequent practice involves the adsorption on activated carbons.

Generally absorption, condensation and adsorption, are used to recover solvents. In condensation processes the entire gas stream is cooled to a temperature below the dewpoint. For absorption processes the extent of recovery depends on the flowrates of the gas stream and the absorber liquid. In the case of adsorption, recovery is complete except for small losses due to incomplete regeneration.

When large volumes of very dilute vapours are treated, the operating costs for condensation and absorption become very high. This is because large volumes of gas have to be refrigerated or stripped from large volume of virtually pure liquid. For this case, adsorption is the best economic choice.

If and when it is employed under appropriate conditions to undertake tasks for which it is fitted, activated carbon will provide effective purification at low cost. In certain situations, carbon can accomplish complete purification by itself, but more often adsorption on carbon is combined with other methods of separation.

Gas separation is also a major problem for the chemical industry. Separation of gases may be accomplished by fractional distillation, solvent extraction, selective adsorption, and similar processes. For example, ethylene purities up to 99.9% are produced by low temperature distillation. Usually 50 to 90 plates and a reflux ratio of between 4 and 6 are required, depending on the composition of feed. Similar separation may be achieved in a single adsorption column of comparatively short length and at much lower cost by using a continuously moving activated adsorbent bed (107). Many of the newly developing applications of oxygen, particularly those which do not require a very high purity of oxygen, are now incorporating pressure swing adsorption processes using zeolite adsorbents (71).

Activated carbons along with molecular sieves, are widely used for the drying and purification of natural gases. The ability to remove moisture and sulphur compounds in a single step operation makes them uniquely suited for sweetening of wet sour natural gas (50). Ethane and propane also recovered from natural gas constitute an important source of supply for the manufacture of polyethylene and polypropylene. Attempts have been made to expand the liquid hydrocarbon processing market to include heavier hydrocarbon fractions, such as the full range of natural gas condensates, natural gasoline, and light naptha. An application of adsorption processes is also found in carbon dioxide removal from manned spacecraft (7).

A review of adsorption processing economics reveals that the major operating costs are found primarily in the desorption stage of the process cycle, rather than in the adsorption step. Desorption is favoured by high temperature, low pressure, and an elutant such as steam. In many systems it is possible to regenerate the adsorbent insitu by desorption, using elevated temperature, reduced pressure, or a solvent. In other cases the adsorbent has to be removed from the adsorber vessel and processed in a furnace either on site or returned to the manufacturer. Activated carbon has a large capacity for repeated adsorption and desorption cycles.

Although the best grades of granular activated carbon are hard and abrasion resistant, methods of handling or conveying which tend to grind the grains should be avoided. The repeated heating and cooling of activated carbon has little effect on its physical structure. In typical solvent recovery plants, 10,000 heating and cooling cycles cause little breakdown of the grains (3). A high velocity of airflow, particularly if it is not uniform or if the top of the activated carbon bed is not held in place by a screen, may cause movement of the particles and rapid wear or breakage of the grains. Upward flow of fluid, particularly at high veocities, should be avoided because it tends to lift the grains and cause channeling.

The material used in this work is Anthrasorb and is produced by the National Coal Board. Anthrasorb is manufactured by gasifying anthracite in a fluidised bed reactor fitted with internal burners. The activation time is up to four hours and temperatures from 850 to 970^{o}C were employed, depending upon the level of activation required. The volatile matter in the coal is driven off leaving an increased carbon content in the residue. The steam reacts not only with the carbon in the surface of the particle but also with that in the walls of existing pores and cracks; so that, as the carbon gasification proceeds, new pores are formed and existing pores are extended and widened. A highly porous structure results. Wilson (120) gives a detailed description of the manufacturing technique, along with the properties and uses of the Anthrasorb.

Adsorption can be carried out either batchwise or continuously. Batch systems are only used where the component or components to be adsorbed are present in small quantities or are very highly adsorbed. A continuous process employs either a fixed, fluidized, or moving bed systems. However due to the high cost of designing, building, and operating fluidized and moving bed systems, fixed beds are more commonly used. A fixed bed is selected for this research work because of its simplicity.

Bowen (21) in his comprehensive chapter entitled 'Sorption Processes' reviews the application of adsorption techniques for process separation. He describes the equipment and provides in some detail the numerous theoretical correlations dealing with adsorption in fixed beds.

The overall objective of this research is to assess the performance of a specific activated carbon (Anthrasorb) as an adsorbent for selected materials under a variety of operating conditions.

Organic vapours considered typical of classes of industrial operations are:

(1) Light paraffins (Separation of similarly low boiling compounds, such as methane, ethane).

(2) Ketones (Solvent recovery and removal in paints, laquers and varnishes industry, such as acetone).

(3) Carbon tetra-chloride (solvent recovery in dry cleaning and fat removal operations).

CHAPTER II

ADSORPTION IN FIXED BEDS

CHAPTER II

ADSORPTION IN FIXED BEDS

2.1. Introduction

Adsorption in fixed beds is a transient phenomenon. Thus the concentration of adsorbate in the effluent stream remains virtually zero for a considerable period and then gradually rises to the value of the stream entering the bed as shown in figure 1. A plot of effluent concentration versus time is termed a breakthrough curve and the point at which the concentration begins to rise rapidly is called the break-point. Adsorption of binary adsorbate mixtures from an inert gas is shown in figure 2. The curve may be divided into four zones. In zone I near the inlet, a plateau zone (constant composition) corresponding to the feed concentration exists. Zone II is a transfer zone (composition changes) in which A is adsorbed and hence causes an increase in the concentration of B not yet adsorbed. A second plateau zone which contains only component B is also present (zone III); in this zone,A displaces B, causing its concentration to rise above the inlet value. Finally zone IV (transfer zone) corresponds to the initial composition of the bed.

This system of zones travels along the bed, until the plateau zone, corresponding to the feed composition, reaches the end of the bed (i.e. equilibrium is reached). The particular shape and the time dependence of the breakthrough curves are very important for the design of adsorption equipment and understanding the fundamental mechanism of mass-transfer during adsorption.

Column performance studies for fixed beds are therefore concerned with prediction of such breakthrough curves. Various analytical solutions proposed are limited to simplified cases because of the unsteady nature of the process. For binary adsorption, further simplified assumptions are required if any analytical methods are to be used. However, the partial differential equations set up to describe these processes are amenable to integration by numerical methods and have been used extensively in this present thesis.

Adsorption in fixed beds can take place under isothermal or adiabatic conditions. As the present work has been carried out under isothermal conditions using low adsorbate concentrations, only this case is considered here in detail. In this chapter, fixed bed theories for single component and binary adsorption are reviewed.

2.2. Adsorption Equilibrium

2.2.1. Introduction

In order to study rate processes, e.g., column studies, an accurate description of the equilibrium isotherms must be provided; since the mass-transfer resistances and the final system state both depend on equilibrium considerations. Furthermore, a good model prediction is contingent upon a satisfactory equilibrium description.

2.2.2. Single Component Systems

The nature of adsorption is determined by the properties of both the adsorbate and the adsorbent. An adsorption isotherm describes how the amount adsorbed depends upon the equilibrium pressure of the gas at constant temperature; it is generally written as:

$$q^* = f(C) \qquad (2.1.)$$

where q* denotes the magnitude of the concentration in the adsorbed phase (e.g. in mol per gram of solid adsorbent) corresponding to equilibrium with C, the concentration in the fluid phase (e.g. in mol per cm^3).

A simple classification for the low concentration range is to characterize the isotherms by their different effects upon column performance. The isotherm is favourable, when the curve is concave to the fluid concentration axis, and unfavourable when the curve is convex. An intermediate case is that of the linear isotherm. These are shown in figure 3(a).

2.2.2.a. Langmuir Isotherm

When the molecules of a gas or vapour collide with the surface of a solid, there is a finite probability that the collision is inelastic, and the molecule stays in contact with the surface for a short length of time. In rare cases, the molecule may be elastically reflected from the surface without any energy exchange taking place. According to Langmuir (68) this time lag is responsible for the phenomenon of adsorption.

Langmuir introduced two assumptions in the derivation of his equation:

(i) The forces of attraction between the adsorbed molecules are negligible.

(ii) Adsorption is confined to a monolayer.

Young and Crowell (123) deal with the derivation of the Langmuir equation in detail. A convenient form of the equation may be written as:

$$v = \frac{v_m \, b \, p}{1 + bp} \qquad (2.2.)$$

Rewriting equation 2.2 in another form and replacing v_m by an empirical parameter 'a':

$$q = \frac{a \, b \, C}{1 + bC} \qquad (2.3)$$

This form of equation is quite useful in describing both chemisorption and physical adsorption on a wide variety of adsorbents (1, 51, 59, 110). The coefficients 'a' and 'b' are normally found empirically by a least square fit to the following rearranged form of equation 2.3:

$$\frac{C}{q} = \frac{1}{a} C + \frac{1}{ab} \qquad (2.4)$$

The coefficient 'b', expressing the degree of non-linearity of the isotherm, can be expressed as a function of temperature in an Arrhenius type of equation, (67). The empirical constant 'a' is normally unaffected by temperature, (67).

Heister and Vermeulen (57) introduced the dimensionless parameter R, for the operation of fixed beds, as:

$$R = \frac{1}{1 + bC_o} \qquad (2.5)$$

The use of this equlibrium parameter, provides the same degree of generality in handling non linear cases of adsorption and ion exchange as the use of a constant relative volatility gives in binary distillation.

The maximum possible concentration in the solid phase is then given by:

$$q_o^* = \frac{a\ b\ C_o}{1 + bC_o} \qquad (2.6)$$

combination of equations 2.3, 2.5 and 2.6 gives another form of the adsorption isotherm, as:

$$\frac{q}{q_o^*} = \frac{C/C_o}{R + (1-R)C/C_o} \qquad (2.7)$$

The different types of equilibrium may be indicated by the value of R as follows:

Favourable equilibrium	$0 < R < 1$
Linear equilibrium	$R = 1$
Unfavourable equilibrium	$R > 1$

2.2.2.b. Freundlich Isotherm

For a heterogeneous surface, Zeldowitch (124), assumed that the adsorption sites are distributed exponentially with respect to the energy (heat) of adsorption; and derived the Empirical Freundlich Isotherm equation.

$$v = K_F p^{1/n} \tag{2.8}$$

Taking the logarithm of equation 2.8:

$$\log v = \log K_F + \frac{1}{n} \log p \tag{2.9}$$

This is a linear equation, suitable for testing the validity of the formula. If a plot of log v against log p gives a straight line, the adsorption data obey the Freundlich equation. The slope of the straight line then gives 1/n while the intercept on the abscissa give log K_F.

Baly (2) showed that the Freundlich equation can also be obtained by assuming that the adsorption is multimolecular, and that each adsorbed layer obeys a separate Langmuir equation with different constants.

2.2.2.c. Polanyi Adsorption Potential Theory

Polanyi (95) considered the energy relations involved in transferring the molecules from the gaseous to the adsorbed state and divided the process into two steps. In the first step he considered the change from the gaseous to the saturated liquid state and calculated the free-energy difference by the equation:

$$\epsilon = \frac{\Delta G}{N_m} = R_g T \ln \frac{Ps}{P} \tag{2.10}$$

The second step involved the free-energy change in passing from the liquid to the adsorbed state. Polanyi concluded that the free-energy change involved in the second step was small in comparison to that for the first step and used the free-energy change for the whole process. This free-energy change was termed the adsorption potential.

Polanyi showed that the adsorption potential was a function of the volume of the adsorbed phase and that its magnitude is virtually independent of temperature. For this reason, the function is called the 'characteristic curve'. Using the characteristic curve, if the adsorption isotherm of a gas on a given adsorbent is known at one temperature, its isotherm at any other temperature can be predicted.

Dubinin et al (26, 27) suggested the equation be written in the form:

$$\frac{\epsilon}{\beta} = \frac{R_g T}{\beta} \ln \frac{Ps}{P} \tag{2.11}$$

where β, the 'affinity coefficient', is a factor causing all the characteristic curves for the various gases to coincide. Numerical values of β for different organic adsorbates are usually between 0.5 and 1.5, relative to benzene as 1.0 (123). The resulting single curve is called the 'correlation curve' for the adsorbent.

Dubinin and Timofeyev (27) also found empirically that the affinity coefficient is directly proportional to the molar volume of the adsorbates, $\bar{V}$, at the adsorption temperature. Thus equation 2.11 can be rewritten as:

$$\frac{\epsilon}{\bar{V}} = \frac{R_g T}{\bar{V}} \ln \frac{Ps}{P} \tag{2.12}$$

Grant et al (48) introduced a modification that would enable one to correlate data above the critical temperature of the solute; their equation is given as:

$$\frac{\epsilon}{V} = \frac{R_g T}{V} \ln \frac{fs}{f} \tag{2.13}$$

where V is the molar volume at the boiling point, and f is the fugacity.

Levan (72) combined the Polanyi-Dubinin equation with the Freundlich and Temkin-Pyzhev isotherms, and termed the resulting function a 'polytherm', which gives both the temperature and pressure dependence. Freundlich and Temkin-Pyzhev isotherm equations employed have the form:

$$\Phi = a_F P^{b_F} \tag{2.14}$$

and

$$\Phi = a_T + b_T \ln P \tag{2.15}$$

respectively. Φ is defined as the volume of the adsorbate (as saturated liquid) at the adsorption temperature ($\Phi = q\bar{V}$); a_F, a_T , b_F

and b_T are constants.

Combination of isotherm equations (2.14) and (2.15) with the adsorption potential equation (2.12) results in a 'polytherm' as follows:

Freundlich polytherm

$$\ln \Phi = \ln \Phi_s - \frac{BRgT}{\bar{V}} \ln \frac{Ps}{P} \qquad (2.16)$$

Temkin-Pyzhev polytherm

$$\Phi = \Phi_s - \frac{B_T R_g T}{\bar{V}} \ln \frac{Ps}{P} \qquad (2.17)$$

where Φ_s is the saturated adsorbate volume and B, B_T are constants.

Using equations (2.16) and (2.17) Levan (72) successfully correlated his experimental results of n-octane and n-decane on activated carbon.

2.2.3. Multicomponent Systems

The adsorption equilibrium isotherm for multicomponent systems at a constant temperature is generally written as:

$$q_1^* = f(C_1, C_2, \ldots) \qquad (2.18)$$

where q_1^* is the adsorbed phase concentration of substance 1 at equilibrium with C_1, C_2, ... the concentrations of substances 1, 2, ... in the fluid phase. There are analogous equations for each of the components of the adsorbing mixture.

A convenient method for presenting multicomponent equilibrium isotherms is shown in Figure 3(b). The total concentration C is defined as the sum of concentrations of the adsorbable components (assuming ideal behaviour in the gas phase), in order to eliminate the influence of inert gases.

2.2.3.a. The Extended Langmuir Isotherm

The extended Langmuir Isotherm equation for substance 1 of a system of n components is given (123) as:

$$q_1^* = \frac{a_1 b_1 C_1}{1 + \sum_{i=1}^{n} b_i C_i} \qquad (2.19)$$

Equation (2.19), derived from kinetic principles by Markham and Benton (80), satisfies the Gibbs isotherm only for the special case where the monolayer capacities of each component are equal (123). This implies that

$$a_1 = a_2 = a_3 = \ldots \qquad (2.20)$$

These, and the corresponding parameters b_i, are equivalent to those in the individual adsorption isotherm. Equation (2.19) is useful for empirical correlation but no physical significance can be attributed to the isotherm.

It is convenient to define a separation factor, $K_{1,2}$, which is a measure of competitive selectivity for the adsorbates 1 and 2,

$$K_{1,2} = \frac{q_1^*/C_1}{q_2^*/C_2} \qquad (2.21)$$

The different types of equilibrium may be indicated by the value of $K_{1,2}$ as follows:

$K_{1,2} > 1$ Component 1 is preferentially adsorbed

$K_{1,2} < 1$ Component 2 is preferentially adsorbed

Adsorption azeotropes will appear, if the isotherm crosses the straight line, $q_B/Q = C_B/C$, as shown in Figure 3(b).

Defining the total gas phase concentration, C, as equal to $(C_1 + C_2)$, and the total adsorbed phase concentration, Q, as equal to $(q_1 + q_2)$, then after some algebraic manipulation, equations (2.19) and (2.21) yield another form of isotherm equation:

$$\frac{q_2^*}{Q} = \frac{C_2/C}{K_{1,2} + (1-K_{1,2})(C_2/C)} \tag{2.22}$$

Equation (2.22) is useful for correlation if adsorption is governed by the Langmuir isotherm.

2.2.3.b. <u>The Ideal Adsorbed Solution Theory</u>

Several thermodynamic approaches to describe adsorption equilibria have been proposed and are quite useful even though they do not result directly in analytic forms for adsorption isotherms. A review of mixed gas adsorption is given by Young and Crowell (123).

Myers and Prausnitz (92) preceded by Hill (58), developed an adsorption solution theory from the Gibbs adsorption isotherm with the following two basic assumptions

1. The adsorbent is considered thermodynamically inert i.e. the change in thermodynamic properties of the adsorbent during an adsorption process at constant temperature are assumed to be negligible compared with similar property changes to the adsorbate.

2. The adsorbent area available for adsorption is independent of temperature and of the adsorbate.

This theory is based on the concept of an ideal adsorbed solution in a manner similar to that used for liquid phase solutions and, using classical surface thermodynamics, an expression analogous to Raoult's law was obtained (92). An ideal solution was defined, in which the partial pressure of an adsorbed component is given by the product of its molefraction in the adsorbed phase and the pressure which it would exert as a pure adsorbed component at the same temperature and spreading pressure as those of the mixture; as is given as

$$Py_i = P_i^o(\Pi)\bar{x}_i \qquad \text{at constant T} \tag{2.23}$$

Spreading pressure is defined in the following form

$$\frac{\Pi A}{R_g T} = \int_o^{P^o} \frac{q}{P}\, dP \tag{2.24}$$

where P_i^o = Vapour pressure of the pure saturated liquid

and Π = Spreading pressure of pure component

There is no experimental technique for measuring the spreading pressure directly, but may be defined as a thermodynamic variable just like entropy or internal energy (92). Kidnay and Myers (65) show that spreading pressure calculations could be greatly simplified or altogether eliminated with little or no loss in the accuracy of the calculations. For a binary mixture of component 1 and 2, equation (2.23) yields a simplified relationship of the form:

$$P = P_1^o \bar{x}_1 + P_2^o \bar{x}_2 \tag{2.25}$$

equation 2.25 is thermodynamically consistent, provided that the spreading pressure of the different adsorbates are equal at a given amount adsorbed.

2.2.3.c. Polanyi Adsorption Potential Theory

The adsorption potential theory has been applied to binary adsorption by assuming that results for single components can be used for the individual components of a mixture (49, 72, 74).

Levan (72) suggested the adsorption potential equation for a binary mixture may be written in the form

$$\epsilon_{1,2} = RgT\ln \left[\frac{f^s_{1,2}}{f_1 + f_2} \right] \tag{2.26}$$

and $f^s_{1,2}$ is given by

$$f^s_{1,2} = \frac{1}{\left[\dfrac{\bar{y}_1}{f^s_1} + \dfrac{\bar{y}_2}{f^s_2} \right]} \tag{2.27}$$

where $\epsilon_{1,2}$ = mixture adsorption potential

$f^{s}_{1,2}$ = fugacity of the mixture at saturation

f_1, f_2 = fugacity of the components

$\bar{y}_1$, y_2 = molefraction of the components in the vapour phase

Equation (2.26) has the same form as equation (2.13) for single components. Levan (72) used equation (2.26) for correlating his results on n-Octane and n-Decane mixtures, and found that the agreement was reasonably good.

2.3. Rate of Adsorption

2.3.1. Introduction

To describe the operation of a fixed bed adsorber it is necessary to be able to predict the concentration in both the solid and gaseous phase at any point in the bed as a function of time. To do this, mass balances in the bed and particle must be set up and then solved for the unknown concentration, making use of known bed and inlet conditions.

The following transport processes may affect the overall rate of the adsorption and therefore must be considered in any model.

1. Transfer of adsorbate from the bulk gas stream to the surface of the adsorbent. This is known as external or boundary film mass transfer since the resistance to transport lies in the boundary film of the stagnant gas surrounding each particle.

2. Transfer of material from external to internal surface of the porous particle by a molecular diffusive mechanism. This diffusive mechanism is made up of two parts:

(a) Pore diffusion in the gaseous phase through the porous structure of the adsorbent.

(b) Surface diffusion in the adsorbed phase along the internal surface of the adsorbent.

These two diffusive mechanisms occur simultaneously, and together they make up intraparticle diffusion. When pore diffusion is important the controlling mass-transfer process occurs before any phase change (i.e. solute deposited on the pore surface), but in surface diffusion it occurs afterwards. At different operating conditions, the same particle can show either surface- or pore-diffusion behaviour, the former being favoured if the pore fluid concentration level is low and the latter being favoured if this level is high.

Clearly, the overall rate of sorption may be controlled by any single step or combination of steps. The differences between the various models used to describe fixed bed behaviour lie in the relative importance ascribed to these individual steps. A number of models, some of them empirical, have been proposed to describe each of the possible rate limiting steps.

2.3.2. Material balances

It is possible to set up material balances for the adsorbate across an infinitesimal section of the adsorption bed and also within an adsorbent particle itself. The derivation of these material balances is in no way dependent upon the assumptions as to the mechanism or mechanisms controlling the removal of the adsorbate from the fluid stream (30).

It is assumed that the system considered consists of a bed of homogeneous spherical particles of uniform radius, contained in a small adsorption column through which the adsorbate flows with a constant linear velocity. Therefore, there is a radial symmetry and the longitudianl dispersion is neglected (84, 97). Hence for the vapour adsorption systems the concentrations of adsorbate in the fluid and on the adsorbent depend solely upon the space variable 'z' and the time variable 't' so that:

$$C = C(z,t) \text{ and } q = q(z,t) \tag{2.28}$$

A mass-balance over the whole bed, assuming a single transfer zone, is given by:

$$\text{Input - Output} = \text{Accumulation + loss by sorption} \tag{2.29}$$

$$\text{Mass into the bed} = FC_o t_e \tag{2.30}$$

$$\text{Mass out of the bed} = FC_o(t_e - t_o) \tag{2.31}$$

$$\text{Accumulation in the bed} = mq_o + EV_b C_o \tag{2.32}$$

$$\text{Loss by sorption} = 0 \tag{2.33}$$

Combining equations (2.30), (2.31), (2.32) and (2.33) give:

$$FC_o t_o = mq_o + EV_b C_o \tag{2.34}$$

t_o is defined as the stoichiometric time, and is given by:

$$t_o = t_n - \frac{\int_0^{tn} C(t)dt}{C_o} \tag{2.35}$$

The stoichiometric time represents the time at which the transfer zone would reach the end of the bed if the concentration were a step function of time (or bed length) as shown in Figure 4.

A mass balance across an infinitesimal element of the bed of volume $A_C \Delta z$ is given by:

$$u \frac{\partial c}{\partial z} + \frac{\partial c}{\partial t} + \rho_b \frac{(1 - E)}{E} \frac{\partial q}{\partial t} = 0 \qquad (2.36)$$

The first term of equation (2.36) represents convection in the axial direction. The second and third represent the rate of accumulation in the fluid phase and the adsorbed phase respectively. It is assumed that the concentration of adsorbate is sufficiently low to make negligible changes in the total flowrate of the fluid phase.

2.3.3. Mass transfer rate controlling mechanisms

The problem of adsorption in fixed beds has been studied and solved for various steps controlling the overall rate of adsorption. For example, with external diffusion controlling the rate, Hougen and Marshall (60), Furnas (38) and others have provided equivalent solutions, whilst Rosen (98), Thomas (109) and Edeskuty and Amundson (30) have solved the problem with intra-particle diffusion controlling. Rosen (97) has also solved the problem considering the combined effects of external and intra-particle diffusion. However, the only solution which considers all three resistances is that due to Masamune and Smith (84). These are defined separately in the following sections.

2.3.3.a. Gas phase mass transfer control

In gas phase mass transfer control, adsorption is limited by the transfer of adsorbate between the bulk of the fluid phase and the outer surface of the adsorbent particles. The rate of mass transfer is given by:

$$\left(\frac{\partial q}{\partial t}\right)_z = K_g.a\,(C - C^*) \qquad (2.37)$$

Where K_g is the film mass transfer coefficient (which can be evaluated by means of several empirical correlation, e.g. that of Hougen and Watson (61)).

Although it is generally recognised that in sorption processes the resistance to external mass transfer alone is not the rate controlling step, the correlation of experimental data with this model provides a useful empirical correlation of sorption data, but then K_g must be regarded as a 'lumped mass transfer coefficient' representing the overall resistance to adsorbate transport.

2.3.3.b. Pore diffusion control

For pore diffusion control, the approximation is made that the amount of solute held in the pores is negligible compared with the amount adsorbed by the solid phase (i.e. although all of the solute is carried through the pores, all of it is held by the solid). The rate of diffusion into a uniformly porous spherical particle is given by Fick's second law

$$\left(\frac{\partial q}{\partial t}\right) = \frac{Dp}{r^2}\,\frac{\partial}{\partial r}\left[\,r^2\left(\frac{\partial c}{\partial r}\right)_t\right] \qquad (2.38)$$

2.3.3.c. Surface diffusion control

Hall et al (52) reported that surface and pore diffusion mechanisms act in parallel, and the more rapid one will control the overall mass transfer process. For surface diffusion control, the rate is expressed by:

$$\left(\frac{\partial q}{\partial t}\right) = \frac{D_s}{r^2}\left[\frac{\partial}{\partial r}\left(r^2\frac{\partial \bar{q}}{\partial r}\right)\right] \tag{2.39}$$

where D_s is the surface diffusivity. Although surface diffusion generally shows a marked concentration dependence, the quantitative relationships are poorly known. A constant surface diffusivity, D_s, is usually assumed.

2.3.4. Mathematical models based on simplifying assumptions

Owing to the non-linear nature of the set of partial differential equations representing most of the adsorption system, rigorous analytical solutions are not readily available. To eliminate these complications, various simplying assumptions have been introduced.

2.3.4.a. Constant pattern behaviour

Breakthrough curves are sometimes encountered which retain a constant shape, regardless of column length. This indicates that all parts of the exchange zone move through the column at a constant rate. In particular, systems having a favourable type of equilibrium isotherm are likely to exhibit such behaviour (52). Under these conditions, the mass balance equation, in the absence of any axial dispersion effects (115), can be written

$$\frac{q}{C} = \frac{q_1}{C_1} \tag{2.40}$$

where q_1 and C_1 are adsorbed and fluid phase concentrations in the plateau zone.

Rosen (97), and Cooney and Lightfoot (18), have shown that a constant pattern is given by an asymptotic solution for favourable equilibria in 'deep' beds. Hall et al (52) assumed a constant pattern condition, and were able to obtain theoretical concentration profiles for the cases where intraparticle diffusion control the mass transfer.

2.3.4.b. Overall particle kinetics equation

These are lumped models in the sense that the rate of transfer of material into the adsorbent particles is given explicitly in terms of the gas phase concentration and some average concentration within the particles. Thus solution of the partial differential equations for diffusion into the particles is not required.

In view of the complexity of the surface diffusion equation (2.39), Glueckauf and Coates (46), assumed that the mass transfer of vapour to adsorbent can be represented by a lumped parameter model.

$$\left(\frac{\partial q}{\partial t}\right)_z = K^I (q^* - q) \tag{2.41}$$

Vermeulen (114) suggested a quadratic form of driving force in the adsorbent granule.

$$\left(\frac{\partial q}{\partial t}\right)_z = \frac{K^{II} (q^{*2} - q^2)}{2q} \tag{2.42}$$

while Hiester and Vermeulen (57) proposed an empirical relationship, which takes into account the equilibrium characteristics of the system

$$\left(\frac{\partial q}{\partial t}\right)_z = K^{III}\left[C(q_o - q) - Rq(C_o - C)\right] \qquad (2.43)$$

Vermeulen and Quilici (116) on the other hand, obtained an empirical correlation for pore diffusion controlling the mass transfer

$$\left(\frac{\partial q}{\partial t}\right)_z = K^{IV} \frac{q^* - q}{\sqrt{1 - (1-R)q}} \qquad (2.44)$$

The kinetic parameters take the form K(t-t'), where t' is the time at which a concentration of C' of the effluent reaches the bed outlet.

It should be stressed that in as much as the physical model assumed is only an empirical approximation without any physical significance. The values of K, which can be evaluated as a result of fitting experimental data to the preceding model, are not related to the actual transport properties and can only be used for prediction purposes in so far as the same model is again employed.

2.3.5. Previous work on single component adsorption

Many mathematical models have been presented for single component adsorption in fixed beds, but only a few of the more important ones will be discussed here. Several good reviews have been given by Carter (12-14). Many empirical design approaches have been tried and notable amongst these are those by

Getty and Armstrong (44), Fleming et al (34), Bunke (11) and Chung (16).

The solution for the isothermal case where external mass transfer only is rate controlling has been solved by Hougen and Marshall (60). Thomas (109) considered the case where adsorption is limited by the rate of physical adsorption, whilst solutions to the problem with external and internal diffusion have been obtained by Kasten, Lapidus and Amundson (63). Eagleton and Bliss (29) assumed that a film similar to the gas film is present in the particle, and thus represents intraparticle diffusion by an additive resistance.

Rosen (97, 98) developed an analytical solution for the problem with both film and intraparticle diffusion rate controlling; and also presented an asumptotic solution which is valid for large bed lengths. A similar solution has also been obtained by Vermeulen (114, 115). However, the most general result obtained for isothermal adsorption with a linear isotherm is that obtained by Masamune and Smith (81-83). They solved the general case where external diffusion, intraparticle diffusion and surface reaction controls the overall rate. They presented their solution as an infinite integral which must be evaluated numerically.

Stuart and Camp (105) have compared the Rosen exact model with the 'kinetic' linear driving model proposed by Hiester and Vermeulen (57), and concluded that the approximate method can be used under some circumstances. Liaw (78) obtained a solution in response to a step change in feed concentration for a linear equilibrium system with consideration of resistance to mass transfer, in both gas and solid phases. Miura (53-55, 89) presents an analytical solution using constant pattern and linear driving force approximations. Both internal and external mass transfer resistances of the particle are taken into account for the analysis. Both Langmuir and Freundlich isotherms were considered. Analytical solutions of the breakthrough curve have also been presented for irreversible isotherms by Cooper (20), while the case for a linear isotherm was solved by Antonson (1), Garg (39-42) and Wheeler (119).

Hall et al (52) used the assumption of constant pattern conditions to develop numerical solutions for adsorption where the Langmuir isotherm is applicable. Their solutions were presented graphically, (for both pore and surface diffusion), as a function of a constant separation factor 'R'. The factor 'R' is a function of the isotherm only and characterises its shape.

Tien and Thodes (11-113) have presented numerical solutions for the case of a non-linear Freundlich isotherm, which both external and intra-particle diffusion contributing the overall rate. However, this solution assumes that all the adsorption occurs at the particle external surface and is more suited for use in ion-exchange columns for which the solution was first developed.

2.3.6. Previous work on multicomponent adsorption

Multicomponent equilibrium sorption has received attention recently, especially from Klein et al (66), Helfferich and Klein (56) and Rhee et al (96). Their predictions allow the calculation of concentrations in the plateau zones between wave fronts, the nature of the wave fronts (e.g. whether they are of the abrupt, self sharpening, shock wave type, or the gradual non-sharpening simple wave type) and the results of wave-wave interactions.

Reports of work on non-equilibrium multicomponent adsorption have been rather limited. Dranoff and Lapidus (24, 25) modelled ion-exchange using a mass action form of the rate equation. Collins and Deans (17) treated the case in which displacements from equilibrium are sufficiently small so that linear perturbation theory is applicable.

Needham et al (93), while presenting hydrocarbon mixture adsorption data on silica gel, concluded that interaction effects complicate mass-transfer to a degree which make it unfeasible to use any simple model to describe the process. Kidnay et al (64) treated their coadsorption data for nitrogen and methane on activated carbon as single component adsorption; Eagelton and Bliss (29), and Engel and Coul (31), utilised empirical models to predict the data.

For binary adsorption of benzene and hexane on silica gel, Shen and Smith (102) found no interactive effects between the components. De Vault's equilibrium theory (23), which assumed that equilibrium was established at all points instantaneously, was applied to predict adsorption of n-hexane.

Cooney and Lightfoot (18), extended the asymptotic solution of the mass balance and rate equations for single solute separation and exchange processes to a multicomponent system. Good agreement with experimental data was reported. Cooney and Strusi (19) extended the solution to non-equilibrium cases for solutes following the Langmuir form of binary isotherms, and showed that the concept of a pseudo binary isotherm is feasible.

Miura (90) derived an analytical solution for three special cases of the Langmuir isotherm by extending the treatment of Cooney and Strusi (19). They clarified the conditions under which the analytical solutions are approximately applicable. In another paper (91), Miura developed a simple method for calculating breakthrough curves under constant pattern conditions and linear driving force approximations. External fluid film mass transfer and intra-particle diffusion resistances were also considered.

Thomas and Lombardi (110) studied the binary adsorption of benzene-toluene mixtures in a fixed bed of activated carbon. They found that, following an initial region of the bed, each wave front assumed an independent constant pattern shape. The rate of adsorption was described by Glueckauf and Coates (46), semi-empirical linear driving force model. Simultaneous rate equations for the two components, were solved numerically by a

Runga-Kutta routine to predict successfully the observed breakthrough of components.

Garipy and Zwiebel (43), and Zwiebel et al (128), studied binary adsorption and desorption in fixed beds. They assumed a mass transfer resistance of the liquid film type. Their predictions display qualitative features similar to those found experimentally by Wastermark (118), Carter and Hussain (15), Spahn (104) and Suzuki (106). Bradley and Sweed (8) treated the case of constant pattern multicomponent adsorption but did not include the effect of diffusional resistance within the adsorbent particles.

Liapis and Rippen (75, 76) developed a general model for the simulation of multicomponent adsorption. Intra-particle pore and solid diffusivities of the components were estimated by matching the predictions of their model to the results of simple multicomponent batch experiments. In a recent paper, Liapis and Rippen (77), proposed a simulation for multicomponent adsorption in a fixed bed with periodic and continuous countercurrent operation. The model used includes the effects of axial diffusion in the columns, mass transfer resistance in the boundary layer surrounding each particle, and fluid diffusion within the porous particles.

2.4. Regeneration of Fixed Beds

The regeneration of fixed beds is usually performed by heating and subsequently purging by a gas stream, or applying vacuum to remove the adsorbate vapour. If both the adsorption and desorption operation in fixed beds could be described as first order, the desorption curves would be mirror images of the adsorption breakthrough curves (98, 126). However, it was shown (127) that even when the desorption step was carried out as an identical complement to the adsorption (i.e. the same flowrate, temperature, etc.) a longer time is required on desorption to return the bed to its initial starting condition.

The deviation from the mirror-image relationship between adsorption and desorption profiles have been attributed to non linearities, especially in the adsorption isotherm (11). Departures from isotherm linearity were also accounted for by Thomas (109), and by Zwiebel et al (125). Both showed significant deviation from the predicted depletion curves of the linear model.

No simple approximation is available for desorption since, if the equilibrium relationship is favourable for adsorption, it will always be unfavourable for desorption. This is true even if the temperature is raised during the desorption cycle. At sufficiently high temperatures, the isotherm will approach linearity, but the curvature will not normally be reversed. The limiting form of the desorption profile will therefore be of the proportionate pattern type (99).

CHAPTER III

APPARATUS AND EXPERIMENTAL

CHAPTER III

APPARATUS AND EXPERIMENTAL

3.1. Introduction

This chapter describes the experimental procedure for all the isothermal adsorption experiments carried out on the two adsorbents Anthrasorb CC818H and CC818M.

The adsorbates studied were:

(a) Methane

(b) Ethane

(c) Methane-Ethane mixtures

(d) Acetone

(e) Carbon tetra chloride.

The experiments were performed at four different temperatures, i.e. -6, 0, 25 and 50^{o}C. The apparatus used for the experimental study is described in the following sections.

3.2. Apparatus

A flow diagram of the experimental set up used for the investigation is shown in Figure 5. In the following description of the apparatus the numbers given in brackets refer to the corresponding items in the flow diagram. Plate 1 shows a photograph of the set up.

The complete apparatus comprised four sections as follows:

(a) Gas sample preparation section.

PLATE NO 1

PHOTOGRAPH OF EXPERIMENTAL APPARATUS

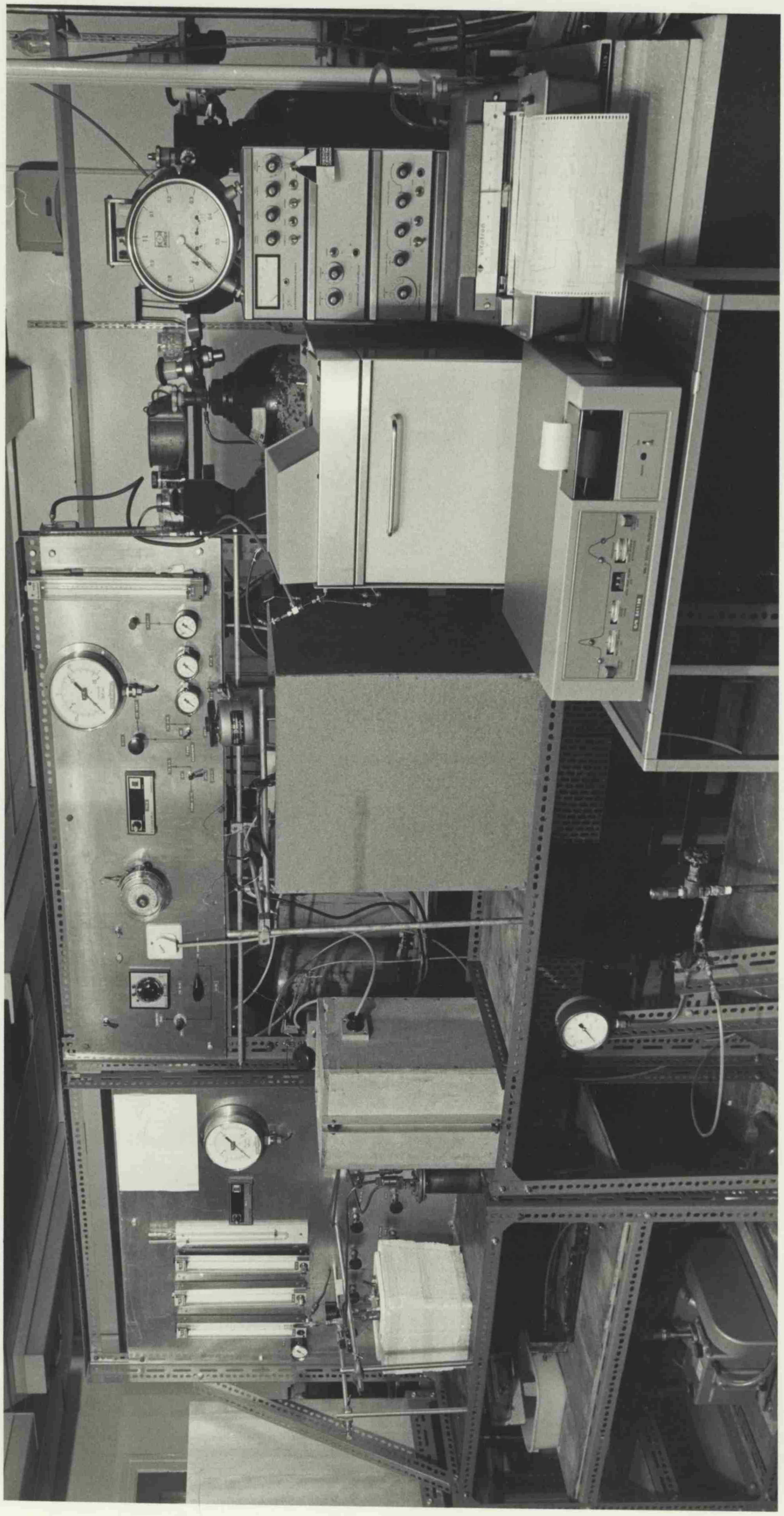

(b) Vapour sample preparation (Saturation) section.

(c) Adsorption and Analysing section.

(d) Regeneration section.

Gas sample preparation consisted of a cylindrical mixing vessel (5) with auxillary tubing. The saturation section comprised a saturator (8) immersed in an ice bath (9) and a mixing vessel (10) partially filled with Raschig rings to enhance mixing. An adsorption column (11) immersed in a water bath (12) with auxillary piping constitutes the adsorption section. The column effluent was analysed in an analysing section consisting of a Flame Ionization Detector, F.I.D., (16), linked with a recorder (17) and coupled with an Integrator (18). The regeneration section had a temperature controlled furnace (23) for desorption.

The outlet flowrate was set by a needle valve (V23) and measured by a bubble flow-meter (BF2). The pressure in the sample loop upstream of the outlet flow control valve was maintained constant at 25 p.s.i.g. by a chromatography grade pressure regulator (PR5); it was employed to match the carrier gas pressure at the column inlet (16) with the sample loop pressure, and to minimise surges in flow when injecting or sampling.

All pipework downstream from the change over valve (V18) and valve (V20), was of 0.16 cm O.D. x 0.08 cm I.D. stainless steel. This tubing was used to minimise dead volume. Stainless steel material was used to withstand the high regeneration temperature used. Adsorbent was regenerated by allowing movement of the adsorption tube between the water bath (12) and the regeneration furnace (21). All other pipework was 0.63 cm O.D. x 0.48 cm I.D. copper tube. The dimensions of the adsorption column were determined after experimenting with different column sizes. The adsorption column chosen was a 0.95 cm O.D. x 34.29 cm l stainless steel tube, which gave a negligible pressure drop when packed. The ends were plugged with glass wool and any dead space remaining after the addition of the adsorbent was filled with 30-60 mesh glass beads.

All materials used for high temperature work were first pressure tested for leaks in a furnace at 500°C. The adsorption column was immersed in a continuously stirred lagged water bath (12). The water bath temperature was maintained by means of a Fison Fi-Monitor regulator and Red Rod immersion heaters (13) to within ± 0.5°C of the required adsorption temperature, and measured by a mercury in glass thermometer (14). The adsorption tube was placed in the water bath and the excess piping (approximately 60 cms) was coiled (15) and immersed in the bath to preheat the inlet gas stream.

The regeneration furnace (23) temperature was controlled with a Pye-Either Mini Temperature Regulator (21) using a chromel-alumel thermo-couple (22). After 8 hours regeneration, the furnace was automatically switched off using an electric time switch (20).

The adsorption column effluent was sampled using a Pye six port rotary sampling valve with a 0.5 cm^3 sample loop. The effluent stream was analysed in a Flame Ionization Detector, F.I.D., (16), Series 104 Chromatograph supplied by W.G. Pye and Co. A Fison chart recorder was connected to the chromatograph, and a Digital Integrator was coupled to the recorder (supplied by Smith Industries Ltd.)

3.3. Gas Analysis

Two techniques were used to determine the hydrocarbon concentration in the effluent stream. Both methods responded quickly and accurately to changes in concentration.

3.3.1. Direct System

For single component gas adsorption experiments, a fraction of the adsorption column effluent was directed into a Flame Ionization Detector, F.I.D., (16), as shown in Figure 6. The signal produced, proportional to the outlet hydrocarbon concentration, was amplified and recorded. This provided continuous monitoring of the effluent concentration (an example is shown in Figure 1).

The process conditions were chosen after some trials, in order to attain both higher sensitivity and good flame stability, and are summarized in Table 3.1. The manner in which calibrations were performed are discussed in section 3.4.

3.3.2. Chromatographic System

A chromatographic system of analysis was used for the binary and single component vapour phase adsorption experiments, and is

Table 3.1. Process Conditions for Gas Analysis

	Direct	Chromotographic
Hydrogen flowrate, $cm^3.min^{-1}$	40	40
Air flowrate, $cm^3.min^{-1}$	600	600
Nitrogen flowrate, $cm^3.min^{-1}$	-	40
oven temperature, ^oC	100	200
Detector temperature, ^oC	150	250

shown diagrammatically in Figure 7.

Prior to the analysis, the effluent from the adsorption column was passed through a 0.5 cm^3 loop via a sampling valve to the exhaust. Nitrogen carrier gas was circulated in the chromatographic column, containing Porapak Q as the stationary phase and located in the oven of the Gas-Chromatograph (16), as shown in Figure 7(a). For analysis a sample was introduced into the chromatographic column by the carrier gas, while the effluent from the adsorption column was connected to the exhaust (shown in Figure 7(b)).

The effluent from the chromatographic column was also analysed using the F.I.D. system (described in section 3.3.1.), the signals from which were recorded and integrated by a digital integrator. It should be pointed out that, in this case, the breakthrough curve is in the form of a succession of periodic chromatographic peaks (a typical example is shown in Figure 8).

In order to obtain a well defined breakthrough curve, it is necessary that the time elapsing between samples should be minimized. On the other hand, overlapping of peaks from different samples should be avoided, by choosing a time interval longer than the retention time corresponding to the slowest moving component (viz. ethane in a methane-ethane mixture).

The process conditions were selected after experimenting with different packing lengths and varying the carrier gas flow rate. The corresponding operating conditions are summarized in Table 3.1. The manner in which calibrations were performed are discussed in section 3.4.

3.4. Calibration

The Flame Ionization Detector (F.I.D.) response was calibrated for each adsorbate, by injecting a known amount of the sample, as shown in Appendix A. A linear relationship between the peak area and concentration was found for all the adsorbates over the range investigated (Figures 9, 10, 11 and 12). The F.I.D. response was checked at the beginning and the end of each experiment.

Pressure gauges were calibrated using a Budenburg standard test gauge. The pressure drop across the adsorption column was found to be negligible (5mm Hg) over the range of flowrate used throughout the experiments.

All the Rotameters were calibrated by a bubble flowmeter. The flow was allowed to pass through a soap solution, and the bubble produced was timed between fixed marks.

The saturator used for the vapour phase adsorption experiments was calibrated for maximum saturation efficiency. The optimum flowrate was obtained by varying the flowrate and noting the corresponding response from the F.I.D. The plot of flowrate versus detector response is shown in Figure 13. It is seen that the detector response increases as the flowrate increases, and remains constant between flowrates of 15 $cm^3.min^{-1}$ and 25 $cm^3.min^{-1}$, and then steadily decreases with further increase of flowrate. A flowrate of 20 $cm^3.min^{-1}$ was therefore chosen, so that the detector response remained constant with any slight fluctuation of flowrate during the experiments.

The effect of the height of liquid in the saturator was also evaluated. A constant flowrate of 20 $cm^3.min^{-1}$ was passed through the saturator and the detector response was noted for different liquid heights (Figure 14). It can be seen from this diagram that the detector response was unsteady below a liquid height of 1 cm, it reached a maximum at a height of 3 cm and the detector response then decreased to a steady value. Since it is imperative to use a height which gives a fairly constant detector response during an experiment, an initial height of 10cm for the liquid in the saturator was selected for all the experiments. The solvent was replaced whenever its height dropped to below 8 cm in the saturator.

The efficiency of saturation was calculated by comparing the theoretical and experimental values of amount adsorbed on to Anthrasorb using the F.I.D. (see section 3.3. for details of the method); and measuring the temperature, flowrate of saturation and diluent streams. Appendix B gives a sample calculation.

3.5. Determination of apparatus dead volume

The apparatus dead volume was determined with the adsorption column packed with 30-60 mesh glass beads. A dilute nitrogen-methane mixture was passed through the bed, and the effluent response recorded by the direct method of analysis (see section 3.3.1.). The same outlet flowrate was used as that employed in the adsorption experiments.

The response on the recorder chart was almost instantaneous for the nitrogen-methane mixture, indicating negligible dead volume. A maximum of 15 s delay was observed, but this is negligible in comparison to the breakpoint times (see Chapter II).

For a run using the direct method of analysis, the time was taken from the instant at which the signal on the recorder chart dropped from the inlet valve to zero. In experiments using the chromatography column, the breakthrough curves contained a succession of periodic peaks; which were obtained by intermittent injection of adsorption bed effluent (see section 3.3.2.). The time was therefore measured from the instant when valve (V18) was turned to allow the adsorbate flow into the adsorption column.

3.6. Materials

Nitrogen, methane and ethane were obtained from Air Products Ltd., and were 99%, 99.7% and 99.7% by volume respectively. Acetone and carbon tetra-chloride were purchased from BDH Chemicals Ltd. They were technical grade chemicals, and were used without further purification.

The activated carbon, Anthrasorb CC818H and CC818M, manufactured by the National Coal Board, is designed for vapour phase applications. Physical properties of this carbon are given in Table 3.2.

Table 3.2. Physical Characteristics of Anthrasorb

	CC 818H		CC 818M	
	Reported	Measured	Reported	Measured
Pore volume, $cm^3.g$	0.47	-	0.40	-
Bed density, g. cm^{-3}	-	0.53	-	0.57
Apparent density, g. cm^{-3}	-	0.95	-	1.04
Void fraction	0.44	0.44	0.44	0.45
CCl_4 uptake, %	79.0	-	65.0	-

The manufacturer provided specifcations for pore volume, void fraction and carbon tetra chloride uptake. Adsorbent bed and apparent densities were measured gravimetrically, while the bed void fraction was measured volumetrically. Sample calculations are shown in Appendix C. Pore size distributions were determined using a Carlo Erba 1500 Mercury Porosimeter. Pore diameters down to 50 Å were determined and as shown in Figure 15.

3.7. Vapour sample preparation (saturation section)

Nitrogen carrier gas was passed through a bed of molecular sieve (4) to dry the gas. The flow was then divided into two different streams, each incorporating two valves in series (coarse valves, V6 and V8, and fine control valves, V7 and V9) to regulate the flow of gas. Two calibrated rotameters, (R1) and (R2) were then included to measure the flow in each stream. To entrain the required concentration of solute vapour, one of the gas streams was sparged through the pure liquid hydrocarbon, contained in a saturator maintained at a constant temperature in an ice bath. The dimensions of the saturator were 6.5 cm O.D. x 15 cm h, and it was made of brass. The saturator was calibrated for its optimum efficiency (see section 3.4.). The saturated stream was then mixed with pure nitorgen in a second mixer of dimension 6.5 cm O.D. x 15 cm h made of brass and filled with Raschig rings to enhance mixing.

3.8. Gas sample preparation

Gas mixtures were prepared in a cylindrical mild steel mixing vessel (5) of dimension 30.5 cm O.D. x 91.4 cm l. Before preparing a gas sample, the vessel and its feed lines were flushed to remove water vapour and the whole apparatus was evacuated for 48 hours.

Samples were then made up as follows:

(a) V3 and V5 were closed, V4 was opened and the vessel (5) filled with methane via V1 and/or ethane via V2 to the required pressure, measured by pressure gauge P1.

(b) Then V1 and V2 were closed, V3 was opened and the vessel filled with nitrogen to the required pressure, indicated by P1.

(c) V3 was then closed.

The minimum time of diffusion for a binary gas mixture was calculated to be approximately 15 minutes (see Appendix D). Thus the time actually allowed, ensured almost complete mixing and this was confirmed with the F.I.D.

3.9. Adsorbent Regeneration

A weighed sample of adsorbent was packed into the adsorption column which was placed in the regeneration furnace. A slow nitrogen purge was passed through the apparatus until the regeneration temperature 150-200°C was reached, and the adsorbent was degassed for about 8 hours (see section 3.2.).

3.10. Experimental procedure

The regenerated and cooled adsorption column (11) was placed in the water bath (12) and each experiment was then started by purging the bed with nitrogen. During this operation a pressure test was performed to ensure leak free equipment. The preheater coil (15) was placed in the water bath and nitrogen continued to pass through the apparatus for 2 hours, so that the adsorbent bed reached the temperature of the water bath. The gas chromatography unit was then switched on and allowed to warm up.

A number of bed effluent samples were analysed to ensure that regeneration was complete and that no impurities were being desorbed and swept away with the carrier gas. The sample gas was then introduced instead of nitrogen using the three way valve (V18) bypassing the adsorption column via valve (V21). Once these conditions were stabilized, the sample was introduced into the adsorption column and the effluent was analysed until breakthrough of all the adsorbates were complete (see Gas Analysis Section 3.3.). The flowrate, ambient temperature and pressure were monitored throughout the experiment.

In order to ensure that the adsorption conditions were well below those which might cause attrition and carryover of the particles in the adsorption column, Ledoux's correlation (70) for the maximum allowable gas velocity was employed. The relevant calculations are shown in Appendix E. In all the experiments the flowrate was chosen to be considerably less than the calculated maximum allowable flowrate (approximately 1.5 $litre.min^{-1}$).

CHAPTER IV

ADSORPTION AND SEPARATION OF METHANE AND ETHANE

CHAPTER IV

ADSORPTION AND SEPARATION OF METHANE AND ETHANE

In this chapter, fixed bed theories for single as well as for multicomponent adsorption are applied to observed experimental results, obtained for methane and etahne on Anthrasorb CC818H and CC818M at various temperatures. Part 1 of this chapter deals with the equilibrium behaviour, while part 2 deals with the transient behaviour,. i.e. the prediction of breakthrough curves.

4.1. Equilibrium Isotherms

4.1.1. Single component adsorption isotherm results

Single component adsorption isotherm experiments were carried out in order to obtain an accurate equilibrium description of all the systems studied. This is necessary to predict binary component adsorption and also breakthrough points.

The following are the single component systems studied

(a) Methane at 0, 25 and 50^{o}C on Anthrasorb CC818H and CC818M

(b) Ethane at -6, 25 and 50^{o}C on Anthrasorb CC818H and CC818M.

Nitrogen carrier gas was used in all experiments. A concentration range (1.23 - 24.85 x 10^{-6} mol.cm^{-3}) for all single component experiments was used. As discussed in Chapter 2, the adsorbate concentration used is sufficiently low to make negligible changes in the total flow rate of the fluid phase.

Equilibrium data for all the single component experiments were obtained by recording the bed effluent concentration as a function of time until the outlet concentration remained steady indicating that equilibrium between adsorbate and adsorbent had been achieved throughout the bed. All the single component results obey a constant pattern profile (discussed in Section 4.2.1.a. of this chapter). When constant pattern behaviour prevails each transfer zone moves through the column at a constant velocity. This therefore simplifies the partial differential form of the continuity equation to a simplified mass-balance equation (see Appendix K). An overall mass-balance equation (section 2.3.2.) is written

$$F C_o t_o = mq_o + EVC_{bo} \tag{2.34}$$

The concept of stoichiometric time is used to derive equation 2.34, and is defined as the time required for a transfer zone (in which mass transfer occurs) to traverse the length of bed if the concentration were a step function of time; it may be calculated from the equation

$$t_o = t_n - \int_o^{tn} \frac{C(t)\ dt}{C_o} \tag{2.35}$$

by applying the trapezoidal rule to breakthrough curves C(t), evaluating the integral between t=0 and the time t_n elapsing before the effluent concentration has reached the initial feed concentration.

The adsorbed-phase concentration of methane, q_{Mo}, (or ethane, q_{Eo}) in equilibrium with the inlet gas-phase concentration, C_{Mo}, (or C_{Eo}) was calculated in terms of the stoichiometric time from a rearranged form of the material balance equation 2.34.

$$q_o = \frac{(Ft_o - EV_b)C_o}{m} \qquad (4.1.)$$

All the quantities in equation 4.1 are therefore known except for q_o. The equilibrium relation was thus established by analysis of the breakthrough curves for all the single component adsorption experiments (discussed in Section 4.1.1.a). Details of all the experiments are tabulated in Appendix I. The computer programme for calculation of the stoichiometric time, and the amount adsorbed at equilibrium is given in Appendix L.

4.1.1.a. Langmuir and Freundlich Isotherms

(i) Methane on Anthrasorb CC818M and CC818H

The experimental results on Anthrasorb CC818M and CC818H are shown in Figures 16 and 17 respectively. An empirical single component Langmuir model represents the data over a range (0-50^{o}C) of temperature. The constants for this model, calculated by a least squares fit to experimental data, are given in Table 4.1.

It is seen from Table 4.1., that the value of the empirical Langmuir constant, b, for methane on Anthrasorb CC818H at 25^{o}C is small. Thus the value of 'bC_o' in the Langmuir equation (2.6) (Section 2.2.2.a.) at very low concentrations would also be small compared with unity. Hence equation (2.6) reduces to a Henry's law form which is

$$q_o = K_H . C_o \qquad (4.2)$$

where K_H is Henry's constant, obtained by a least squares fit of

Table 4.1. Empirical Langmuir Constants

Adsorbate	Adsorbent	Temperature (^{o}C)	$a \times 10^{3}$ ($mol.g^{-1}$)	$b \times 10^{-4}$ ($cm^{3} mol^{-1}$)	$b^{1} \times 10^{-4}$ ($cm^{3} mol^{-1}$)
Methane	CC818M	0	0.72	5.91	
		25	0.86	2.96	1.44
		50	0.80	2.16	
	CC818H	25	8.56	0.48	
Ethane	CC818M	-6	3.99	20.06	
		25	2.87	11.43	2.53
		50	2.26	10.55	
	CC818H	-6	4.64	15.61	
		25	3.55	11.25	
		50	4.82	4.30	

the equation (4.2) to experimental points. Figure 17 shows that Henry's law fits the experimental data. For dilute systems, a number of theretical isotherm equations (notably that of Langmuir) reduce to Henry's law (123).

The experimental isotherms may also be expressed in terms of a Freundlich model over the whole range of adsorbate concentration and temperature, as shown in Figure 18. The model coefficients, obtained by a least squares fit of the equation 2.9 (section 2.2.2.b) to experimental points, are given in Table 4.2.

The temperature dependence is clearly seen from Figure 16 by a marked decrease in adsorption with increasing temperature. The value of Langmuir constant 'a' in equation (2.6) (section 2.2.2.a) was found fairly constant for the three temperatures of 0, 25 and 50°C studied (Table 4.1.), thus showing the independence of 'a' on adsorption temperature. On the other hand, when the logarithm of b is plotted against the reciprocal of temperature a straight line results, thus showing the dependence on temperature (shown in Figure 19).

(ii) Ethane on Anthrasorb CC818M and CC818H

The results for ethane adsorbed at 25, 50 and -6°C on Anthrasorb CC818M and CC818H are shown in Figures 20 and 21 respectively. An empirical Langmuir model gives a good representation of the results. The model coefficients, obtained by a least squares fit to experimental data, are given in Table 4.1. The temperature dependence of the empirical Langmuir constant, b, in equation (2.6)

Table 4.2. Empirical Freundlich Constants

Adsorbate	Adsorbent	Temperature (^{o}C)	$K_F \times 10^4$ ($cm^3 g^{-1}$)	n
Methane	CC818M	0	0.89	2.12
		25	0.44	1.56
		50	0.22	1.27
Ethane	CC818M	-6	8.51	2.17
		25	4.38	1.97
		50	2.69	1.69
	CC818H	-6	6.89	1.72
		25	4.54	1.73
		50	2.48	1.38

(section 2.2.2.a) is shown in Figure 19. Freundlich's empirical model, however, did not fit the experimental data as well as the Langmuir model, as shown in Figures 22 and 23. The deviation is significant at low temperature and high concentrations. The constants for the Freundlich model, calculated by a least squares fit to experimental data, are given in Table 4.2.

4.1.1.b. Application of the Polanyi adsorption potential theory. Methane and Ethane on Anthrasorb CC818M and CC818H

A unique relationship was found between adsorbate volume and the Polanyi adsorption potential for methane and ethane. Correlation curves are shown in Figures 24 and 25 for methane and ethane at various temperatures on Anthrasorb CC818M and CC818H respectively. Therefore, the assumption of 'liquid' adsorbate behaviour would appear to be correct (see Section 2.2.2.C).

Figure 26 shows the experimental data obtained for methane and also ethane adsorbed as single components on Anthrasorb CC818M at various temperatures; along with the data of Grant et al (48) for methane, ethane, propane, n-butane and n-pentane adsorbed on type BPL carbon. The methane points appear to be slightly above the correlation curve and this was also reported by Grant. However the Polanyi adsorption potential theory, equation 2.13, (Section 2.2.2.c) is in excellent agreement with the experimental results. It can also be observed from Figure 26, that the experimental data are in good agreement with the results of Grant's even though different types of carbon were employed for the analysis.

Levan's correlations (72), (equation 2.16 and 2.17) (Section 2.2.2.c) also apply to the experimental data of ethane on Anthrasorb CC818M and CC818H, as shown in Figures 27 and 28. A Freundlich 'polytherm' (see Section 2.2.2.c) appears to fit the data better than a Temkin-Pyzhev 'polytherm'. Physical properties of methane and ethane are given in Table 4.3. The model coefficients, obtained by a least squares fit to the experimental data, are given in Table 4.4.

Comparing Polanyi's correlation curves of Anthrasorb CC818M and CC818H (Figures 24 and 25), it can be seen that the adsorption capacity of Anthrasorb CC818H is higher than Anthrasorb CC818M at all temperatures.

4.1.2. Isosteric heats of adsorption

The isothermal data of methane and ethane at different temperatures on Anthrasorb CC818M and CC818H can be used to evaluate Isosteric heats of adsorption, using the following relationship (123):

$$q_{st} = -R_g \left[\frac{\partial \ln C}{\partial (1/T)}\right]_{q*} \tag{4.3}$$

Curves of log C_o versus 1/T at constant amount adsorbed, q*, were prepared (Figures 29 and 30) from data obtained by cross plotting the isotherms shown in Figures 16 and 21. The resulting plots were straight lines indicating that the variation of q_{st} with temperature is insignificant. The slope of the straight lines, according to equation 4.3 is q_{st}/R_g. The heat of adsorption for

Table 4.3. Physical Properties of Methane and Ethane

Adsorbate	Temperature (^oC)	Ps (Bar)	fs (Bar)	V ($cm^3.mol^{-1}$)
Methane	0	230.00	159.60	37.75
	25	310.00	232.50	37.75
	50	405.00	335.23	37.75
Ethane	-6	20.00	15.85	54.67
	25	40.50	28.98	54.67
	50	64.00	41.92	54.67

Table 4.4. Empirical Constants used with Polanyi Adsorption Potential Theory

Adsorbent	Temkin - Pyzhez		Freundlich	
	Φ_s ($cm^3.g^{-1}$)	$2.3B_T \times 10^3$ ($cm^3.{}^oK^{-1}.mol^{-1}$)	Φ_s ($cm^3.g^{-1}$)	$2.3\ BR_g \times 10^2$ ($cm^3.{}^oK^{-1}mol^{-1}$)
CC818M	0.15	6.11	68.39	8.89
CC818H	0.10	5.60	62.66	7.74

methane and ethane are obtained in this way.

Typical plots for methane and ethane on Anthrasorb CC818H are displayed in Figure 31. For methane, the isosteric heat, q_{st}, decreases rapidly with the amount adsorbed, thus demonstrating the heterogeneity of the carbon employed. On the other hand for ethane the heat of adsorption appears to remain constant with increasing values of coverage thus pointing to a degree of homogeneity. This difference in behaviour may arise because of possible differences in the spatial requirements for adsorption between the two adsorbates. If ethane requires two adsorption sites per molecule rather than one, then the heterogeneity displayed by methane may be masked, especially if the original heterogeneity is not very marked or if the distribution of heats of adsorption amongst sites is broad.

4.1.3. Binary adsorption isotherm results

In order to investigate the capacity of Anthrasorb CC818M and CC818H to adsorb and separate mixtures of light paraffins, methane-ethane mixtures of varying concentrations were employed at 25^{o}C. Binary component equilibrium data were correlated with the empirical equations based on single component models.

As in the case for single component experiments (Section 4.1.1) low adsorbate concentration were also employed for binary mixtures of methane and ethane. The concentration range used for each component is 1.36 - 10.32 x 10^{-6} mol.cm^{-3}. Nitrogen was used as a diluent. In Section 4.2.2.a., it is shown that the binary adsorption breakthrough curves develop constant pattern behaviour. This implies that for a binary mixtures (in zone III, see Figure 2), the constant pattern equation 2.40 (Section 2.3.4.a) can be written as

$$\frac{q_{Eo}}{C_{Eo}} = \frac{q_{M1} - q_{Mo}}{C_{M1} - C_{Mo}} \tag{4.4}$$

since $C_{E1} = q_{E1} = 0$ (Figure 2). Thus the advantage of using low adsorbate concentrations together with a constant pattern profile is to simplify the continuity equation (Appendix K) to an algebraic equation. The prediction of binary breakthrough curves then reduces to the solution of two simultaneous ordinary differential rate equations (one for each component). Details of the calculation are shown in section 4.2.2.b. By this method the computing time was enormously reduced.

The amount adsorbed in equilibrium with the initial fluid phase concentration is obtained by applying an overall mass balance equation of the same form as equation 2.34 (Section 2.3.2.). It is evident from Figure 2, that the ethane concentration in zone III, in which no mass transfer occurs, is zero. Thus $C_{E1} = 0$. The overall mass balance for ethane in the binary mixture is:

$$FC_{Eo}t_{Eo} = mq_{Eo} + EV_bC_{Eo} \tag{4.5}$$

On the other hand, the concentration of methane is not zero in zone III and therefore the analogous equation for methane is

$$Ft_{Mo}C_{Mo} = mq_{Mo} + EV_bC_{Mo} + FC_{M1}(t_{Mo} - t_{M1}) \quad (4.6)$$

By simple manipulation of equation 4.5 and 4.6, the following relations are obtained:

$$q_{Eo} = \frac{(Ft_{Eo} - EV_b)C_{Eo}}{m} \quad (4.7)$$

$$q_{Mo} = \frac{(Ft_{Mo} - EV_b)C_{Mo} - FC_{M1}(t_{Mo} - t_{M1})}{m} \quad (4.8)$$

Equations 4.7 and 4.8 are employed to evaluate the adsorbed phase concentrations, q_{Eo} and q_{Mo}, the stoichiometric times t_{Eo} (= t_{Mo}) and t_{M1} having been calculated by application of the equation.

$$t_{M1} = t_m - \int_o^{t_m} \frac{C_M(t)dt}{C_{Mo}} \quad (4.9)$$

and equation 2.35 to the breakthrough curves. It was therefore necessary to record the concentration changes as a function of time and note the times t_m and t_n when the concentration profiles had flattened out into plateau zones.

The corresponding results are also tabulated in Appendix I.

4.1.3.a. The Extended Empirical Langmuir Model

The multicomponent Langmuir isotherm is based on the assumption of equal monolayer capacities, i.e. $a_1 = a_2$ (Section 2.2.3.a). By observation of Table 4.1, this condition is not fulfilled. The assumption of a constant separation factor, $K_{1,2}$, was tested by plotting the data in terms of C_MQ/q_MC versus C_M/C, as illustrated in Figure 32. The experimental points can be fitted to the following rearranged form of equation 2.25:

$$\frac{C_M/C}{q_M/Q} = K_{1,2} + (1 - K_{1,2}) \frac{C_M}{C} \tag{4.10}$$

However, the scattering of the data suggests that the separation factor is not constant (varies from 3.33 to 6.27).

From the foregoing discussion, it may be concluded that the multicomponent Langmuir model is not suitable. However, an extended empirical Langmuir model of the following form is employed:

For methane

$$q_M = \frac{a_M b_M c_M}{1 + b_M C_M + b_E^1 C_E} \tag{4.11}$$

Equation 4.11 was rearranged to calculate the value of constant b_E^1, as

$$\frac{a_M b_M C_M}{q_M} - (1 + b_M C_M) = b_E^1 C_E \tag{4.12}$$

The values of constants a_M and b_M are taken from single component experiments (Table 4.1). Plotting the left hand side member against C_E, the best value of b_E^1 was then obtained by means of the least square method, and is tabulated in Table 4.1. In the same manner, the constant b_M^1 was also calculated and tabulated in Table 4.1.

The curves predicted by equation 4.11 for methane-ethane mixtures adsorbed on Anthrasorb CC818M and CC818H are compared with the experimental points in Figures 33 and 34 respectively. The experimental data were well represented by this model.

4.1.3.b. Kidnay and Myers Model

Kidnay and Myers model (65) based on the so-called Ideal adsorbed solution theory of Myers and Prausnitz (92), (see Section 2.2.3.b), was also employed to correlate the binary adsorption data. Kidnay and Myers suggested that, if the plots of log C versus log q (the individual isotherms) are parallel, then the adsorbates have the same relationship between the spreading pressure and adsorbed phase concentration. The individual isotherms for methane and ethane are plotted in Figure 35, the curves obtained are fairly parallel.

For methane, the model used has the form:

$$q_M = \frac{a_M b_M C_M \left[1 + (1 - \frac{a_E}{a_M}) b_E C_E\right]}{1 + b_M C_M + b_E C_E} \qquad (4.13)$$

For ethane, an analogous form of equation 4.13 was used. The results obtained are compared with the experimental points, in Figures 33 and 34. The model does not predict the experimental data satisfactorily.

4.1.3.c. Application of the Polanyi adsorption potential theory

A unique relationship was also found for binary adsorption, between adsorbate volume and the Polanyi adsorption potential (Figure 36). The adsorption potential (equation 2.26) was plotted versus the total volume of solute adsorbed, Φ , obtained from single component adsorption experiments (Figures 24 and 25). Excellent agreement was obtained between the Polanyi adsorption potential theory and the experimental points.

4.1.4. Conclusions

Equilibrium isotherms for the single component adsorption of methane and ethane, on Anthrasorb CC818M and CC818H can be fitted by Langmuir type equations. The experimental results for methane and ethane was well represented over a wide range of temperatures. A Freundlich empirical relation also represents the experimental data fairly well.

The potential theory developed by Polanyi and Dubinin and extended by Levan to combine the standard isotherm equations, can be applied to the system studied. The Freundlich isotherm, when combined with the potential theory('Polytherm'), gave a good representation of the results, while the Temkin-Pyzhev polytherm failed to correlate the results.

The Polanyi potential correlation curve for methane and ethane gave good agreement with the results of Grant et al, considering the different type of activated carbon employed. Thus this type of correlation can predict adsorption values at higher or lower pressures, and also at various temperatures, with a minimum of experimental data. In addition, the adsorption isotherm of other different hydrocarbon gases on the same adsorbent may be predicted.

The extended empirical Langmuir model correlates the binary adsorption data satisfactorily even though the empiriical Langmuir coefficients, a_1 and a_2 (Table 4.1) are not equal, and the separation factor (Figure 32) is not constant. Kidnay and Myers model based on the Ideal adsorbed solution theory fails to predict the binary adsorption points. The treatment of multicomponent adsorption developed from the potential theory of Polanyi and Dubinin provides a simple method for predicting the volume of adsorbate in equilibrium with a mixed vapour. This model successfully correlates the experimental equilibrium data.

4.2. Rate of Adsorption

4.2.1. Single component breakthrough curves

Breakthrough curves were obtained for a wide range of temperature (-6 to 50^{o}C) and concentrations (1.39 - 34.72 x 10^{-6} mol.cm^{-3}) for methane and ethane on Anthrasorb CC818M and CC818H as shown in Figures 37 to 46 inclusive. It can be observed from Figures 47 and 48 that there was more adsorption at the low temperature than at high temperatures. Experiments were performed to check the reproducibility and reliability of the apparatus. Figures 49 and 50 show the result obtained for methane on Anthrasorb CC818H and CC818M respectively.

4.2.1.a. Constant pattern behaviour

A breakthrough curve observed in a fixed-bed adsorption column tends to develop with time in one of two basic ways. Depending on the general nature of the distribution relationship, the solute 'front' will be either continuously broadening or self-sharpening in nature. In the former case, the asymptotic limit of the profile consists of an infinitely broad front, while in the latter situation the asymptotic state is a relatively sharp S-shaped front of invariant form - that is, a 'constant pattern' front.

The complete description of the shape of the concentration profiles as a function of time may be obtained by solving, simultaneously, the equation of continuity and a mass transfer rate expression for the solute, subject to appropriate boundary conditions. The assumption of a constant pattern condition offers a considerable advantage, for it permits the reduction of the system continuity equation from partial to ordinary differential form. This decreases the amount of numerical calculation time required for solution by an order of magnitude.

A constant pattern behaviour prevails only in these circumstances where the adsorbate concentration is low, e.g. in a suitable carrier gas. On adsorption,changes in flowrate are then negligible and a constant fluid velocity in the bed can be assumed (see Appendix K). This also implies that any transport processes which determine the rate of adsorption within the bed will remain equally important at all points along the bed.

In this work, analytical solutions of the linear driving force (46)(Section 4.2.1.e) and pore diffusion models (116) (Section 4.2.1.c) were used. These are based on the assumption of a constant pattern condition. It was therefore of interest to discern if such behaviour was also observed for each individual breakthrough curve of methane and ethane. A series of experiments, in which approximately the same feed concentration was passed through beds of different lengths, was performed and the corresponding breakthrough curves obtained are shown in Figures 51 and 52 (methane) and Figures 53 and 54 (ethane).

It can be seen that, for a given inlet concentration, the shapes of the breakthrough curves remain approximately constant for various bed lengths. In order to standardise all breakthrough curves, the normalised concentration C/C_o is plotted as a function of $(t - t_{0.5})$, where $t_{0.5}$ is the time elapsing before C/C_o reaches a value of 0.5 at the bed outlet. Figures 55 and 56, for methane and ethane respectively, illustrate the constant pattern obtained.

4.2.1.b. External mass transfer control

In order to evaluate the effect of external mass transfer, the flowrate at which the feed entered the bed was varied as well as the length of the bed. Results are shown in Figures 51 to 54 inclusive. The constant shape of the breakthrough curves suggest that there is little or no resistance to mass-transfer between the bulk fluid and the particles within the bed.

A more quantitative estimation of the importance of mass-transfer from fluid to solid was obtained by solving the continuity equation 2.36, and the rate equation 2.37, together with the isotherm equation 4.2 governing the equilibrium behaviour for a particular system (methane adsorbed on Anthrasorb CC818H at 25°C) The boundary conditions were taken a $C(0,t) = C_o$. A finite difference method was used to solve the differential equations. The detailed numerical procedure is outlined in Appendix F. In the computer solution given in Appendix M, there was an inherent oscillation about the base line until the calculated break-point was reached. In order to reduce this oscillation to a negligible amount, the value of the spatial and time integration increments had to be quite low. It was necessary to reduce the time increment to 0.01 s and the ratio of spatial increment to bed length to approximately 0.02.

Figures 57 and 58 show the predicted breakthrough curves along with the experimental points for methane adosrbed on Anthrasorb CC818H at 25°C. The model fails to predict the data, for the experimental conditions employed. Hence it is concluded that external mass-transfer effects are negligibly small compared to internal mass-transfer.

4.2.1.c. Pore diffusion model

Vermeulen and Quilici (116) proposed a square-root driving force model which approximates pore diffusion behaviour. Their equation takes the form outlined in equation 2.44 (Section 2.3.4.b). For a favourable isotherm and under constant pattern conditions, these authors integrate the equation 2.44, and obtain the following analytical solution:

$$\frac{1}{\psi}\left\{\left[-2\sqrt{1-(1-R)(C/C_o)}\right]-\right.$$

$$\left[\frac{R}{1-R}\right]\ln\left[\frac{1+\sqrt{1-(1-R)(C/C_o)}}{1-\sqrt{1-(1-R)(C/C_o)}}\right]+$$

$$\left[\frac{\sqrt{R}}{1-R}\right]\ln\left[\frac{\sqrt{1-(1-R)(C/C_o)}+\sqrt{R}}{\sqrt{1-(1-R)(C/C_o)}-\sqrt{R}}\right]$$

$$I = K^{IV}(t-t_o) \qquad (4.14)$$

The factor ψ is an adjustable parameter which enables the results to be matched with the mid-point slope of the three dimensional solution of Hall et al (52). Vermeulen et al obtained the following correlation for

$$\psi = \frac{1.0}{R^{2.0} + 1.83(1-R)^{0.92}} \qquad (4.15)$$

The constant of integration, I, appearing in equation 4.14 was also found by comparing the results calculated (using equation 4.14) with those given by Hall (52). Vermeulen et al (116), reported that the integration constant is a function of the equilibrium parameter R, and give the following relation

$$I = 2.44 - 2.15R \qquad (4.16)$$

Figures 59 to 63 inclusive, show the theoretical and experimental breakthrough curves for methane and ethane adsorbed on Anthrasorb CC818M and CC818H, using equation 4.14. It should be pointed out, that the rate constant K^{IV} does not remain constant over the range of concentration studied. Although with different given values of K^{IV}, the predicted breakthrough curves approximate the experimental points well. The values of K^{IV} are obtained by fitting the theoretical curves to the experimental data, and the one which fits the experimental breakthrough curve is thus the required value of K^{IV}. This procedure is outlined in Appendix H. The values of K^{IV} are tabulated in Table 4.5, and it is also shown that K^{IV} is merely an empirical constant and to which no physical significance is attributed. The computer programme used is outlined in Appendix N.

4.2.1.d. Surface diffusion model

Surface diffusion model predictions were compared with the experimental breakthrough curves, in Figures 64 and 65, for methane and ethane respectively. The model is solved numerically, using a finite difference scheme, and the detailed procedure is outlined in Appendix G, the corresponding computer programme in Appendix P. The rate constant used in the numerical scheme is evaluated using Hall's (52) procedure, and is outlined in Appendix H.

It can be seen that the breakthrough curves are represented reasonably accurately over most of the concentration range though there is some divergence at higher concentration. The small discrepancy between the solutions is a result of using a fairly coarse mesh for the finite difference network (see Appendix G). In order to keep the solution stable very small time steps had to be used. Hence the computer time available only one simulation could be attempted for each adsorbate (methane and ethane). Because

Table 4.5. Kinetic Parameters

Adsorbate	Adsorbent	Temperature (^oC)	K^{IV} (min^{-1})	K^{I} (min^{-1})
Methane	CC818M	0	20-25	20
		25	50-90	60
		50	95	95
	CC818H	25	500-600	500
Ethane	CC818M	-6	5	5
		25	10	10
		50	20-25	20
	CC818H	-6	3-5	5
		25	10	10
		50	20	20

of the complexities involved with this model, it was thought more economical (in computer time) to use simplified models.

4.2.1.e. Linear driving force model

Linear driving force model have been used by many authors (53, 54, 55, 110) due to its simplicity. Glueckauf and Coates (46) integrate equation 2.41, for the cases where the adsorption is governed by the favourable isotherm, and under constant pattern conditions, and presented the following result:

$$\frac{R}{1-R}\ \ln\left(\frac{C_{0.5}(C_o-C)}{C(C_o-C_{0.5})}\right) + \ln\left(\frac{C_o - C}{C_o - C_{0.5}}\right) = K^I\ (t-t_{0.5}) \quad (4.17)$$

where t and $t_{0.5}$ represent the values of time when the concentrations at the bed outlet are C and $C_{0.5}$ respectively. For convenient, $t_{0.5}$ is the time when $(C/C_O) = 0.5$, and $C_{0.5}$ is the concentration corresponding to that time.

Equation 4.17 was utilized to predict the theoretical breakthrough curves. Appendix Q gives the computer programme used. The value of constant, K^I, used in this model, is obtained by matching the theoretical to the experimental breakthrough curves, and the procedure is outlined in Appendix H. It can be observed from Figures 66 to 73 inclusive, that the model fits the data fairly well, for all the temperature range (-6 to 50°C) and the concentration range ($1.39 - 34.72 \times 10^{-6}\ mol.cm^{-3}$) studied. A slight variation in the value of K^I at high concentrations were observed. Average values of K^I are tabulated in Table 4.5.

4.2.1. f. Comparison of models used for correlation

In section 4.2.1.b. it was established that external mass-transfer has no appreciable effect on the breakthrough curves, and the main resistance to mass-transfer is intra-particle diffusion. In Figures 74 and 75, various models are compared. Figure 74 clearly shows that external mass-transfer is not rate controlling. Although Vermeulen and Quilici's pore diffusion approximation (116) fits the experimental data well, ~~however~~, the rate constant, K^{I}, was not constant over the concentration range studied (Table 4.5). A model in which surface diffusion is assumed to be the rate controlling process fits the experimental breakthrough curves. Nevertheless, on grounds of simplicity Glueckauf and Coates's linear driving force model (46) is perfectly satisfactory as an empirical entity. The advantage of the linear driving force model is that it is superior to other single parameter models in matching the breakthrough curves for single components, and also matches the multicomponent data well, as reported by previous investigators (18, 90, 91, 110).

4.2.2. Multicomponent breakthrough curves

Twenty four binary adsorption experiments were carried out, and the results are tabulated in Appendix I. The concentration range ($1.36 - 10.32 \times 10^{-6}$ mol. cm^{-3}) were used for each component viz. methane and ethane. Two activated carbons were used for the investigation, namely - Anthrasorb CC818H and CC818M at $25^{o}C$. A carrier gas, Nitrogen, was used in all the experiments, so that the adsorbate concentration is low enough for the assumption of a constant velocity in the bed.

Typical examples are shown in Figures 76 to 79 respectively. The adsorptive capacity of Anthrasorb CC818H and CC818M is compared in Figure 80 and 81. The mixture of composition 6.69% CH_4, 3.31% C_2H_6 and 90% N_2 by volume (shown in Figure 80) first completely adsorbs and when the bed is saturated, methane begins to breakthrough as a single component. Ethane does not break through the bed until well after all the methane has been desorbed and thus Anthrasorb is potentially useful for purposes of separating ethane from an ethane-methane mixture (e.g. ethane from North Sea gas).

4.2.2.a. Constant pattern behaviour

A series of experiments in which approximately the same feed concentration was passed through a bed of different lengths were performed and the corresponding breakthrough curves are shown in Figures 82 to 86 respectively. It can be observed that, for a given inlet concentration, the shapes of the breakthrough curves remain approximately constant for variation of the bed length, thus implying that constant pattern behaviour exists.

4.2.2.b. Prediction of breakthrough curves

A breakthrough curve for a binary mixture may be divided into four zones, as discussed in Section 2.1., and is shown in Figure 2. Two different types of zone can be observed, one of constant composition (plateau zone)(Zones I and III) and one in which the composition changes (transfer zone) (zones II and IV). The ethane concentration drops to zero in zone II, whereas the methane concentration first increases in zone II and subsequently falls to zero in zone IV. Therefore, for each run, there exists two transfer zones and two plateau zones for methane, but only one transfer zone and one plateau zone for ethane. Zone I corresponds to the initial feed concentration of the methane-ethane mixture.

(i) Zone II

To predict the concentration profile in the first transfer zone requires the simultaneous solution of two kinetic equations, since methane as well as ethane will appear in the vapour phase. Since the Glueckauf's linear driving force model (46) successfully predicts the single component experiments, therefore, it is applied to calculate the concentration profiles in the first transfer zone. Thus the equations

$$\left(\frac{dq_E}{dt}\right)_{Z=L} = K_E^I \, (q_E^* - q_E) \tag{4.18}$$

and

$$\left(\frac{dq_M}{dt}\right)_{Z=L} = K_M^I \, (q_M^* - q_M) \tag{4.19}$$

are combined with the constant pattern relation (equation 4.4) and the adsorption isotherm equation 4.11 to give:

$$\left(\frac{dC_E}{dt}\right)_{Z=L} = \frac{K_E^I}{q_{Eo}/C_{Eo}} \left[\frac{a_E b_E C_E}{1+b_E C_E + b_M^1 C_M} - \frac{q_{Eo}}{C_{Eo}} \, C_E \right] \tag{4.20}$$

and

$$\left(\frac{dC_M}{dt}\right)_{Z=L} = \frac{K_M^I}{\left(\dfrac{q_{M1}-q_{Mo}}{C_{M1}-C_{Mo}}\right)} \left[\frac{a_M b_M C_M}{1+b_M C_M + b_E^1 C_E} \right. -$$

$$\left(\frac{q_{M1} - q_{Mo}}{C_{M1} - C_{Mo}}\right) \left[C_M - C_{Mo}\right] \qquad - q_{Mo}\Bigg] \tag{4.21}$$

Equations 4.20 and 4.21 are then solved simultaneously by the Runga-kutta-Merson (Kutmer) method (35), using the following initial conditions:

$$C_M = C_{M1}, \quad C_E = C_{E1} = 0 \tag{4.22}$$

However, the right-hand sides of equations 4.20 and 4.21 tend to zero at the initial conditions, so that integration cannot be started. To overcome this difficulty the integration was started from a small C_E value (10^{-7} was employed) and the corresponding C_M value. To determine the C_M value, equation 4.21 was divided by equation 4.20 which produces a relation of the form

$$\frac{dC_M}{dC_E} = f\,(C_M, C_E) \tag{4.23}$$

L'Hopital's rule was applied at the initial condition, $C_M = C_{M1}$ and $C_E = 0$, to obtain the initial value of dC_M/dC_E. Then the C_M value corresponding to $C_E = 10^{-7}$ mol.cm^{-3} was obtained by the Runga-Kutta-Merson (Kutmer) method (Appendix R)

(ii) Zone III

As shown by Cooney and Lightfoot (18), for a constant pattern profile, the following relationship holds (see Section 4.1.3)

$$\frac{q_{Eo}}{C_{Eo}} = \frac{q_{M1} - q_{Mo}}{C_{M1} - C_{Mo}} \tag{4.4}$$

Since, in this system (see Figure 80), $C_{E1} = q_{E1} = 0$. The equilibrium relationship appropriate to the second plateau zone (zone III) is

$$q_{M1} = \frac{a_M b_M C_{M1}}{1+b_M C_{M1}} \tag{4.24}$$

Combination of equations 4.4 and 4.24 yields

$$C_{M1} = \frac{-M + \sqrt{M^2 - (4b_M\, q_{Eo}/C_{Eo})(q_{Mo} - C_{Mo}q_{Eo}/C_{Eo})}}{2\, b_M q_{Eo}/C_{Eo}} \tag{4.25}$$

where

$$M = q_{Eo}/C_{Eo} + b_M(q_{Mo} - q_{Eo}C_{Mo}/C_{Eo}) - a_M b_M \tag{4.26}$$

Equilibrium data obtained from the single and binary component experiments (Appendix I and Table 4) are used to estimate C_{M1}.

(iii) Zone IV

As in the case of single component experiments, a Linear driving force model is used to simulate the binary breakthrough curves. In the second plateau zone (zone III), C_{M1}, is used as initial concentration in equation 4.17, and the rate constant, K^I (obtained from the single component experiments (Table 4.5)) is used for the calculation.

The complete breakthrough curves are compared (Figures 87 and 88) with some of the experimental results obtained for binary mixtures. The close agreement between the experimental points and the semi-empirical curves (computed from Glueckauf and Coates linear driving force model) indicates that the numerical solution of a model based upon a pair of equations containing first order driving force terms, provides a reasonable but simple representation of the system. The computer programme used for these predictions is summarised in Appendix R.

4.2.3. Conclusions

A linear driving force model gives a good representation of both single and binary adsorption of methane and ethane on Anthrasorb CC818H and CC818M over the range of experimental conditions studied. The assumption that the interaction between the two components is described by a simple binary Langmuir isotherm proves sufficient. Thus Anthrasorb may well be a suitable adsorbent for the separation of ethane from ethane-methane mixtures. Hence there is the possibility that it may be a cheap and effective adsorbent for removing, and subsequently recovering, ethane from North Sea gas. Further experiments at high pressures up to about 100 bar would be necessary to establish this unequivocally.

CHAPTER V

ADSORPTION AND REMOVAL OF ACETONE AND CARBON TETRA-CHLORIDE

CHAPTER V

ADSORPTION AND REMOVAL OF ACETONE AND CARBON TETRA-CHLORIDE

Experimental results for acetone and carbon tetra-chloride vapours, adsorbed on Anthrasorb CC818H and CC818M at 25^{o}C, are discussed in this chapter. Breakthrough curves for desorption are also reported. Details of all the experiments are tabulated in Appendix J.

5.1. Equilibrium Isotherms

5.1.1. Langmuir and Freundlich Isotherms

The experimental data are well represented by both empirical Langmuir and Freundlich isotherms (Figures 89, 90, 91 and 92). Tables 5.1 and 5.2 give the various model parameters obtained by a least squares fit to the experimental data. It can be seen from Figures 89 and 90 that carbon tetra chloride (a non-polar adsorbate, immiscible in water) adsorbs at 25^{o}C on Anthrasorb CC818H preferentially to CC818M. On the other hand, acetone (a polar substance soluble in water) is held at 25^{o}C by Anthrasorb CC818H more tenaciously than CC818M.

On grounds of molecular symmetry of the carbon tetra chloride molecule, the dipole moment is zero, whereas for acetone a dipole moment of 2.88Debye units exist. Thus the total adsorption forces comprise both dispersion and dipole elements for acetone, but only dispersion forces are present when the non-polar carbon tetra chloride is adsorbed.

Table 5.1. Empirical Langmuir Constants at 25°C

Adsorbate	Adsorbent	$a \times 10^3$ ($mol.g^{-1}$)	$b \times 10^{-4}$ ($cm^3.mol^{-1}$)
Acetone	CC818M	15.36	179.40
	CC818H	9.09	335.40
Carbon tetra-chloride	CC818M	9.63	890.58
	CC818H	13.71	612.77

In addition to the dissimilarities in polarity, the two molecules are quite different in size and shape: a carbon tetra chloride molecule is large (mol.wt = 153.82) as compared to acetone (mol. wt = 58.08). The molecular configuration for both molecules are shown below:

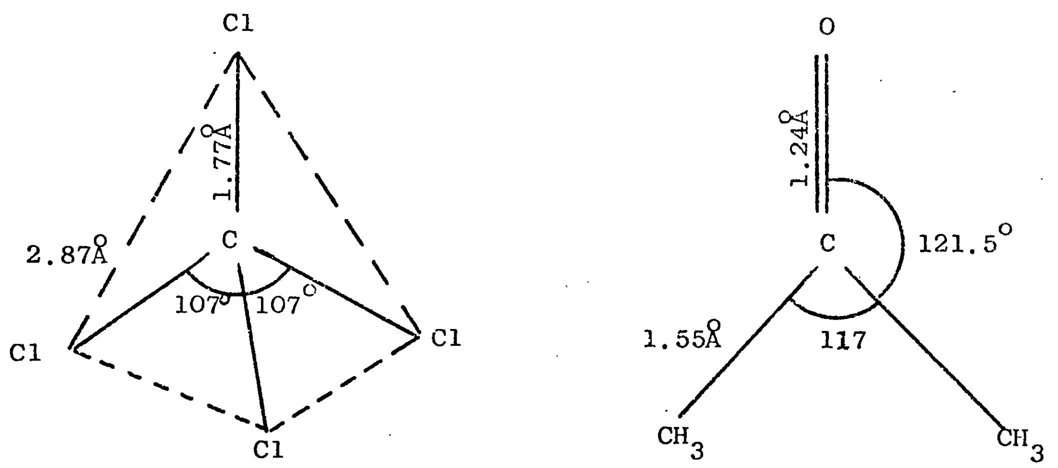

Carbon tetra-chloride
(Tetrahedral)

Acetone
(Trigonal planer with respect to C-C-O, and tetrahedral within the methyl group).

The dissimilarities described above will undoubtedly contribute to the differences in adsorption.

Six experiments were performed on regenerated Anthrasorb CC818H, and the equilibrium data is plotted in Figure 90 together with the experimental points obtained from a fresh charge of Anthrasorb CC818H. The results obtained match closely, thus showing the reproducibility and regenerative quality of Anthrasorb CC818H.

Table 5.2. Empirical Freundlich Constants at 25°C

Adsorbate	Adsorbent	$K_F \times 10^4$ ($cm^3.g^{-1}$)	n
Acetone	CC818M	25.10	1.47
	CC818H	26.30	2.13
Carbon tetrachloride	CC818M	48.42	3.11
	CC818H	51.76	2.05

5.1.2. Application of Polanyi adsorption potential theory

The Polanyi adsorption potential theory was successfully applied to acetone and carbon tetra-chloride adsorption experiments. A unique relationship between the adsorbate volume and the Polanyi adsorption potential is found on Anthrasorb CC818M and CC818H (Figures 93 and 94). The assumption of liquid adsorbate at the adsorption temperature by Dubinin (26), enables the polanyi characteristic curves for the various gases to coincide (Section 2.2.2.C). This assumption proves to be valid for the experimental results obtained for acetone and carbon tetra-chloride.

Freundlich 'polytherm' (see Section 2.2.2.C) gives a good representation, on Anthrasorb CC818M and CC818H, for both acetone and carbon tetra-chloride vapours at 25^{o}C (Figures 95 and 96). On the other hand, the Temkin-Pyzhev 'polytherm' fails to predict the results so well, also shown in Figures 95 and 96. The physical properties of acetone and carbon tetra-chloride are listed in Table 5.3. The empirical constants for the Freundlich and Temkin-Pyzhev 'polytherms', obtained by a least squares fit to the experimental points, are given in Table 5.4.

5.2. Rate of adsorption

In the following sections the mathematical models, discussed in Chapter II, are applied to the experimental breakthrough curves for acetone and carbon tetra-chloride vapours adsorbed on Anthrasorb CC818M and CC818H. Desorption breakthrough curves for acetone are also discussed.

Table 5.3. Physical Properties of Acetone and Carbon tetrachloride

Adsorbate	P_s (Bar)	V ($cm^3.mol^{-1}$)
Acetone	0.29	74.04
Carbon-tetrachloride	0.14	97.34

Table 5.4. Empirical Constants used with Polanyi Adsorption Potential Theory

Adsorbent	Temkin - Pyzhev		Freundlich	
	Φ_s ($cm^3.g^{-1}$)	$2.3B_TRg$ ($cm^3.^oK^{-1}.mol^{-1}$)	Φ_s ($cm^3.g^{-1}$)	2.3 BRg ($cm^3.^oK^{-1}mol^{-1}$)
CC818M	1.10	0.11	2.03	0.12
CC818H	1.32	0.15	2.82	0.14

5.2.1. Adsorption breakthrough curves

Typical experimental adsorption breakthrough curves are shown in Figures 97 to 102 inclusive. It is observed that, both adsorbates (i.e. acetone and carbon tetra-chloride) are strongly adsorbed on Anthrasorb CC818M and CC818H.

5.2.1.a. Constant pattern behaviour

Figures 103 to 105 inclusive show that constant pattern conditions also prevail for acetone and carbon tetra-chloride vapours. However, the shape of the breakthrough curves are only approximately constant with the variation of the bed length. This may be due to experimental error in duplicating the process conditions. It was not possible to make a 'pre mixed vapour' as was done for methane and ethane gases (see Section 3.7).

5.2.1.b. Pore diffusion model

The pore diffusion model proposed by Vermeulen and Quilici (116) (equation 4.7) was also tested for acetone and carbon tetra-chloride adsorption experiments. Theoretical curves were matched with the experimental curves on Anthrasorb CC818M and CC818H (Figures 108 to 111 respectively). The Rate constant, K^{IV}, remains almost constant over the range of concentration studied, as shown in Table 5.5. The values of K^{IV} are obtained by fitting the theoretical curves to the experimental data, and the one which fits the experimental breakthrough curve is thus the required value of K^{IV}. This procedure is outlined in Appendix H. The computer programme used for fitting the data is presented in Appendix N.

Table 5.5. Kinetic Parameters

Adsorbate	Adsorbent	K^{I} (min^{-1})	K^{IV} (min^{-1})
Acetone	CC818M	0.19	0.15
	CC818H	0.19	0.15
Carbon tetra-chloride	CC818M	0.11	0.12
	CC818H	0.11	0.12

5.2.1.c. Surface diffusion model

The breakthrough curves predicted by the surface diffusion model, along with the experimental points are shown in Figures 106 and 107. The model barely fits the experimental breakthrough curves. Numerical solution of the model and the fitting of experimental results is presented in Appendix G; the computer programme is listed in Appendix P.

5.2.1.d. Linear driving force model

In Figures 112 to 117 inclusive, the experimental breakthrough curves were compared with the theoretical curves calculated from the Glueckauf and Coates's (46) linear driving force model (equation 4.10). The model closely matches the experimental breakthrough curves. The empirical kinetic constant, K^I, obtained by matching the theoretical curve with the experimental data (see Appendix H) is tabulated in Table 5.5. Appendix Q shows the computer programme used.

Pore diffusion and linear driving force models were compared in Figures 118 to 121 respectively. Both models fit the experimental breakthrough curves fairly well.

5.2.2. Desorption breakthrough curves

5.2.2.a. Description

It is possible to describe the desorption or regeneration process by considering two inter related aspects.

(i) where regeneration is carried out primarily to restore the adsorptive capacity of the adsorbent, so that any recovered adsorbates are of little value or use, e.g. in the large scale removal of general odours from the atmosphere of industrial premises, or the drying of gases.

(ii) where regeneration is carried out primarily to recover significant quantities of a valuable adsorbate; and the restoration of the adsorbent capacity is a side factor, e.g. in the large scale recovery of volatile solvents used by a particular chemical process and discharged from the process at a low concentration in an inert carrier fluid.

After a complete adsorption cycle (i.e. when the bed reaches an equilibrium state) a regenerative fluid is then passed through the bed. The adsorbate content of the regenerative fluid increases as adsorbate is transferred from the particle to the fluid. The concentration profile for an isothermal and non-heated regeneration fluid as a function of time is illustrated by Figure 122. The S-shaped curve suggests that the breakthrough of material in desorption may be the mirror image of the adsorption breakthrough wave (98, 126).

Generally, desorption is carried out by a heated regenerative fluid, which will supply the required heat of desorption. A set of general non-linear (favourable) isotherms are shown diagrammatically by Figure 123. For an adsorption isothermal temperature of Ta, the maximum loading on the adsorbent is q_o given by an inlet concentration of C_o. For a bed at a loading of q_o, and a regenerative fluid of temperature Tb, then the maximum concentration of adsobrate leaving with the regenerative fluid is C_b (note that C_b is greater than C_o). If the regenerative fluid is at Tc, then the maximum adsorbate concentration in the regenerative fluid is at C_c (note that C_c is greater than C_b).

Hence, a heated regeneration fluid effects an increase (several orders of magnitude of its inlet value during the adsorption period) in the adsorbate concentration. This means that far less fluid is required (if heated) to regenerate a bed, than during the adsorption period. Also, regeneration can be carried out in a time less than that required for the adsorption period, under the same flow conditions.

5.2.2.b. Experimental results and discussion

Six desorption experiments were performed under different process conditions; they are tabulated in Appendix J, and diagrammatically shown in Figures 124 through 129. It can be seen that the experimental results concur with the description given in Section 5.2.2.a. A temperature range (150-250^{o}C) was used for the desorption experiments. Nitrogen was used as the regenerative fluid. After the start of a desorption cycle, the gas-phase concentration rapidly reaches a maximum (several orders of magnitude of its inlet value during the adsorption cycle), and then decreases until all the adsorbate is removed. An insignificant amount of acetone vapour emerged from the bed (i.e. regeneration is completed). It should be noted that, using the heated carrier gas, the desorption time drastically decreased as compared with the adsorption time (Figures 98 and 127).

5.3. Conclusions

Equilibrium isotherms for acetone and carbon tetra-chloride vapours were well represented by the empirical Langmuir and Freundlich relations. Correlation curves developed from the Polanyi potential theory fit the experimental data well. A Freundlich polytherm gave a better representation of the results than the Temkin-Pyzhev polytherm.

There was little to choose between the Vermeulen and Quilici's pore diffusion and Glueckauf and Coates's linear driving force models. Both models predict the theoretical curves, which closely matched the experimental breakthrough curves.

A temperature of 150-250^{o}C was used to regenerate the Anthrasorb CC818H from the acetone vapours using nitrogen as the carrier gas. The experimental profiles obtained confirm the description given.

NOMENCLATURE

NOMENCLATURE*

Symbol	Interpretation	Dimensions
A_C	Cross sectional area of adsorption column	L^2
a	Coefficient in empirical Langmuir equation	$N\ M^{-1}$
a_F	Coefficient in empirical Freundlich equation	$M^{-2}L^4T^2$
a_T	Coefficient in empirical Temkin-Pyzhev equation	$M^{-1}L^3$
B	Coefficient in Freundlich polytherm equation	$N^{-1}L^3\ \theta^{-1}$
B_T	Coefficient in Temkin-Pyzhev equation	$N^{-1}L^3\ \theta^{-1}$
b	Coefficient in empirical Langmuir equation	$N^{-1}L^3$
b_F	Constant in Freundlich equation	-
b_T	Coefficient in Temkin-Pyzhev equation	$M^{-2}L^4T^2$
b^1	Empirical coefficient in extended empirical Langmuir equation	$N^{-1}L^3$
C	Gas phase concentration	$N\ L^{-3}$
C*	Gas phase concentration at equilibrium	$N\ L^{-3}$
D	Longitudinal dispersion coefficient	L^2T^{-1}
D_p	Pore diffusion coefficient	L^2T^{-1}
D_s	Surface diffusion coefficient	L^2T^{-1}
E	Total Bed voidage	-
F	Voumetric flowrate	L^3T^{-1}
f	Gas phas fugacity	$ML^{-1}T^{-2}$

*M, L, T represent the dimensions of mass, length and time respectively in any set of self consistent units. θ , N and H represent dimensions of temperature, moles and heat respectively. (H is equivalent to ML^2T^{-2}).

Symbol	Interpretation	Dimensions
f_s	Gas phase fugacity at saturation	$ML^{-1}T^{-2}$
$f_{1,2}$	Fugacity of the mixture (component 1 and 2)	$ML^{-1}T^{-2}$
$f^s_{1,2}$	Fugacity of the mixture at saturation	$ML^{-1}T^{-2}$
ΔG	Gibb's free energy change	HN^{-1}
I	Integration constant in pore diffusion model	-
K^I	Kinetic parameter in linear driving force model	T^{-1}
K^{II}	Kinetic parameter in quadratic driving force model	T^{-1}
K^{III}	Kinetic parameter in empirical adsorption-desorption model	T^{-1}
K^{IV}	Kinetic parameter in pore diffusion model	T^{-1}
K_F	Empirical coefficient in Freundlich equation	$M^{-1}L^3$
$K_g a$	Mass transfer film resistance	T^{-1}
K_H	Coefficient in empirical Henry's law	$M^{-1}L^3$
$K_{1,2}$	Separation factor in binary mixtures	-
m	Mass of adsorbent	M
N_m	No of molecules	-
N	No of transfer units	-
n	Freundlich constant	-
P	Partial pressure	$ML^{-1}T^{-2}$
Ps	Partial pressure at saturation	$ML^{-1}T^{-2}$
P^o	Vapour pressure of the pure saturated liquid	$ML^{-1}T^{-2}$
Q	Total adsorbed phase concentration	NM^{-1}
q	Adsorbed phase concentration	NM^{-1}

Symbol	Interpretation	Dimensions
q^*	Adsorbed phase concentration at equilibrium	NM^{-1}
q_{st}	Isosteric heat of adsorption	HN^{-1}
R	Equilibrium parameter (dimensionless)	-
R_o	Dimensionless radius of particle	-
R_g	Universal gas constant	-
r	radius of particle	L
T	Temperature	Θ
T_o	Throughput parameter (dimensionless)	-
t_o	Stoichiometric time	T
t_e	Time at which the bed is at equilibrium	T
t_n, t_m	Time at which transfer zones flatten out to plateau zone	T
$t_{0.5}$	Time when $C/C_o = 0.5$	T
u	Interstitial gas velocity	LT^{-1}
$\bar{u}$	Wave velocity through the bed	LT^{-1}
V	Molar volume at boiling point	$N^{-1}L^3$
$\bar{V}$	Molar volume at the adsorption temperature	$N^{-1}L^3$
V_b	Bed volume	L^3
v	Volume adsorbed	NM^{-1}
v_m	Maximum volume adsorbed	NM^{-1}
x	Dimensionless gas phase concentration (C/C_o) (local)	-
$\bar{x}$	mole fraction in liquid phase	-
X	Dimensionless gas phase concentration in equilibrium	-
y	Dimensionless adsorbed phase concentration (local)(q/q_o)	-

Symbol	Interpretation	Dimensions
$\bar{y}$	Mole fraction in vapour phase	-
Y	Mean adsorbed phase concentration (dimensionless)	-

Greek Letters

β	Affinity coefficient	-
ϵ	Adsorption potential	ΘNL^{-3}
$\epsilon_{1,2}$	Adsorption potential of the mixture (component 1 and 2)	ΘNL^{-3}
γ	Radius of mixing cylinder	L
ρ_b	Bed density	ML^{-3}
Φ	Volume of adsorbate	$M^{-1}L^{3}$
Φ_s	Saturated adsorbate volume	$M^{-1}L^{3}$
ψ	Adjustable parameter in pore diffusion model (dimensionless)	-

Subscript

A	Acetone
C	Carbon tetrachloride
E	Ethane
M	Methane
O	Initial conditions
1	Plateau zone concentration

REFERENCES

REFERENCES

1. Antonson, C.R., and Dranoff, J.S. A.I.Ch.E. Symp. Ser, (1969) 65, No. 96, 27.

2. Baly, E.C.C. Proc. Roy, Soc., (1937), A160, 465.

3. Barnebey, H.L. A.I.CH.E. Symp. Ser, (1971), 67, No. 117, 108.

4. Bering, B.P,, Dubinin, M.M., and Serpinski, V.V. Dokl. Akad. SSSR, (1961), 138, 1373.

5. Bering, B.P., Dubinin, M.M., and Serpinski, V.V. J. Colloid and Interface Sci., (1966), 21, 378.

6. Bering, B.P., Gordeva, V.A., and Dubinin, M.M. Izv. Akad. Nauk. SSSR. Ser. Khim, (1971), 1, 22.

7. Blakely, R.L., and Taylor, B.R. A.I.CH.E. Symp. Ser., (1965), 65, No. 96, 89.

8. Bradley, W.G., and Sweed, N.H. A.I.Ch.E. Symp. Ser., (1975), 71, No. 152, 59.

9. Brunauer, S. "The Adsorption of Gases and Vapours". Oxford University Press, (1944).

10. Brunauer, S., Deming, L.S., Deming, W.S., and Teller, E. J.Am.Chem.Soc., (1940), 62, 1723.

11. Bunke, G., and Gelbin, D. Chem. Engng. Sci., (1978), 33, 101.

12. Carter, J.W. Chem. Proc. Engng., (1960), 47, 37.

13. Carter, J.W. Chem. Proc. Engng., (1960), 47, 70.

14. Carter, J.W. Brit. Chem. Engng., (1968), 13, 229.

15. Carter, J.W., and Hussain, H. Chem. Engng. Sci., (1974), 29, 267.

16. Chung, I.J., and Hus, H.W. Chem. Engng. Sci., (1978), 33, 399.

17. Collins, C.G., and Deans, H.A. A.I.Ch.E.J., (1968), 14, 25.

18. Cooney, D.O., and Lightfoot, E.N. Ind. Engng. Chem. Proc. Des. Dev., (1966), 5, 25., I & EC Fund, (1965), 4, 233.

19. Cooney, D.O., and Strusi, F.P. Ind. Engng. Chem. Fundamentals, (1972), 11, 123.

20. Cooper, R.S. Ind. Engng. Chem. Fundamentals, (1969), 8, 193.

21. Coulson, J.M., and Richardson, J.F. "Chemical Engineering", Volume 3, Chapter 7, Pergamon Press, (1975).

22. Crank, J. "Mathematics of Diffusion", Oxford (1956), **44**.

23. De Vault, D. J. Am. Chem. Soc., (1943), 65, 532.

24. Dranoff, J., and Lapidus, L. Ind. Engng. Chem. Fundamentals, (1958), 50, 1648.

25. Dranoff, J., and Lapidus, L. Ind. Engng. Chem. Fundamentals, (1961), 53, 71.

26. Dubinin, M.M., and Radushkevich, L.V. Compt. Rend. Acad. Sci. U.R.S.S., (1947), 55, No. 4, 327.

27. Dubinin, M.M., and Timofeyev, D.P. Compt. Rend. Acad. Sci. U.R.S.S., (1946), 54, No. 8, 701; (1947), 55, No. 2, 137.

28. Dubinin, M.M., Zaverina, E.D., and Timofeyev, D.P., Zhur, Fiz. Khim, (1949), 23, 1129.

29. Eagleton, L., and Bliss, H. Chem. Engng. Prog., (1953), 49, 543.

30. Edeskuty, F.J., and Amundson, N.R. J. Phys. Chem. (1952), 56, 148.

31. Engel, H.C., and Coull, J. Trans. Am. Inst. Chem. Engrs., (1942), 38, 947.

32. Everett, D.H. Trans. Faraday Soc., (1950), 46, 942.

33. Fernbacker, J.M., and Wenzel, L.A. A.I.Ch.E. Symp. Ser., (1969), 65, No. 96, 457.

34. Fleming, A.B., Getty, R.J., and Townsend, F.M. Chem. Engng., (1964), 71, 69.

35. Fox, L. "Numerical Solution of Ordinary Differential Equations". Pergarmon Press (1962)

36. Freundlich, H. "Colloid and Capillary Chemistry", Dutton, New York, (1926).

37. Friederick, R.O., and Mullins, J.C. Ind. Engng. Chem. Fundamentals, (1972), 11, No. 4, 457.

38. Furnas, C.C. U.S. Bur. Mines. Bull., (1932), 361.

39. Garg, D.R., and Ruthven, D.M. Chem. Engng. Sci., (1972), 27, 417.

40. Garg, D.R., and Ruthven, D.M. Chem. Engng. Sci., (1974), 29, 571.

41. Garg, D.R., and Ruthven, D.M. Chem. Engng. Sci., (1975), 30, 1972.

42. Garg, D.R., and Ruthven, D.M. A.I.Ch.E.J., (1975), 21, 200.

43. Gariepy, J.W., and Zwiebel, I. A.I.Ch.E. Symp. Ser., (1971), 67, No. 117, 17.

44. Getty, R.J., and Armstrong, W.P. Ind. Engng. Chem. Proc. Des. Dev., (1964), 3, 60.

45. Glessna, A.J., and Myers, A.L. A.I.Ch.E. Symp. Ser., (1969), 65, No. 96, 73.

46. Glueckauf, E., and Coates, J.I. J. Chem. Soc., (1947), p 1315.

47. Grant, R.J., Manes, M., and Smith, S.B. A.I.Ch.E.J., (1962), 8, 403.

48. Grant, R.J., and Manes, M. Ind. Engng. Chem. Fundamentals, (1964), 3, No. 3, 221.

49. Grant, R.J., and Manes, M. Ind. Engng. Chem. Fundamentals, (1966), 5, No. 4, 490.

50. Gustafson, K.J., and Healey, M.J. Proc. Gas. Cond. Conf., (1968), G-1-G-10.

51. Habgood, H.W. Can. J. Chem., (1958), 36, 1384.

52. Hall, K.R., Eagleton, L.C., Acrivos, A., and Vermeulen, T. Ind. Engng. Chem. Fundamentals, (1966), 5, No. 2, 212.

53. Hashimoto, K., Miura, K. J. Chem. Engng. Japan, (1976), 9, 388.

54. Hashimoto, K., Miura, K., and Tsukano, M., J. Chem. Engng. Japan, (1977), 10, 27.

55. Hashimoto, K., Mirua, K., and Nagata, S. J. Chem. Engng. Japan, (1975), 8, 367.

56. Helfferich, F., and Klein, G. "Multicomponent Chromatography", Marcel Deckker Inc., New York, (1970).

57. Hiester, N.K., and Vermeulen, T. Chem. Engng. Prog., (1952), 48, 505.

58. Hill, T.L. J. Chem. Phys., (1949), 17, No. 6, 520.

59. Hoori, S.E., and Prausnitz, J.M. A.I.Ch.E. Symp. Ser., (1967), 63, No. 74, 3.

60. Hougen, O.A., and Marshall, W.R. Chem. Engng. Prog., (1947), 43, No. 4, 197.

61. Hougen, O.A., Watson, K.W., and Ragatz, R.A. "Chemical Process Principles", Part II, Wiley, New York, (1959).

62. Jain, J.S., and Snoeyink, V.L. J.W.P.C.F., (1972), 45, 2463.

63. Kasten, P.R., Lapidus, and Amundson, N.R. J. Phys. Chem., (1952), 56, 683.

64. Kidnay, A.J., Hiza, M.J., and Dickson, P.F. Adv. Cryogenic. Engng., (1969), 14, 41.

65. Kidnay, A.J., and Myers, A.L. A.I.Ch.E.J., (1966), 12, No. 5, 981.

66. Klein, G., Tondeur, D., and Vermeulen, T. Ind. Engng. Chem. Fundamentals, (1967), 6, 339.

67. Kondis, E.F., and Dranoff, J.S. A.I.Ch.E. Symp. Ser., (1971), 67, No. 117, 25.

68. Langmuir, I. J.Am. Chem. Soc., (1918), 40, 1361.

69. Lapidus, L., and Amudson, N.R. J. Phys. Chem., (1952), 56, 984.

70. Ledoux, E. Chem. Engng., (1948), No. 3., 118.

71. Lee, H., and Stahl, D.E. A.I.Ch.E. Symp. Ser., (1973), 69, No. 134, 1.

72. Levan, M.D. Ph.D. Thesis, University of California, Berkeley, (1976).

73. Lewis, W.K., Gilliland, E.R., Chertow, B., and Cadogan, W.P. Ind. Engng. Chem., (1950), 42, No. 7, 1326.

74. Lewis, W.K., Gilliland, E.R., Chertow, B., and Cadogan, W.P. Ind. Engng. Chem., (1950), 42, No. 7, 1319.

75. Liapis, A.I., and Rippen, D.W.T. Chem. Engng. Sci., (1977), 32, 619.

76. Liapis, A.I. and Rippen, D.W.T. Chem. Engng. Sci., (1978), 33, 593.

77. Liapis, A.I., and Rippen, D.W.T. A.I.Ch.E.J., (1979), 25, No. 3, 455.

78. Liaw, C.H., Wang, J.S.P., Greenkorn, R.A., and Chao, K.C. A.I.Ch.E.J., (1979), 25, No. 2, 376.

79. Lombardi, J.L. Ph.D. Thesis, University of Wales, (1968).

80. Markham, E.C., and Benton, A.F. J.Am. Chem. Soc., (1931), 53, 497.

81. Masamune, S., and Smith, J.M. A.I.Ch.E.J., (1962), 8, No. 2, 217.

82. Masamune, S., and Smith, J.M. J. Chem. Engng. Data, (1963), 8, 54.

83. Masamune, S., and Smith, J.M. Ind. Engng. Chem. Fundamentals, (1964), 3, No. 2, 179.

84. Masamune, S., and Smith, J.M. A.I.Ch.E.J., (1964), 10, 246.

85. Maslan, F.D., Altman, M., and Aberth, E.R. J. Phys. Chem., (1953), 57, 106.

86. Mathews, A., Ph.D. Thesis, Michigan University, (1975).

87. Mattson, J. J. Colloid. Interface Sci., (1969), 31, 116.

88. Michaels, A.S. Ind. Engng. Chem., (1952), 44, 1922.

89. Miura, K., and Hashimoto, K. J. Chem. Engng. Japan, (1977), 10, No. 6, 490.

90. Miura, K., and Hashimoto, K. J. Chem. Engng. Japan, (1979), 12, No. 4, 329.

91. Miura, K., Kurahashi, H., Inokuchi, Y., and Hashimoto, K. J. Chem. Engng. Japan, (1979), 12, No. 4., 281.

92. Myers, A.L., and Prausnitz, J.M. A.I.Ch.E.J., (1965), 11, 121.

93. Needham, R.B., Campbell, J.M., and McLeod, H.C. Ind. Engng. Chem. Proc. Des. Dev., (1966), 5, 122.

94. Perry, J.H. "Chemical Engineering Handbook", Fourth Edition, McGraw Hill, New York, (1963).

95. Polanyi, M. Verh. Deut. Phsik. Ges., (1914), 16, 1012.; ibid, (1916), 18, 55.; Z Elecktrochem., (1920), 26, 370.

96. Rhee, H.H., Aris, R., and Amundson, N.R. Phil. Trans. Royal Soc. London, (1970), A267, No. 1182, 419.

97. Rosen, J.B. J. Chem. Phys., (1952), 20, 387.

98. Rosen, J.B. Ind. Engng. Chem. (1954), 46, No. 8, 1596.

99. Ruthven, D. A.I.Ch.E.J., (1978), 24, No. 3, 540.

100. Schay, G.J. Chem. Phys. Hungary, (1973), 69, 691.

101. Shen, J., and Smith. J.M. Ind. Engng. Chem. Fundamentals, (1968), 7, No. 1, 100.

102. Shen, J., and Smith, J.M. Ind. Engng. Chem. Fundamentals, (1968), 7, No. 1, 106.

103. Sherwood, T.K., Pgford, R.L., and Wilke, C.R. "Mass Transfer", McGraw Hill, (1975), 17.

104. Spahn, H., and Schlunder, E.U. Chem. Engng. Sci., (1975), 30, 529.

105. Stuart, F.X., and Camp, D.T. Ind. Engng. Chem. Fundamentals, (1967), 6, No. 1, 157.

106. Suzuki, M., and Kowazoe, K.J. J. Chem. Engng. Japan, (1974), 7, 346.

107. Szirmay, L.V. A.I.Ch.E. Symp. Ser., (1975), 71, No. 152, 104.

108. Temkin, M.I., and Pyzhev, V. Acta. Physiochim. U.R.S.S., (1940), 12, 327.

109. Thomas, H.C. J. Am. Chem. Soc., (1944), 66, No. 10. 1664.

110. Thomas, W.J., and Lombardi, J.L. Trans. Inst. Chem. Engng., (1971), 49, 240.

111. Tien, C., and Thodos, G. A.I.Ch.E.J., (1960), 6, No. 3, 364.

112. Tien, C., and Thodos, G. A.I.Ch.E.J., (1961), 7, No. 3, 411.

113. Tien, C., and Thodos, G. A.I.Ch.E.J., (1965), 11, No. 5., 845.

114. Vermeulen, T. Ind. Engng. Chem., (1953) 45, 1664.

115. Vermeulen, T. Adv. Chem. Engng. (1958), 2, 148.

116. Vermeulen, T., and Quilici, R.E. Ind. Engng. Chem. Fundamentals, (1970), 9, No. 1, 179.

117. Weber, W.J., and Morris, J.C. J. San. Engng. Div. ASCE, (1964), SA3, 79.

118. Westermark, M. W.P.C.F.J., (1975), 47, 704.

119. Wheeler, J.M., and Middleman, S. Ind. Engng. Chem. Fundamentals, (1970), 9, 624.

120. Wilson, J., and Bachelor, J.S. Colliery Guardian, (1973), No. 6, 217.

121. Yaws, C.L. "Physical Properties", McGraw Hill, New York, (1977).

122. Yon, C.M., and Turnock, P.H. A.I.Ch.E. Symp. Ser., (1971), 67, No. 117, 75.

123. Young, D.M., and Crowell, A.D. "Physical Adsorption of Gases", Butterworth, London, (1962).

124. Zeldowitsh, J. Acta Physiochem. U.R.S.S., (1934), 1, 961.

125. Zwiebel, I. Ind. Engng. Chem. Fundamentals, (1969), 8, 803.

126. Zwiebel, I., and Schnitzer, J.J. A.I.Ch.E. Symp. Ser., (1973), 69, No. 134, 18.

127. Zwiebel, I., Gariepy, R.L., and Schnitzer, J.J. A.I.Ch.E.J., (1972), 18, No. 6, 1139.

128. Zwiebel, I., Kralik, C.M., and Schnitzer, J.J. A.I.Ch.E.J., (1974), 20, 915.

FIGURES

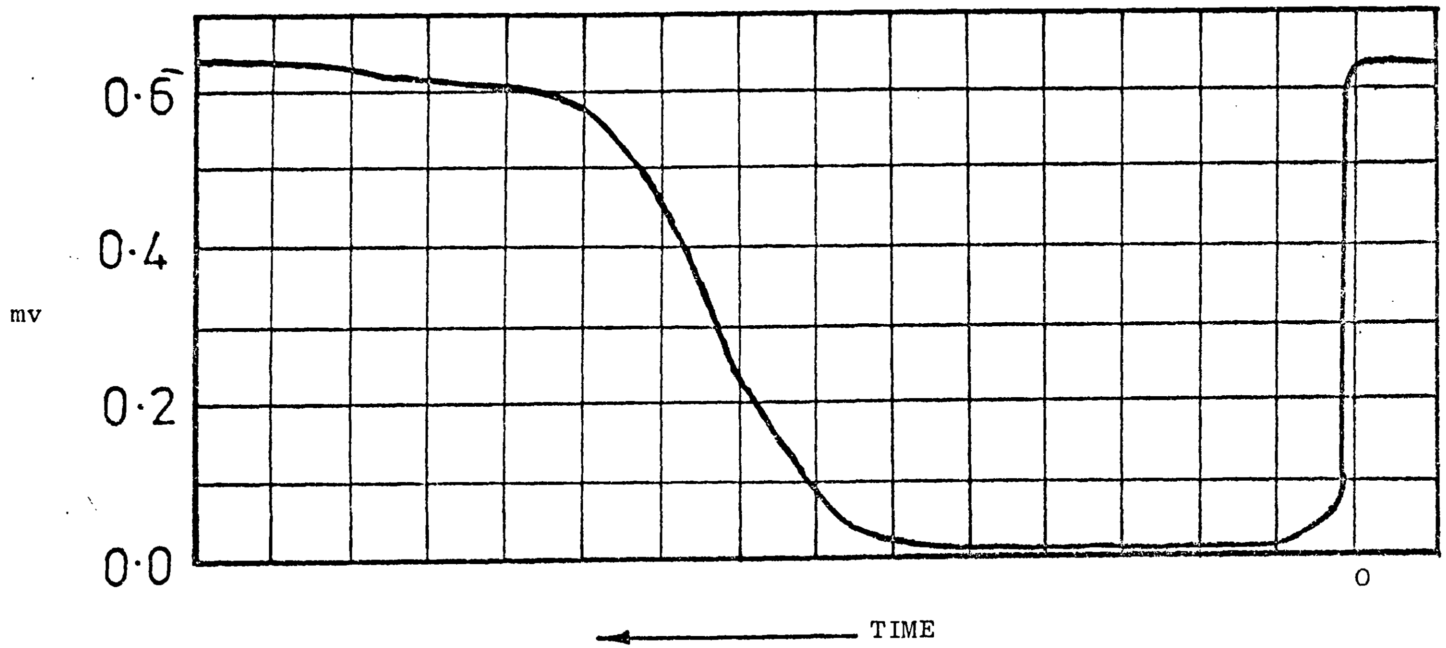

Figure 1: Typical recorded curve for the direct method of analysis.

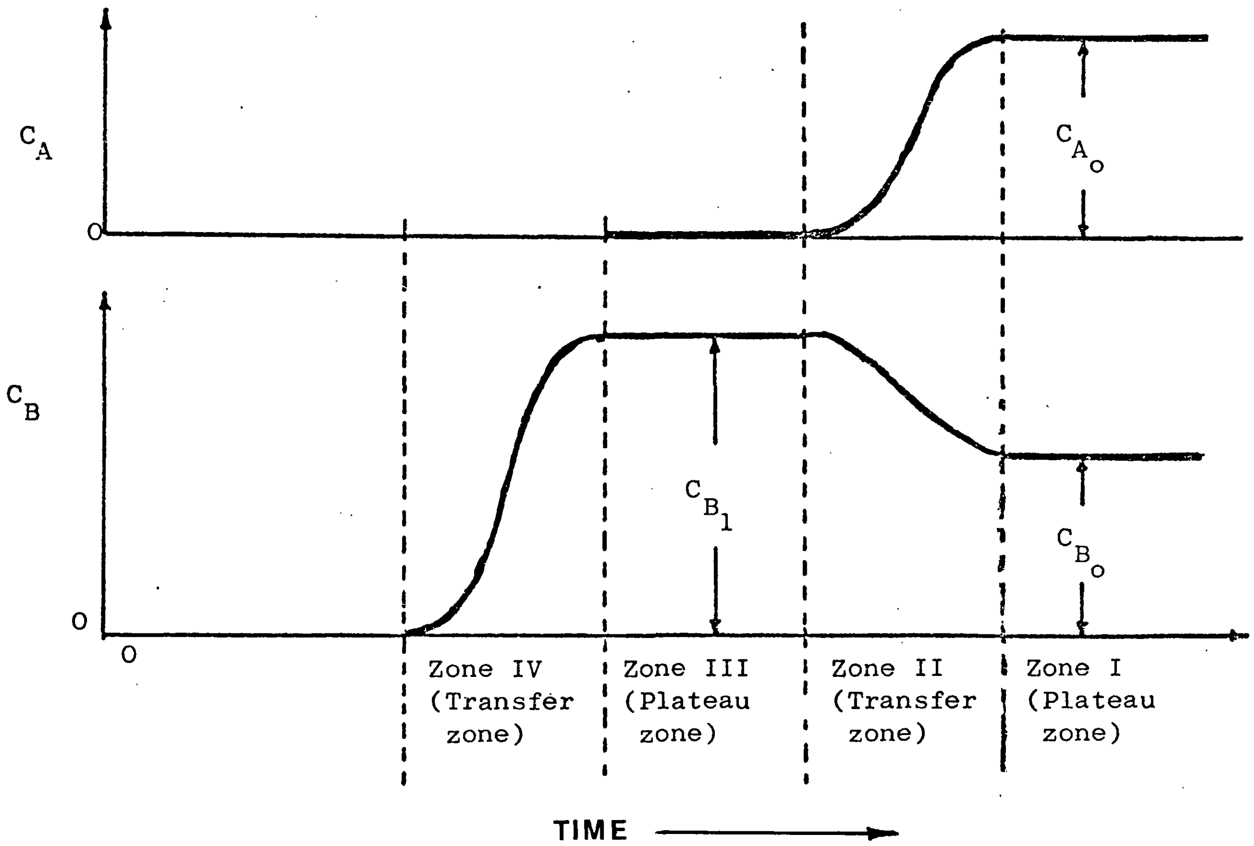

Figure 2: Breakthrough curves for A and B

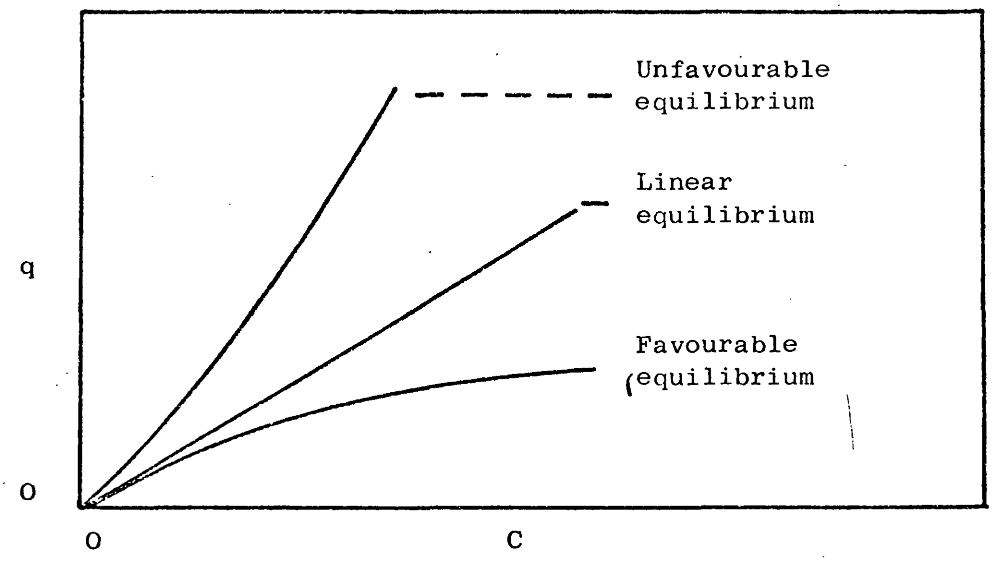

Figure 3(a): Examples of isotherms for single component adsorption

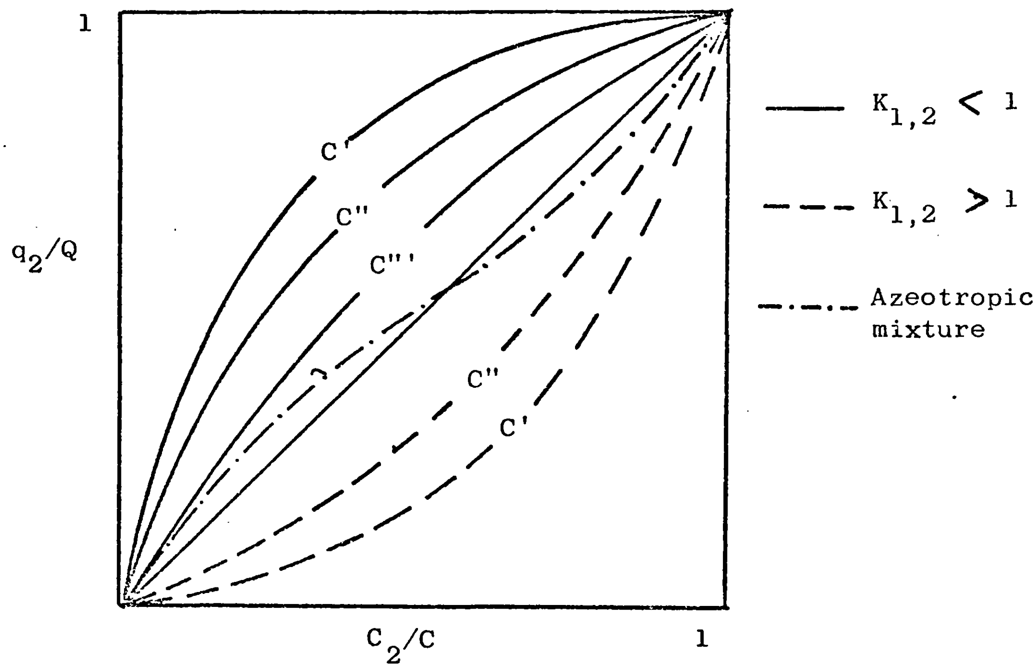

Figure 3(b): Examples of isotherms for binary mixtures

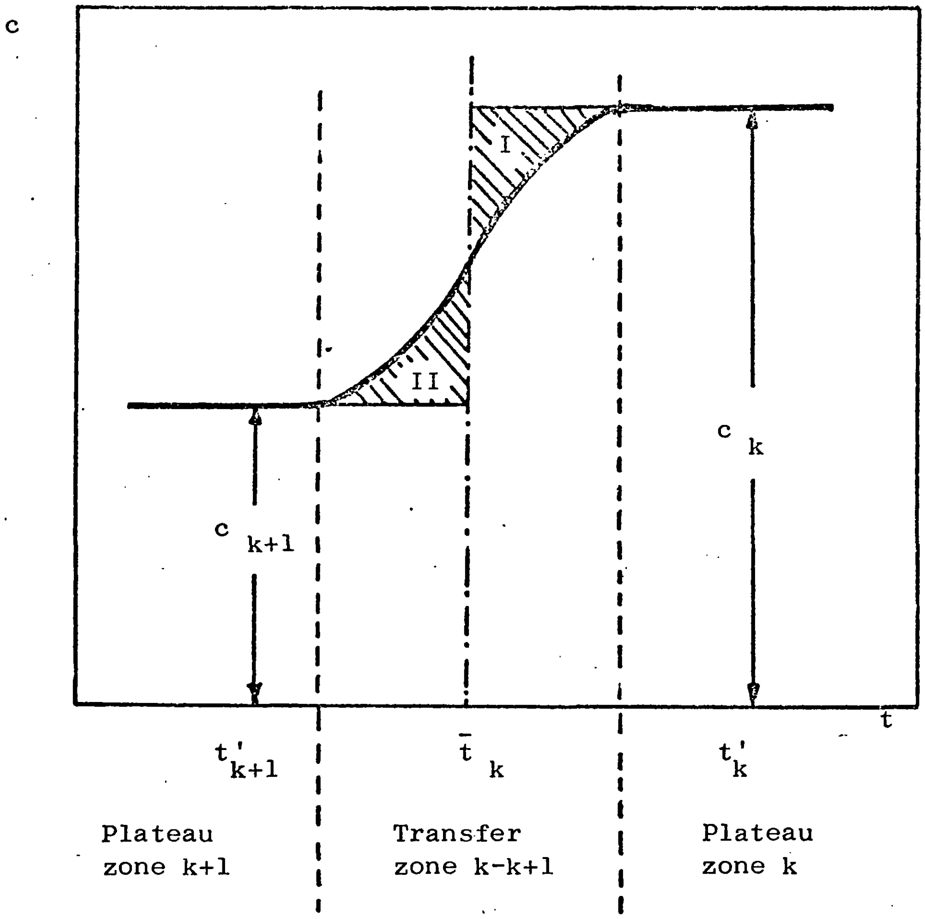

Figure 4: Stoichiometric time in the transfer zone k-k+1

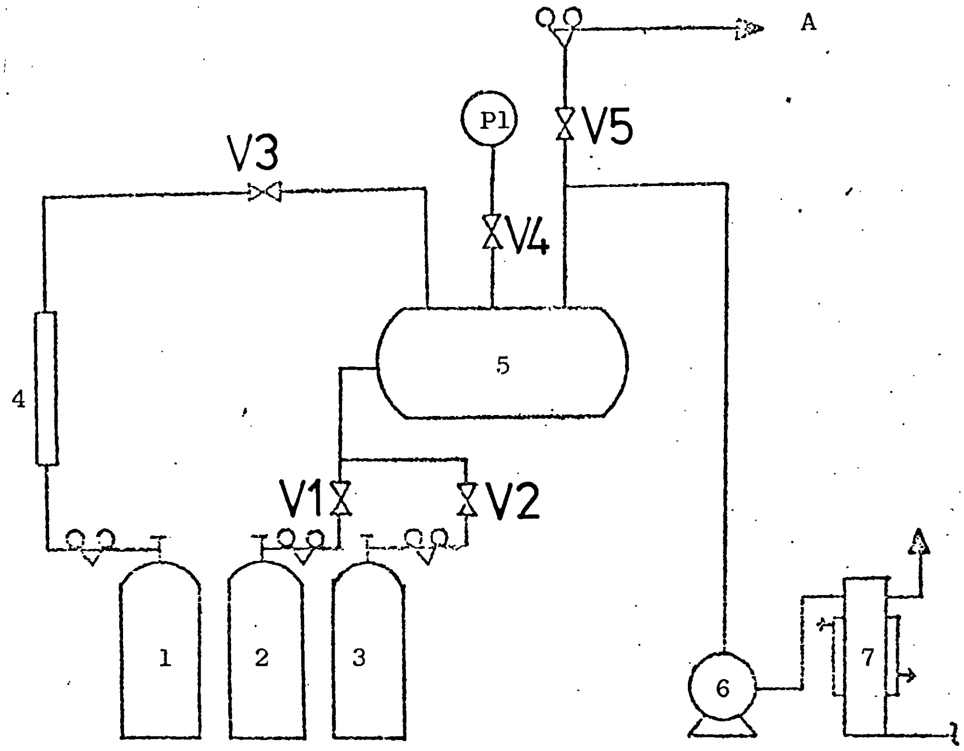

(a) gas mixture preparation section

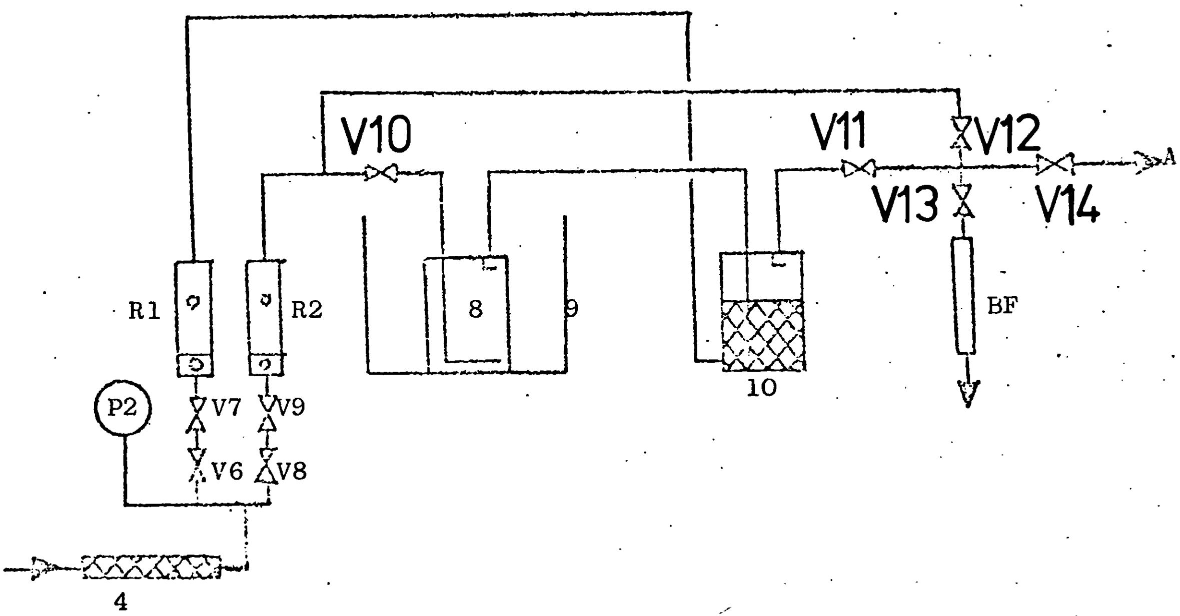

(b) Saturation section

Figure 5: Scheme of apparatus

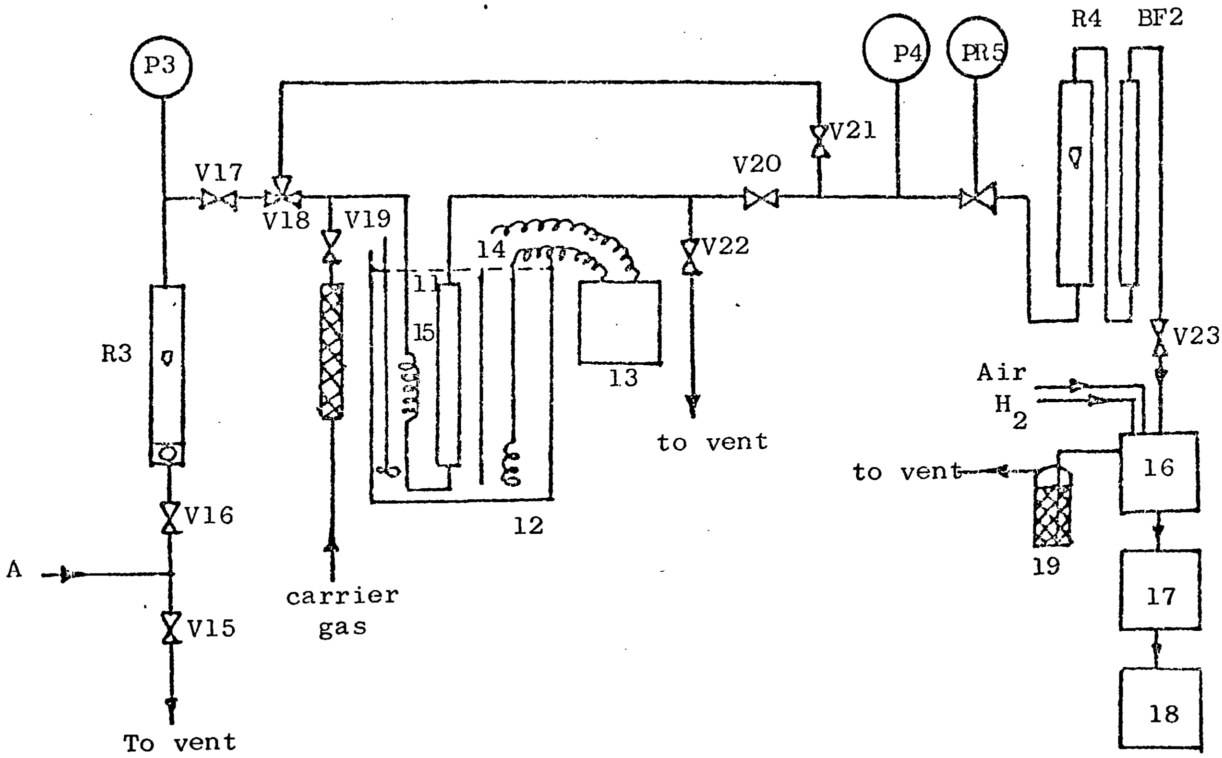

(c) Adsorption and Analysing Section

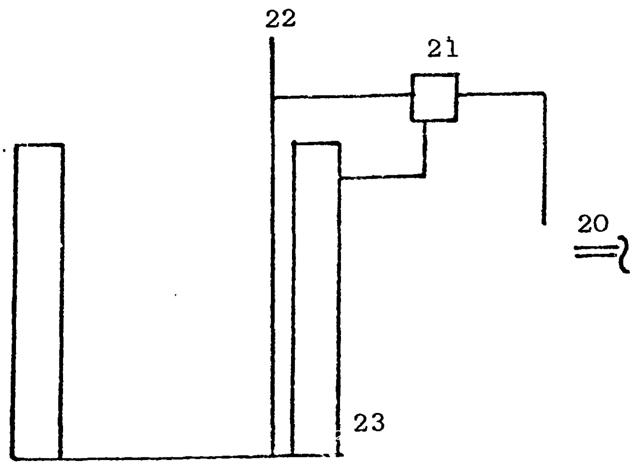

(d) Regeneration Section

Figure 5 (cont.): Scheme of Apparatus

Key to Figure 5

1	Nitrogen gas cylinder
2	Methane gas cylinder
3	Ethane gas cylinder
4	Molecular sieve drying column
5	Mixing vessel
6	Edward rotary vacuum pump
7	Diffusion pump
8	Saturator
9	Ice bath
10	Mixer
11	Adsorption column
12	Water bath
13	Temperature controller
14	Hg in Glass ~~in~~ thermometer
15	Preheater coil
16	Gas Chromatograph Unit
17	Recorder
18	Integrator
19	Molecular sieve
20	Electric time switch
21	Pye-Ether temperature regulator
22	Chromed-Alumed thermocouple
23	Regeneration furnace
BF	Bubble flowmeter
P	Pressure gauge
PR	Pressure regulator
R	Rotameter
V	Valves

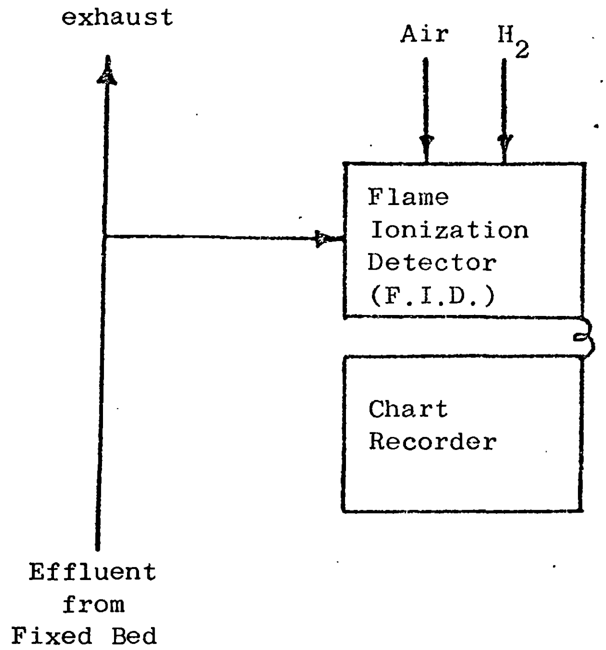

Figure 6: Continuous sampling detector (direct system).

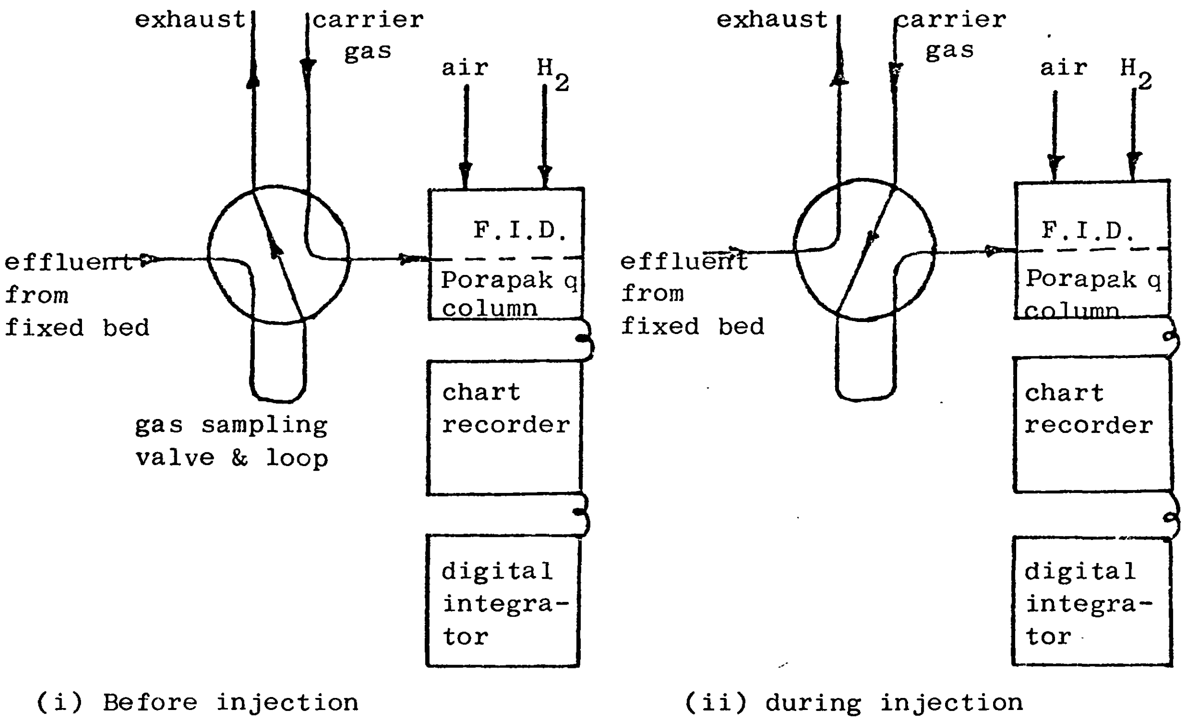

Figure 7: Discrete sampling detector (chromatographic system)

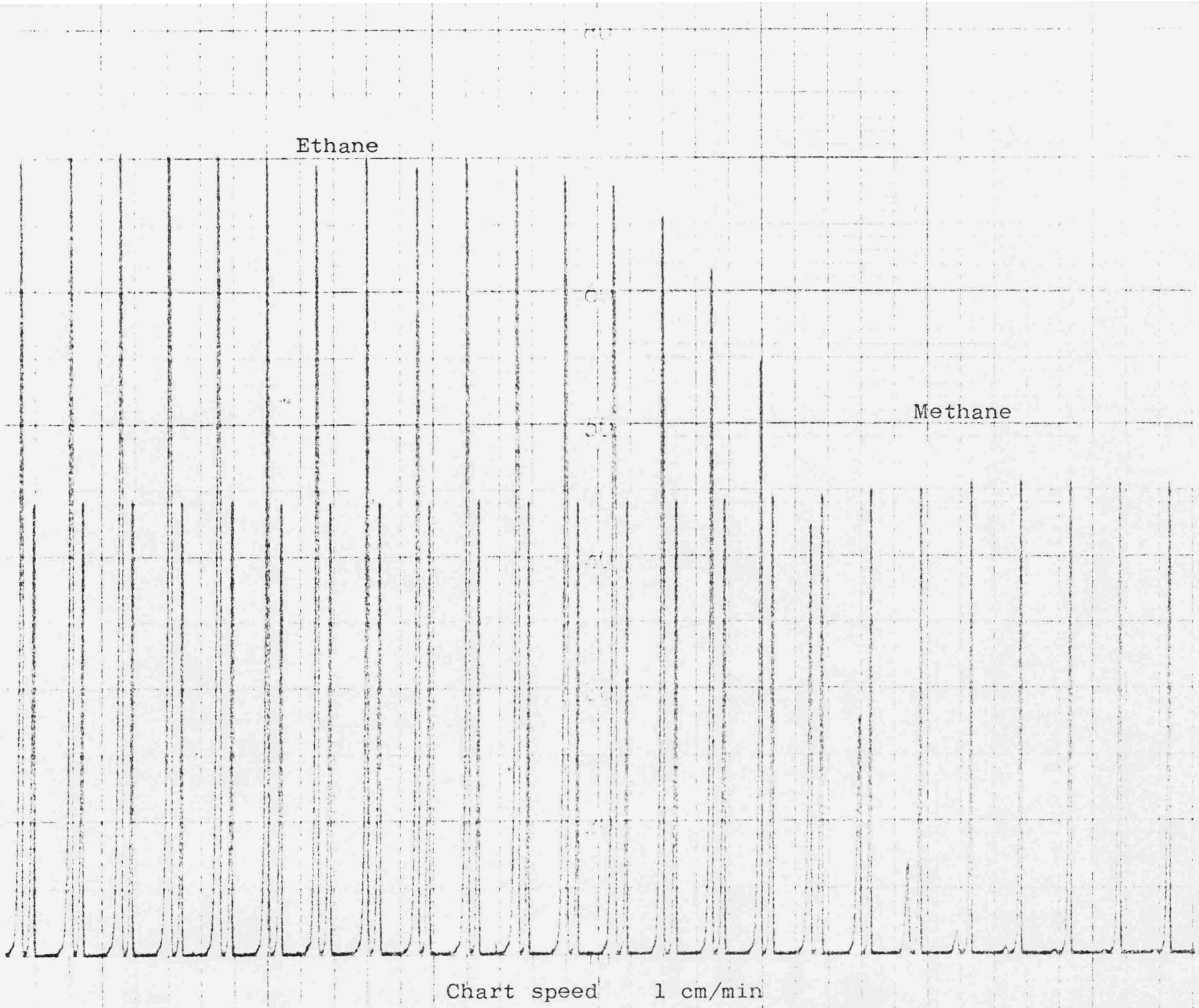

Figure 8: Typical gas sample chromatogram for binary adsorption.
For complete chromatographic breakthrough curve see back cover

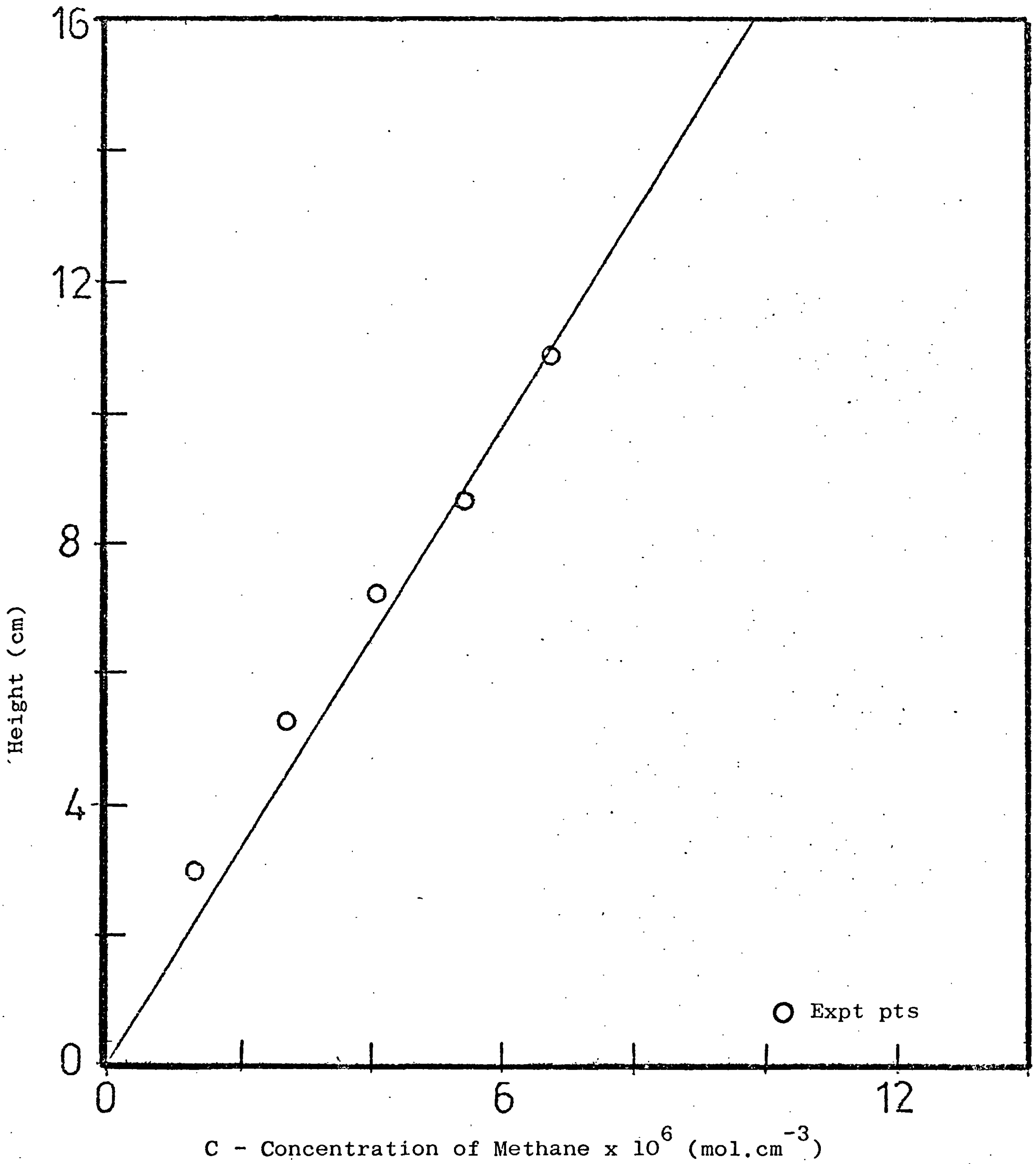

Figure 9: Calibration of Direct System (Methane)

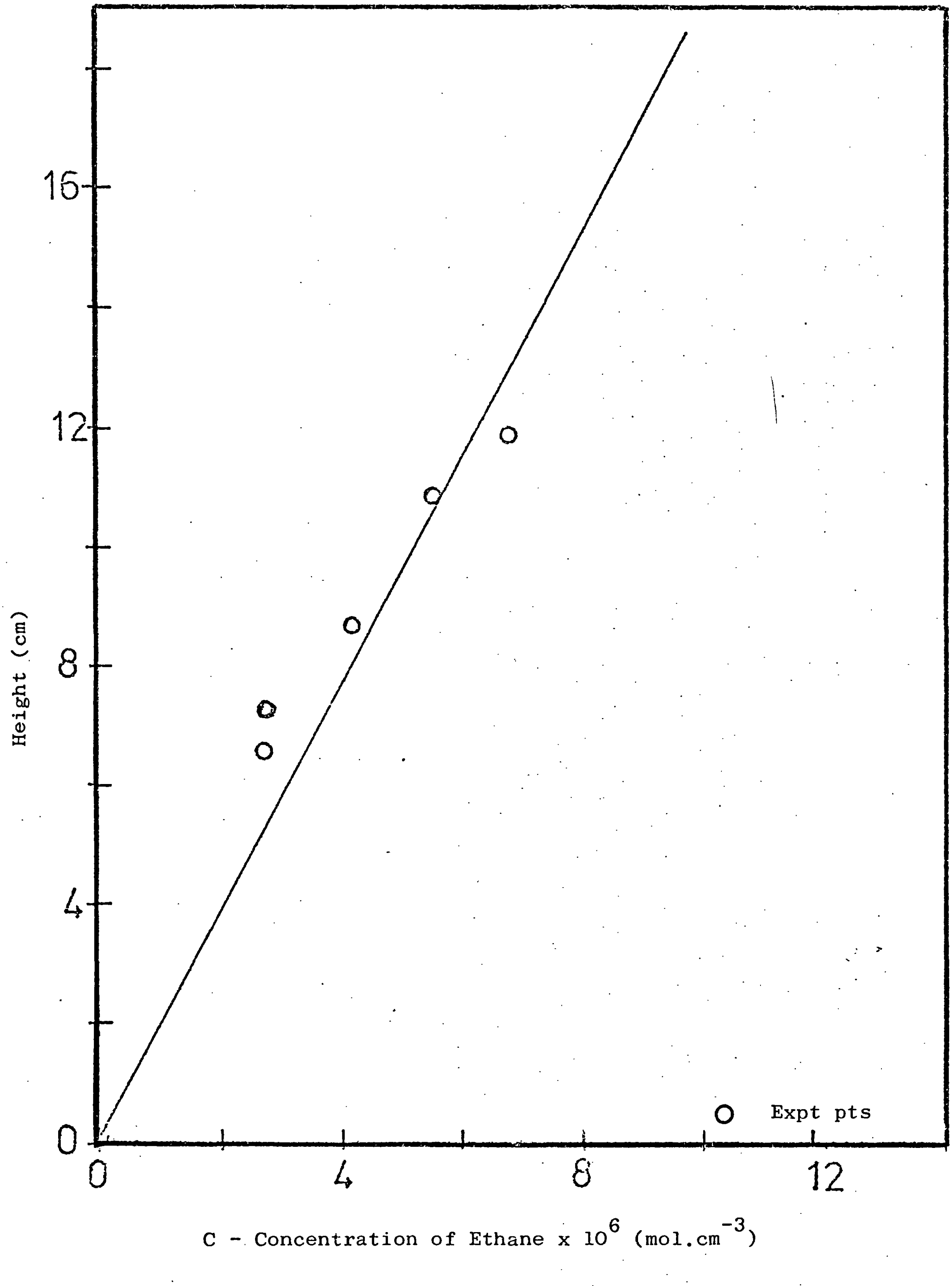

Figure 10: Calibration of Direct system (Ethane)

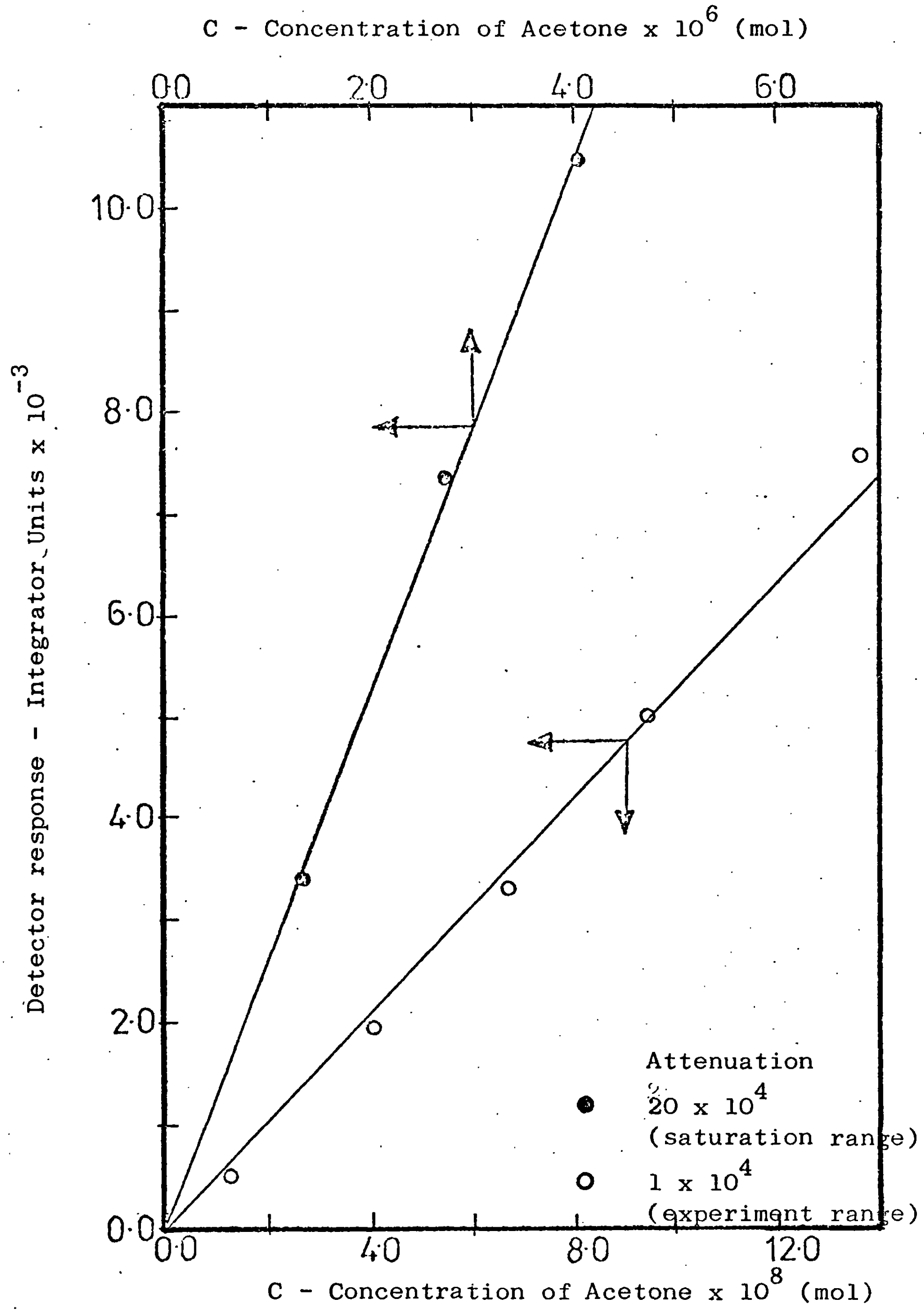

Figure 11: Calibration of Chromatographic System (Acetone)

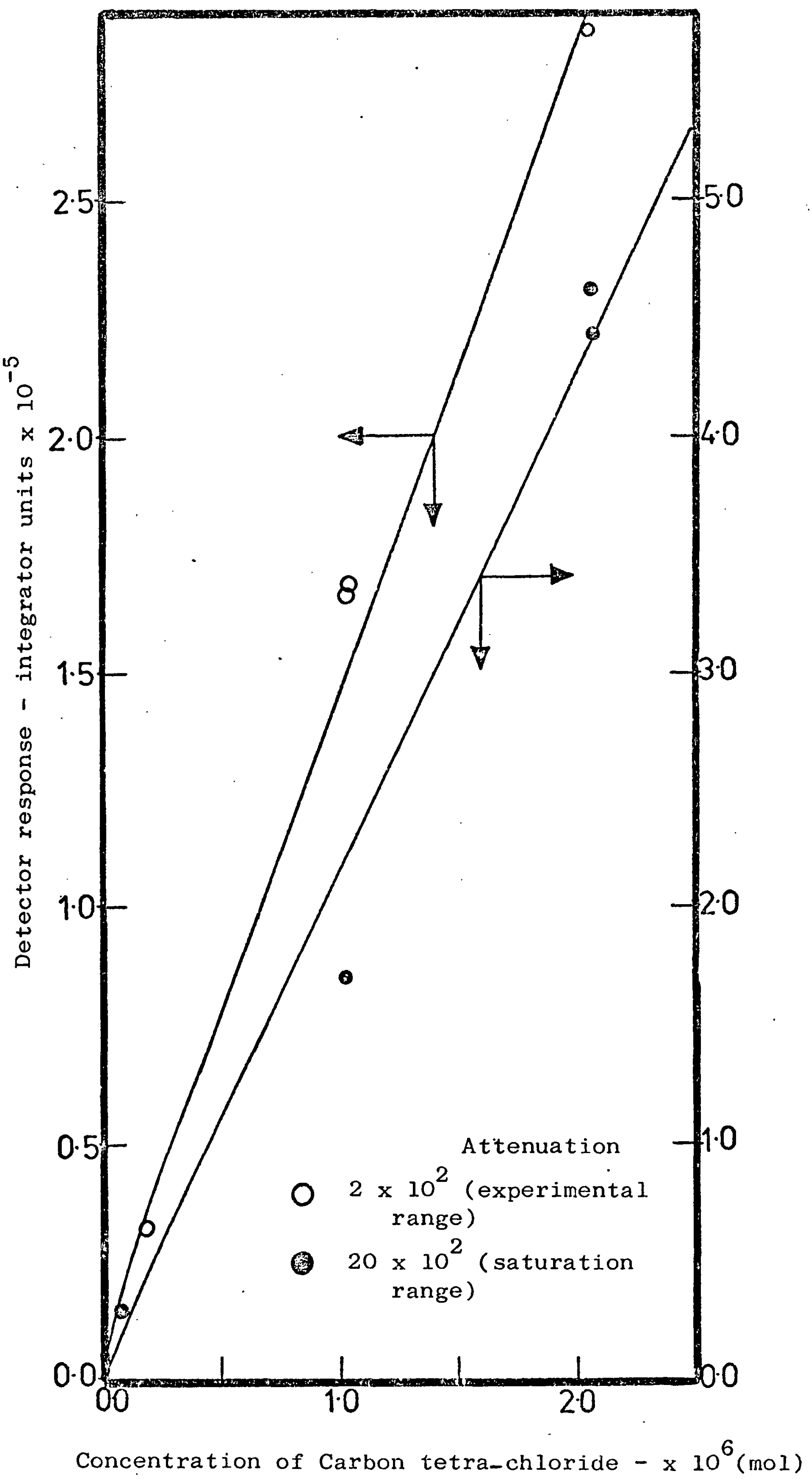

Figure 12: Chromatographic system calibration (carbon tetra chloride)

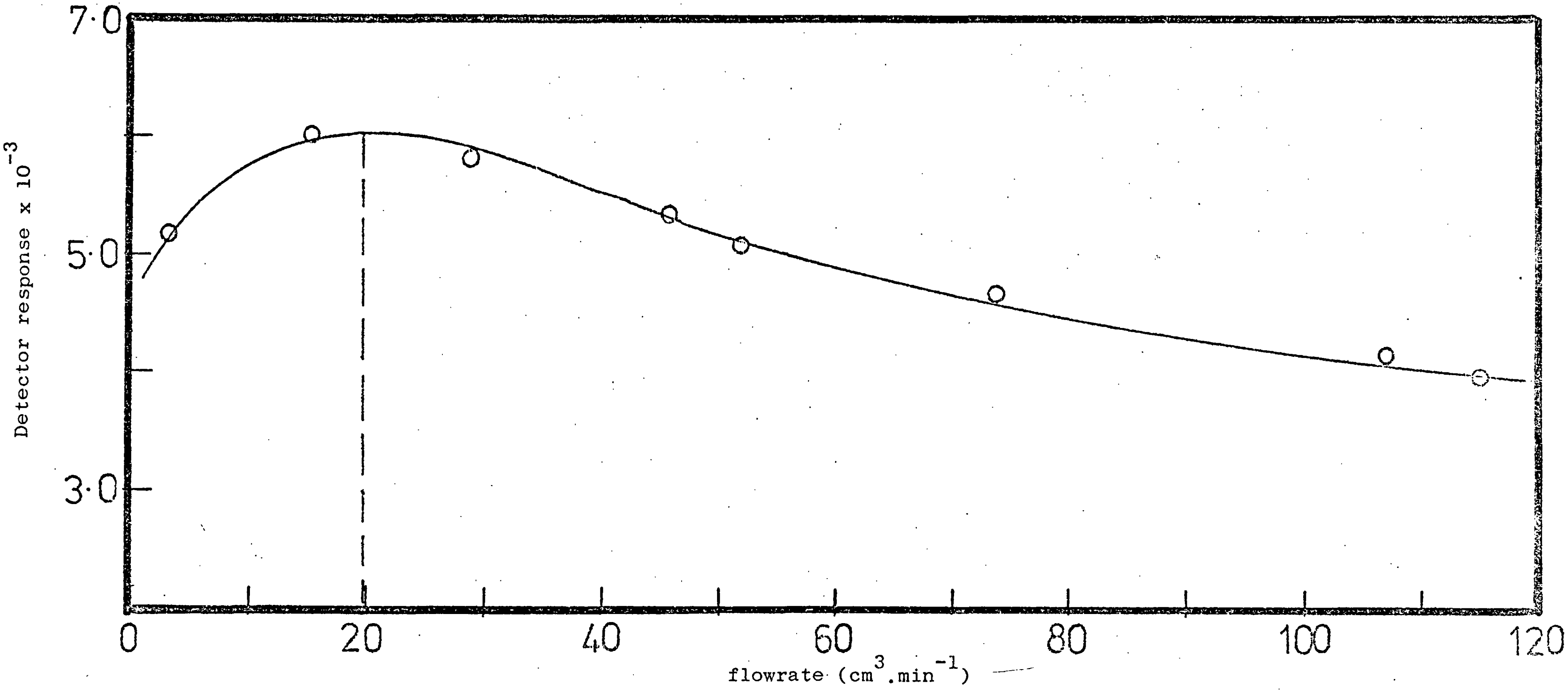

Figure 13: Effect of carrier gas flowrate on saturation.

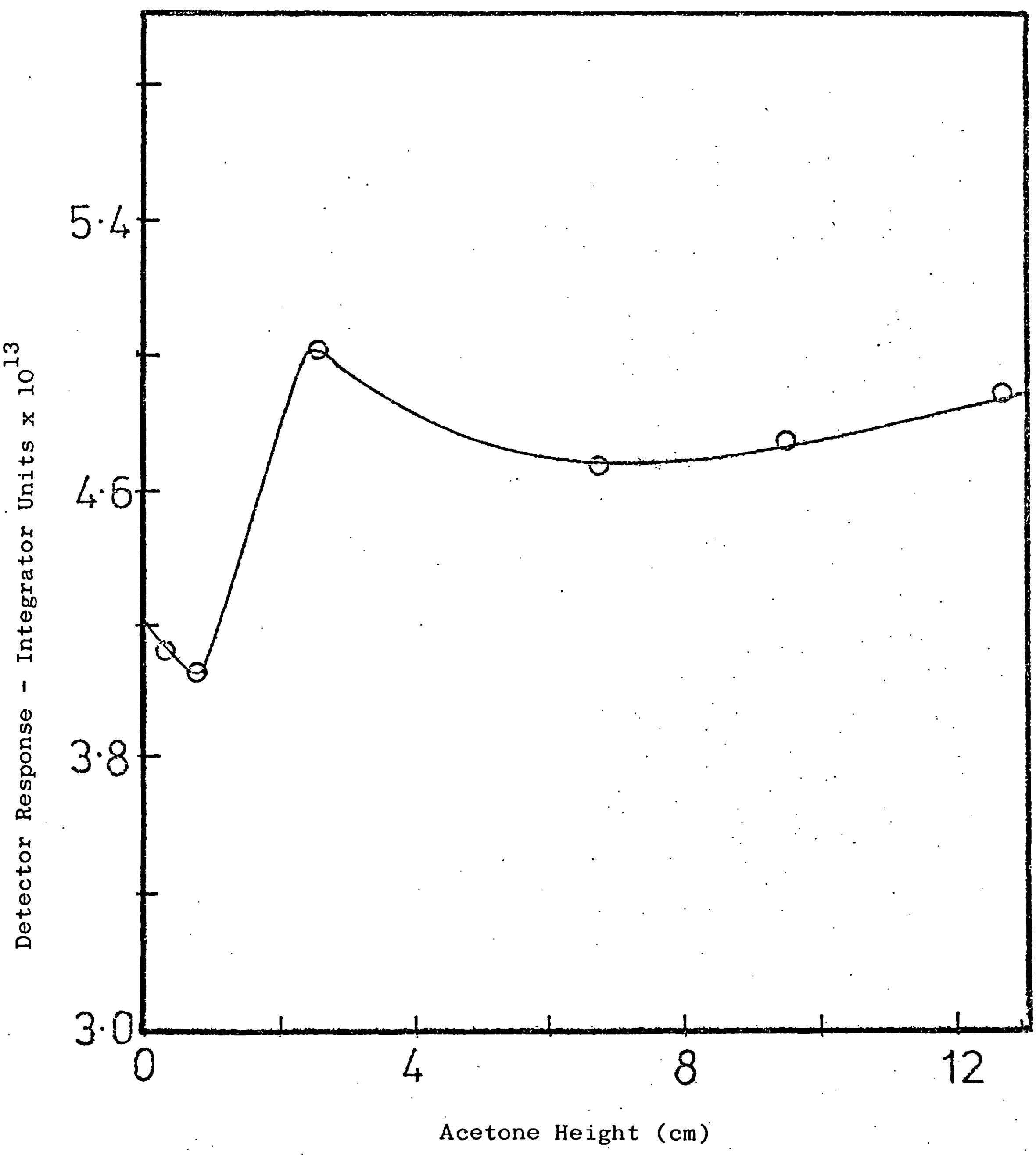

Figure 14: Effect of acetone height on saturation

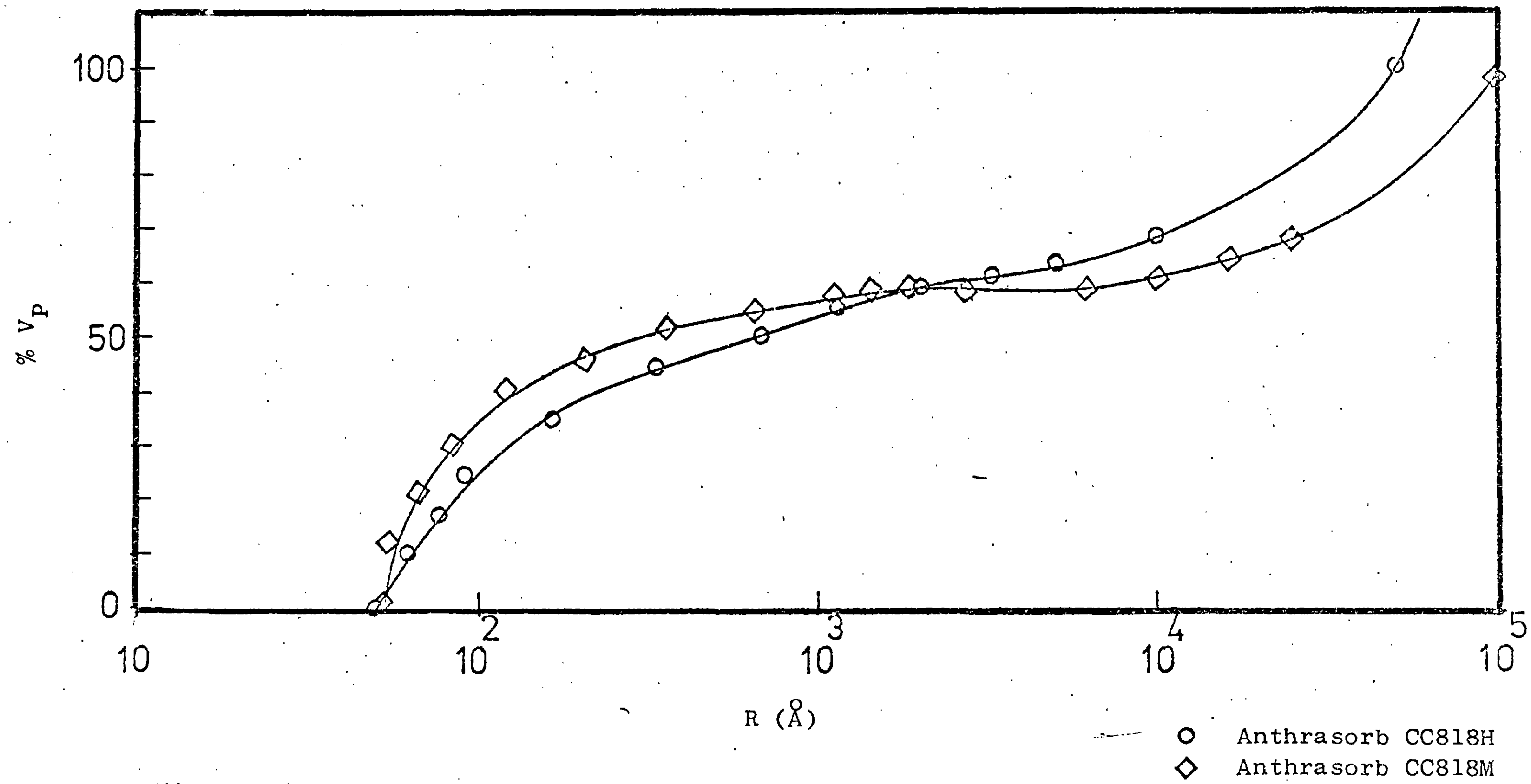

Figure 15: Pore size distribution for Anthrasorb

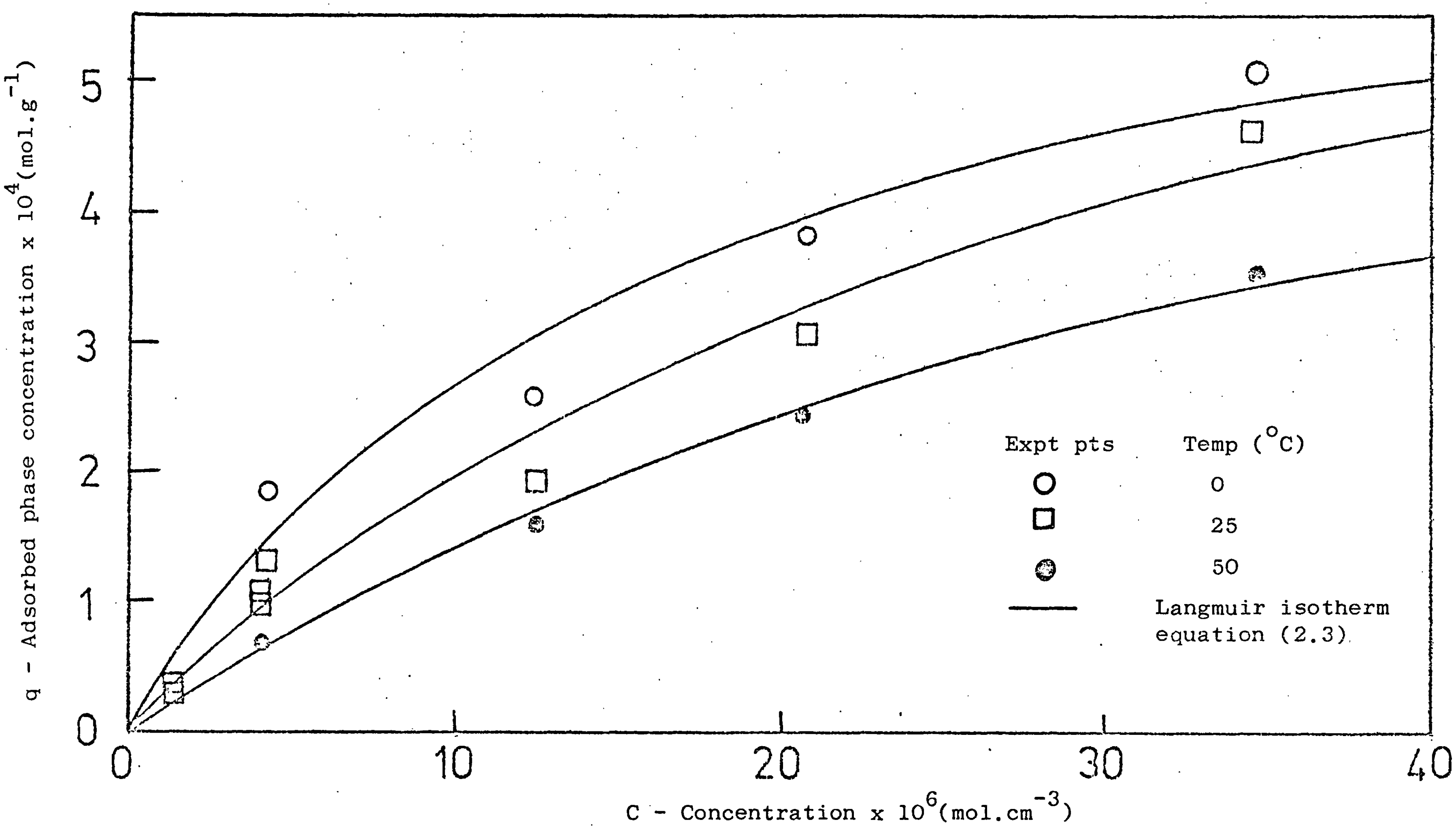

Figure 16: Langmuir isotherms of methane on Anthrasorb CC818M at various temperatures.

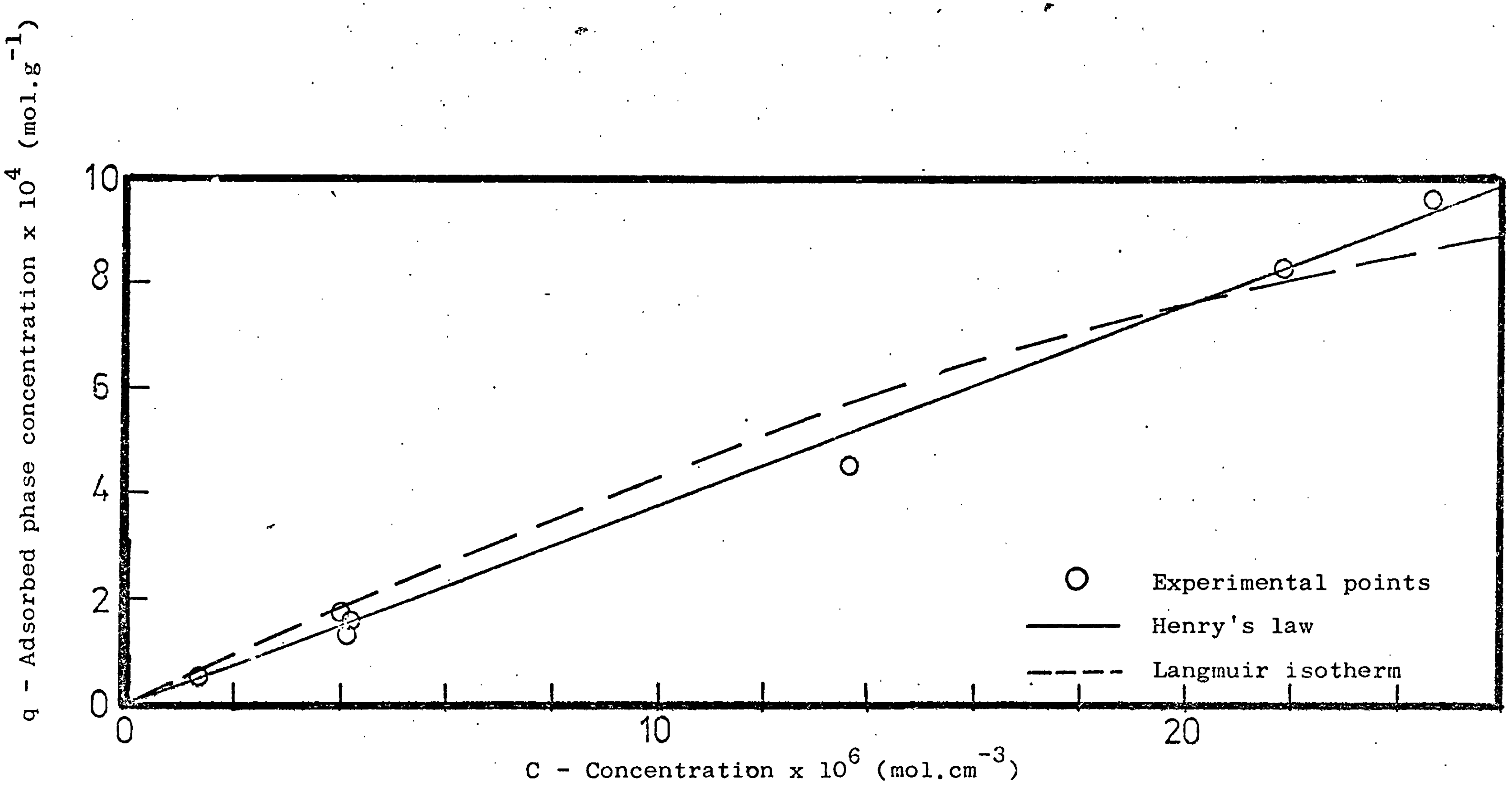

Figure 17: Henry and Langmuir isotherms of methane on Anthrasorb CC818H at 25°C.

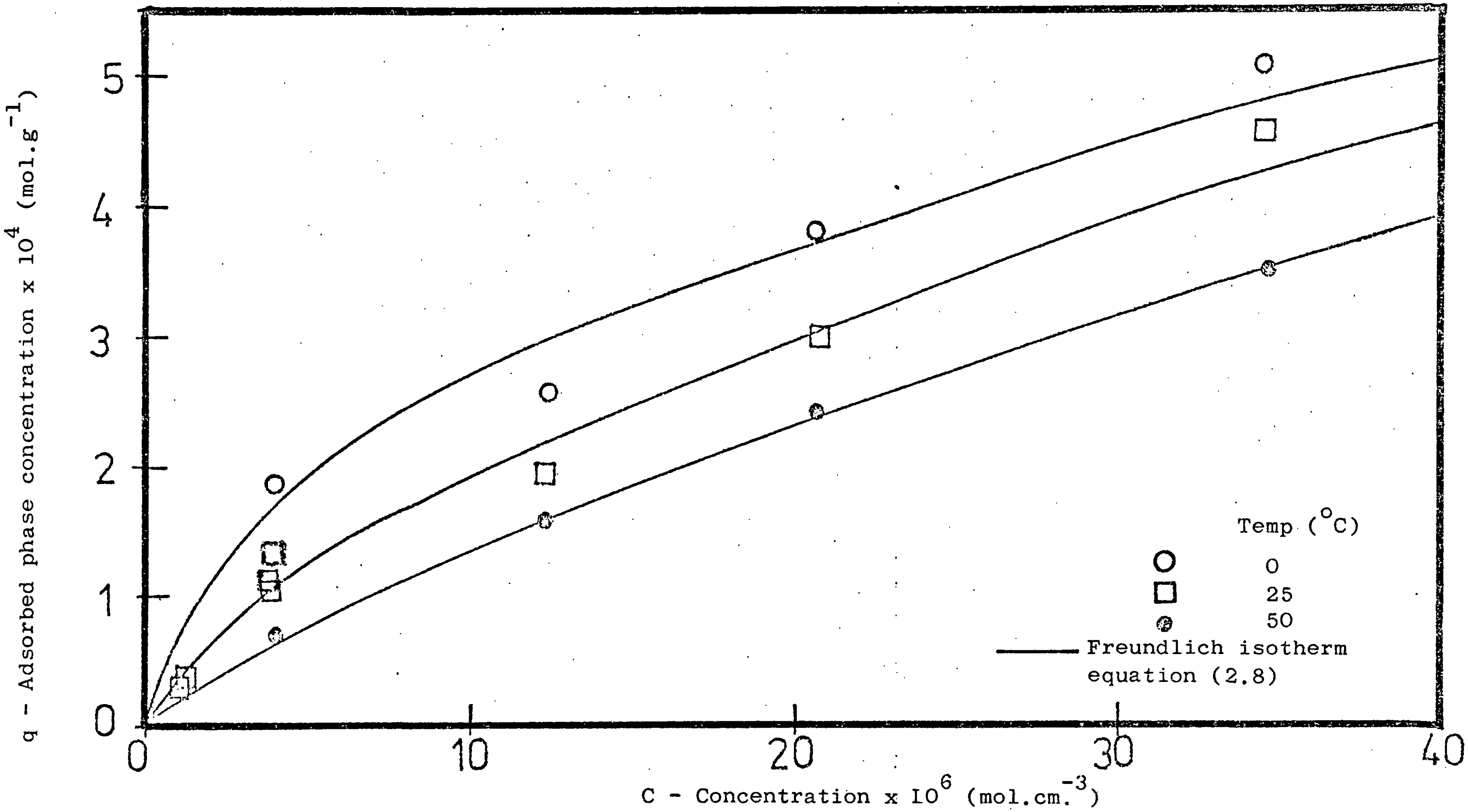

Figure 18: Freundlich isotherm of methane on Anthrasorb CC818M at various temperatures.

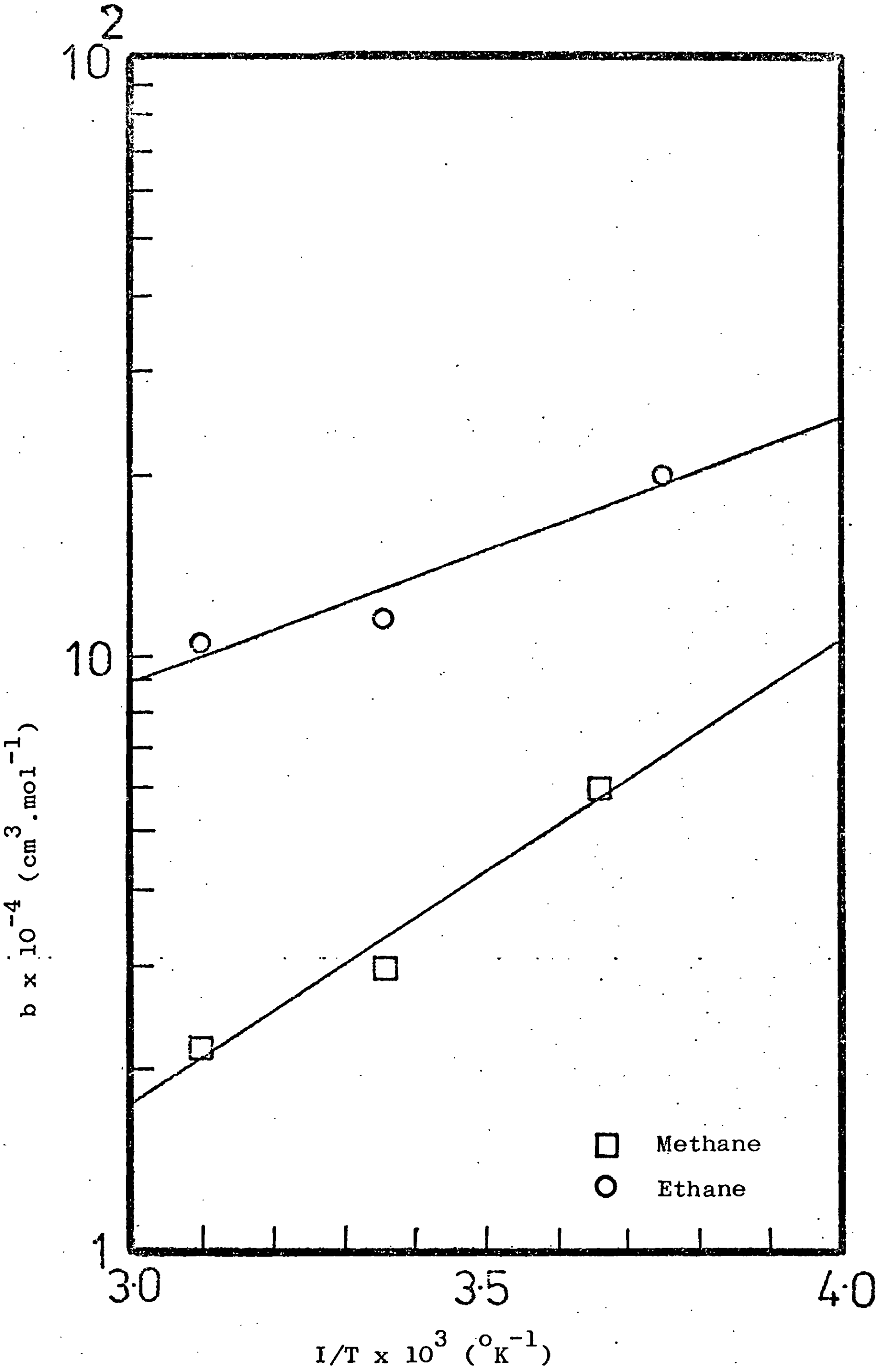

Figure 19: Temperature dependence of the Langmuir equilibrium constant 'b' on Anthrasorb CC818M

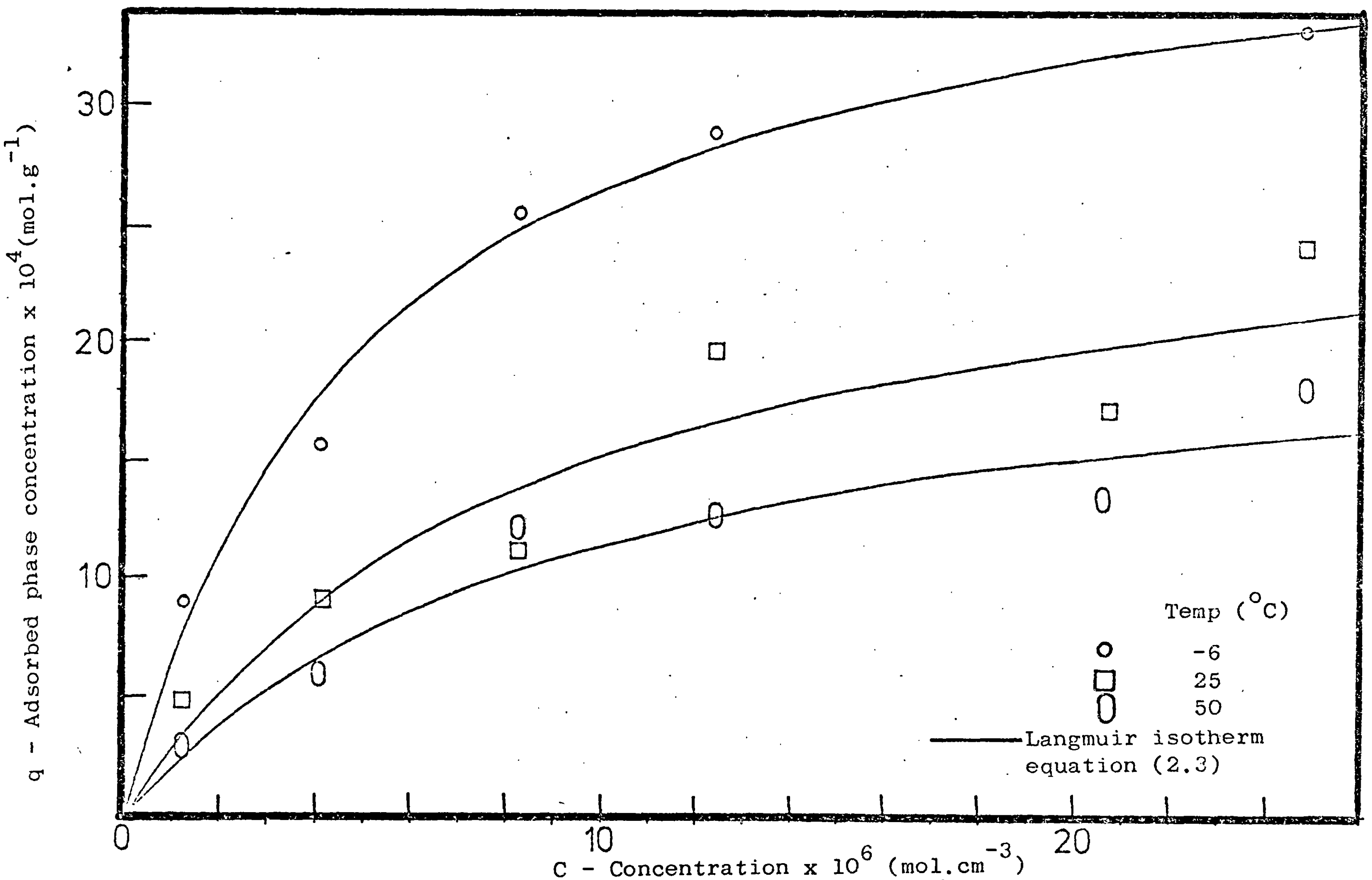

Figure 20: Langmuir isotherms of ethane on Anthrasorb CC818M at various temperatures.

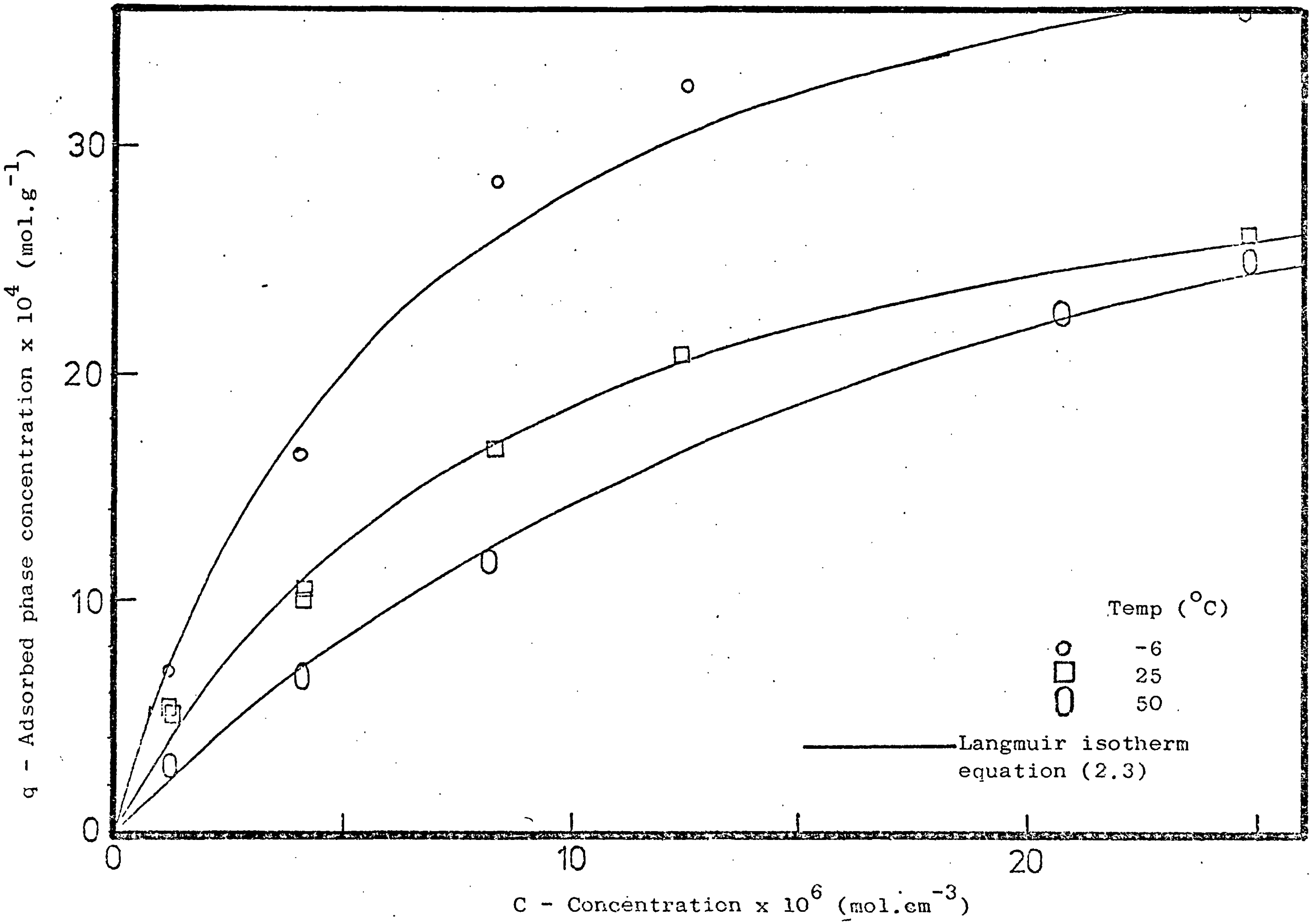

Figure 21: Langmuir isotherms of ethane on Anthrasorb CC818H at various temperatures.

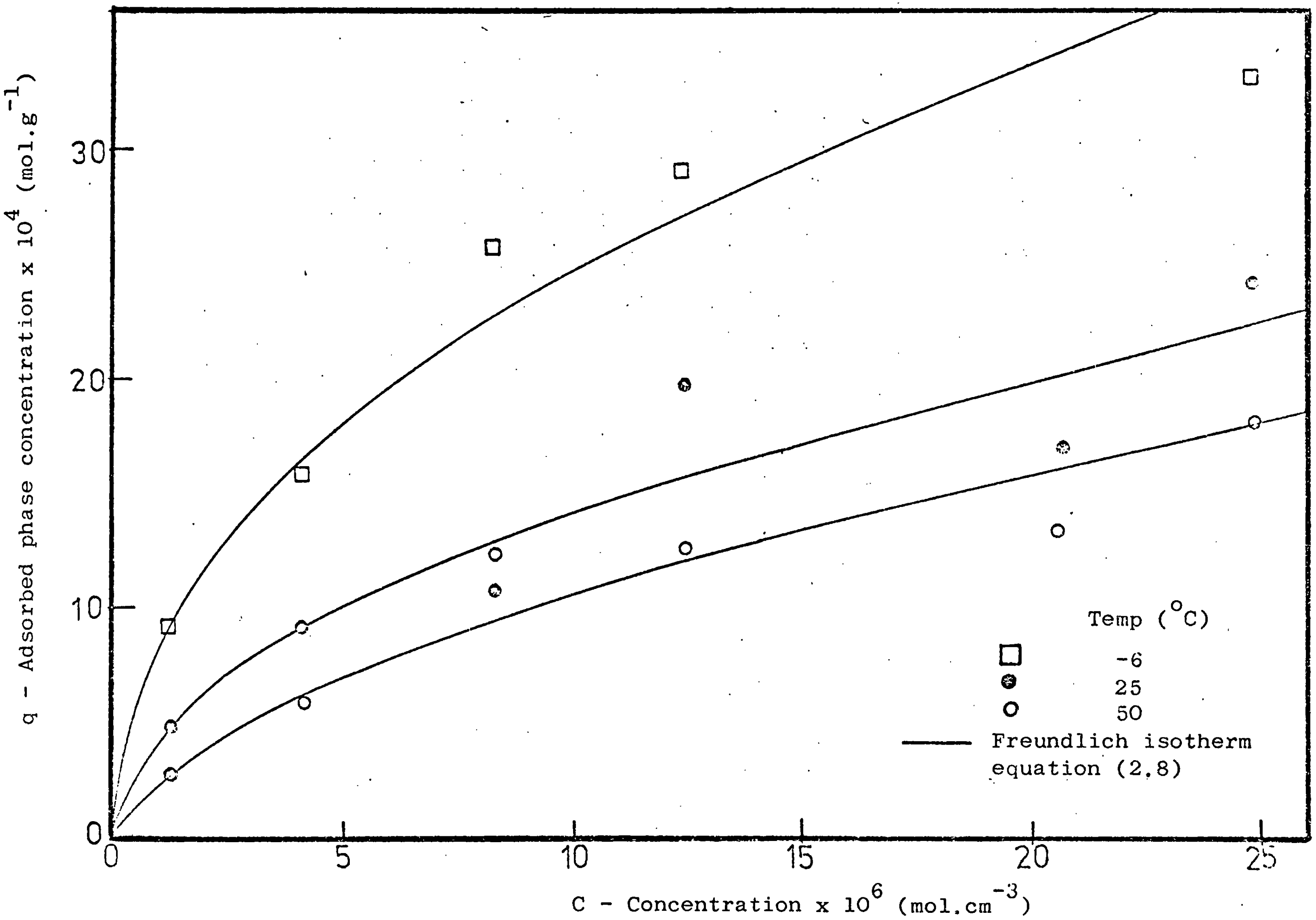

Figure 22: Freundlich isotherms of ethane on Anthrasorb CC818M at various temperatures.

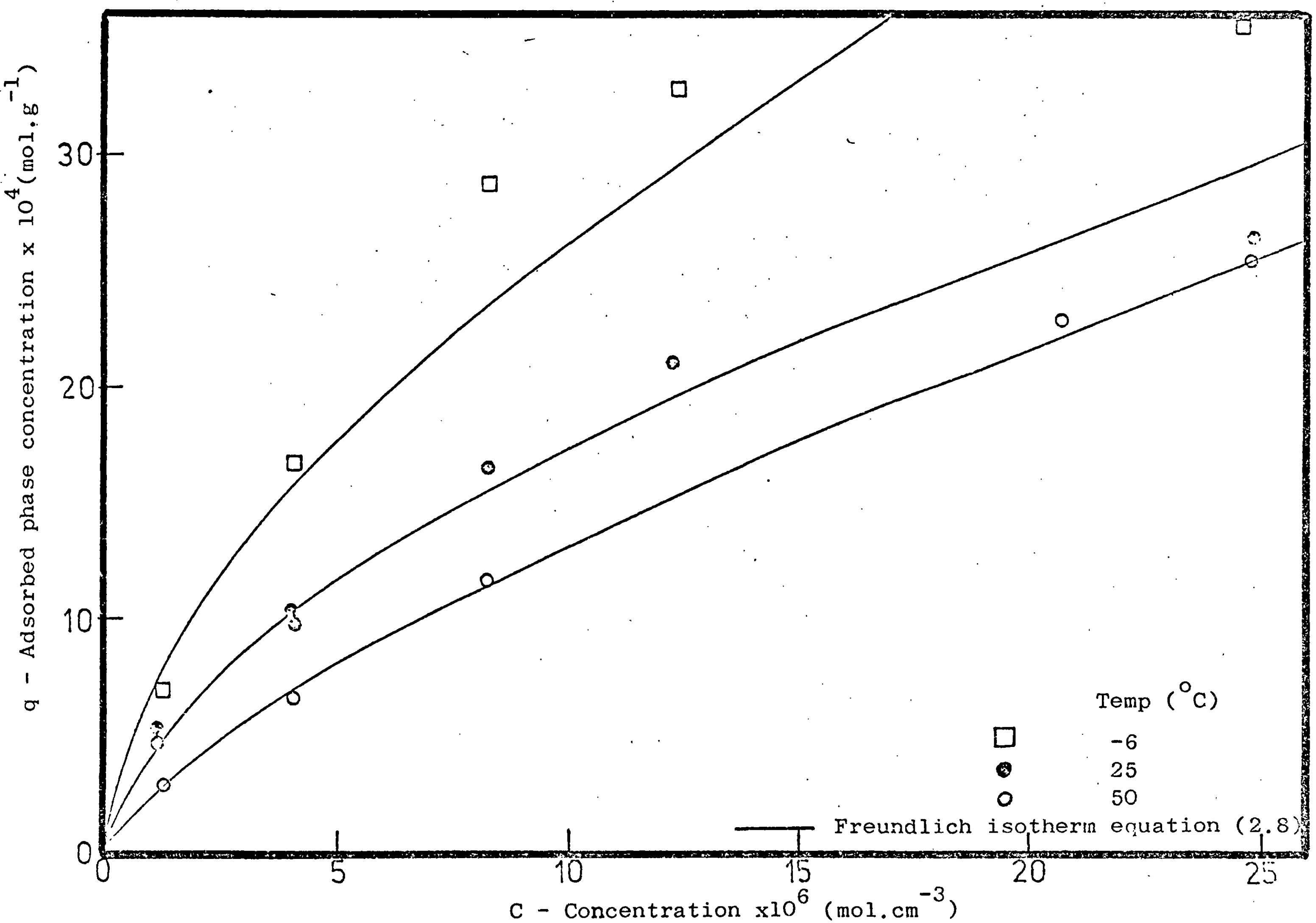

Figure 23: Freundlich isotherms of ethane on Anthrasorb CC818H at various temperatures.

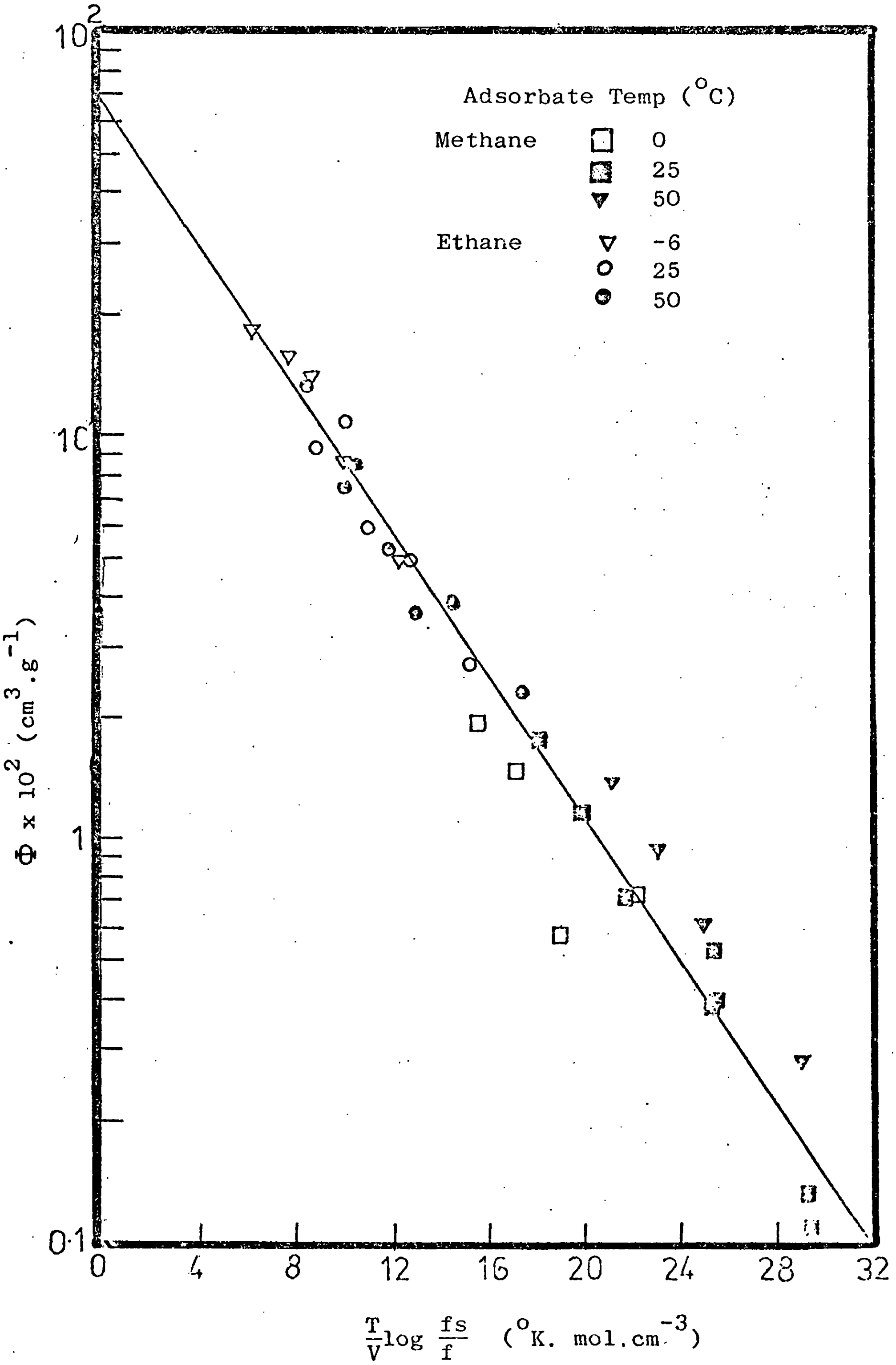

Figure 24: Correlation curve for methane and ethane on Anthrasorb CC818M at various temperatures.

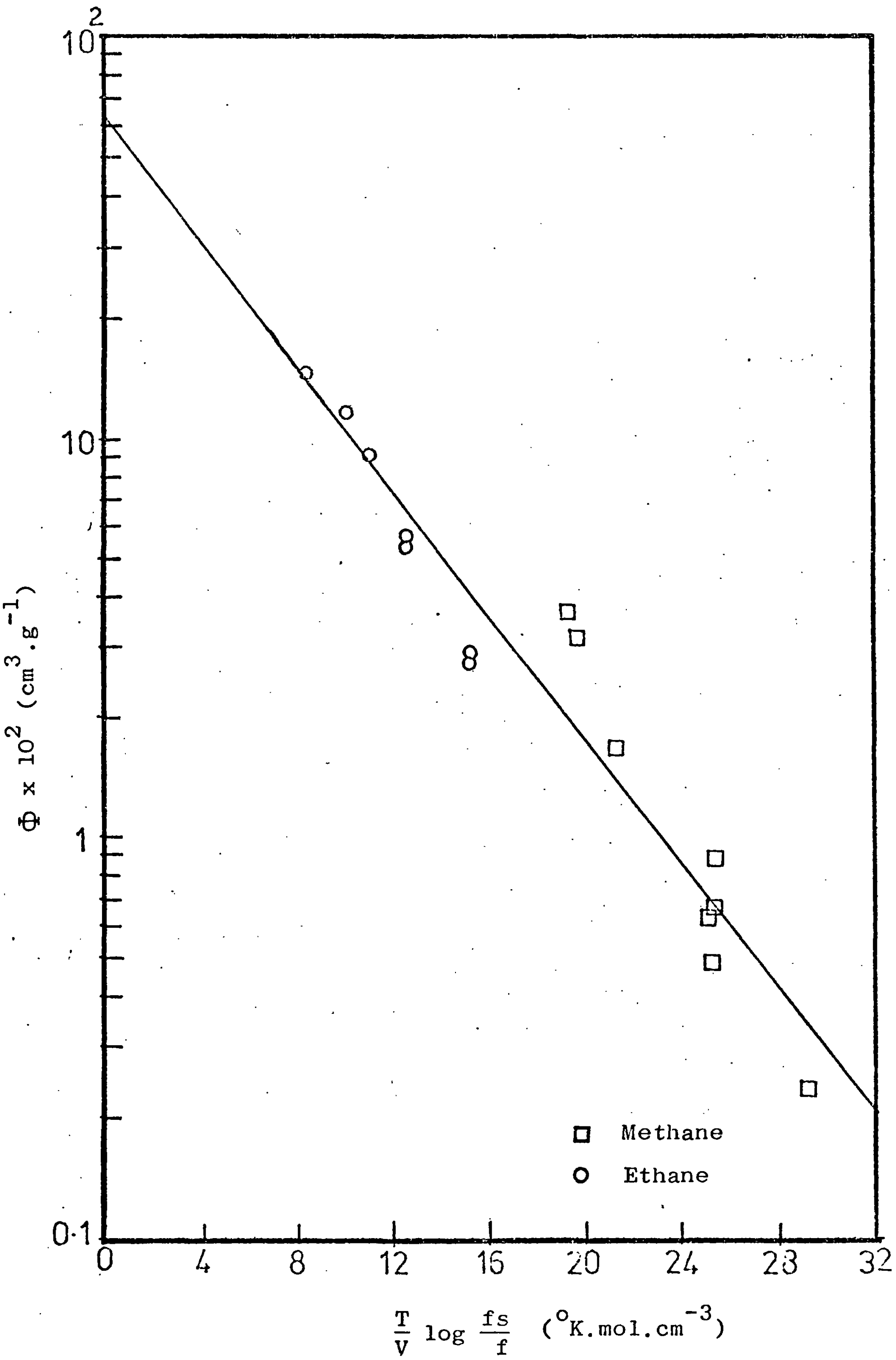

Figure 25: Correlation curve for methane and ethane on Anthrasorb CC818H at 25^{o}C.

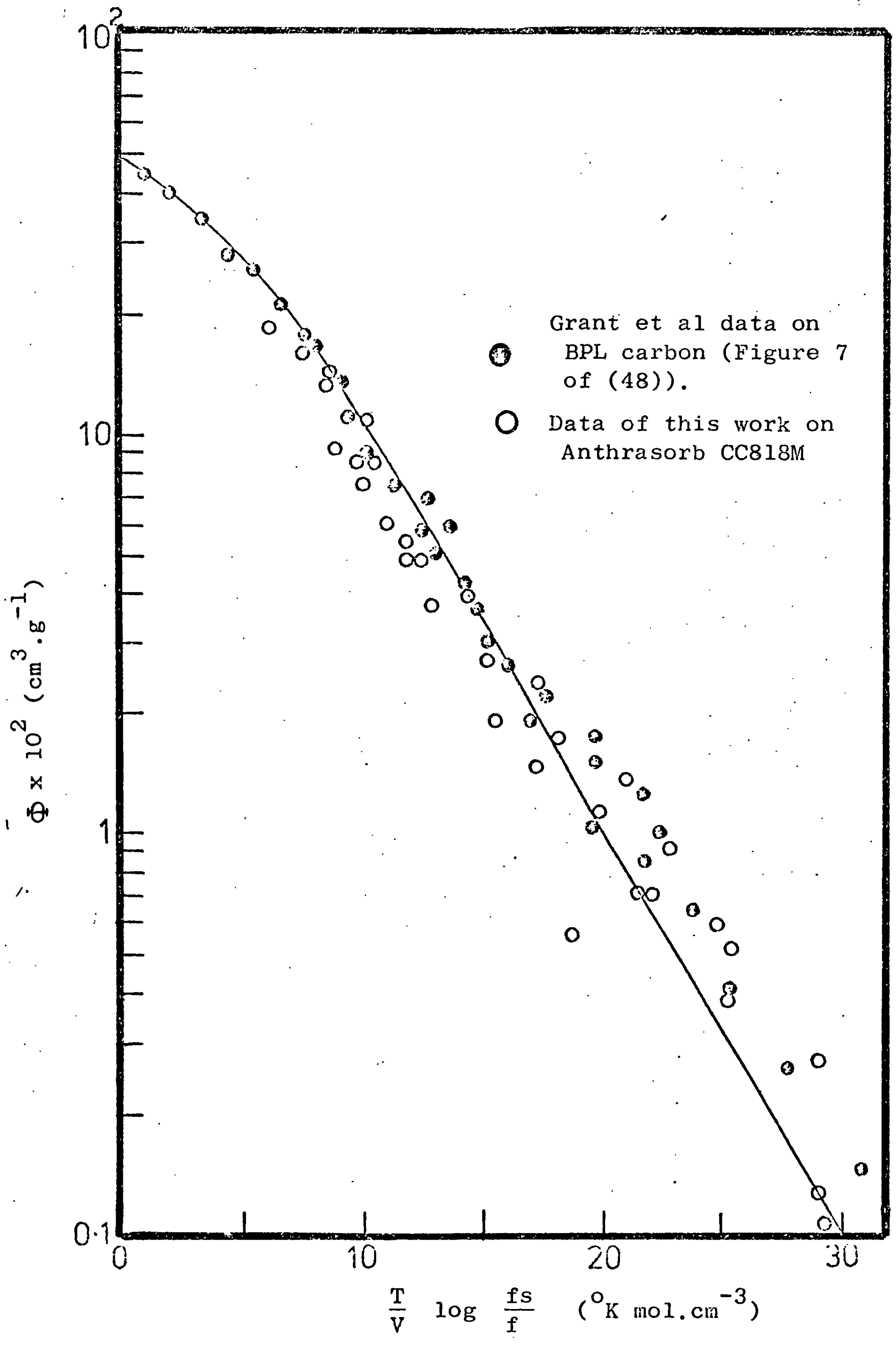

Figure 26: Generalized adsorption correlation of normal paraffins.

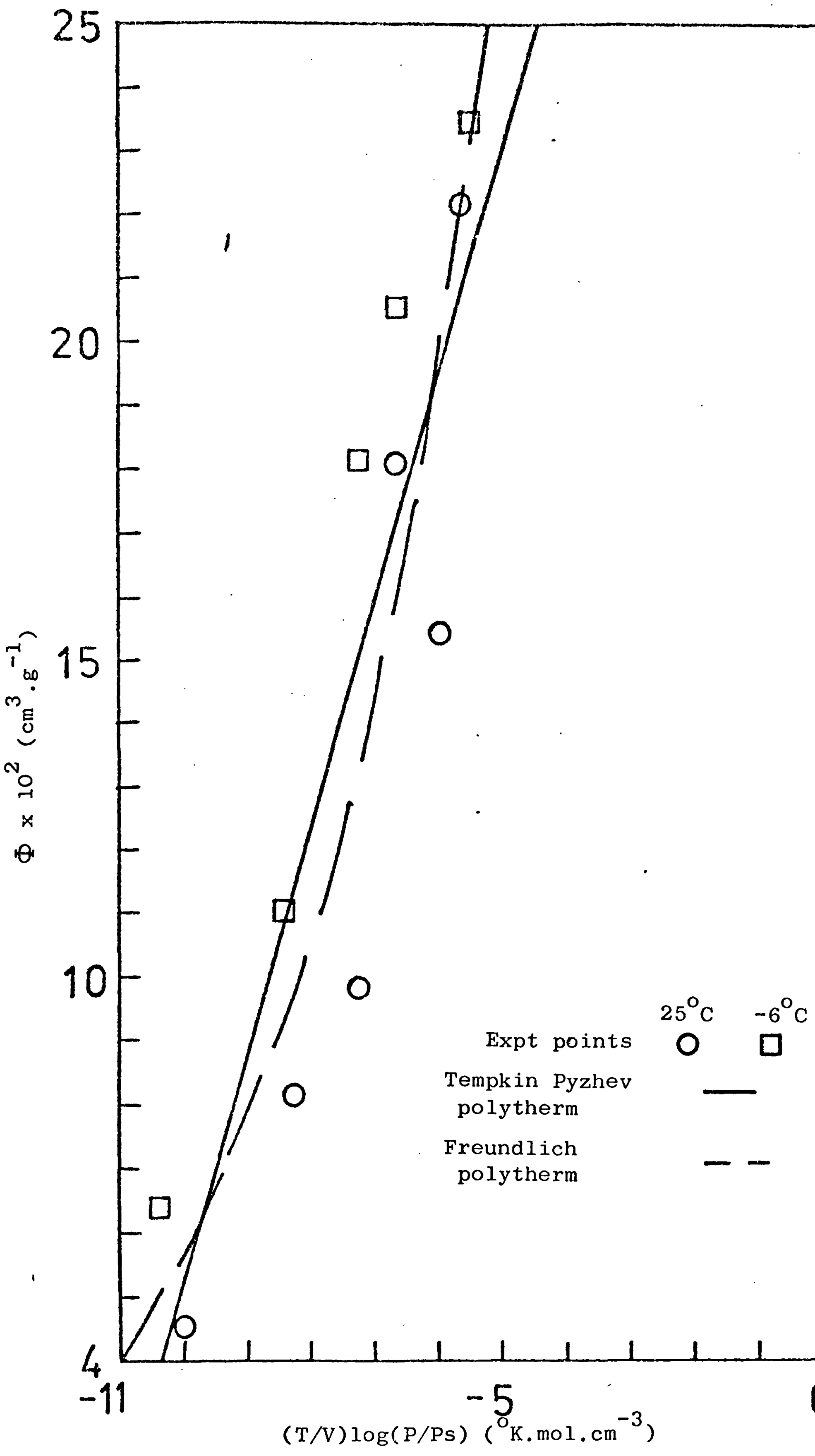

Figure 27: Tempkin-Pyzhev & Freundlich polytherm of ethane on Anthrasorb CC818M at various temperatures.

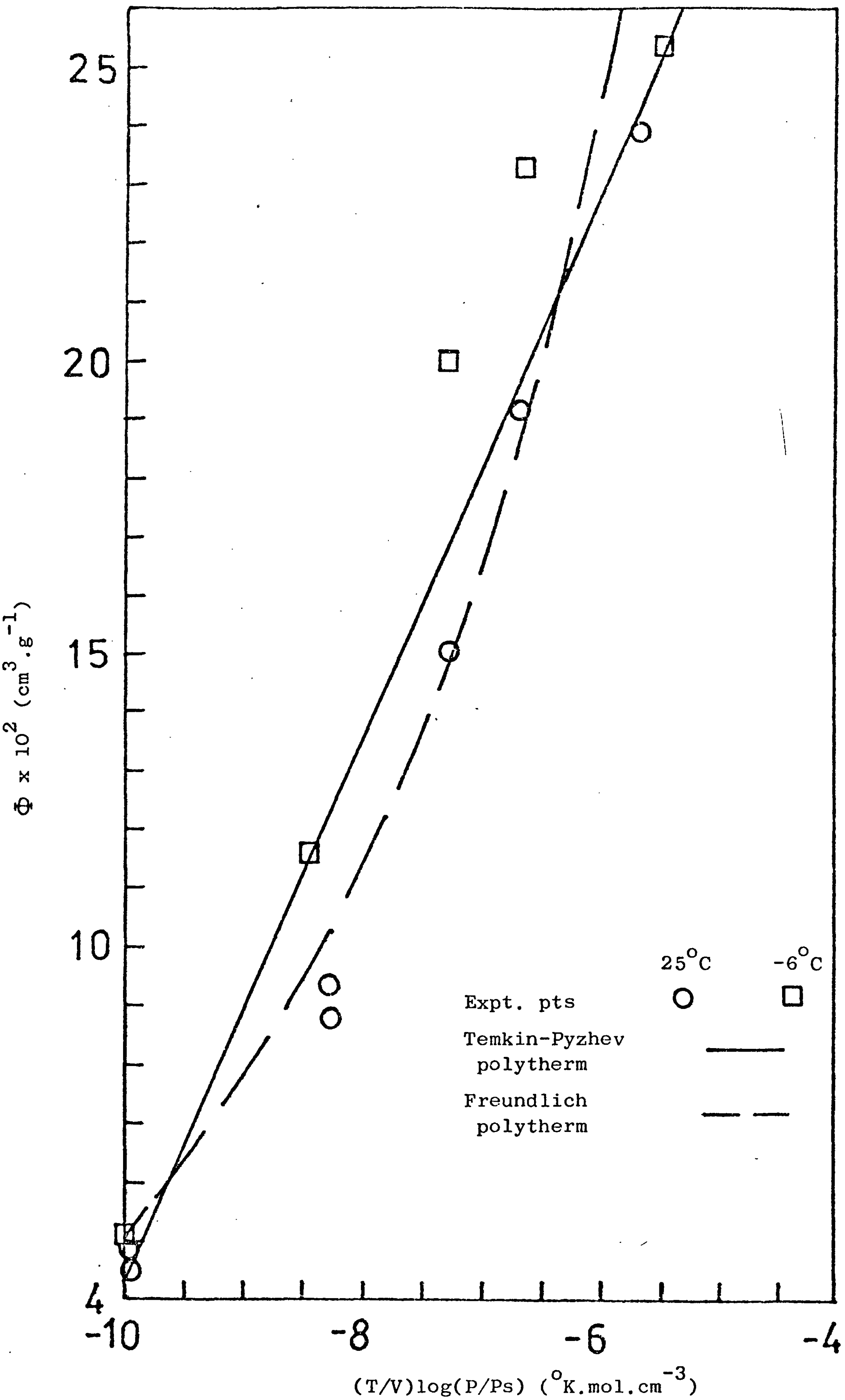

Figure 28: Freundlich and Temkin-Pyzhev polytherms for ethane on Anthrasorb CC818H

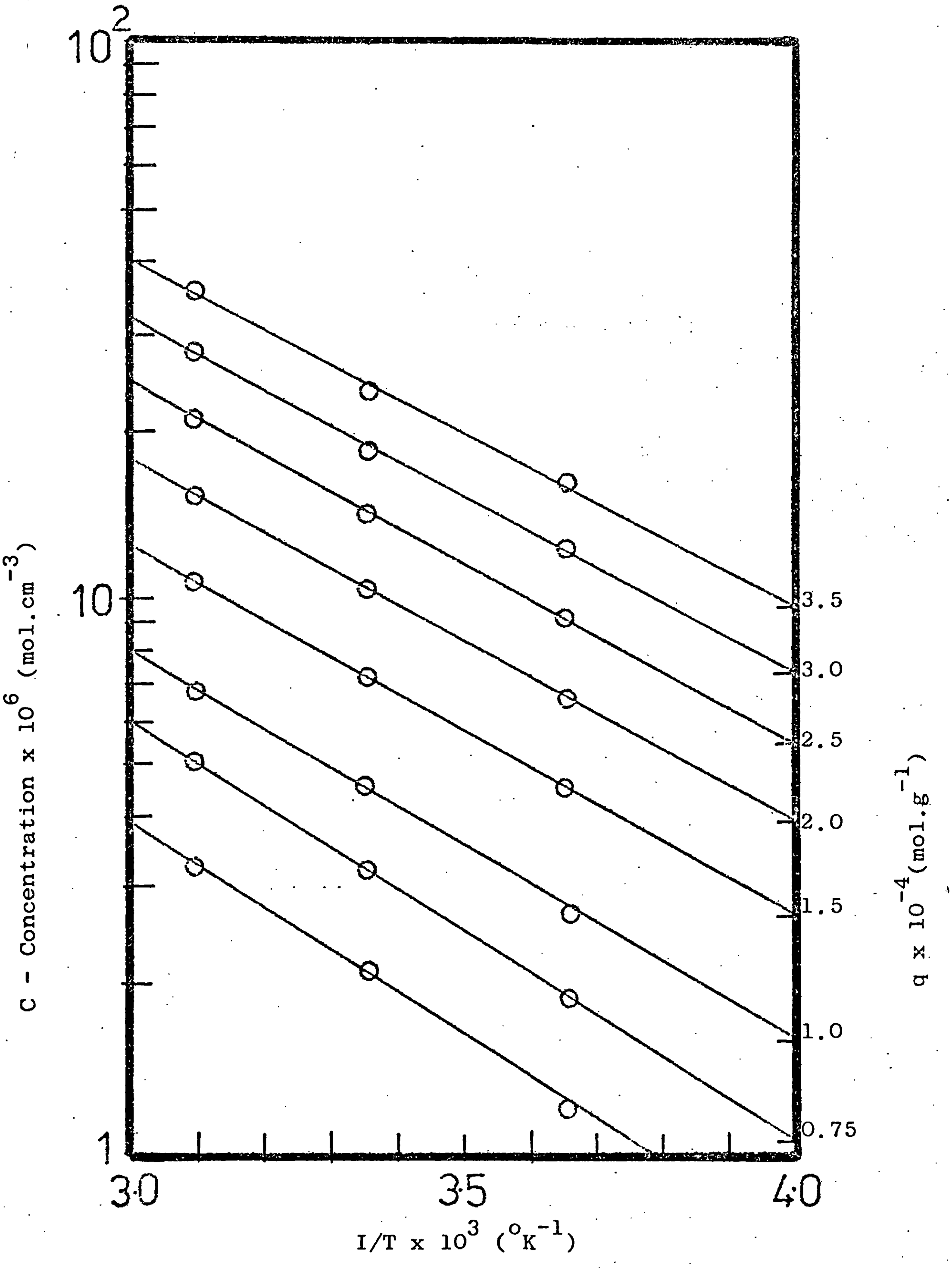

Figure 29: Equilibrium isosters for methane on Anthrasorb CC818M

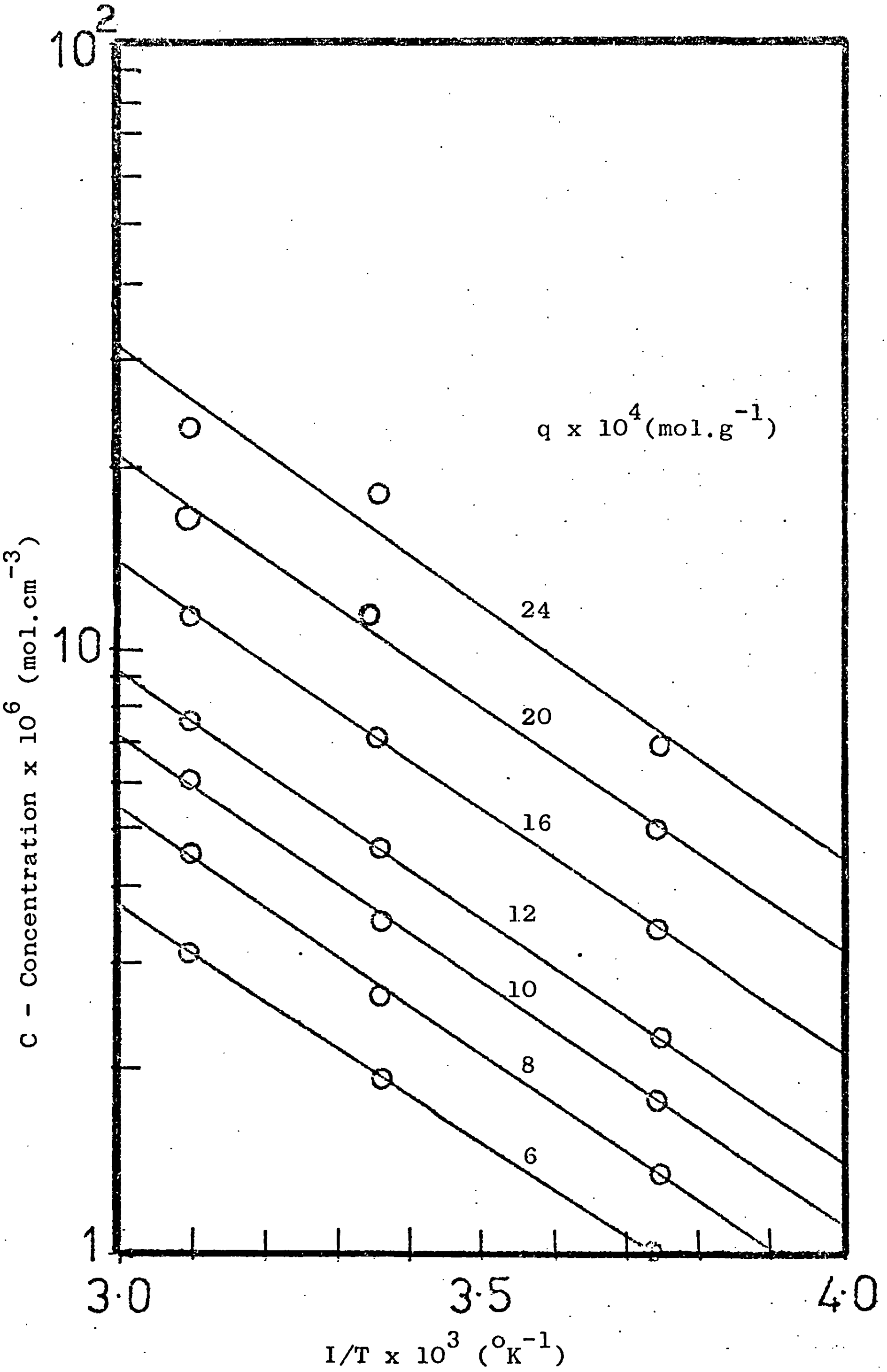

Figure 30: Equilibrium isosters for ethane on Anthrasorb CC818H

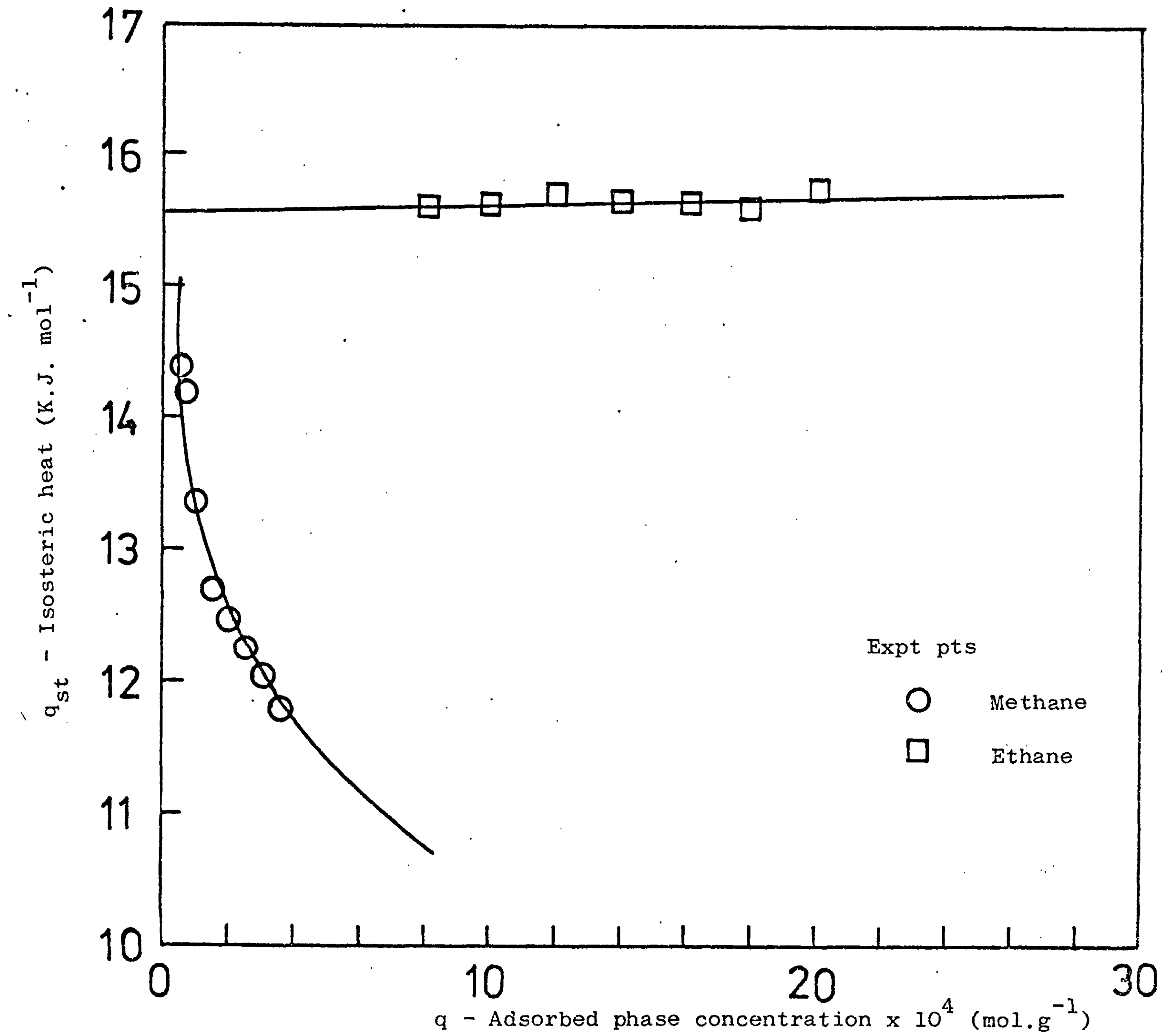

Figure 31: Isosteric heat of adsorption for methane and ethane on Anthrasorb CC818M

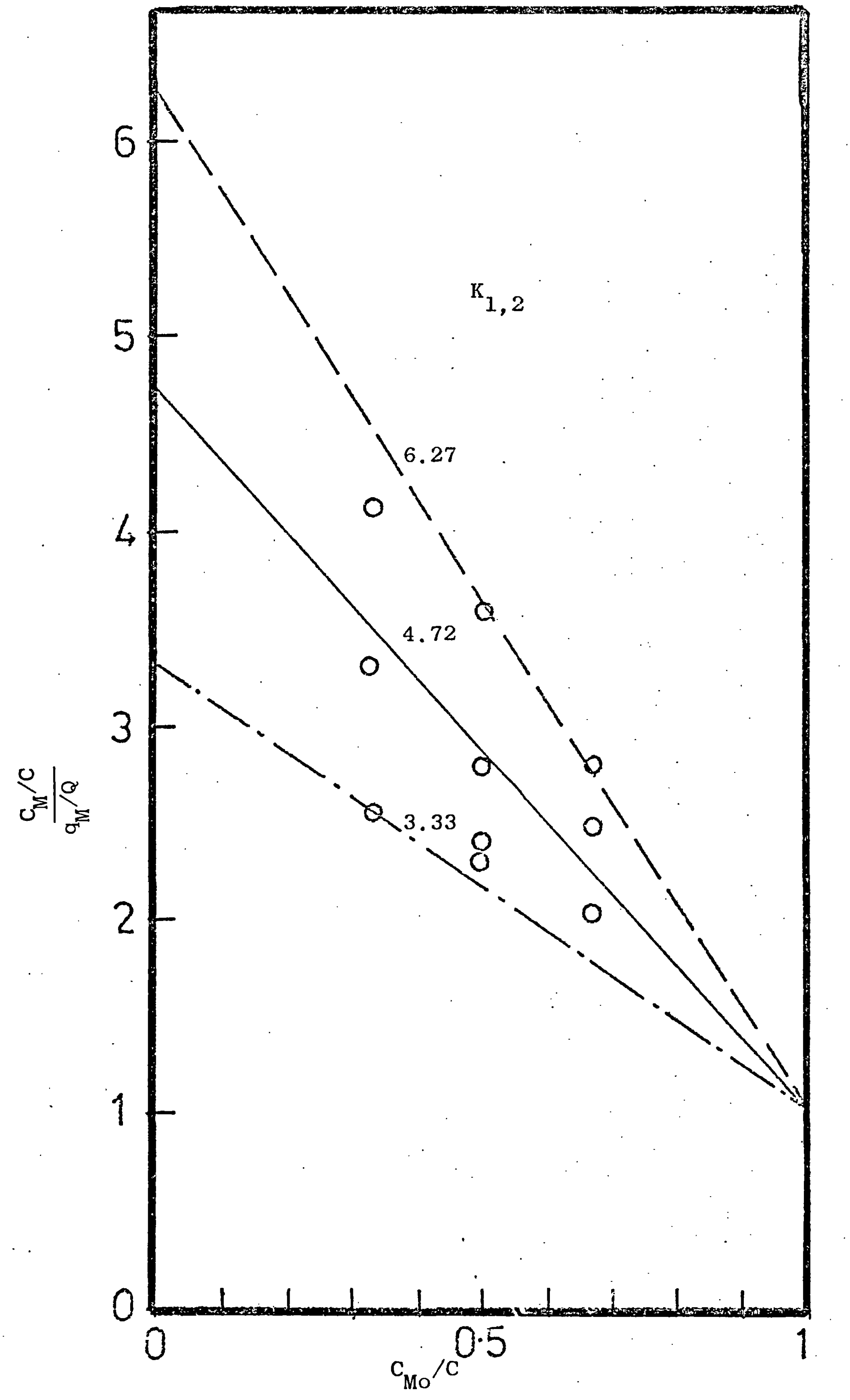

Figure 32: Binary adsorption data on Anthrasorb CC818M

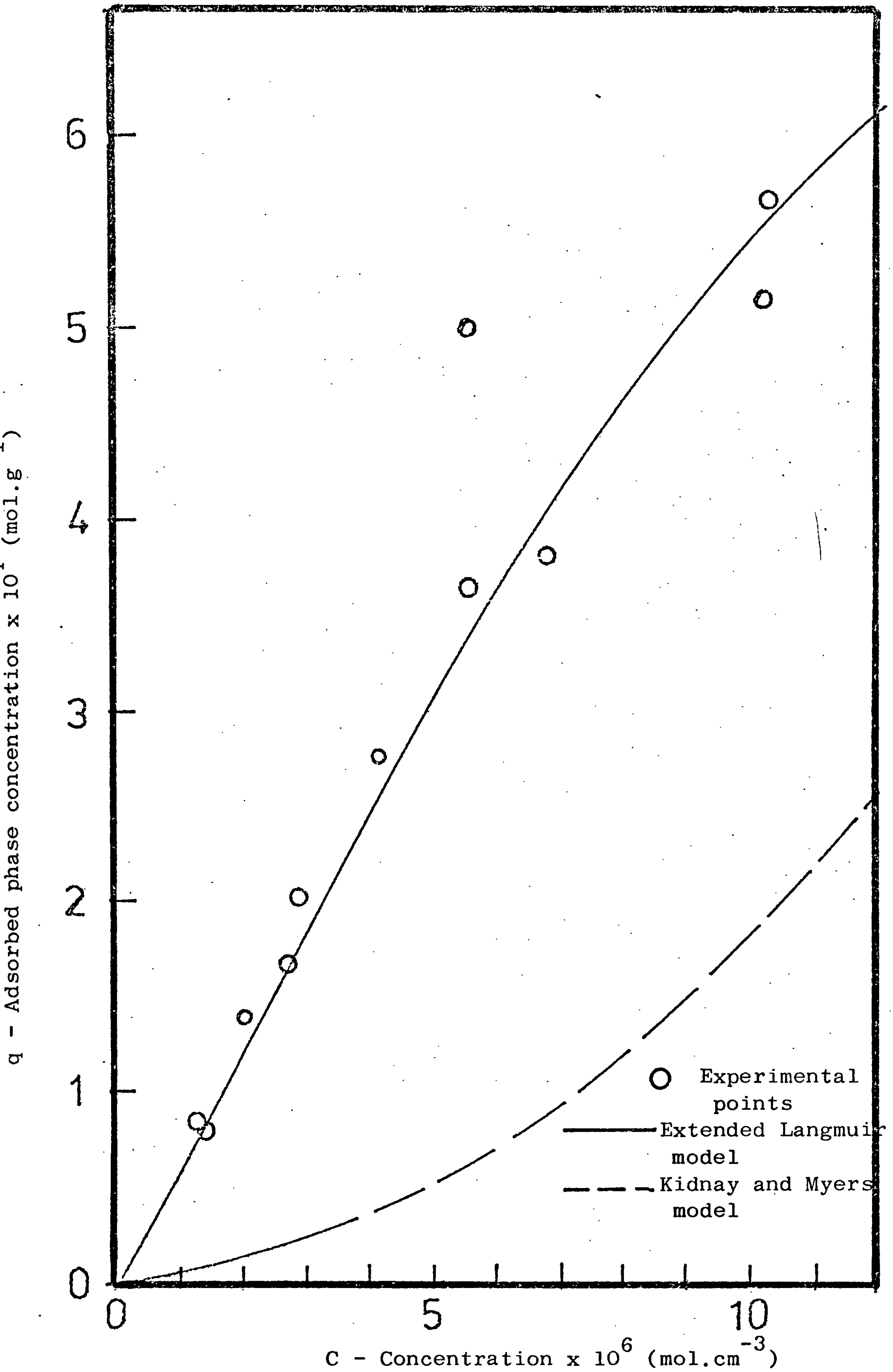

Figure 33: Binary correlation of methane on Anthrasorb CC818M

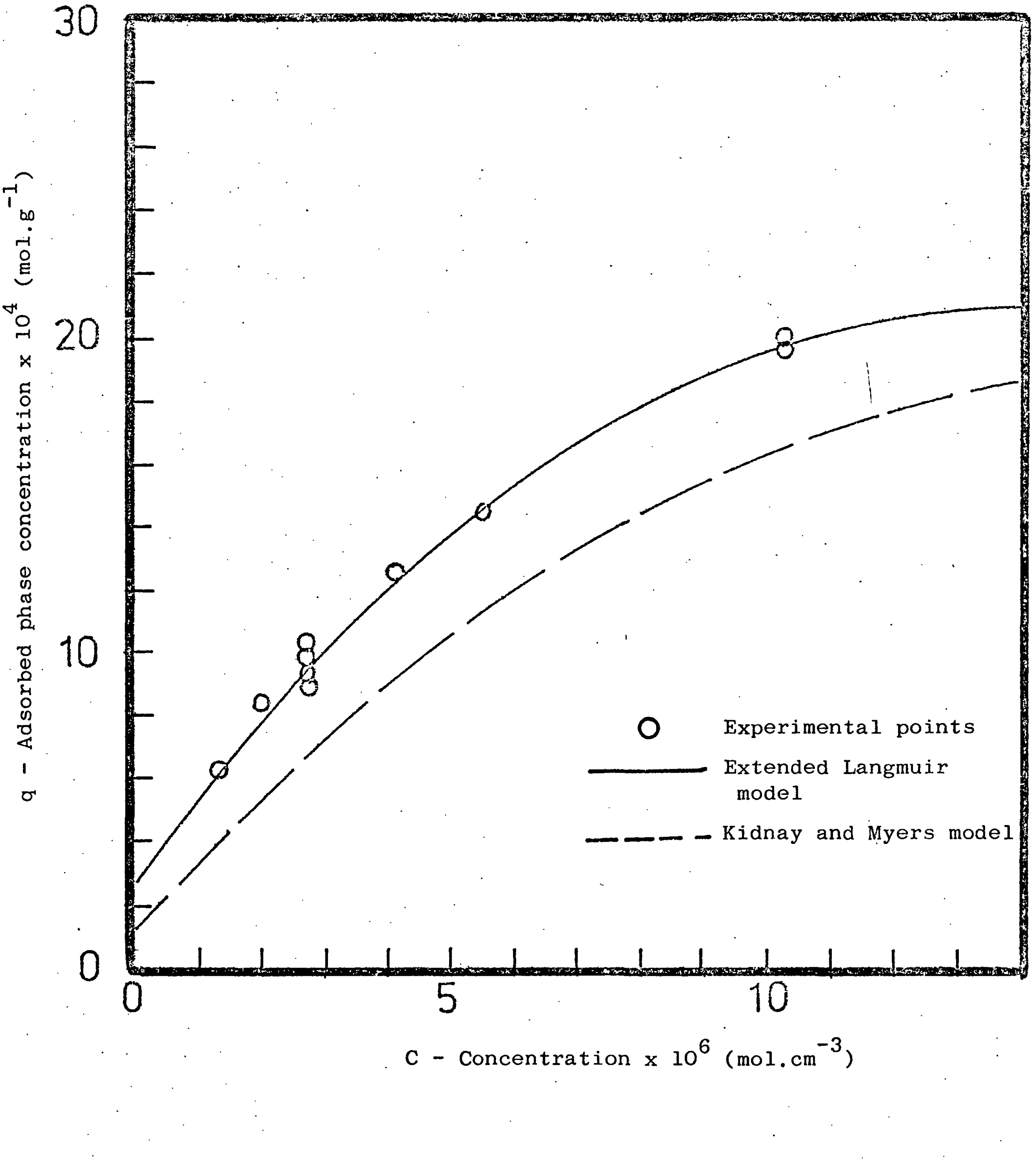

Figure 34: Binary correlation of ethane on Anthrasorb CC818M

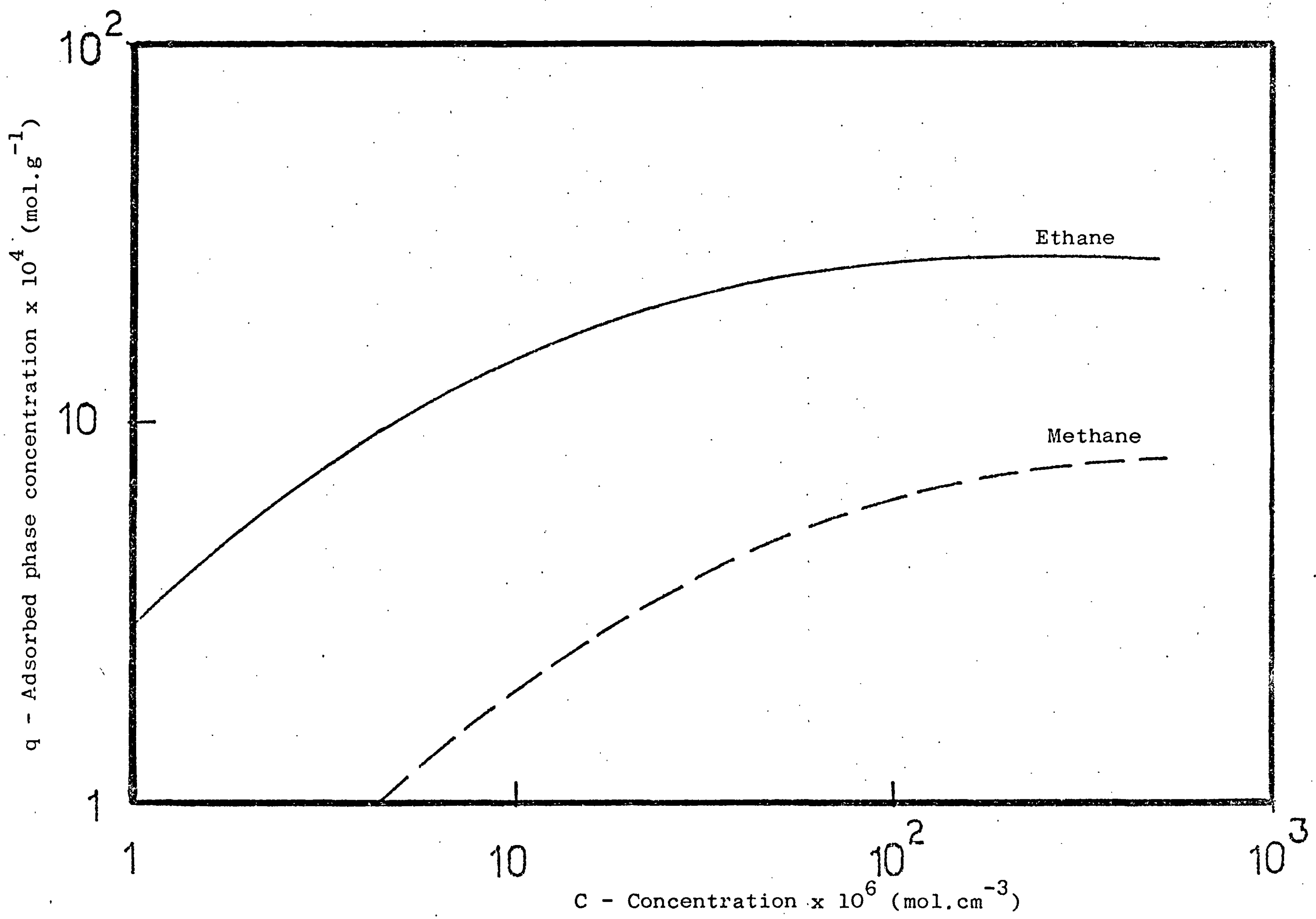

Figure 35: Single component isotherm logarithmic plots displaying variation of separation factor $K_{1,2}$

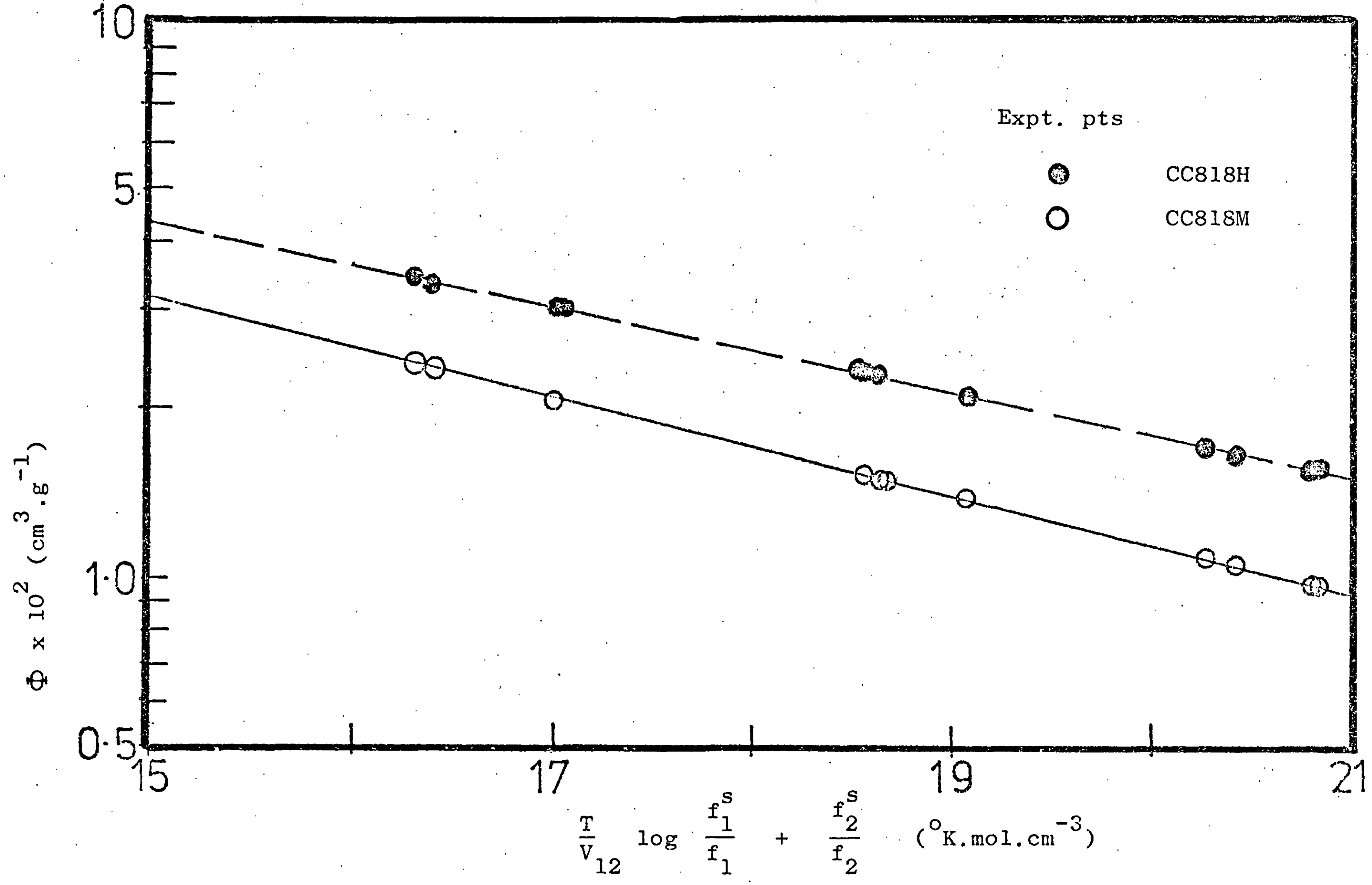

Figure 36: Correlation curves for methane-ethane mixtures on Anthrasorb CC818H and CC818M at 25°C.

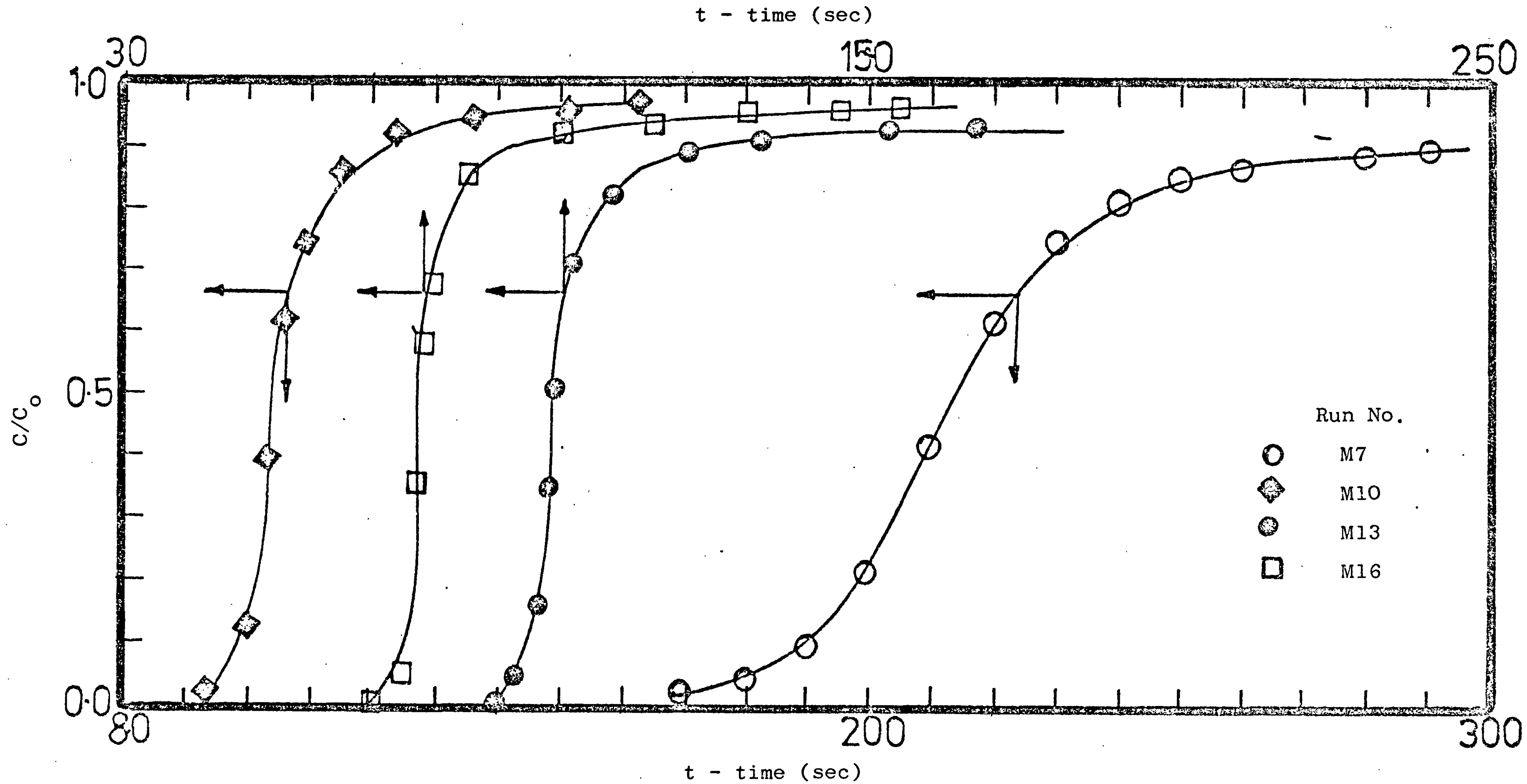

Figure 37: Experimental breakthrough curves for methane on Anthrasorb CC818M at $0^{o}C$

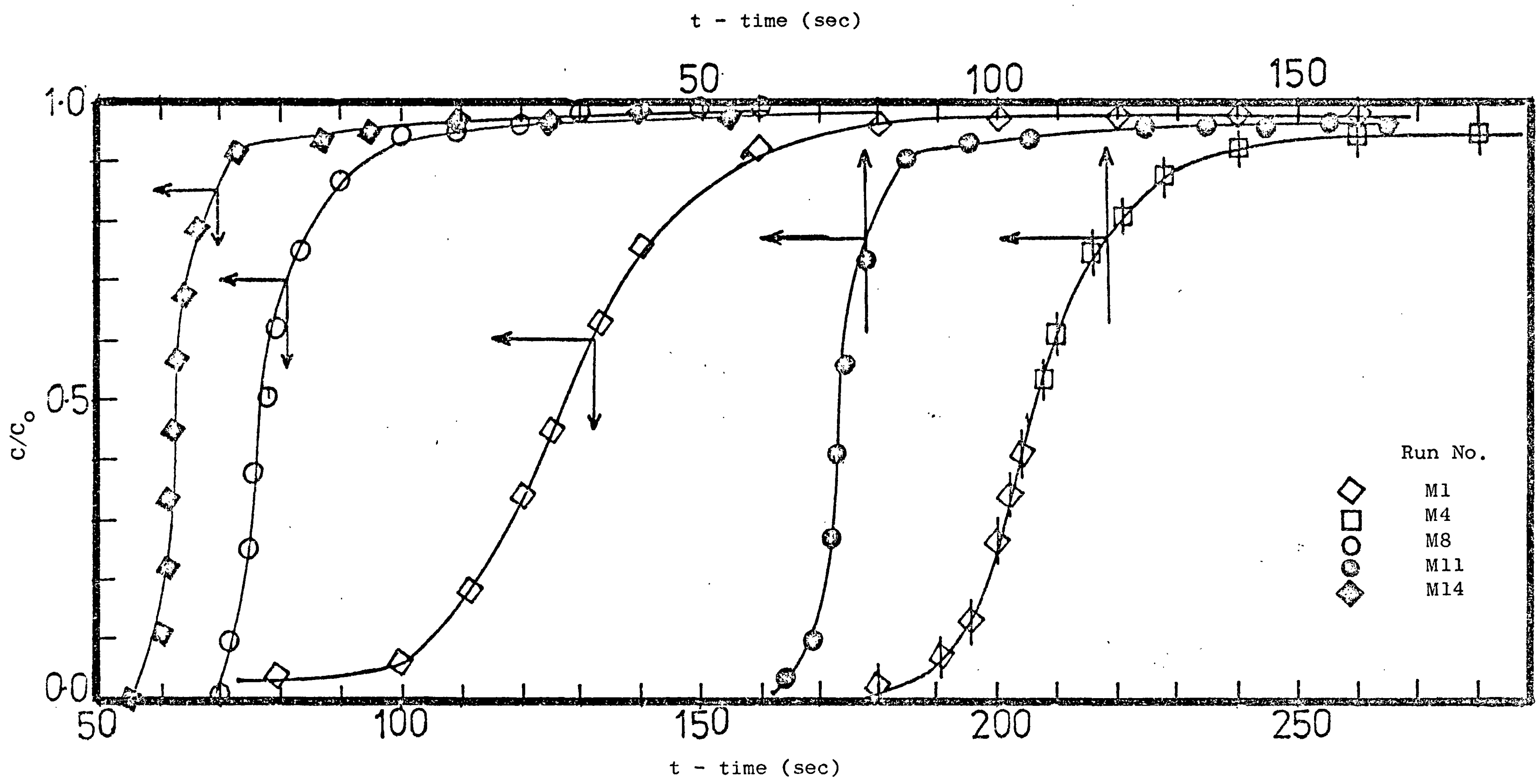

Figure 38: Experimental breakthrough curves for methane on Anthrasorb CC818M at 25^{o}C.

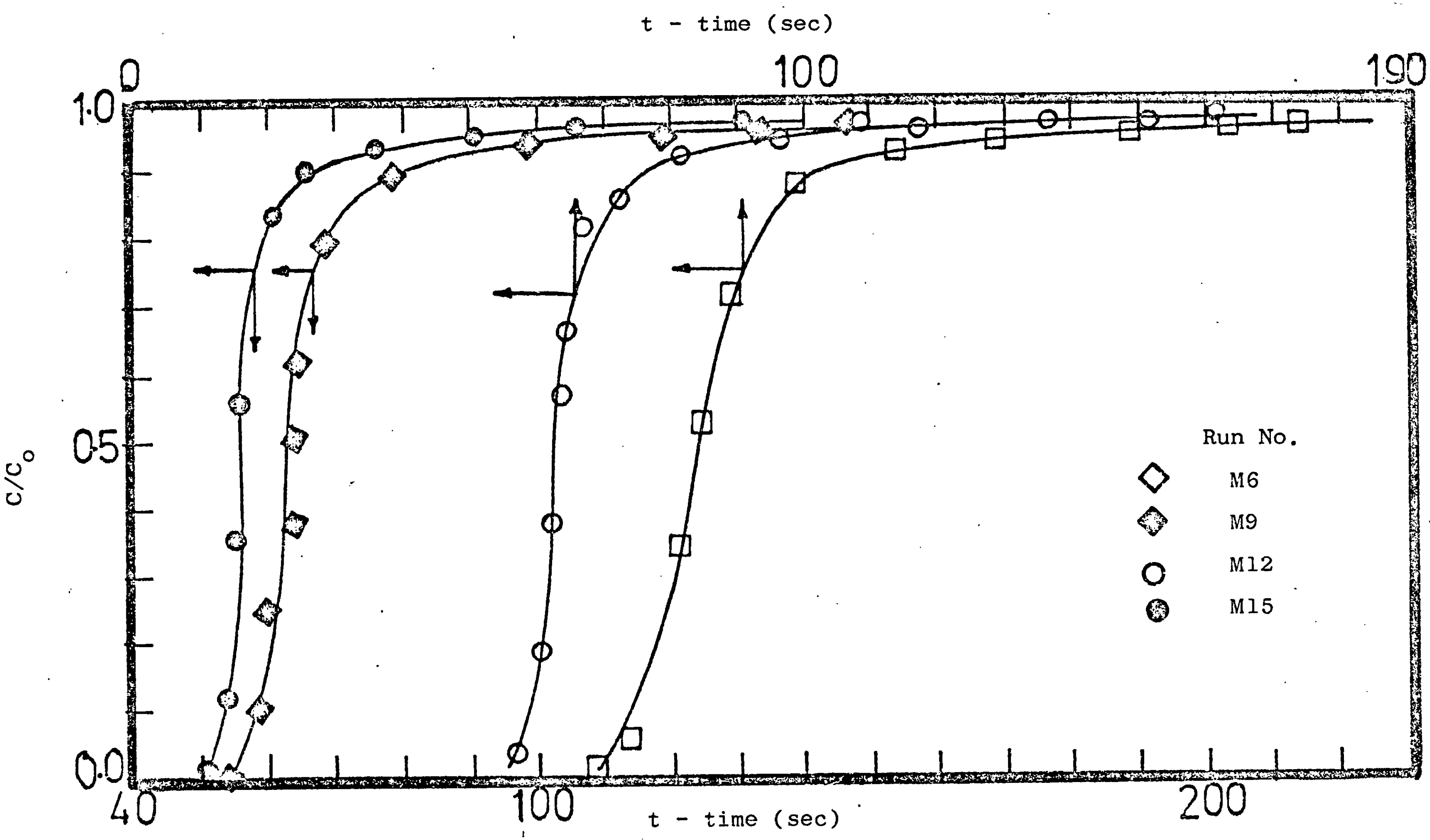

Figure 39: experimental breakthrough curves for methane on Anthrasorb CC818M at 50^{o}C

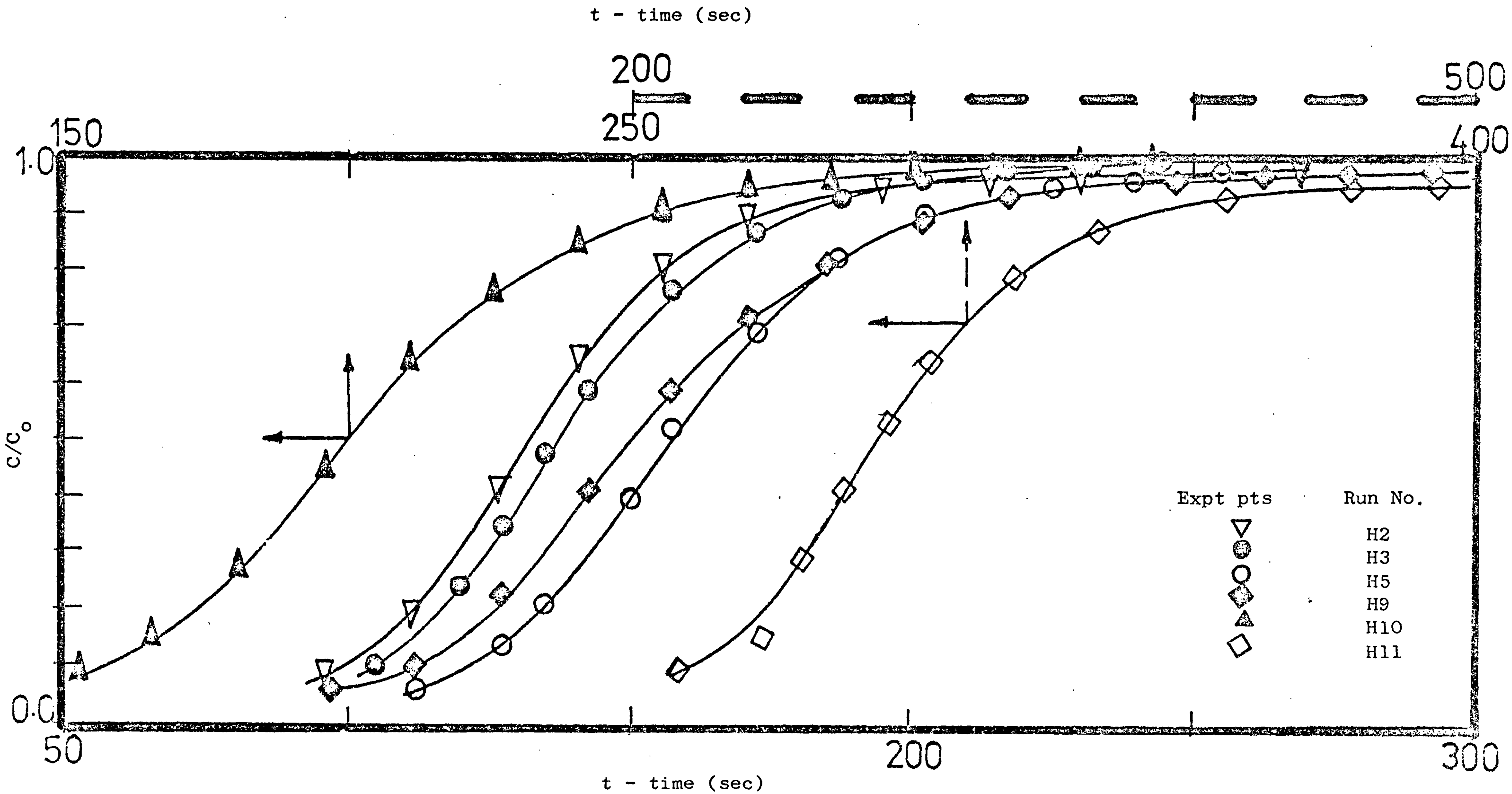

Figure 40: Experimental breakthrough curves for methane on Anthrasorb CC818H at 25°C.

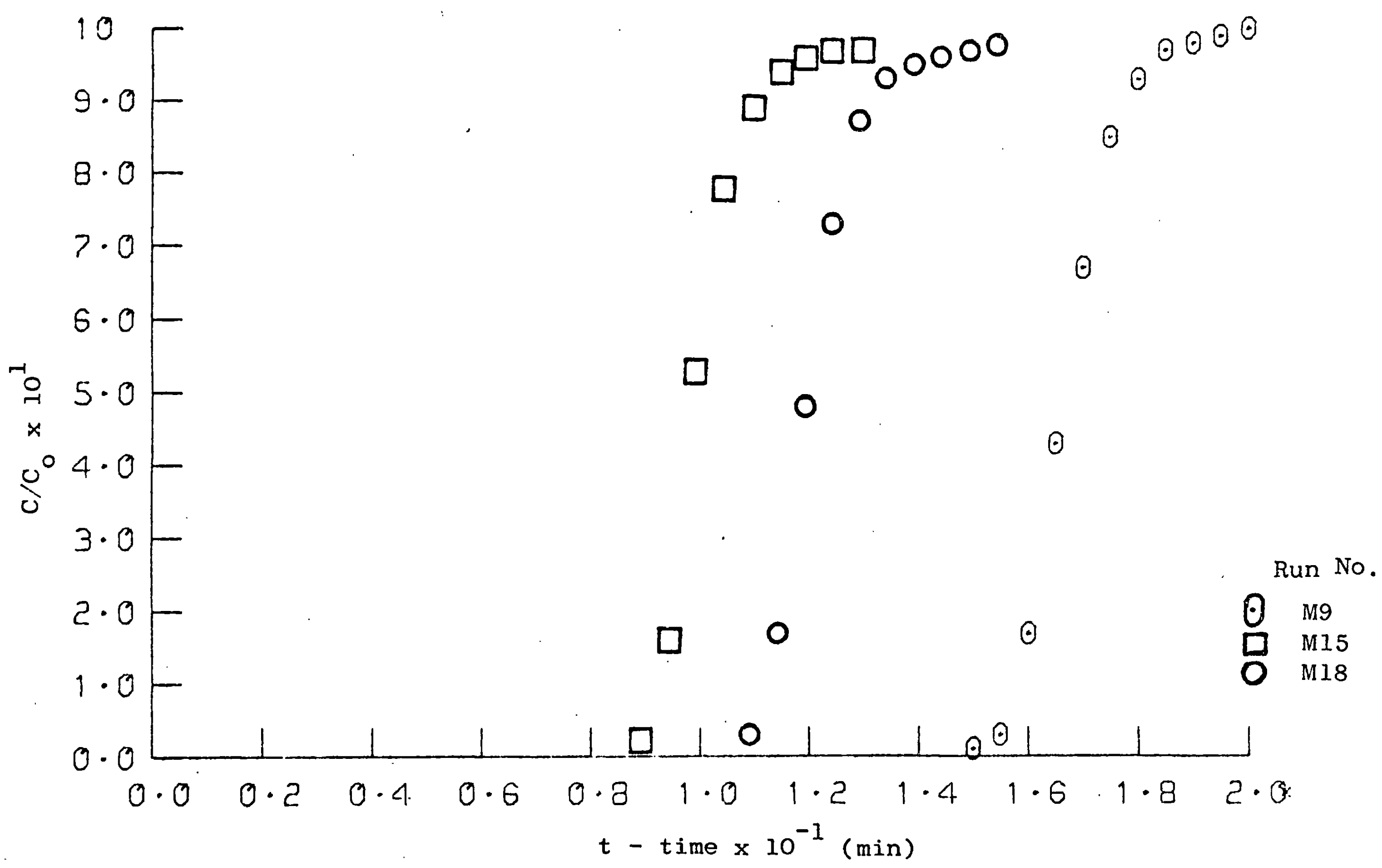

Figure 41: Experimental breakthrough curves for ethane on Anthrasorb CC818M at -6°C.

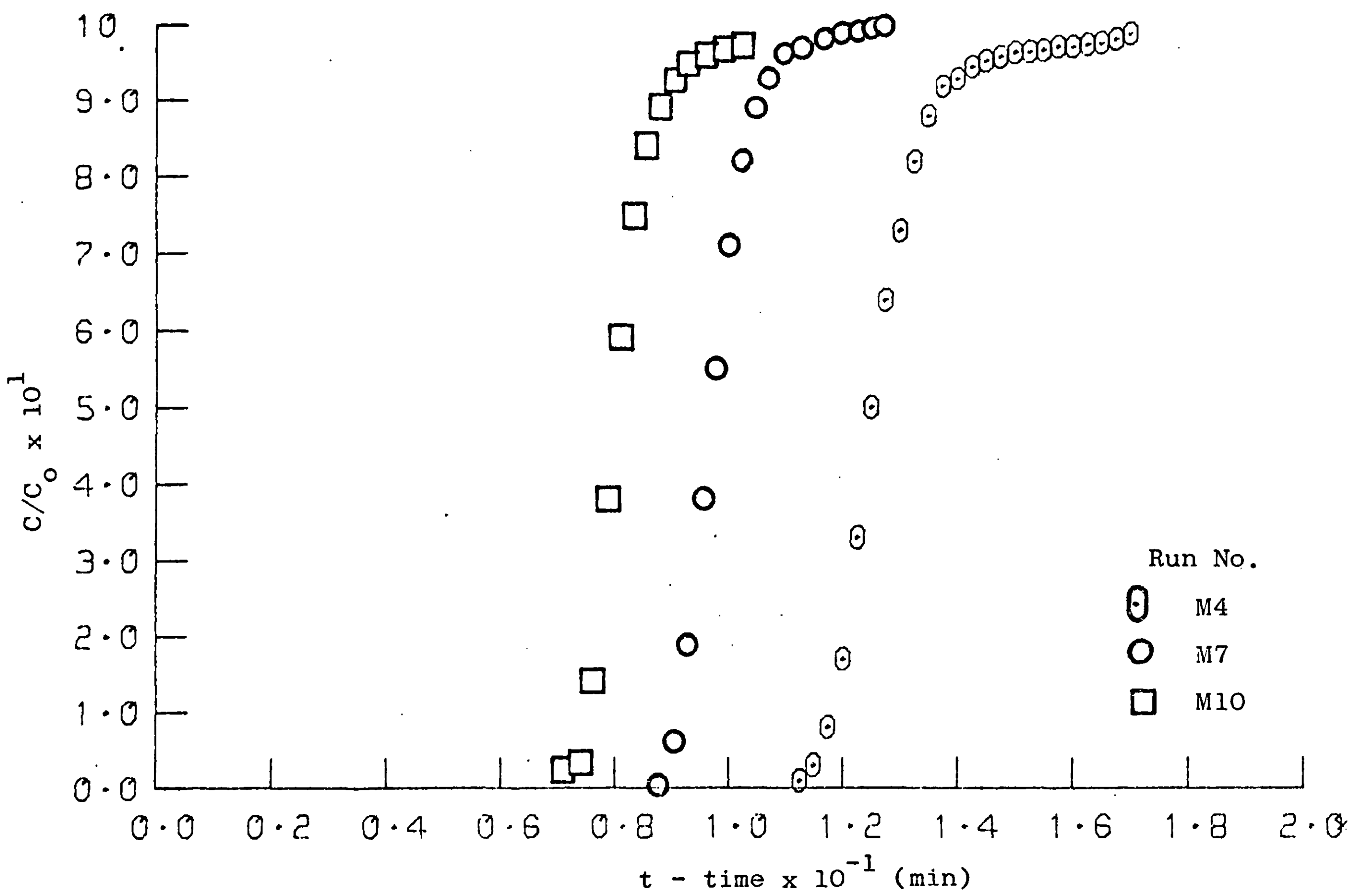

Figure 42: Experimental breakthrough curves for ethane on Anthrasorb CC818M at 25^{o}C.

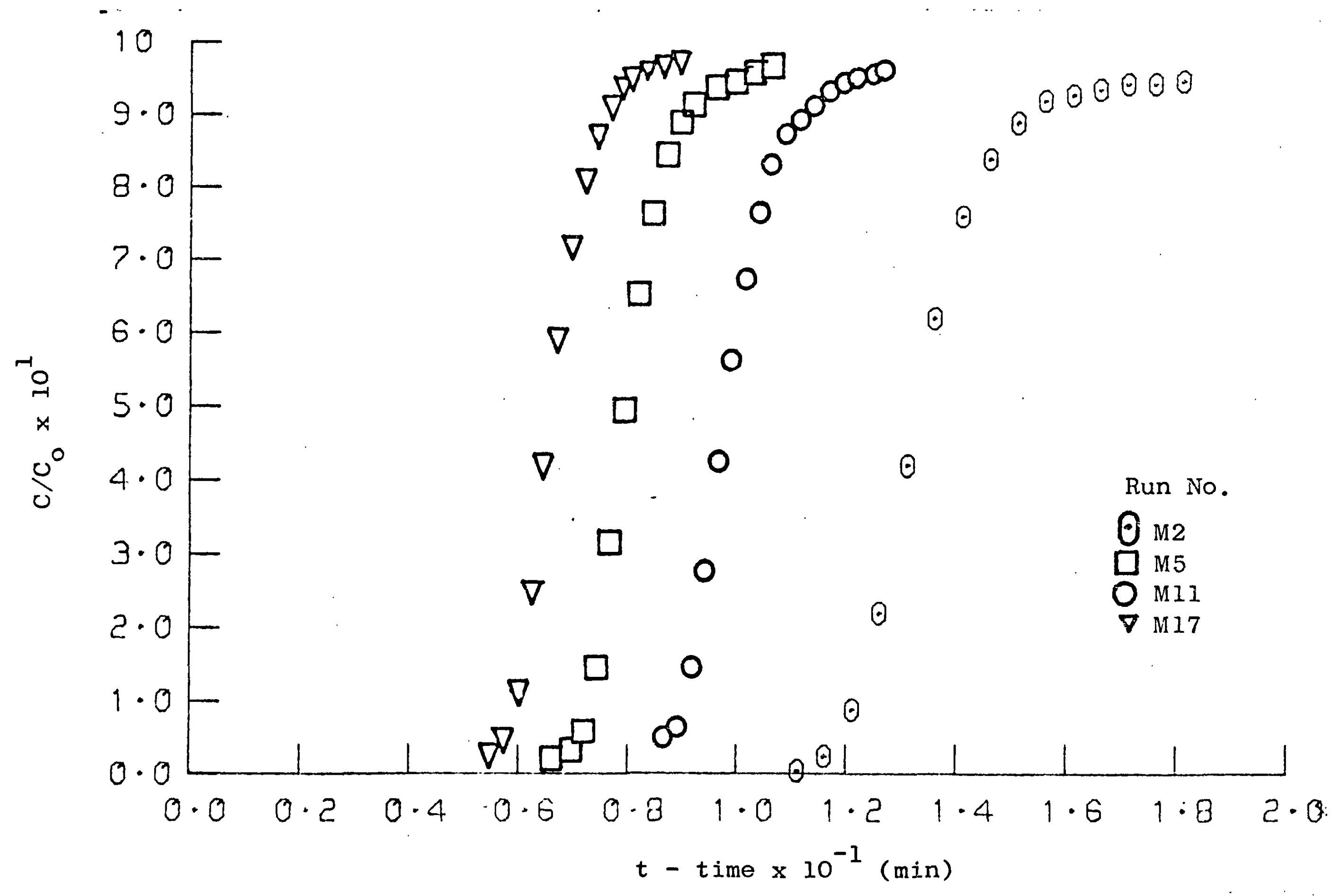

Figure 43: Experimental breakthrough curves for ethane on Anthrasorb CC818M at 50°C.

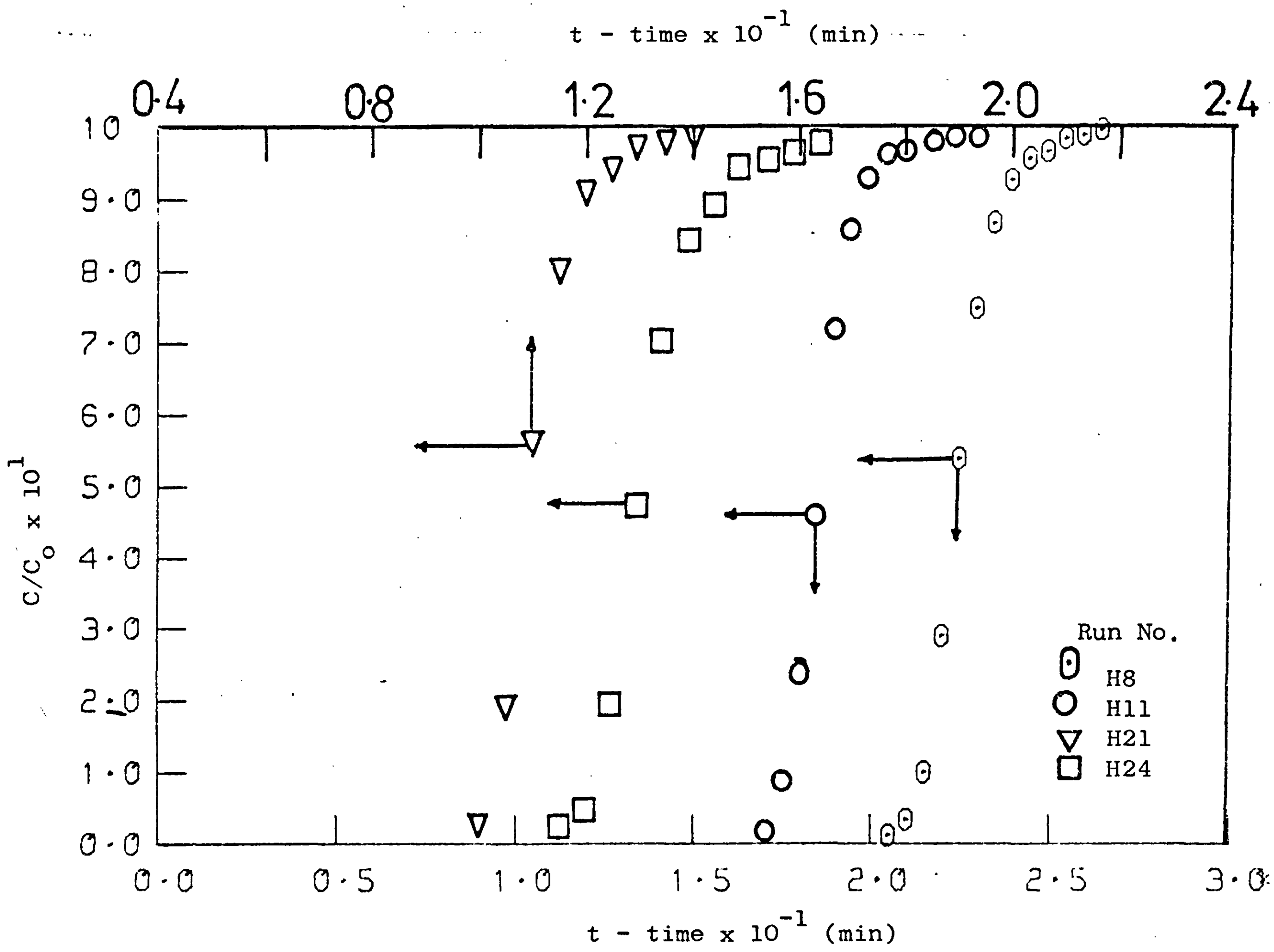

Figure 44: Experimental breakthrough curves for ethane on Anthrasorb CC818H at $-6^{o}C$.

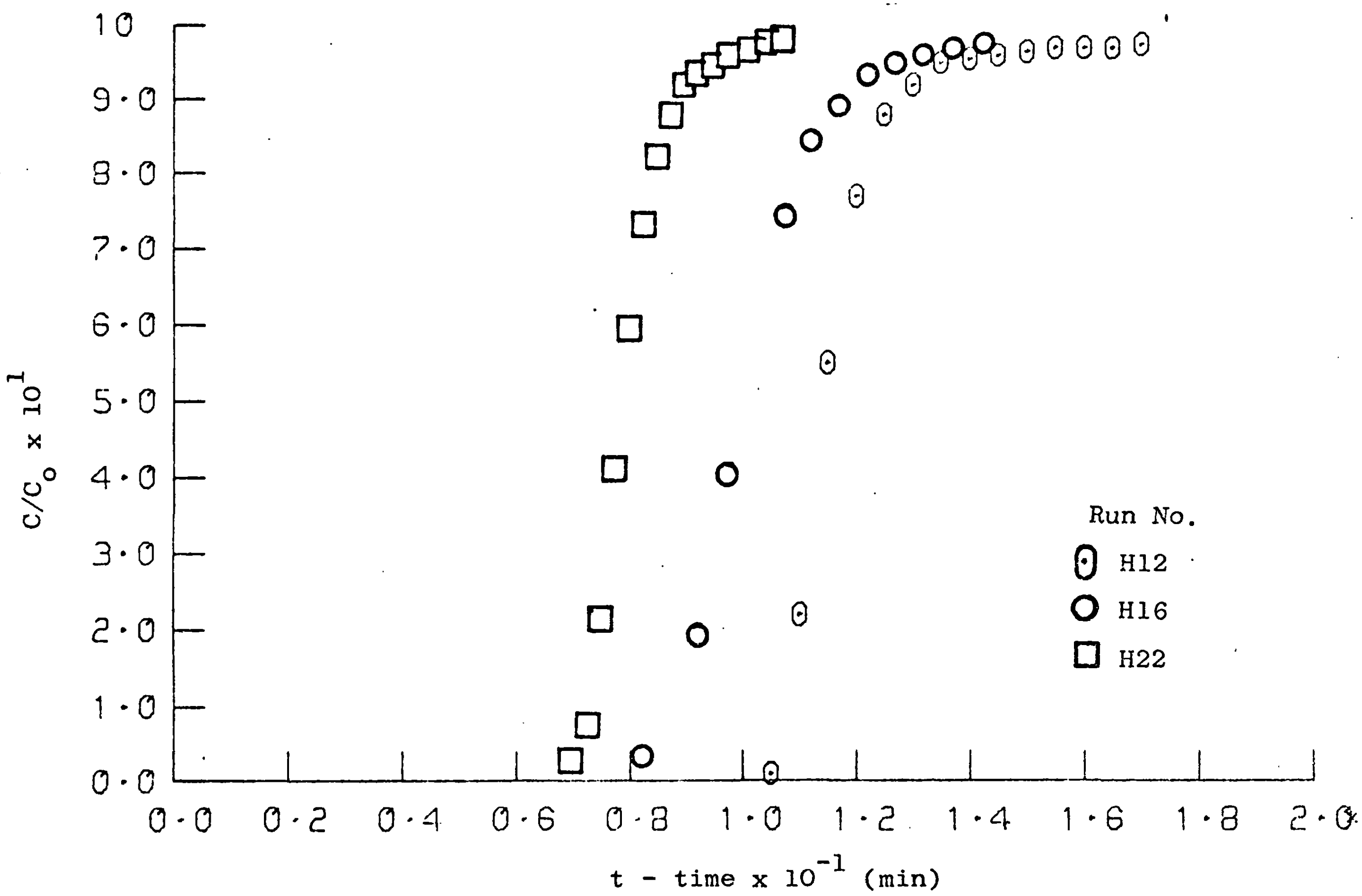

Figure 45: Experimental breakthrough curves for ethane on Anthrasorb CC818H at $25^{o}C$.

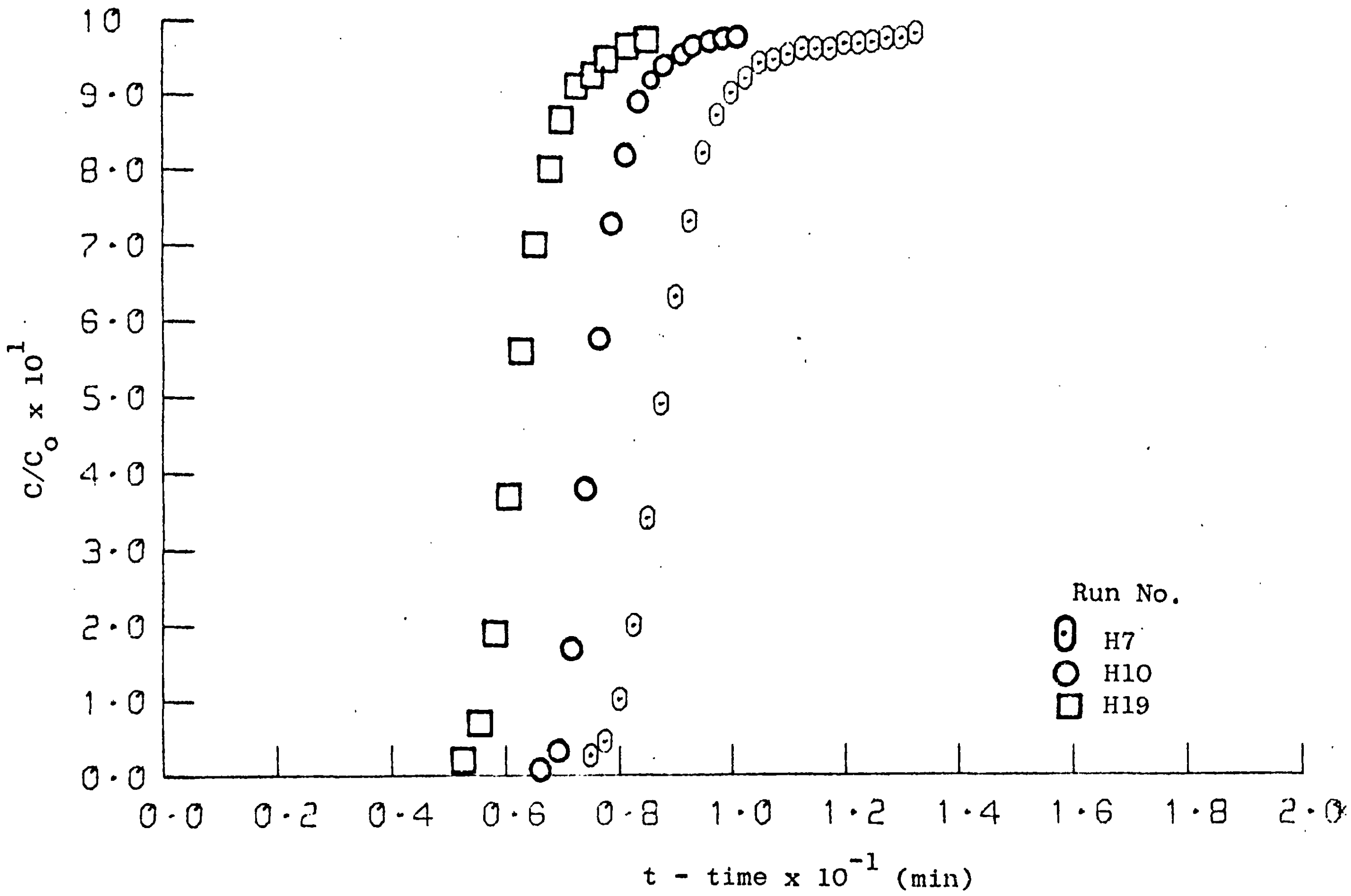

Figure 46: Experimental breakthrough curves for ethane on Anthrasorb CC818H at 50°C.

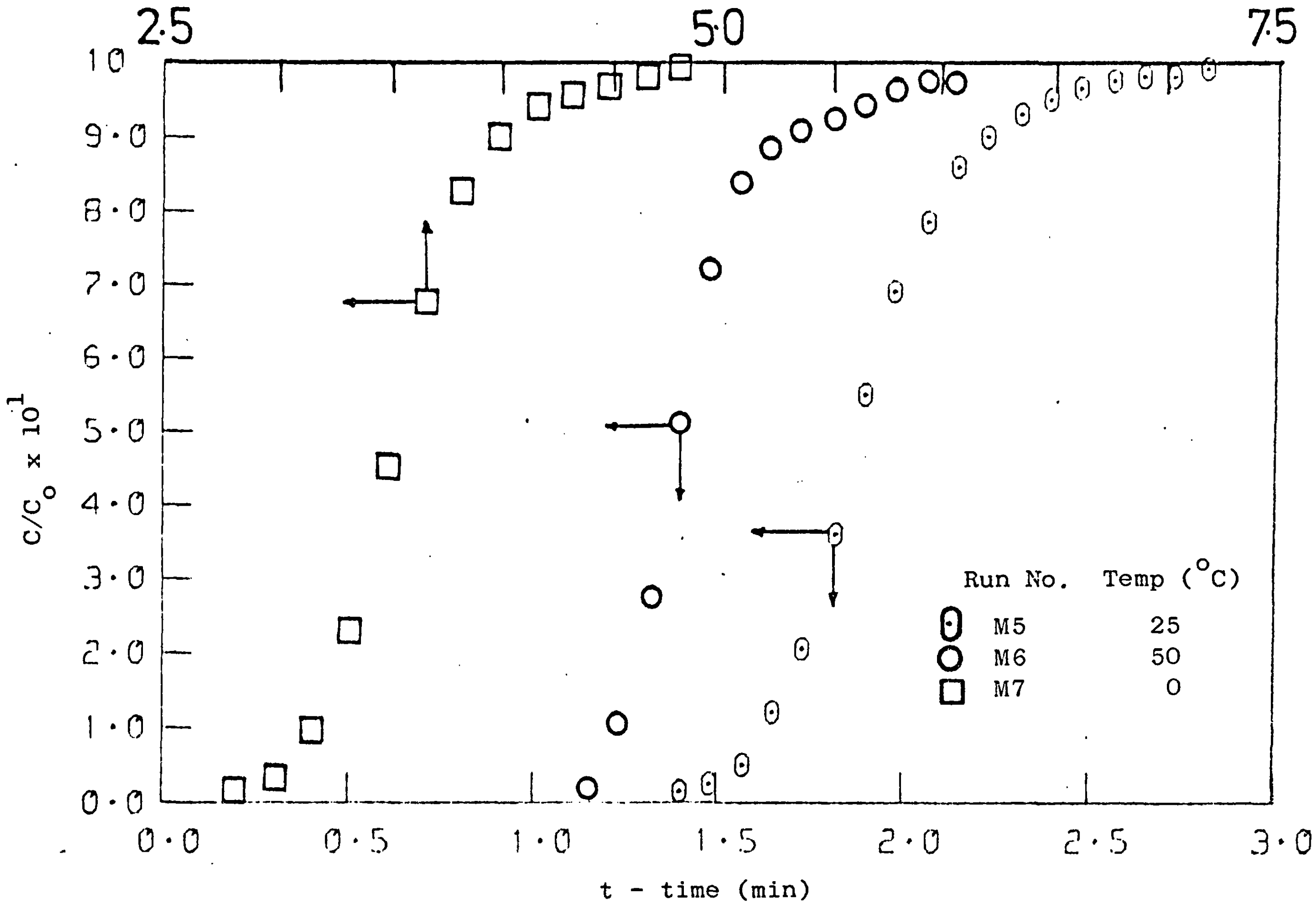

Figure 47: Experimental breakthrough curves for methane on Anthrasorb CC818M at various temperatures.

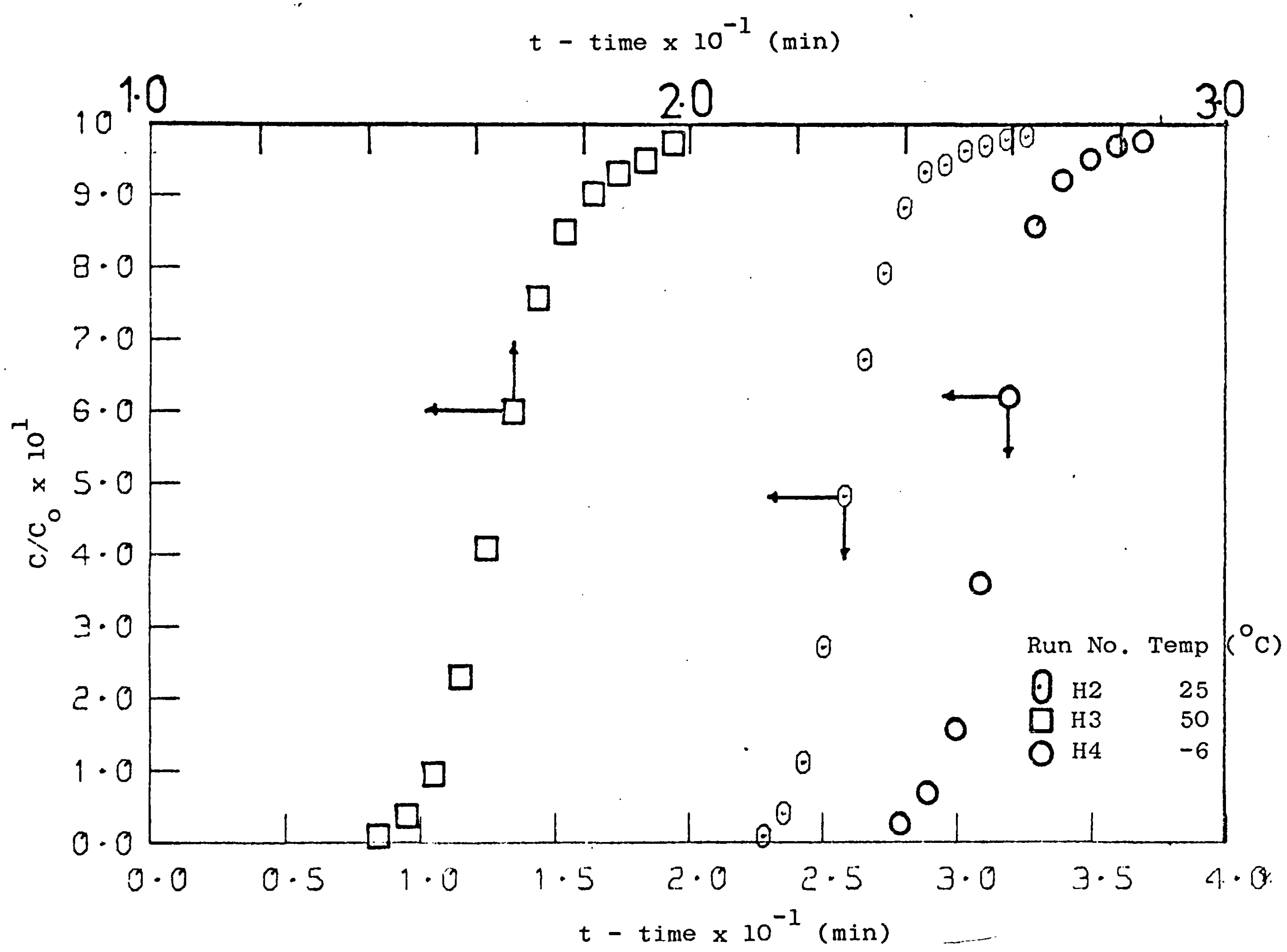

Figure 48: Experimental breakthrough curves for ethane on Anthrasorb CC818H at various temperatures.

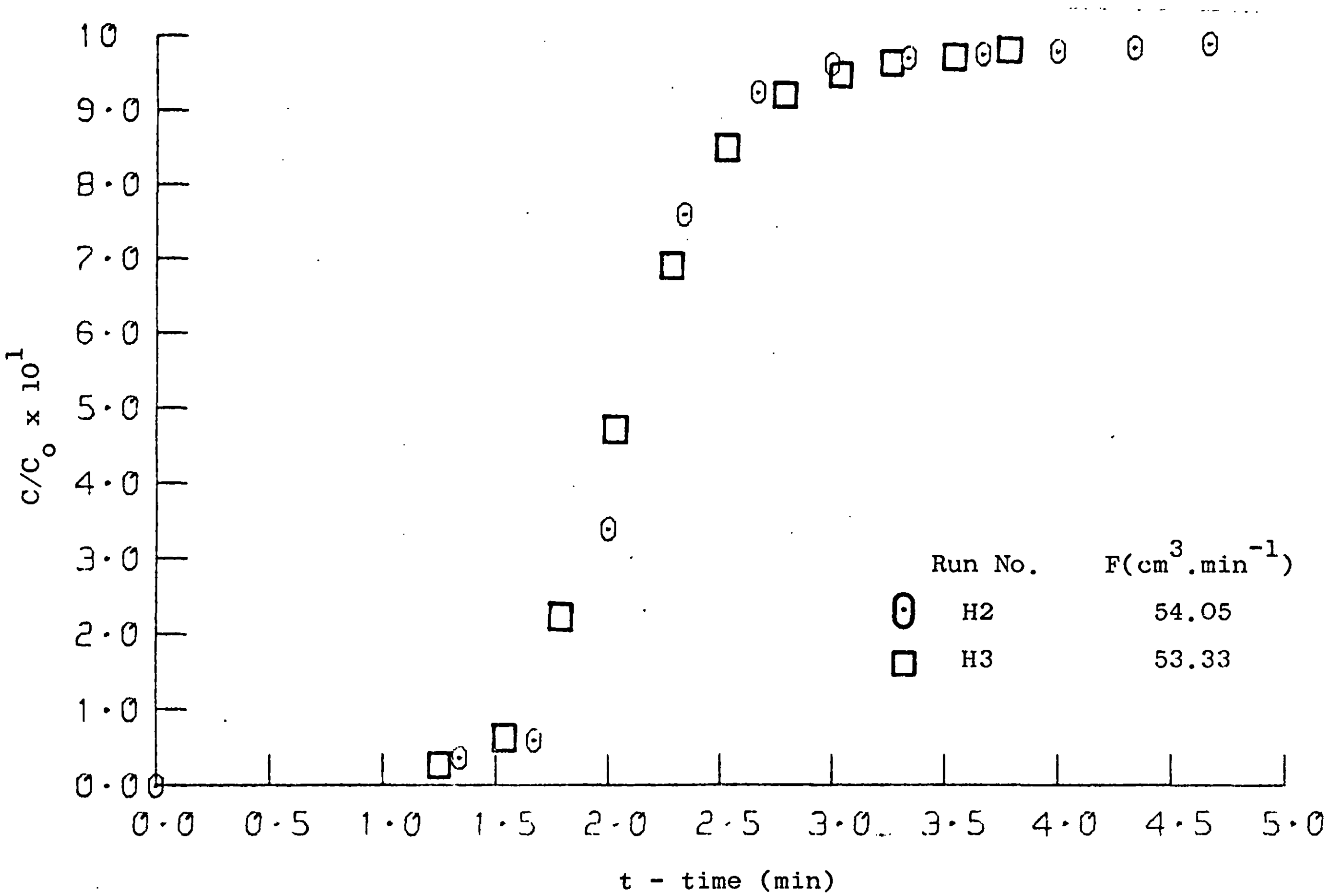

Figure 49: Reproducibility test for methane on Anthrasorb CC818H at 25°C.
$C_o = 4.17 \times 10^{-6}$ mol.cm^{-3}, $m = 3.0$ g

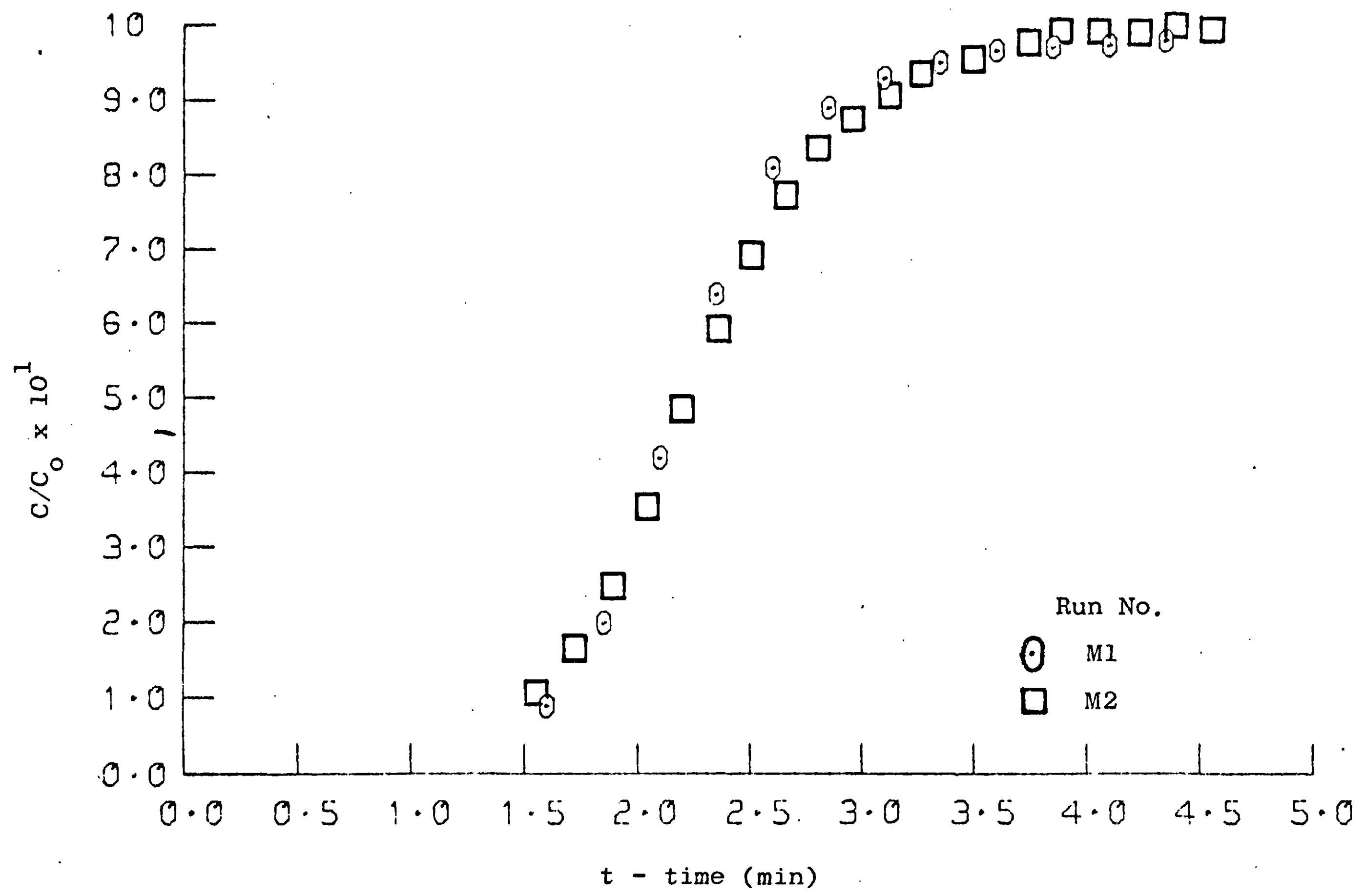

Figure 50: Reproducibility test for methane on Anthrasorb CC818M at 25°C.

$C_o = 1.39 \times 10^{-6}$ mol.cm^{-3}, m = 3.0 g, F = 35 cm^3.min^{-1}

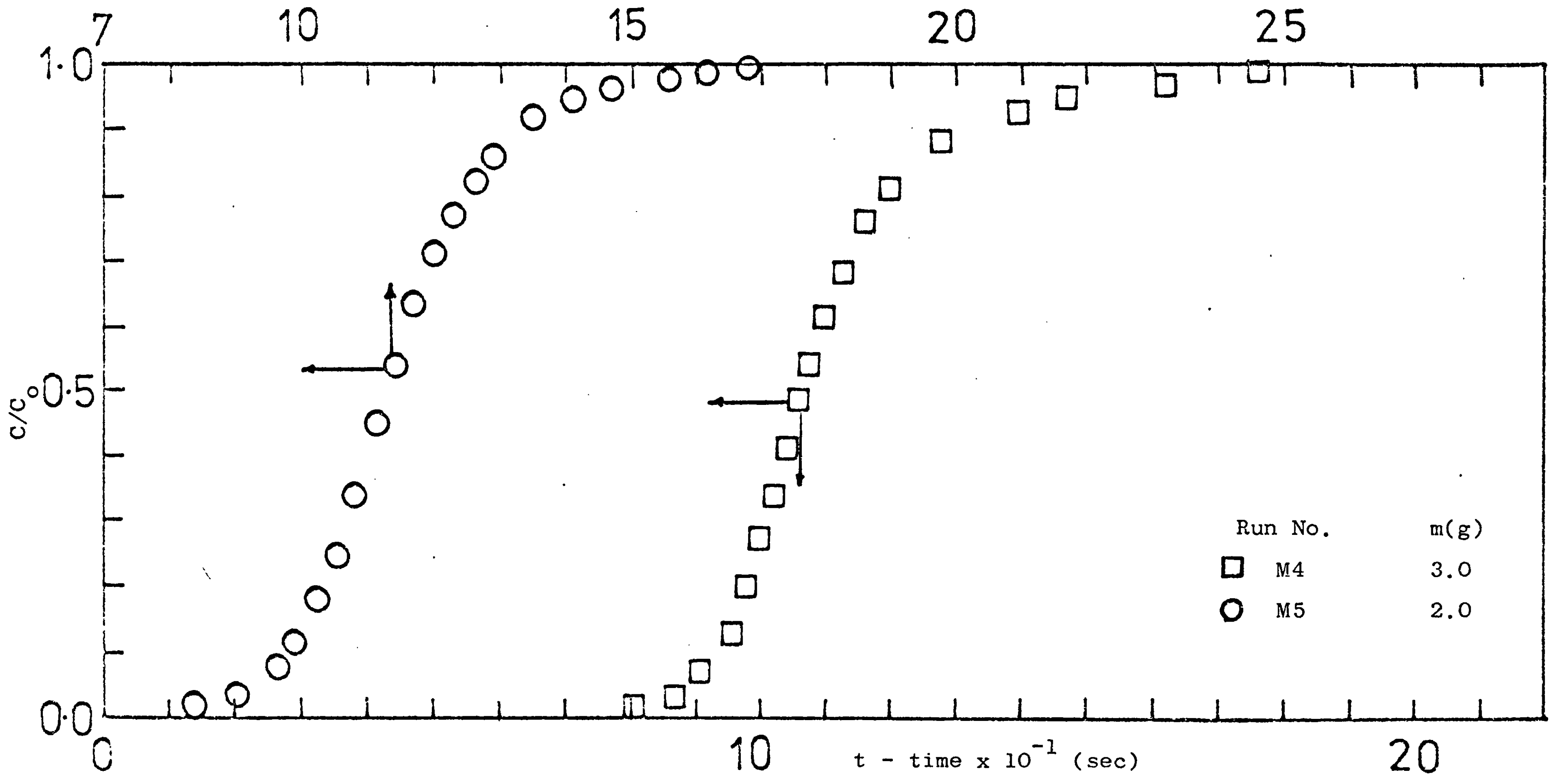

Figure 51: Constant pattern behaviour for methane on Anthrasorb CC818M at 25°C.

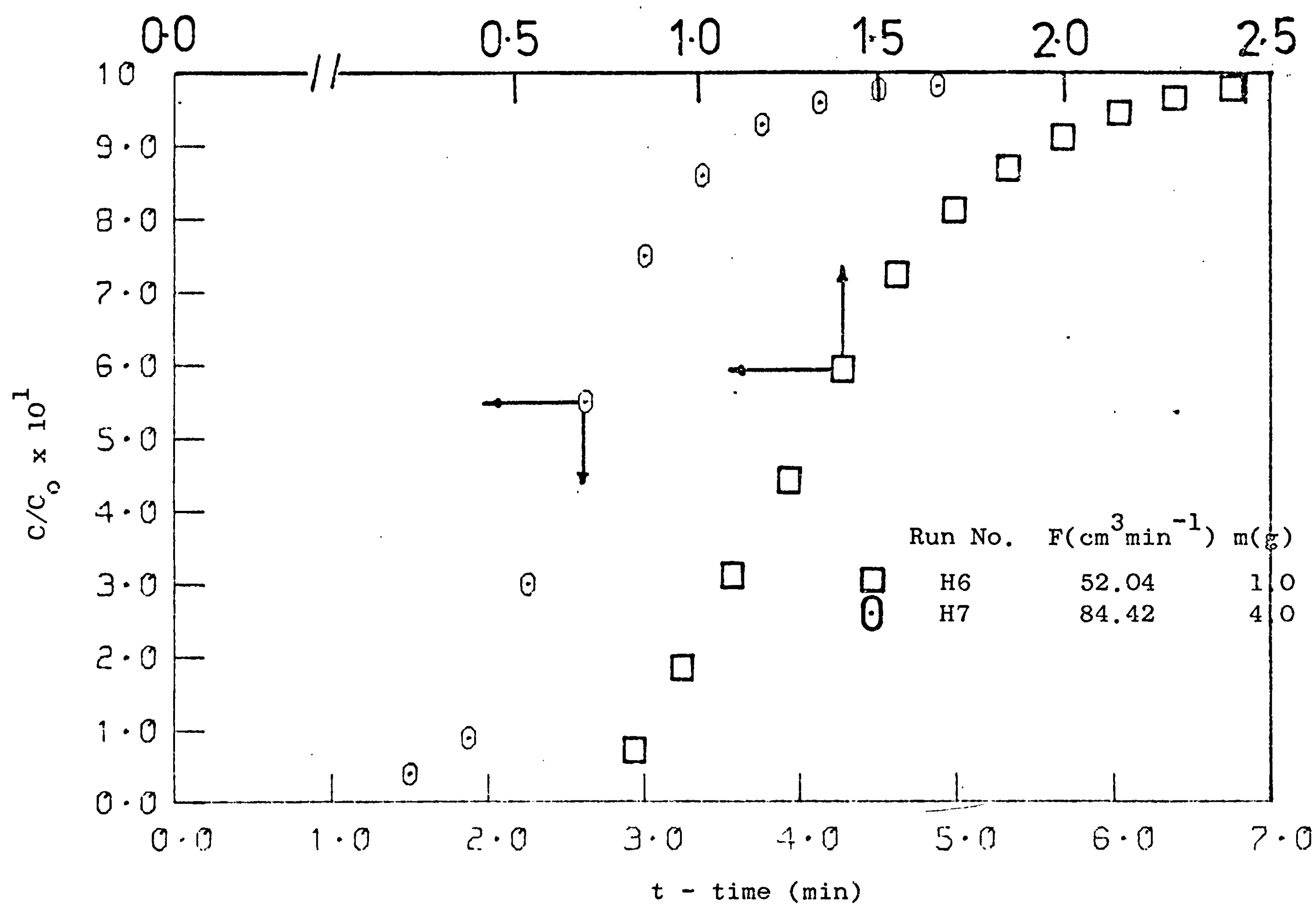

Figure 52: Constant pattern behaviour for methane on Anthrasorb CC818H

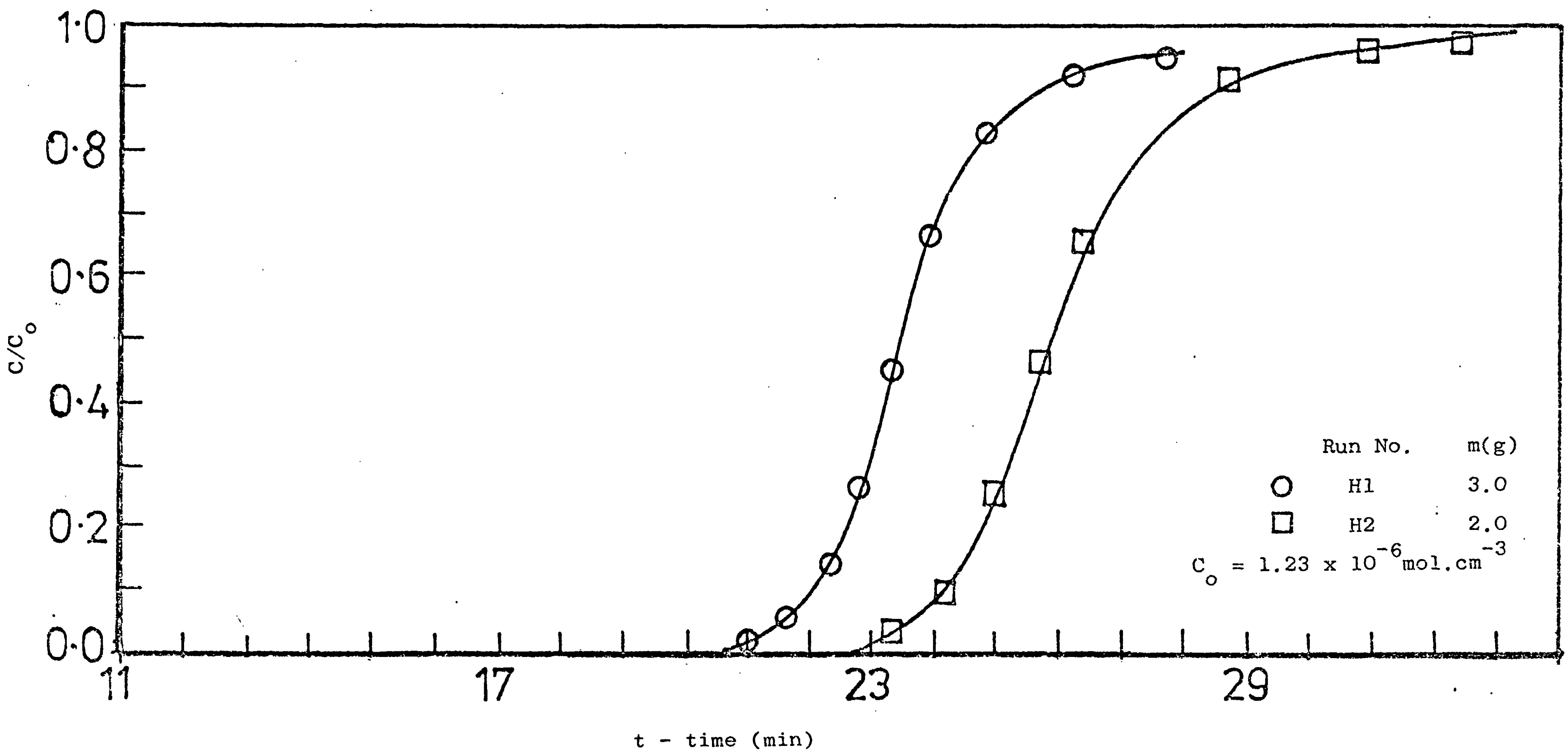

Figure 53: Constant pattern behaviour for ethane on Anthrasorb CC818H at 25°C.

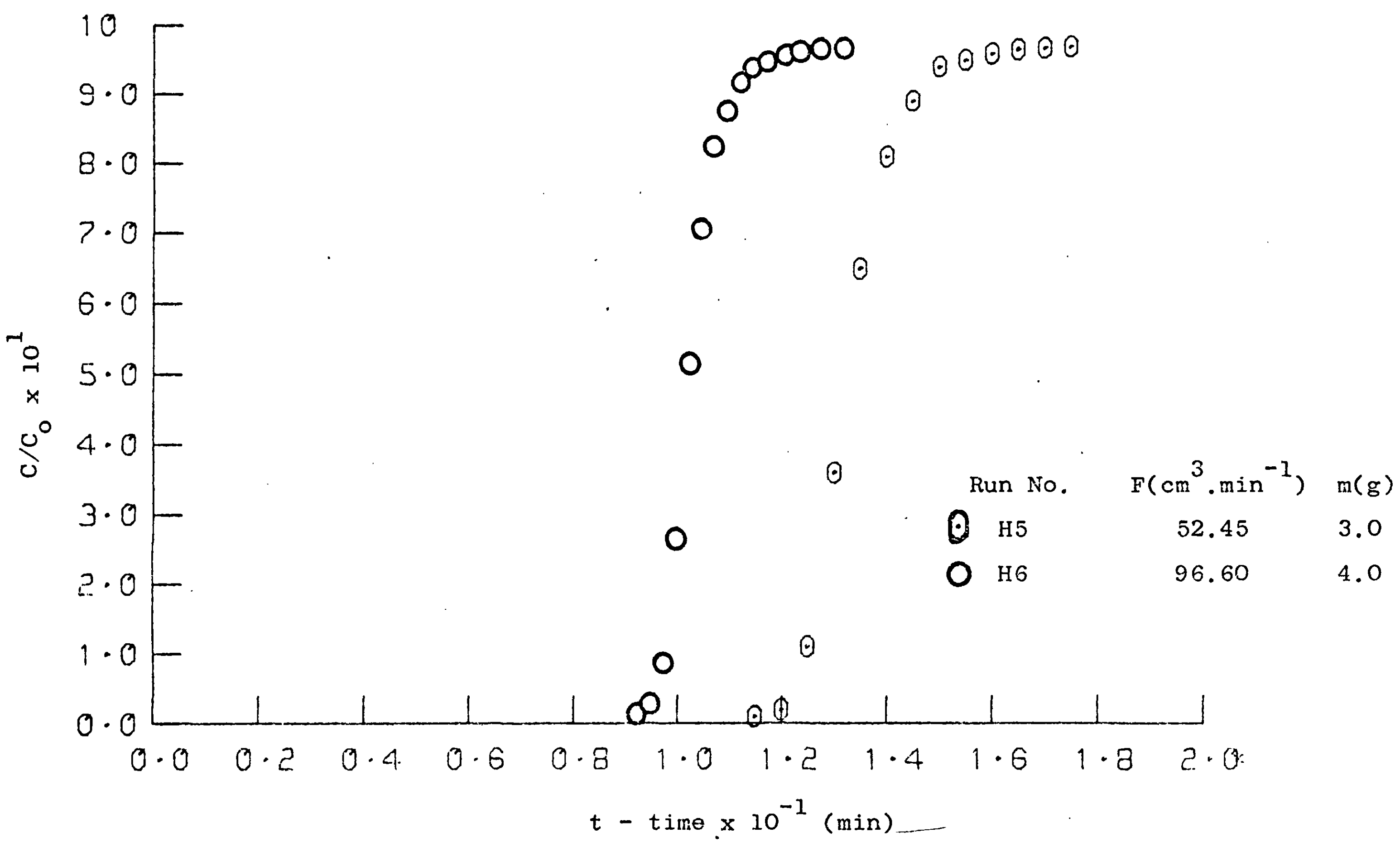

Figure 54: Constant pattern behaviour for ethane on Anthrasorb CC818H at 25°C.

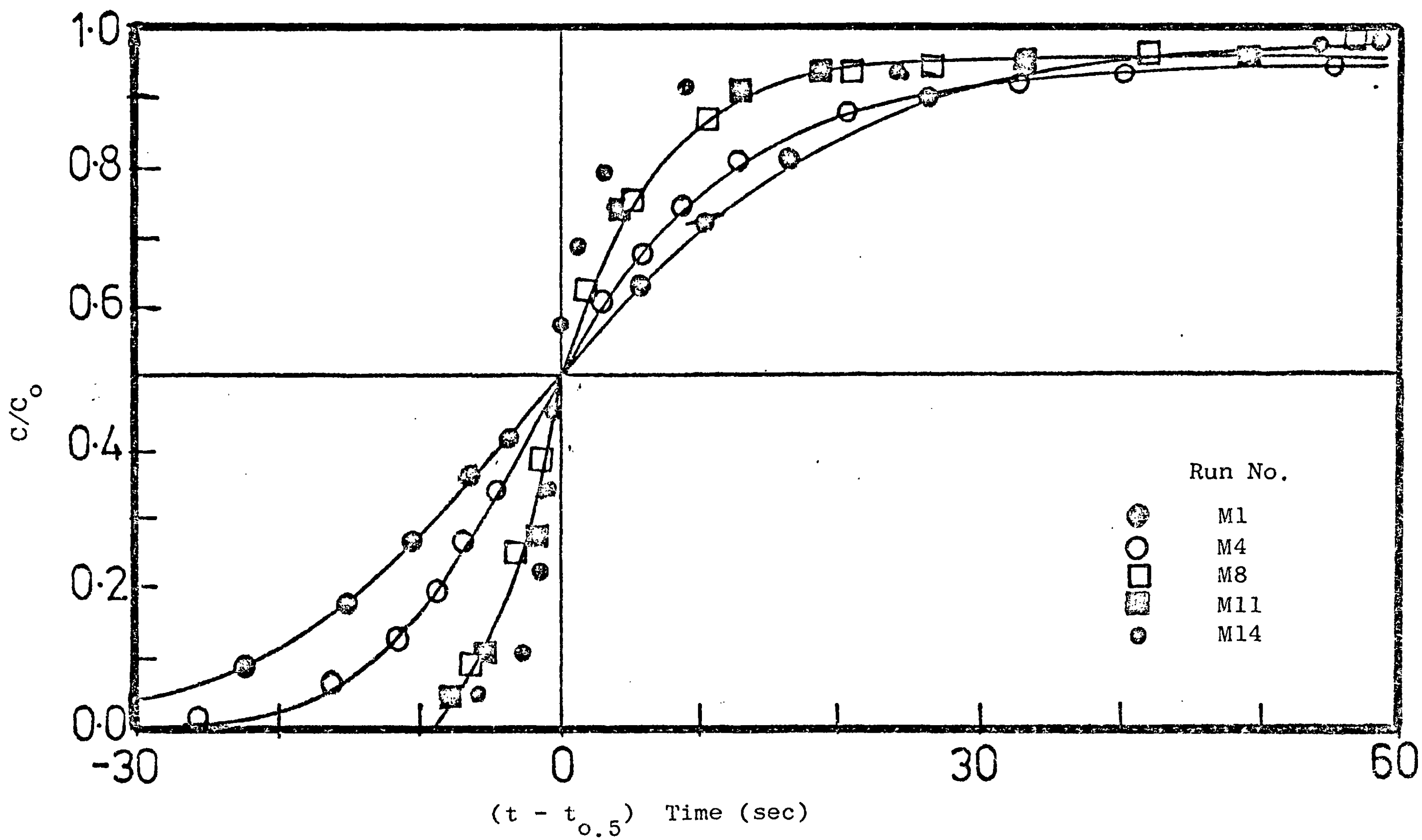

Figure 55: Experimental results for methane plotted as C/C_o against $(t-t_{0.5})$

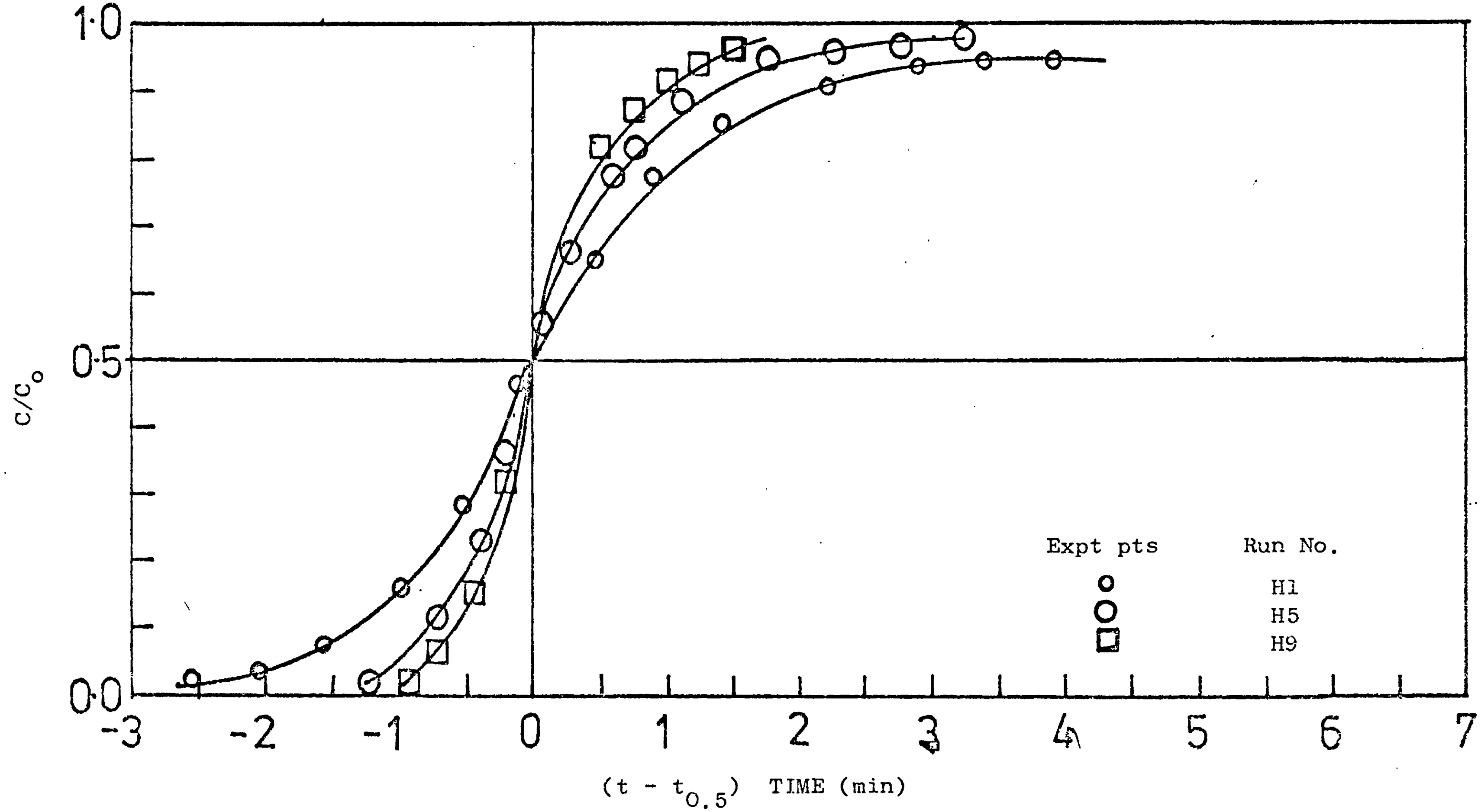

Figure 56: Experimental results for ethane as a single component experiments plotted as C/C_o against $(t - t_{0.5})$.

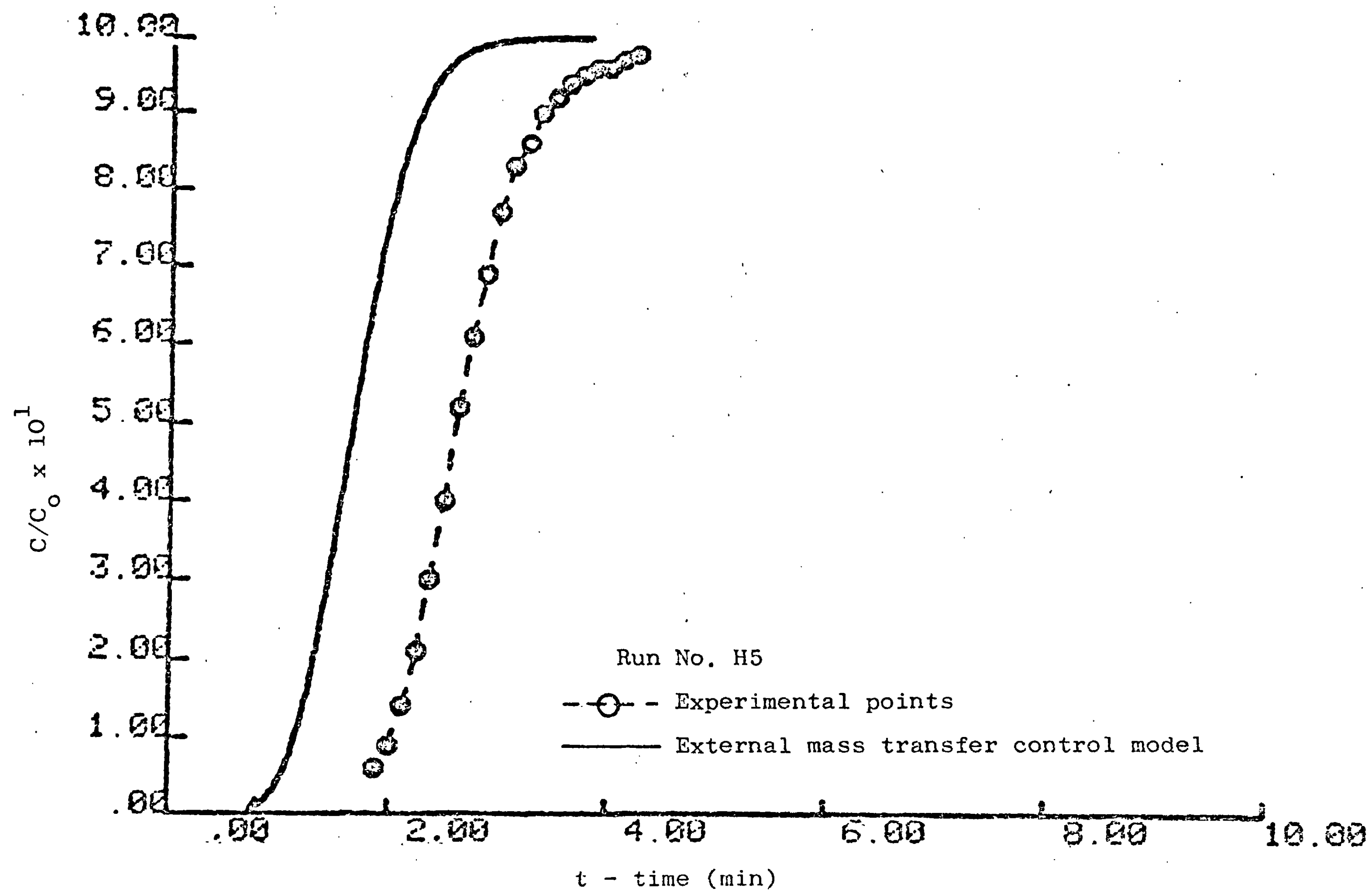

Figure 57: Comparison of experimental and predicted breakthrough curves for methane on Anthrasorb CC818H at 25°C.

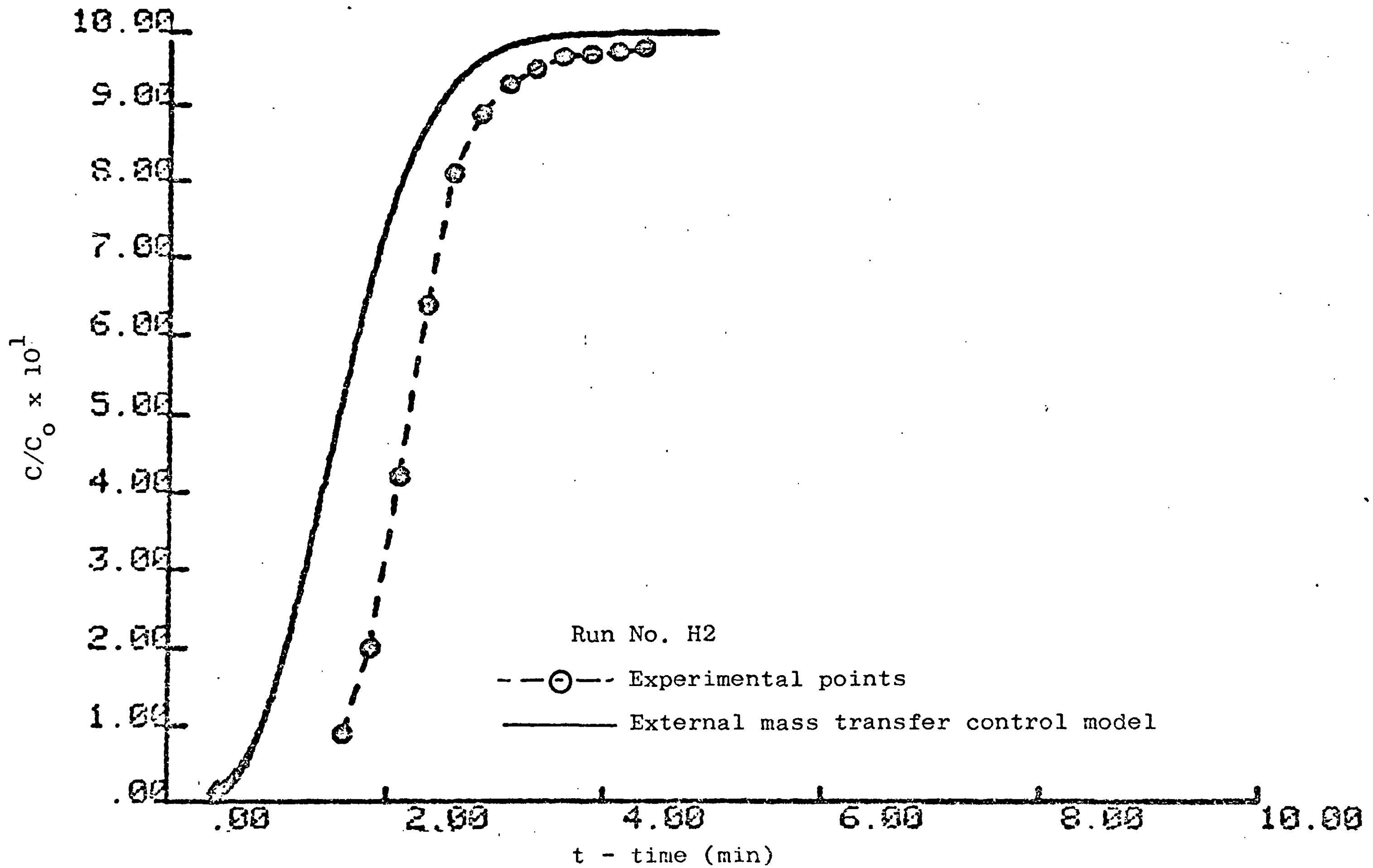

Figure 58: Comparison of experimental and predicted breakthrough curves for methane on Anthrasorb CC818H at 25°C.

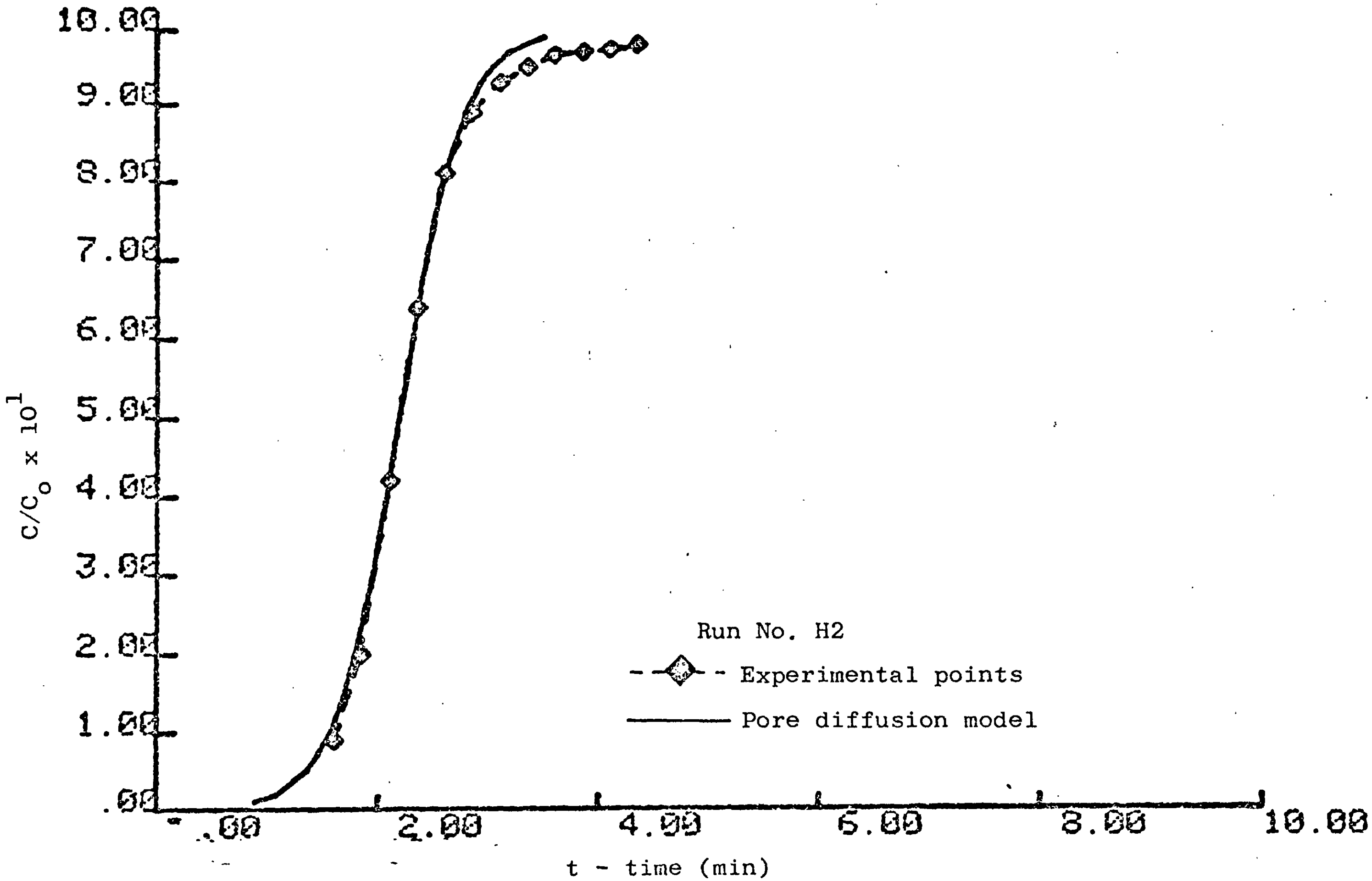

Figure 59: Comparison of experimental and predicted breakthrough curves for methane on Anthrasorb CC818H at 25°C.

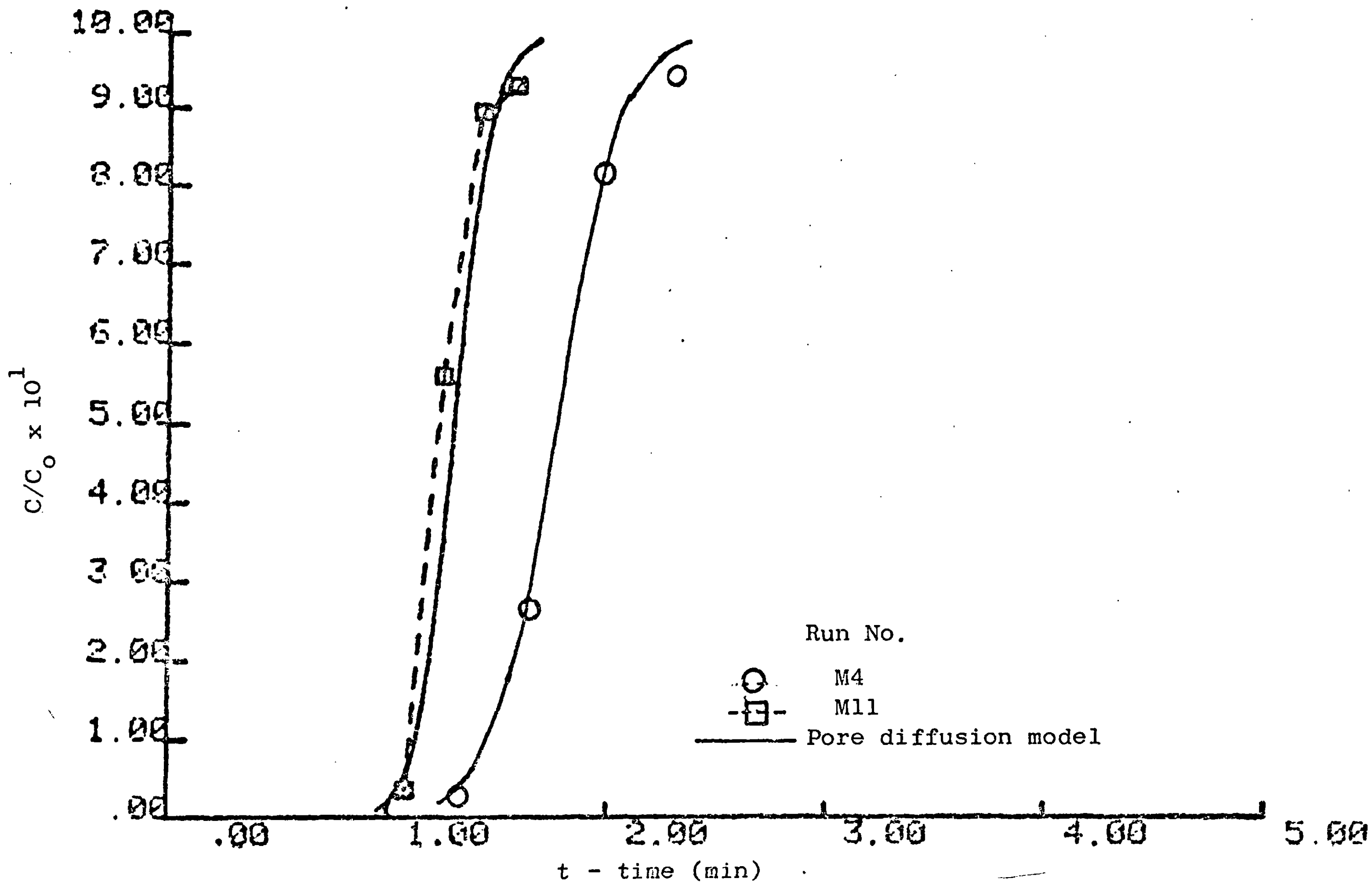

Figure 60: Comparison of experimental and predicted breakthrough curves for methane on Anthrasorb CC818M at 25°C.

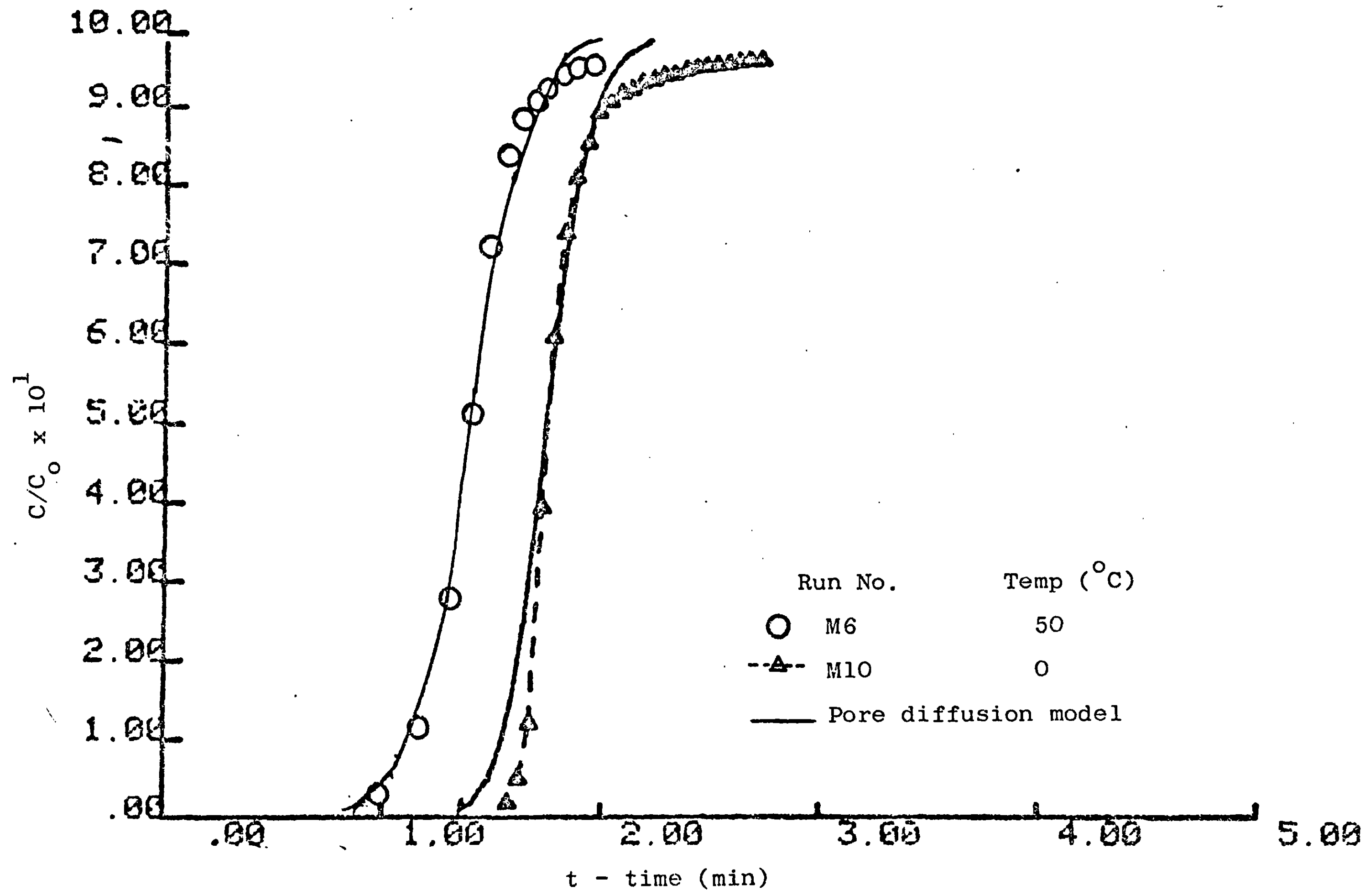

Figure 61: Comparison of experimental and predicted breakthrough curves for methane on Anthrasorb CC818M at various temperatures.

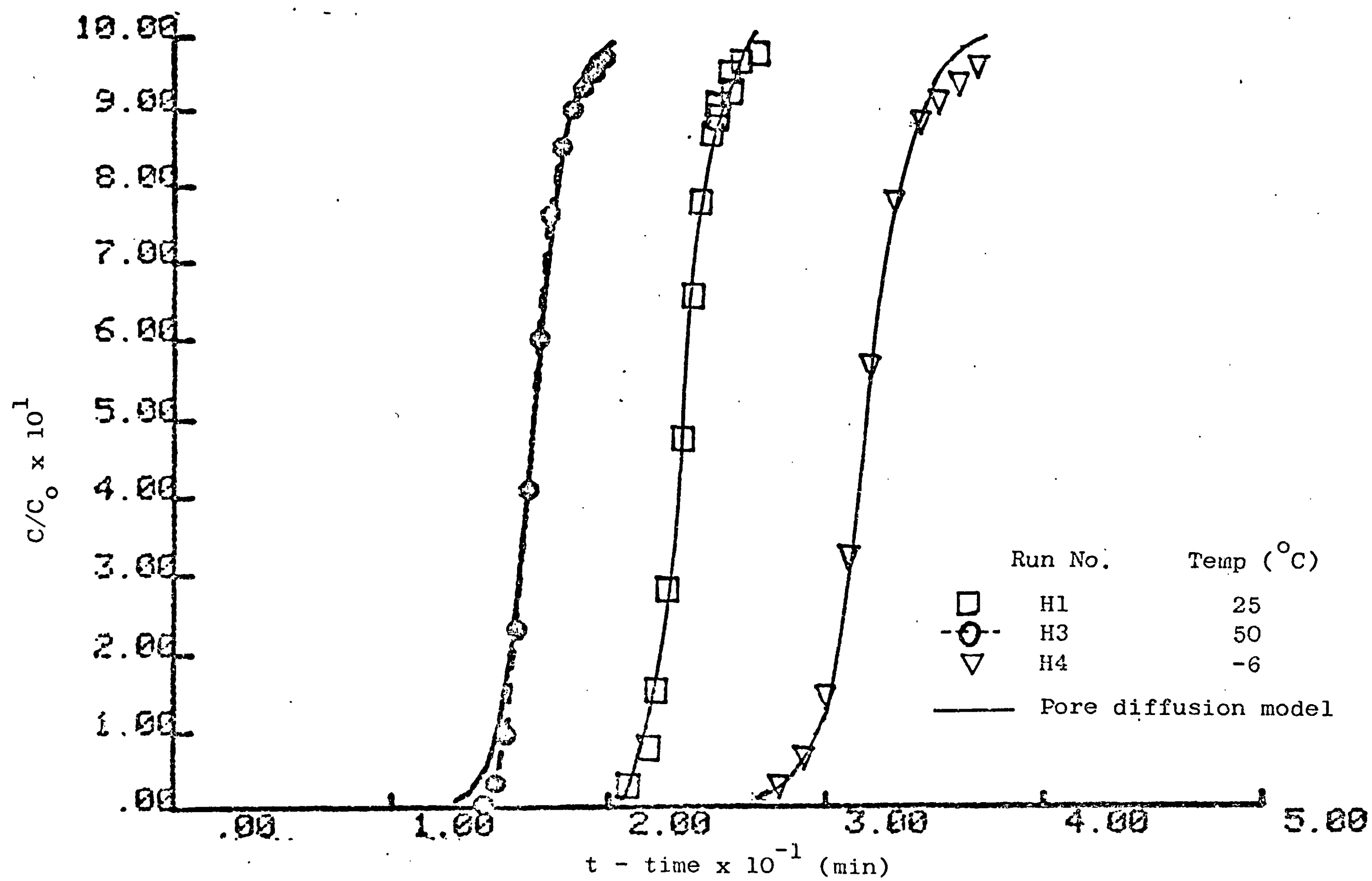

Figure 62: Comparison of experimental and predicted breakthrough curves for ethane on Anthrasorb CC818H at various temperatures.

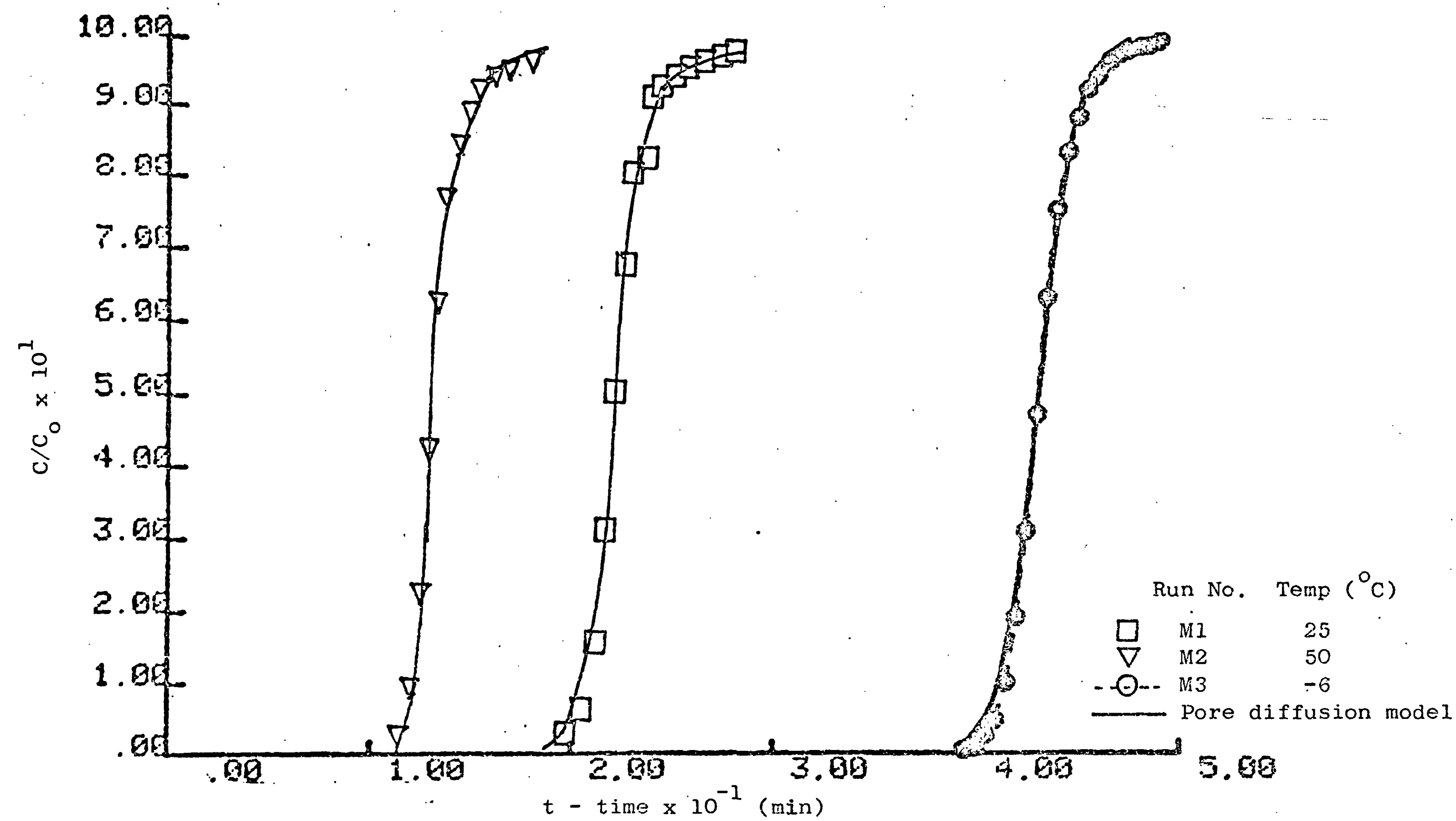

Figure 63: Comparison of experimental and predicted breakthrough curves for ethane on Anthrasorb CC818M at various temperatures.

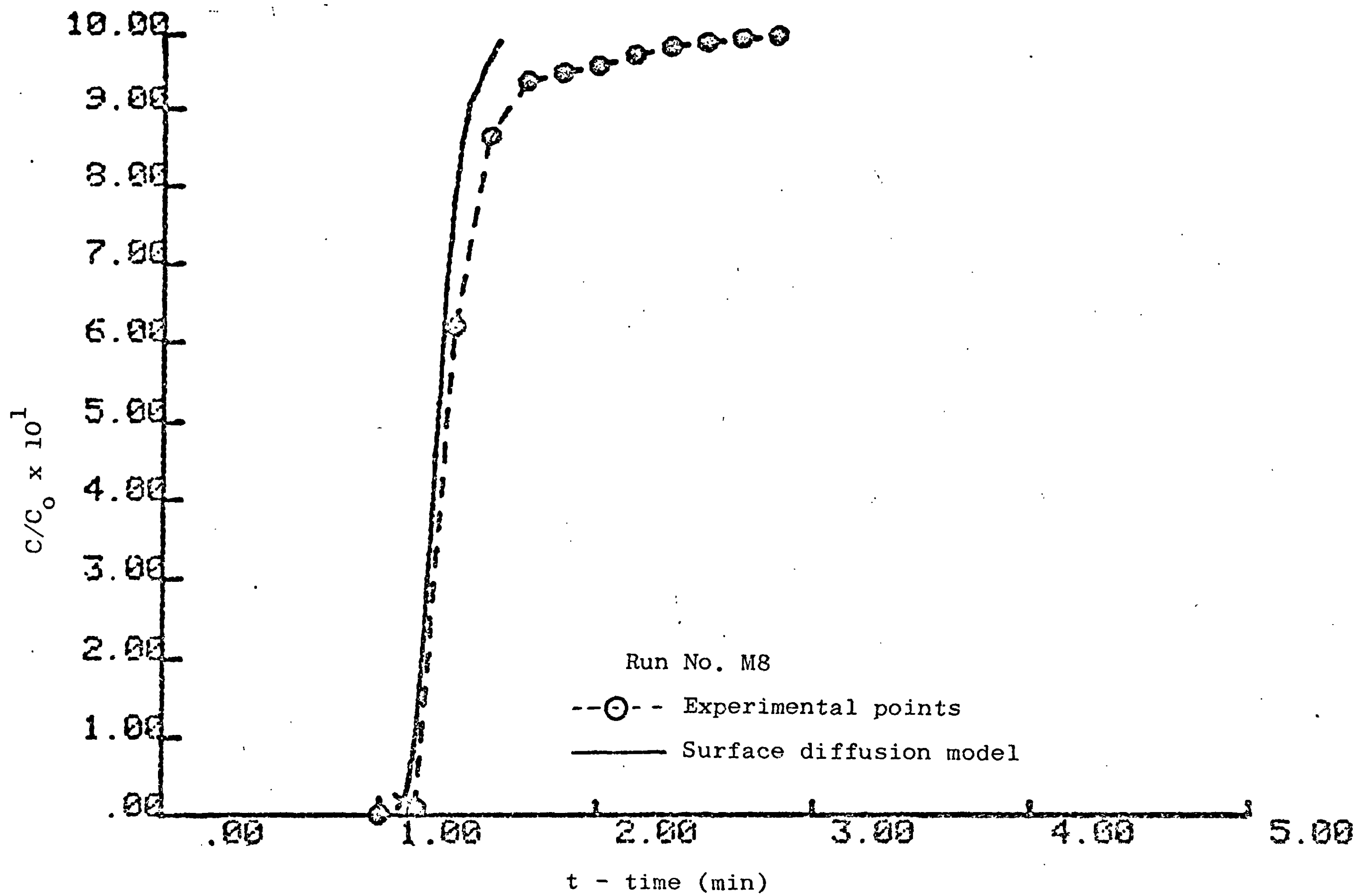

Figure 64: Comparison of experimental and predicted breakthrough curves for methane on Anthrasorb CC818M at 25^{o}C.

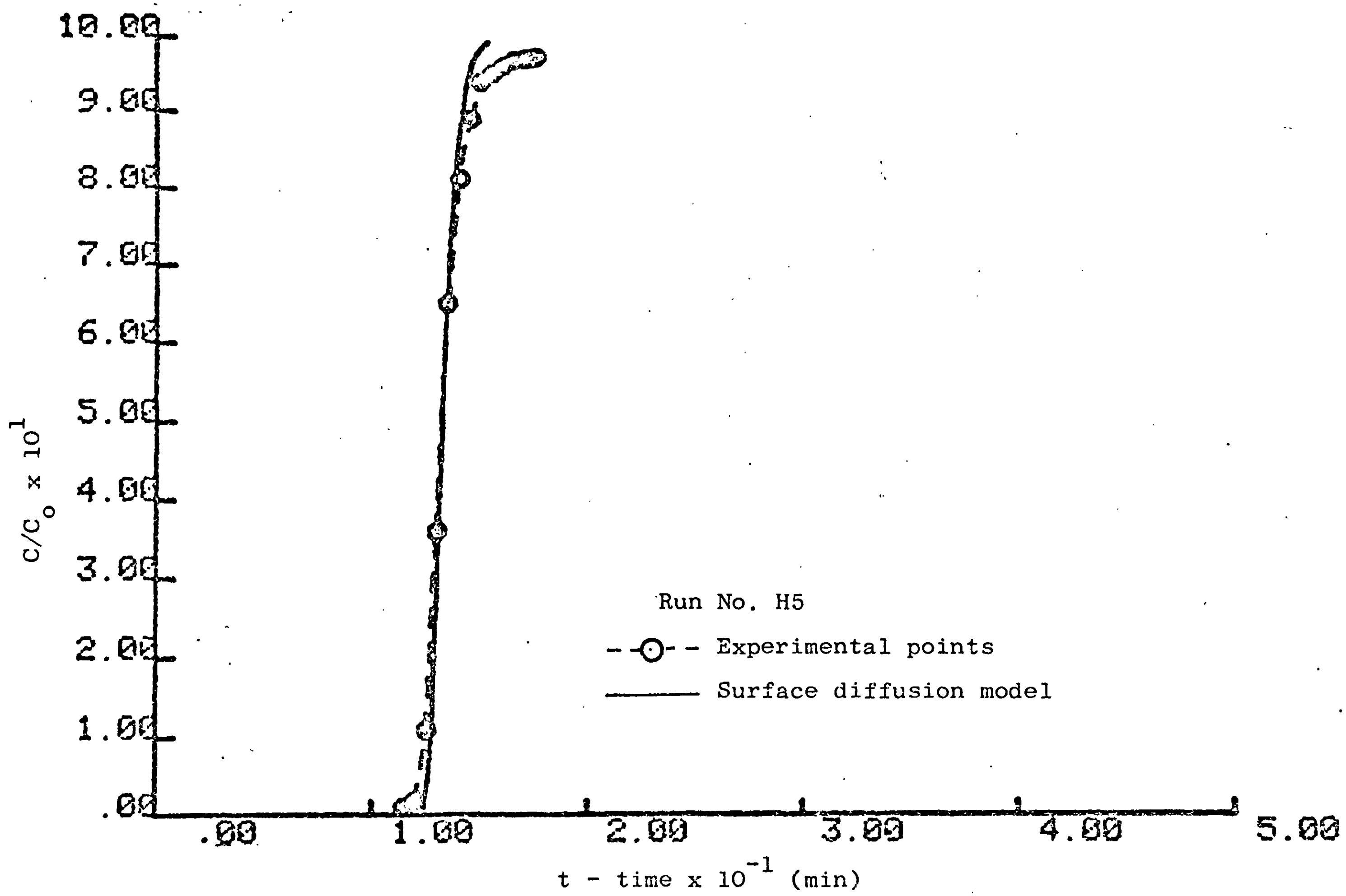

Figure 65: Comparison of experimental and predicted breakthrough curves for ethane on Anthrasorb CC818H at 25°C.

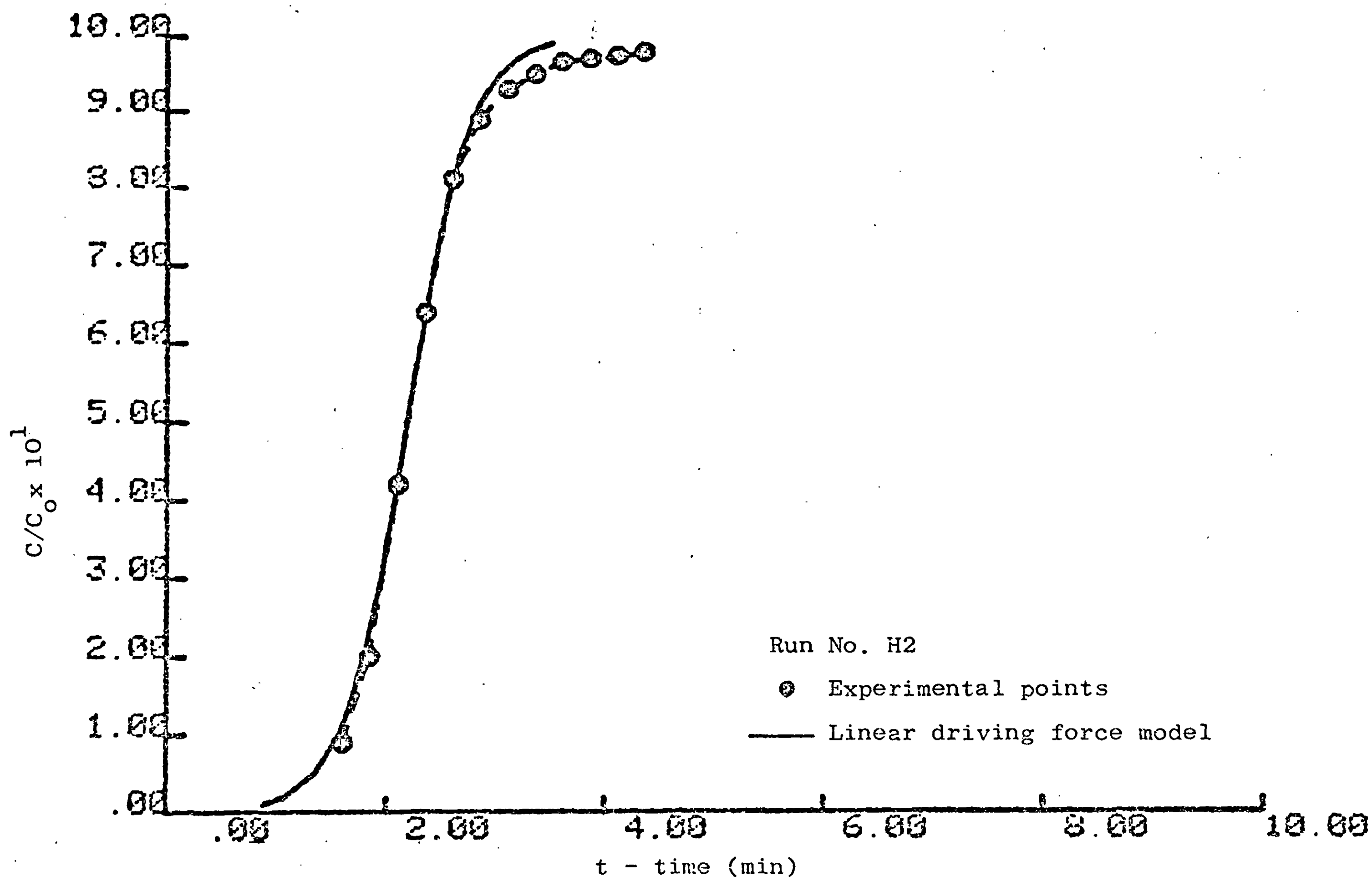

Figure 66: Comparison of experimental and predicted breakthrough curves for methane on Anthrasorb CC818H at 25°C.

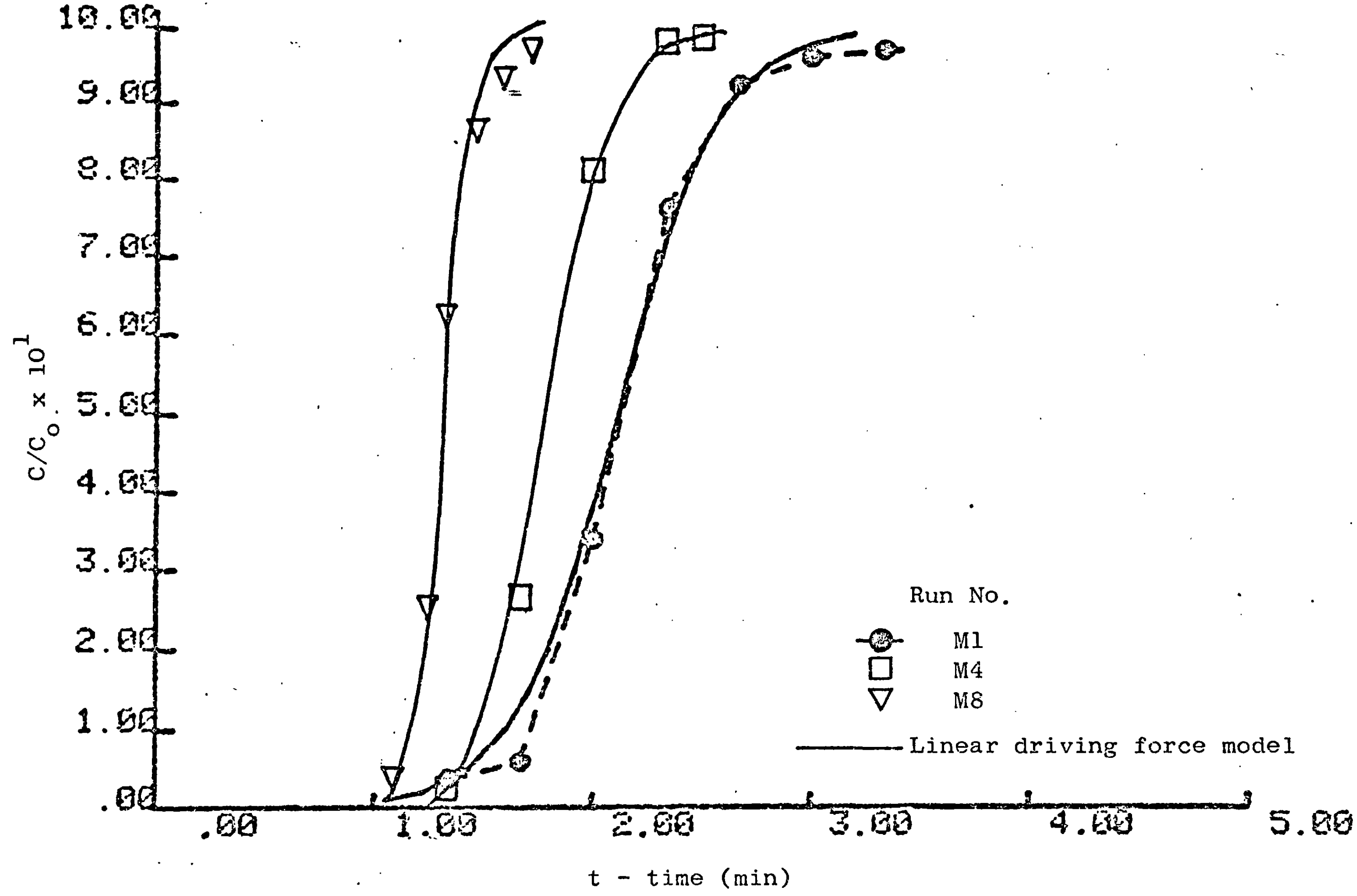

Figure 67: Comparison of experimental and predicted breakthrough curves for methane on Anthrasorb CC818M at 25°C.

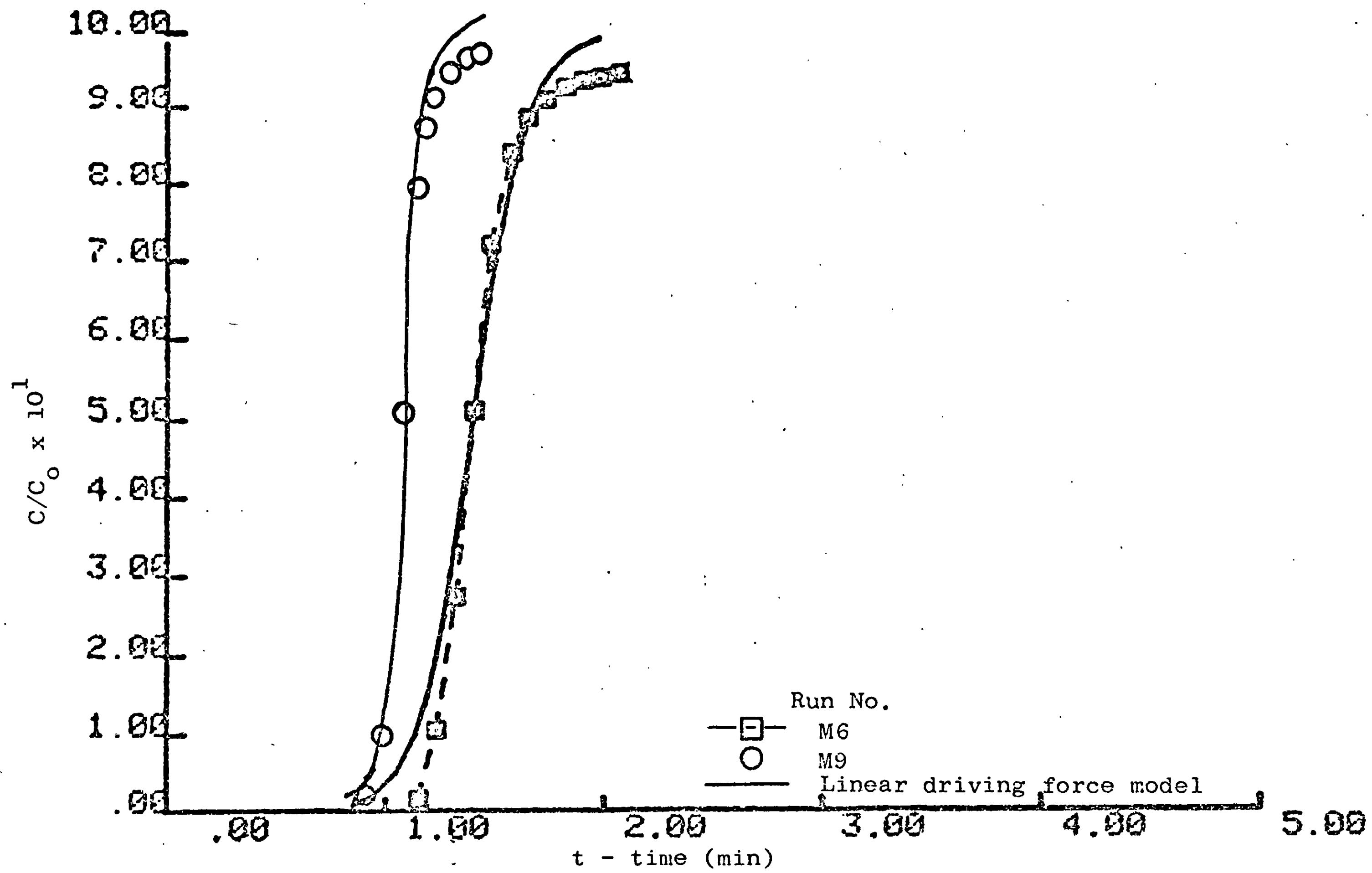

Figure 68: Comparison of experimental and predicted breakthrough curves for methane on Anthrasorb CC818M at 50°C.

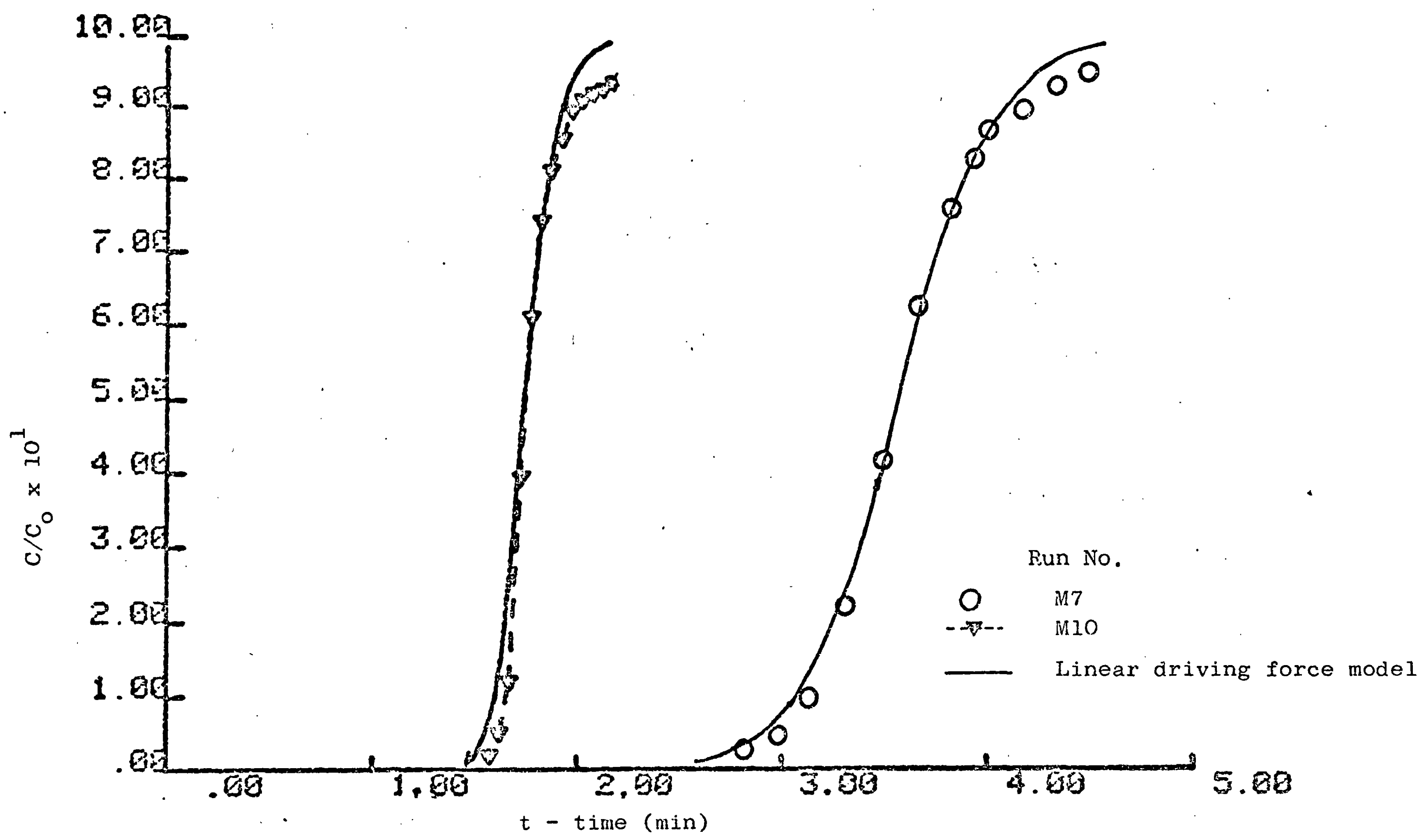

Figure 69: Comparison of experimental and predicted breakthrough curves for methane on Anthrasorb CC818M at $0^{\circ}C$.

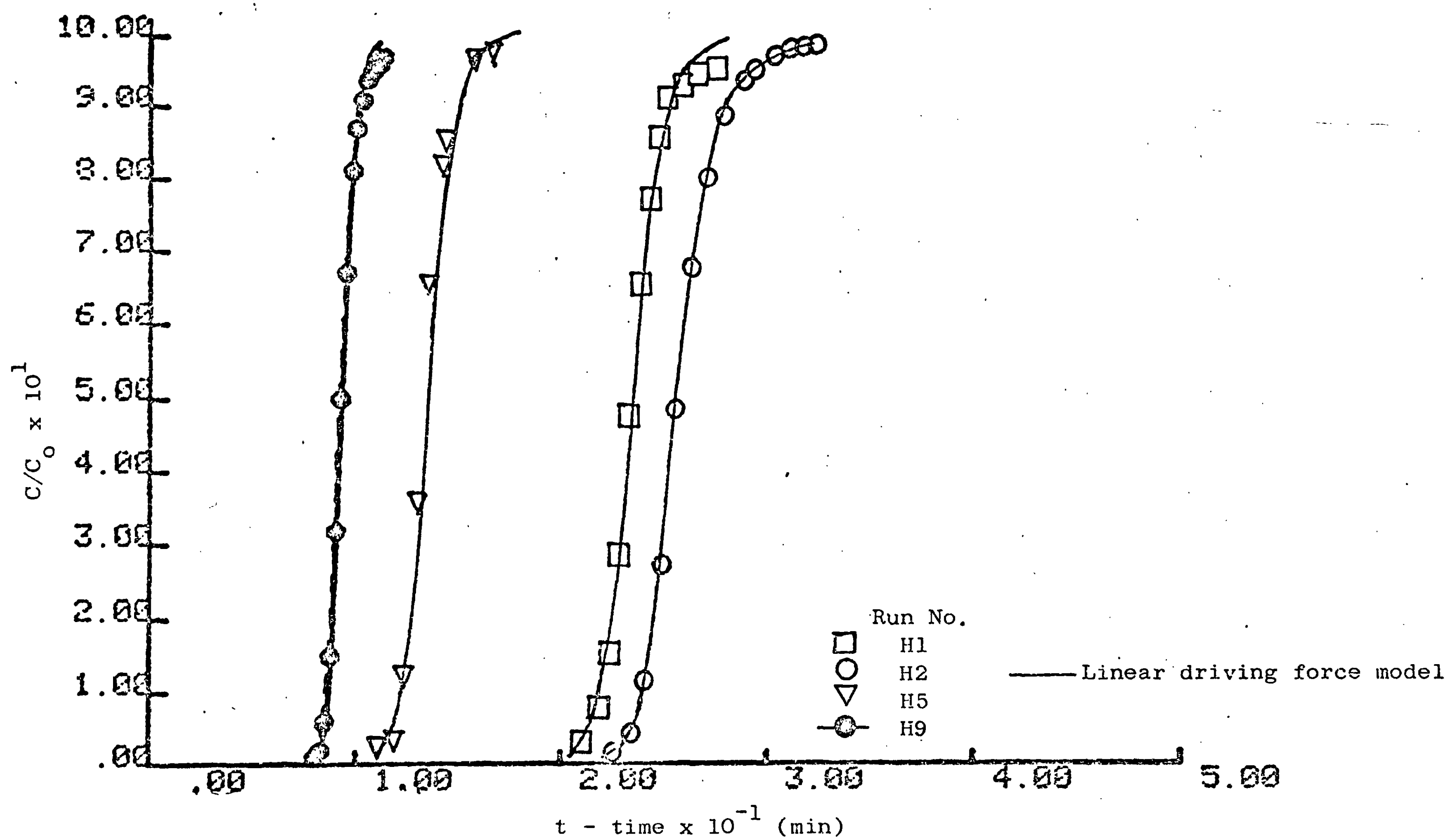

Figure 70: Comparison of experimental and predicted breakthrough curves for ethane on Anthrasorb CC818H at 25°C.

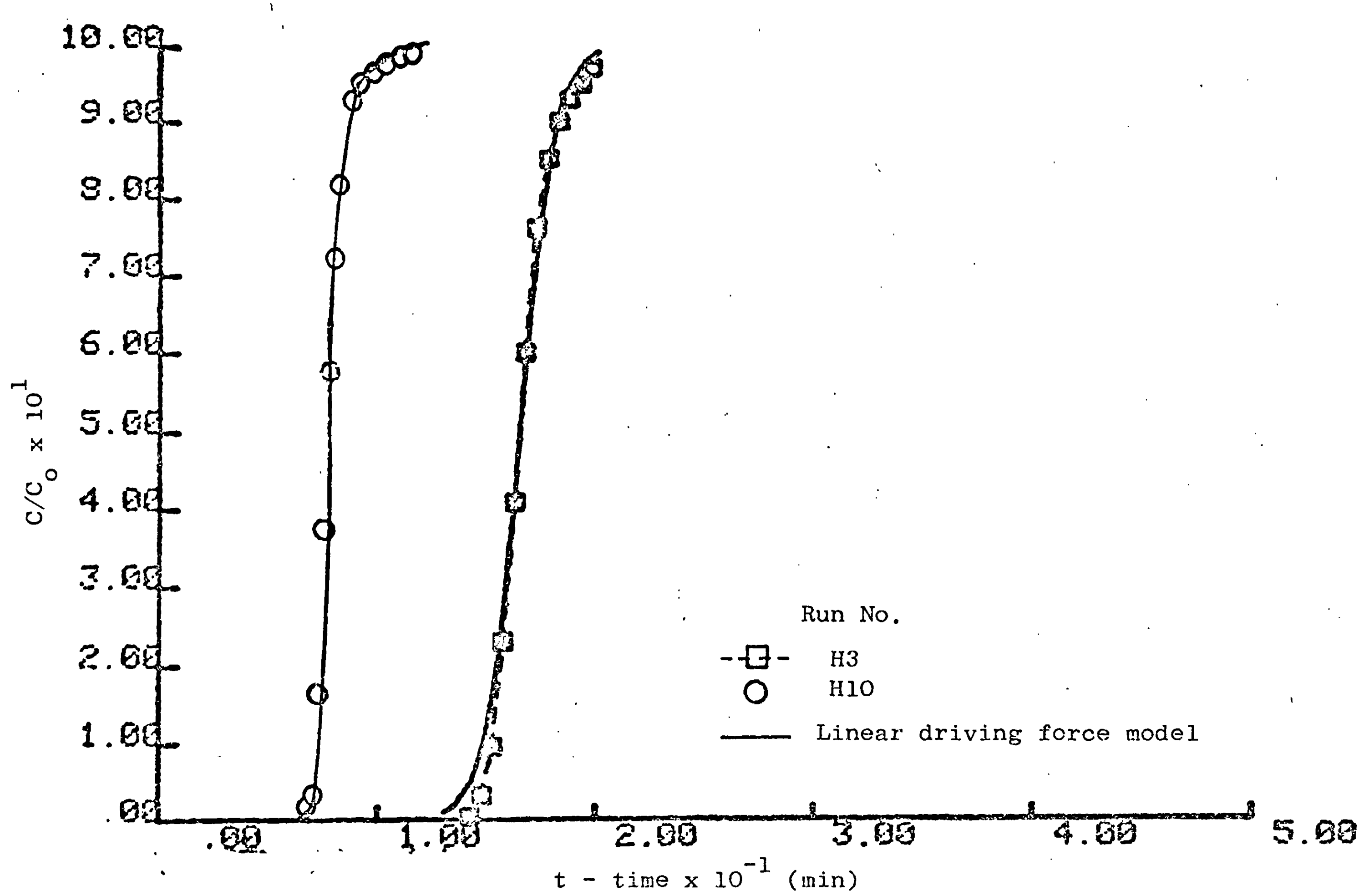

Figure 71: Comparison of experimental and predicted breakthrough curves for ethane on Anthrasorb CC818H at 50°C.

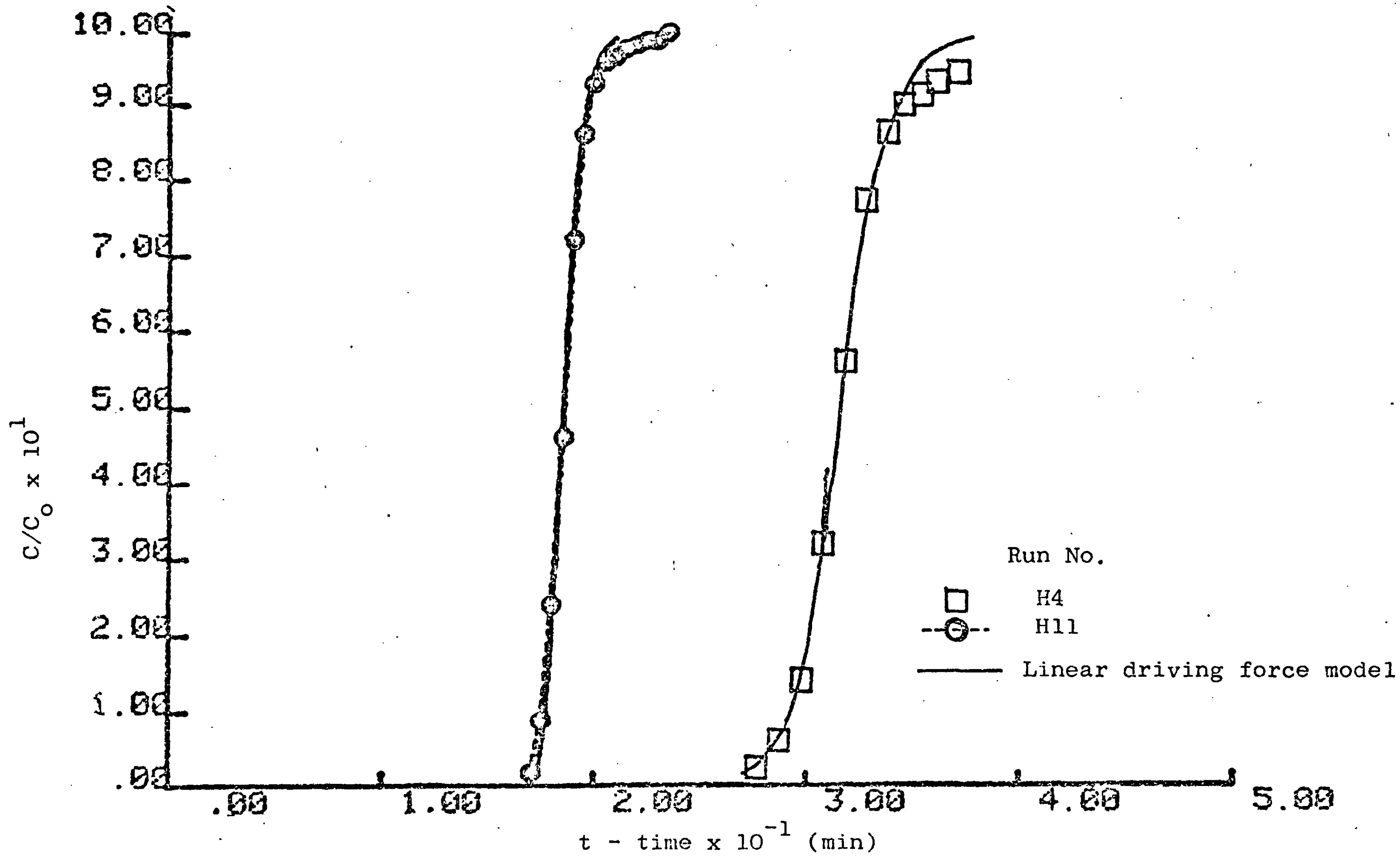

Figure 72: Comparison of experimental and predicted breakthrough curves for ethane on Anthrasorb CC818H at -6°C.

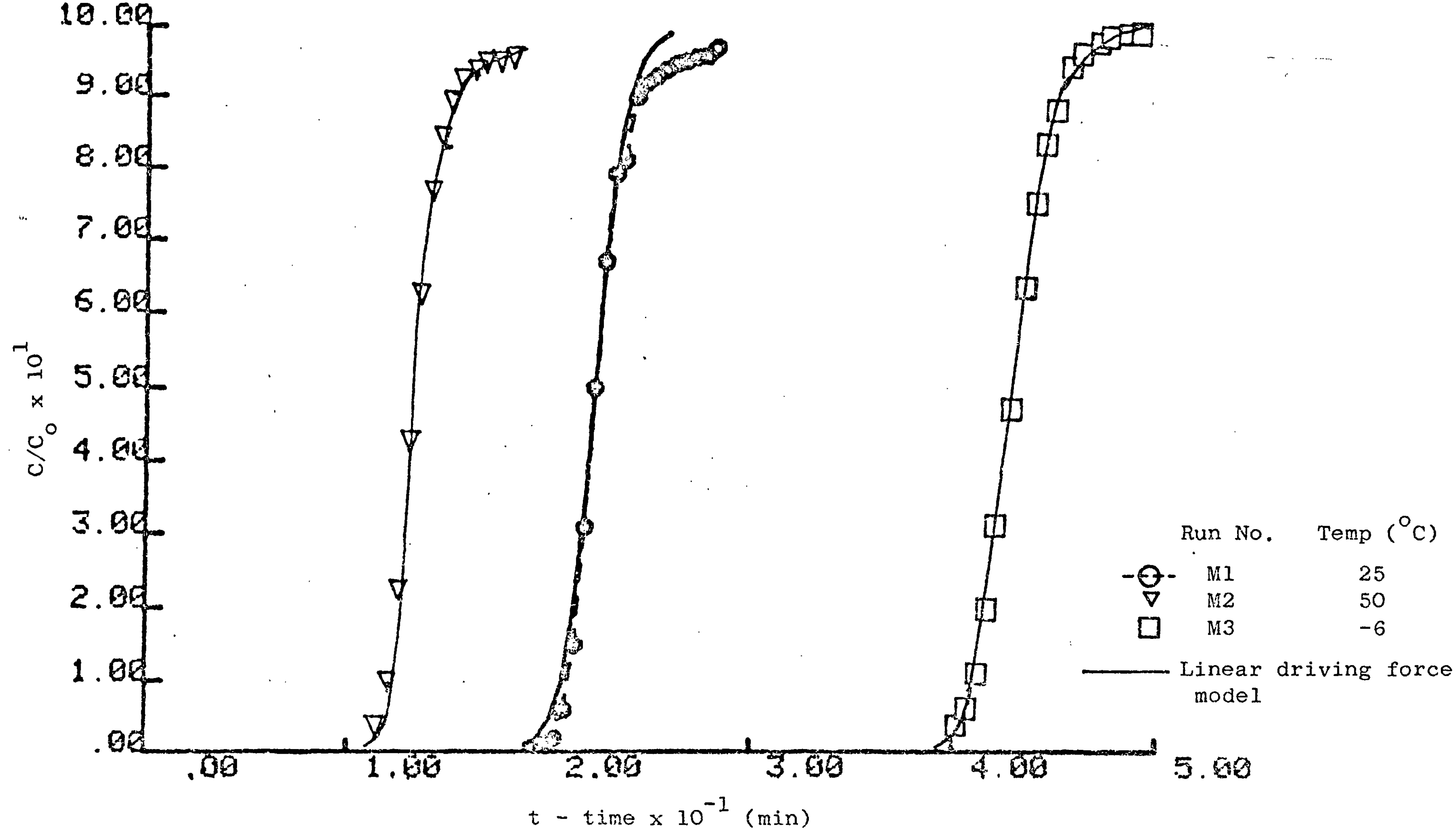

Figure 73: Comparison of experimental and predicted breakthrough curves for ethane on Anthrasorb CC818M at various temperatures.

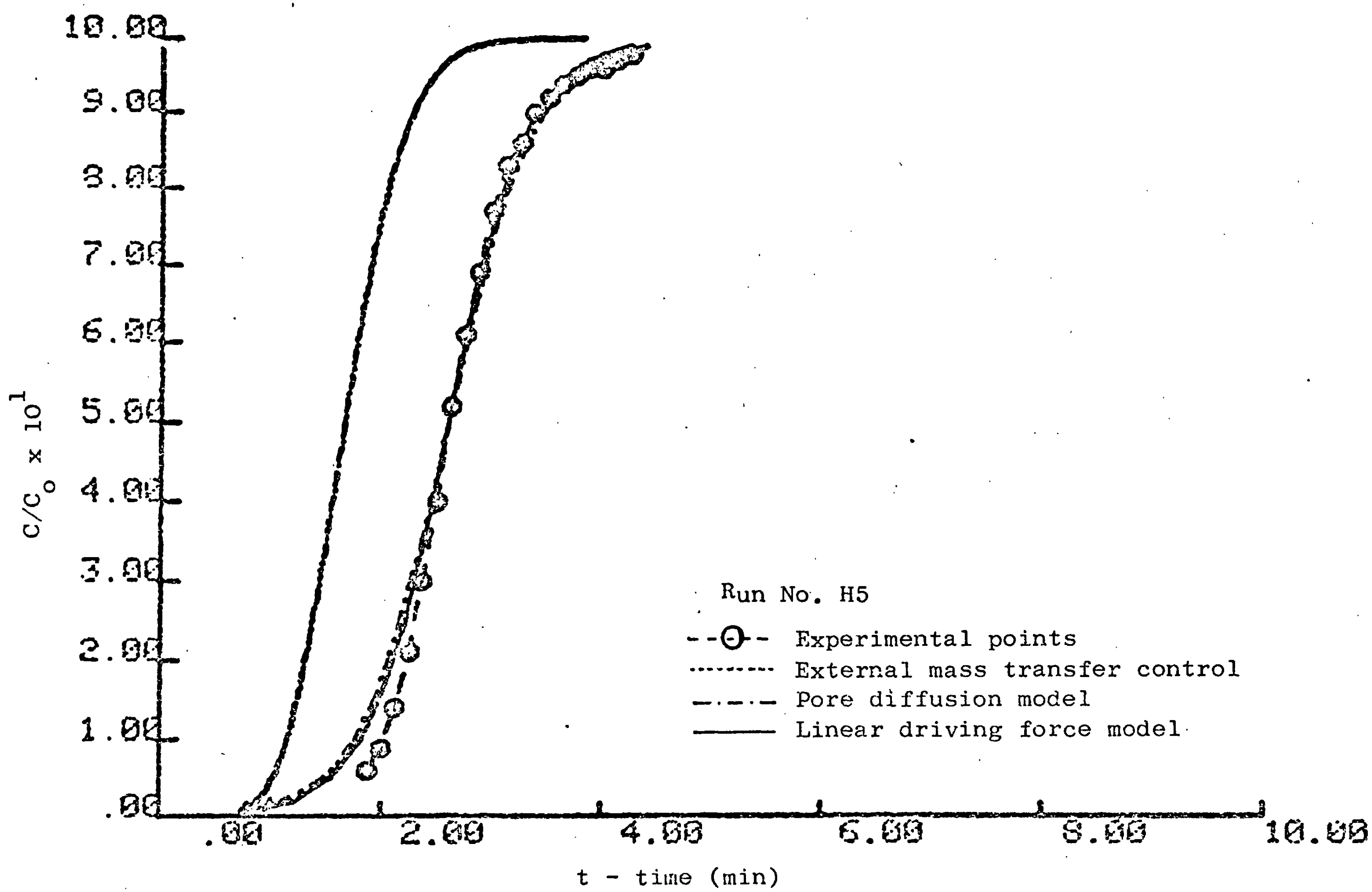

Figure 74: Comparison of experimental and predicted breakthrough curves for methane on Anthrasorb CC818H at 25°C.

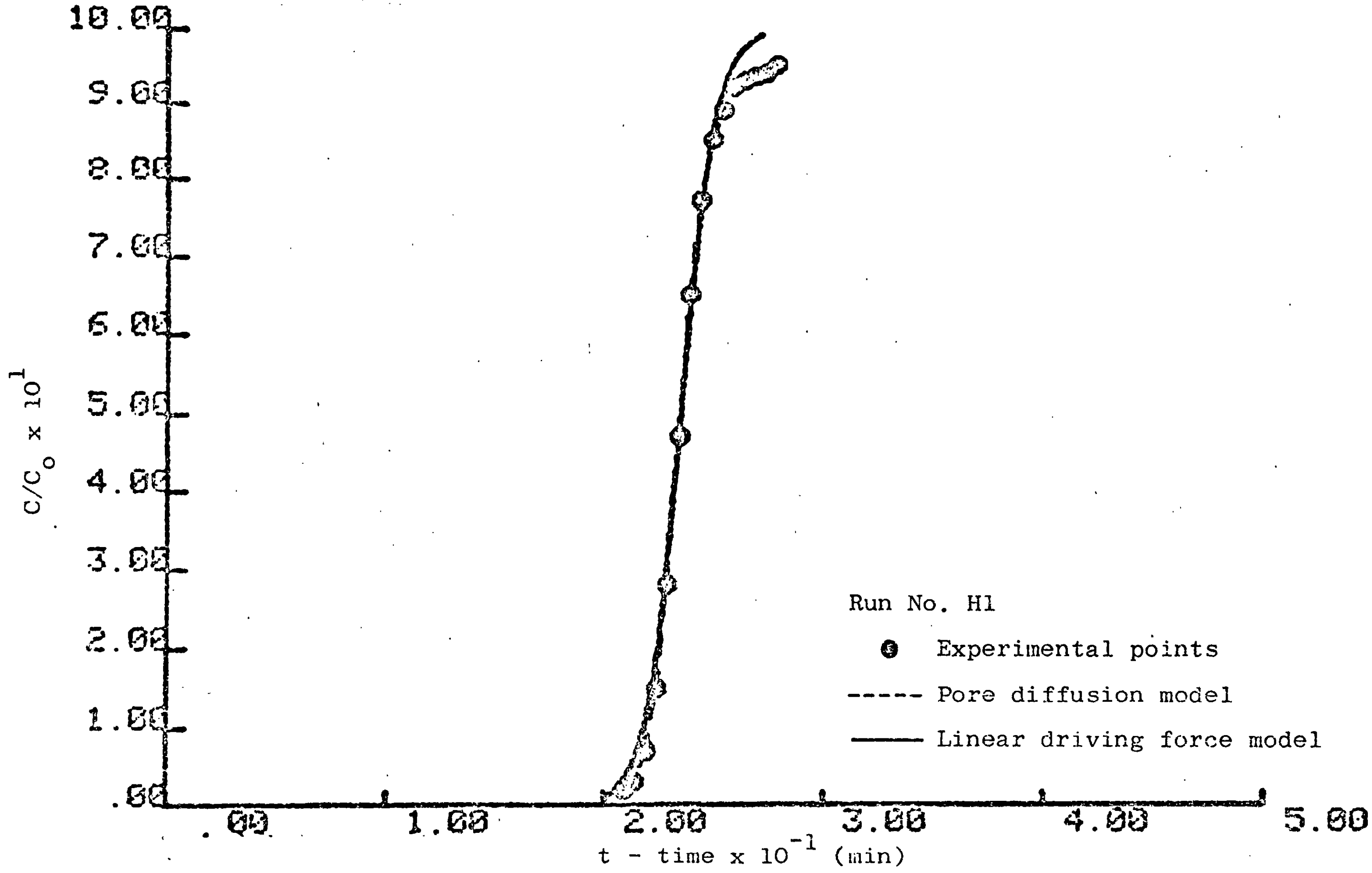

Figure 75: Comparison of experimental and predicted breakthrough curves for ethane on Anthrasorb CC818H at 25^{o}C.

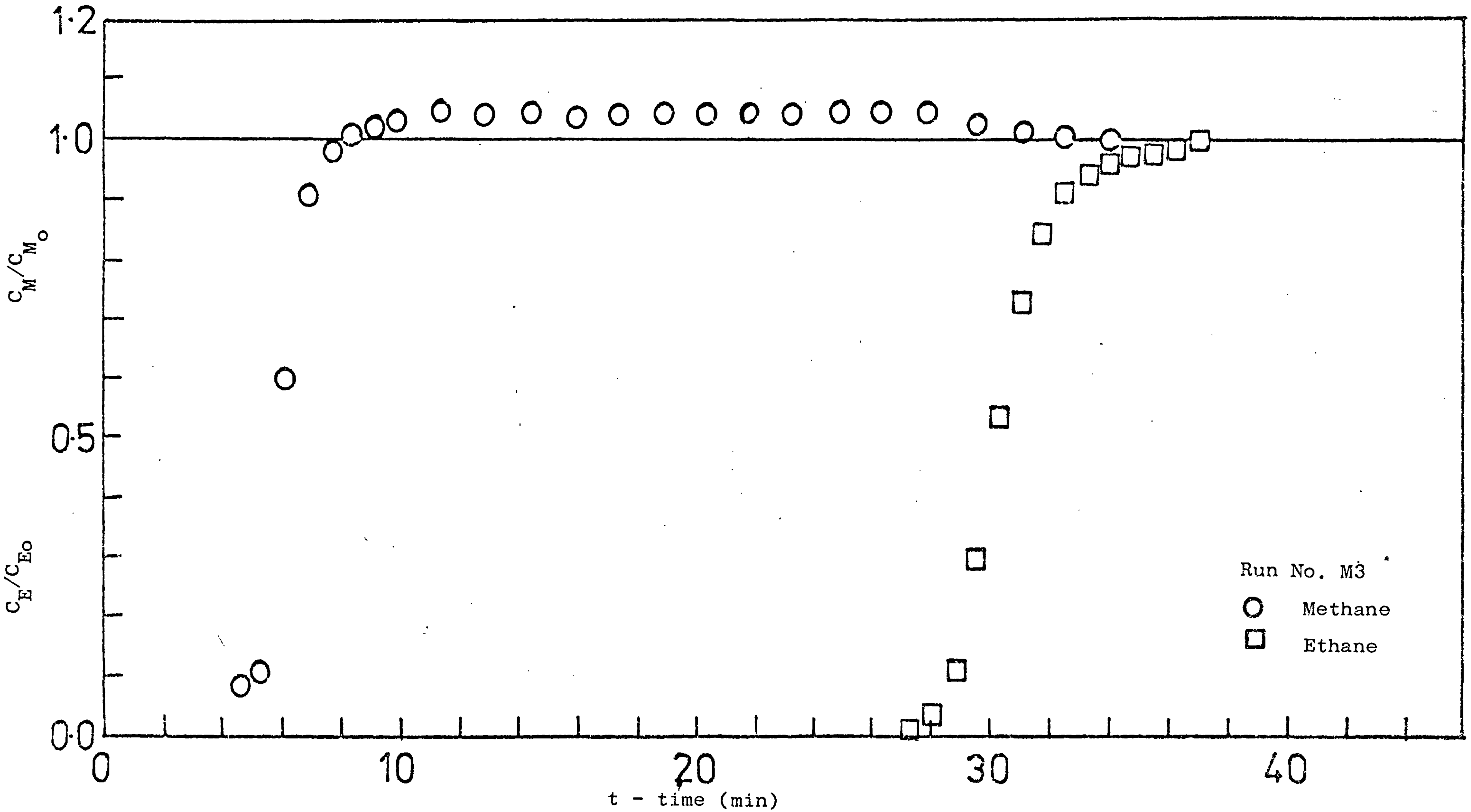

Figure 76: Experimental breakthrough curves for methane-ethane mixture on Anthrasorb CC818M at 25°C.

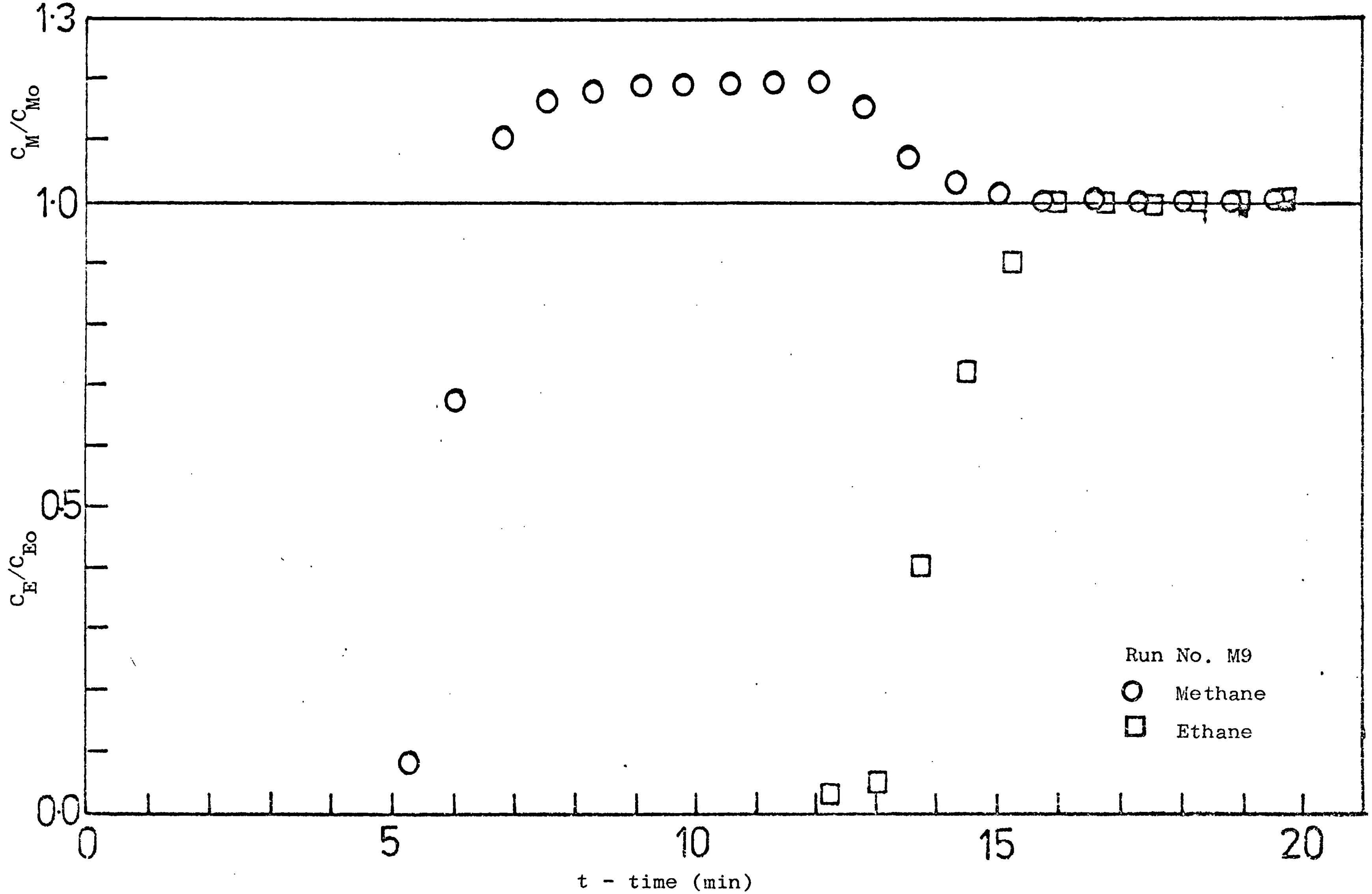

Figure 77: Experimental breakthrough curves for methane-ethane mixture on Anthrasorb CC818M at 25°C

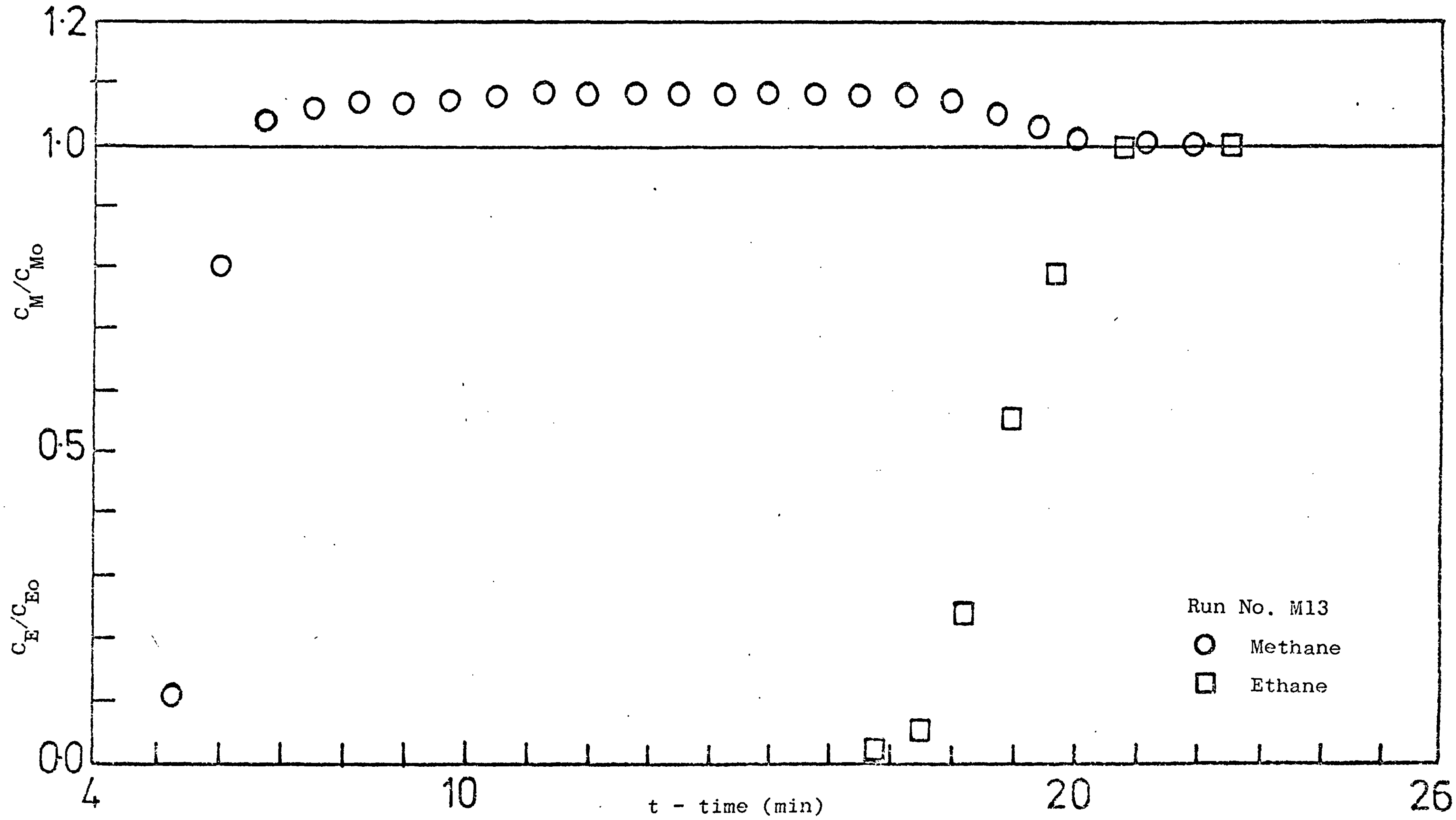

Figure 78: Experimental breakthrough curves for methane-ethane mixture on Anthrasorb CC818H at 25°C.

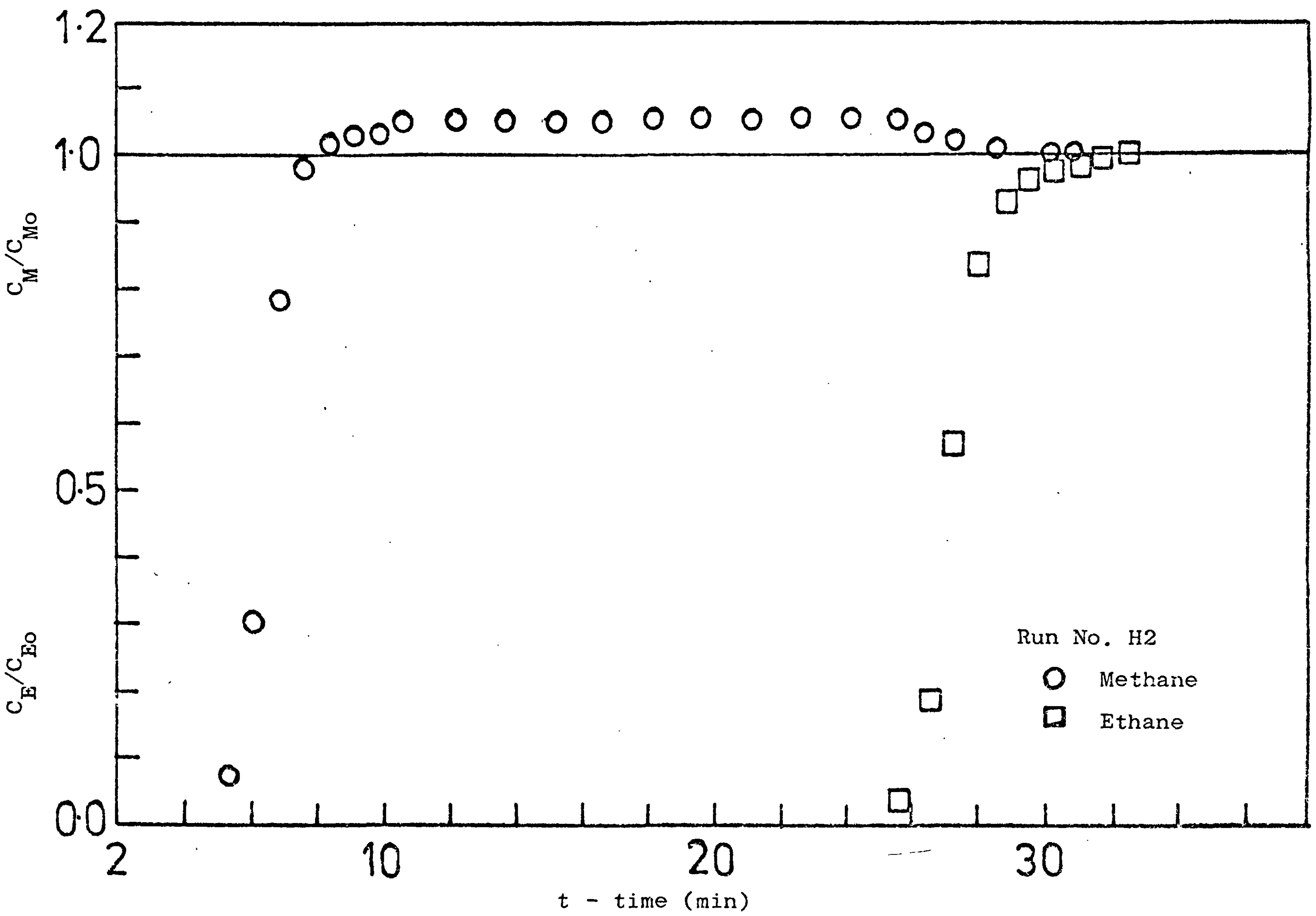

Figure 79: Experimental break through curves for methane-ethane mixture on Anthrasorb CC818H at 25°C.

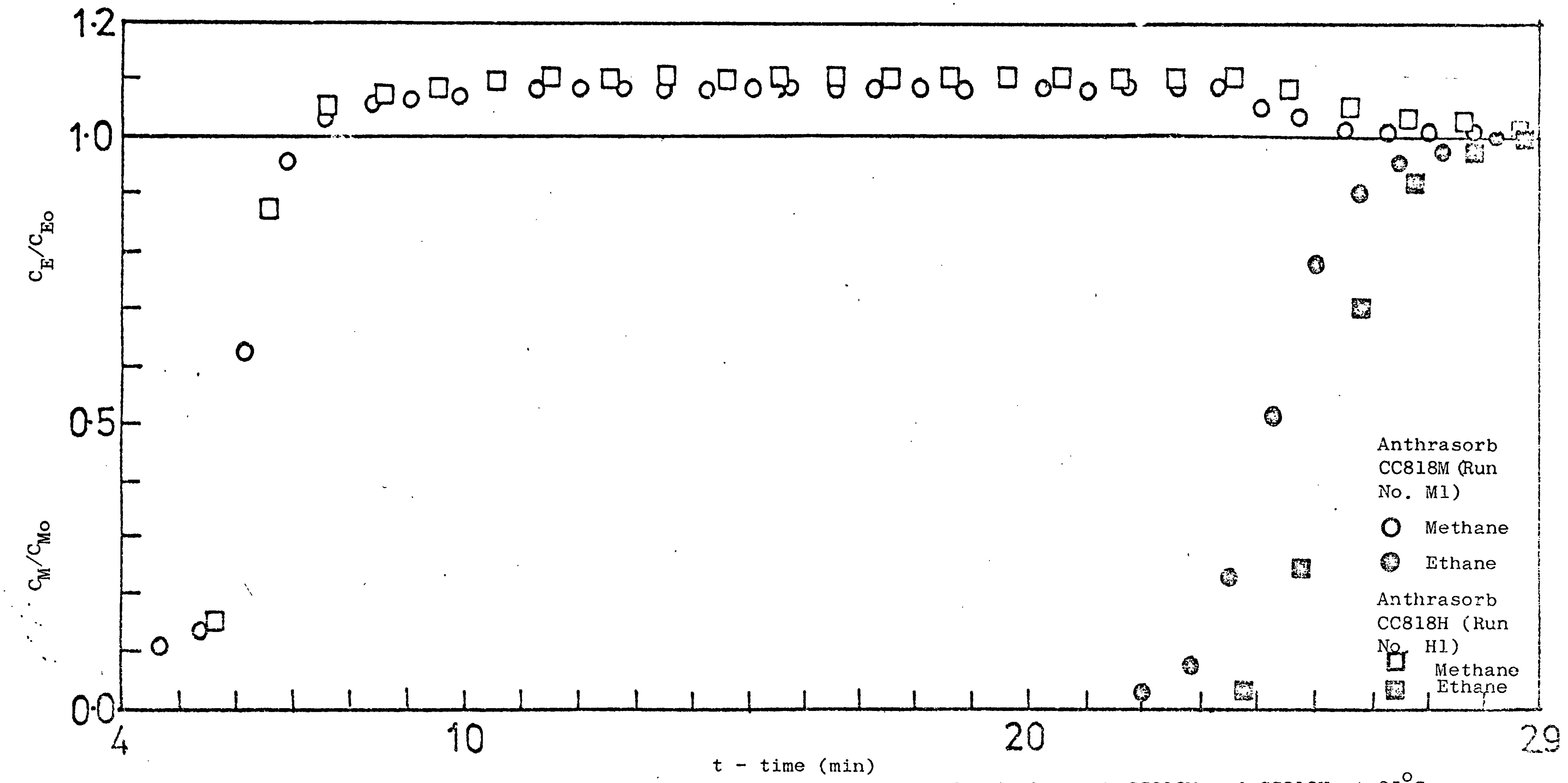

Figure 80: Comparison of experimental binary breakthrough curves for Anthrasorb CC818M and CC818H at 25°C

$m = 3.0g$, $C_2H_6 = 2.76 \times 10^{-6}$ mol.cm^{-3}, $CH_4 = 1.36 \times 10^{-6}$ mol.cm^{-3}

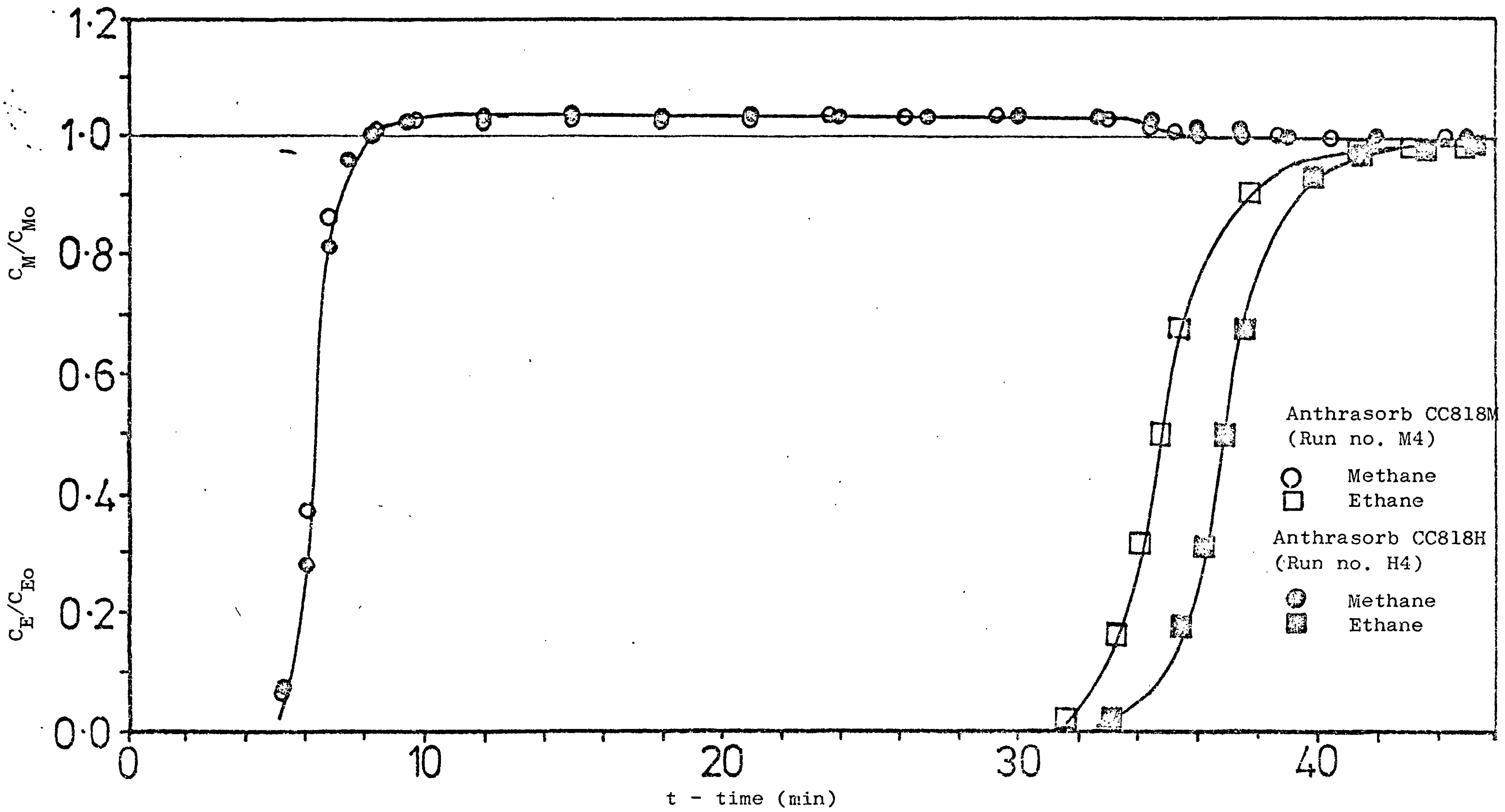

Figure 81: Comparison of experimental binary breakthrough curves for Anthrasorb CC818M and CC818H at 25°C.

m = 3.0g, C_2H_6 = 3.31 vol %, CH_4 = 6.69 vol %, N_2 = 90 vol %

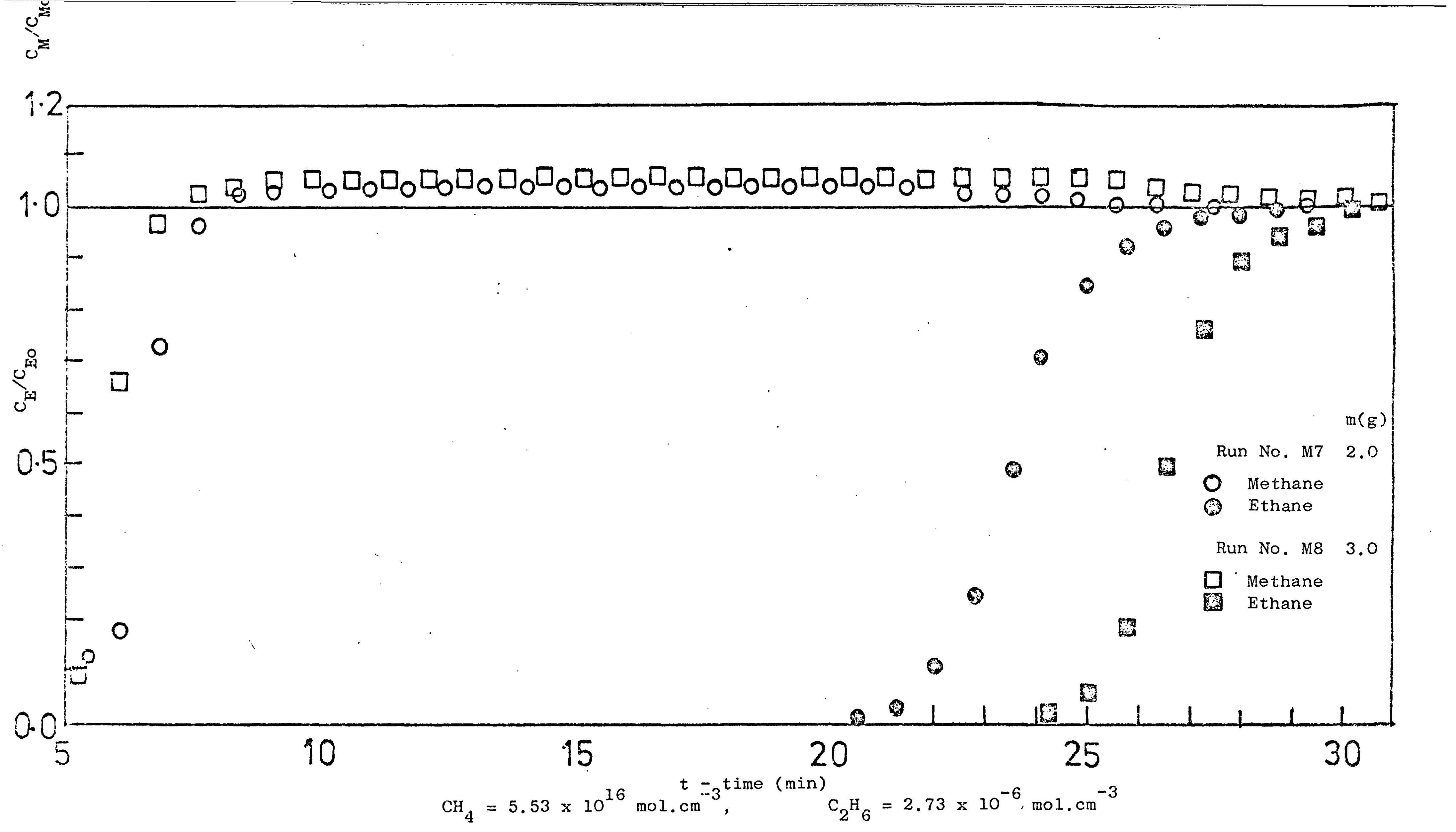

$CH_4 = 5.53 \times 10^{16}$ mol.cm^{-3}, $C_2H_6 = 2.73 \times 10^{-6}$ mol.cm^{-3}

Figure 82: Constant pattern behaviour for binary mixtures on Anthrasorb CC818M at 25°C.

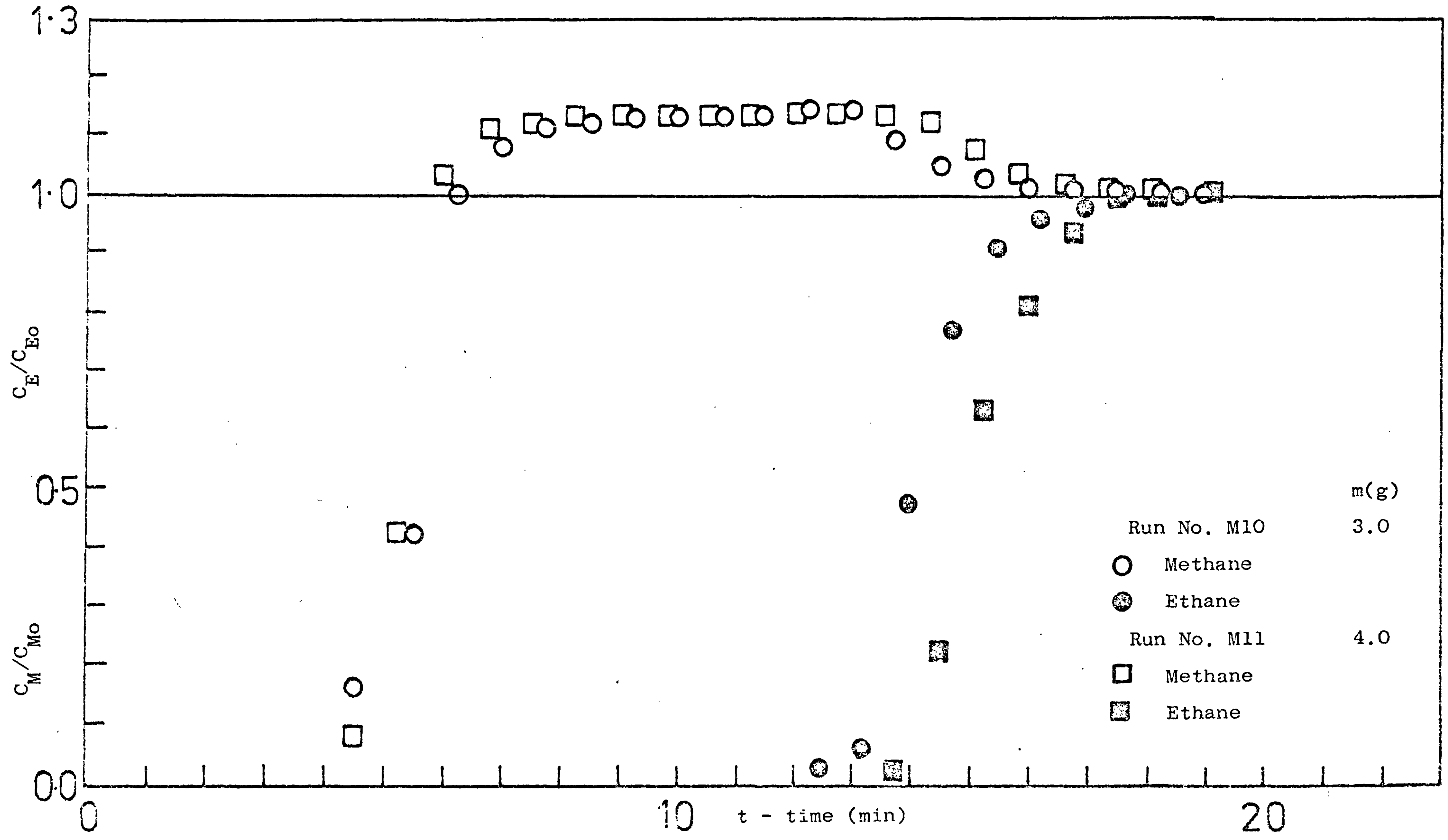

Figure 83: Constant pattern behaviour for binary mixtures on Anthrasorb CC818M at 25^{o}C.

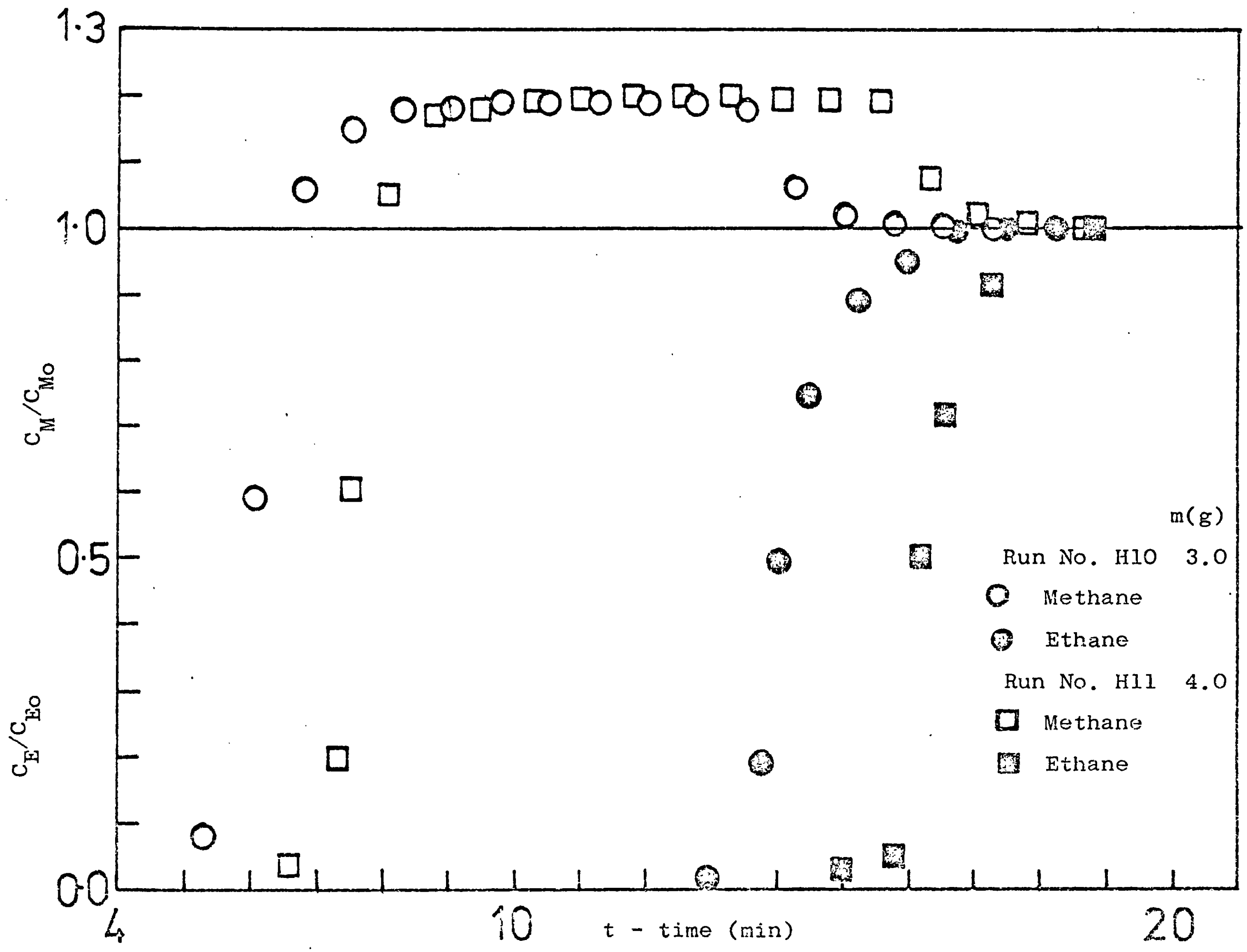

Figure 84: Constant pattern behaviour for binary mixtures on Anthrasorb CC818H at 25°C.

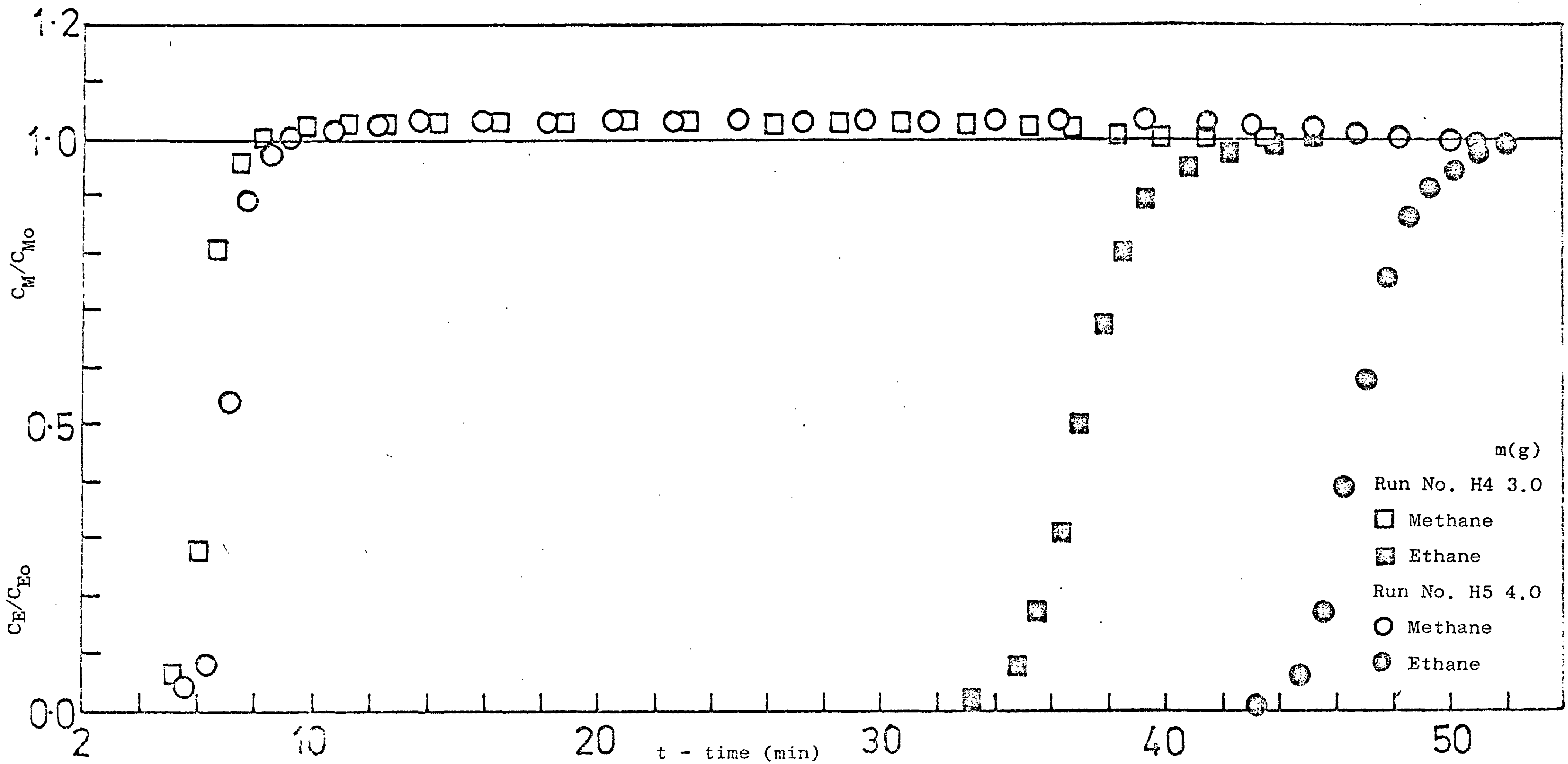

Figure 85: Constant pattern behaviour for binary mixtures on Anthrasorb CC818H at 25°C.

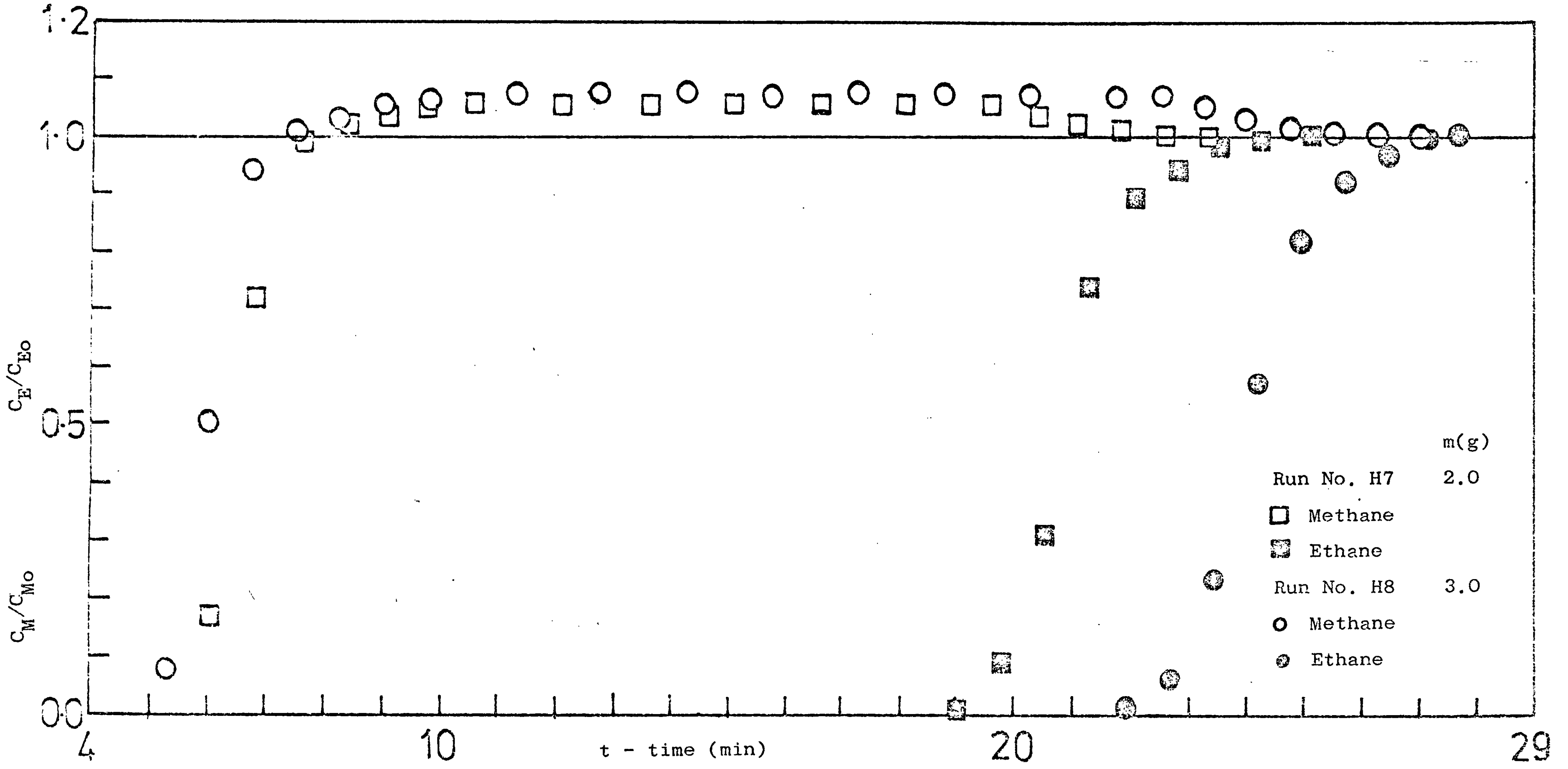

Figure 86: Constant pattern behaviour for binary mixtures on Anthrasorb CC818H at 25°C

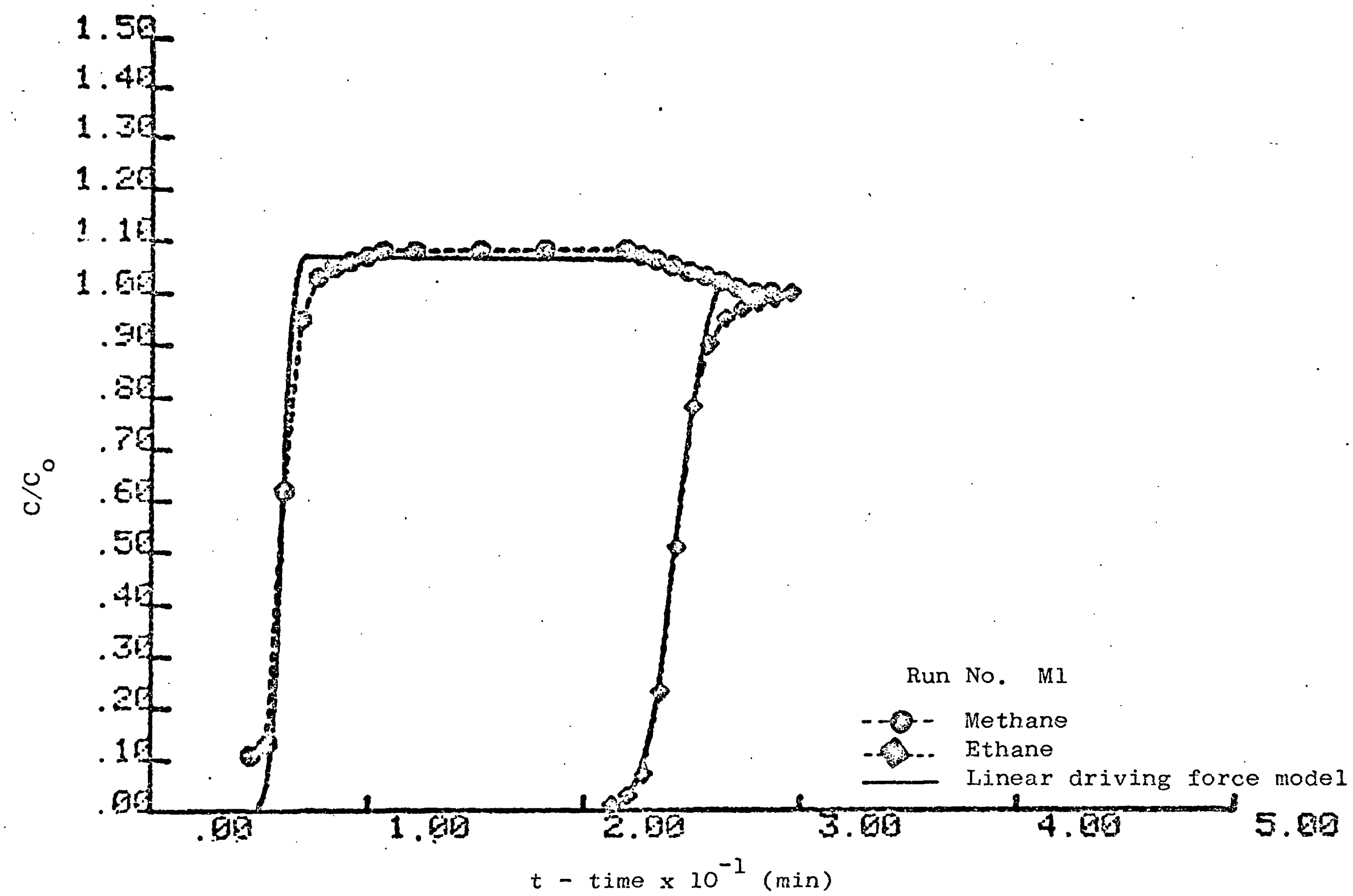

Figure 87: Comparison experimental and predicted breakthrough curves for methane-ethane mixture on Anthrasorb CC818M at 25°C.

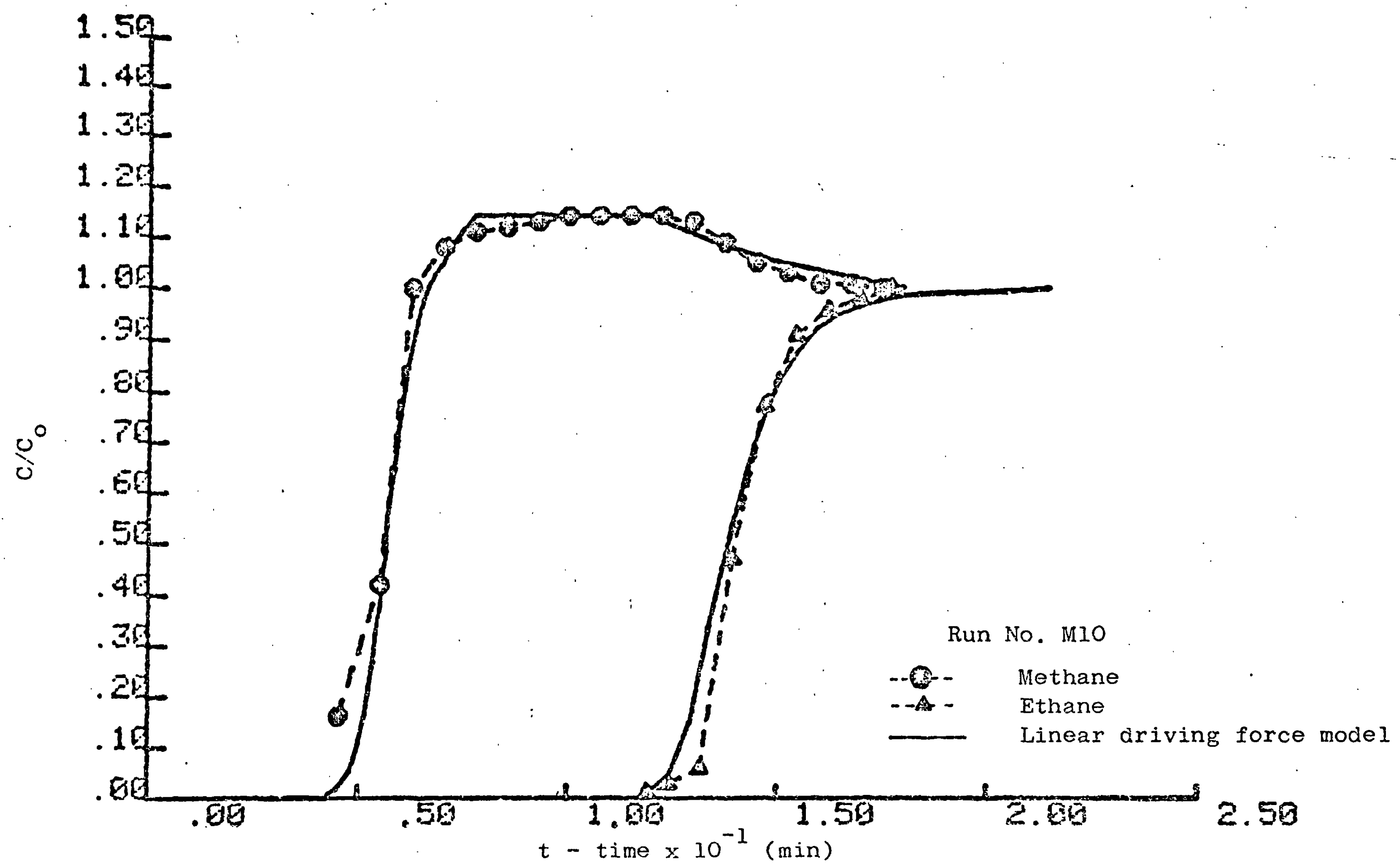

Figure 88: Comparison of experimental and predicted breakthrough curves for methane-ethane mixture on Anthrasorb CC818M at 25°C.

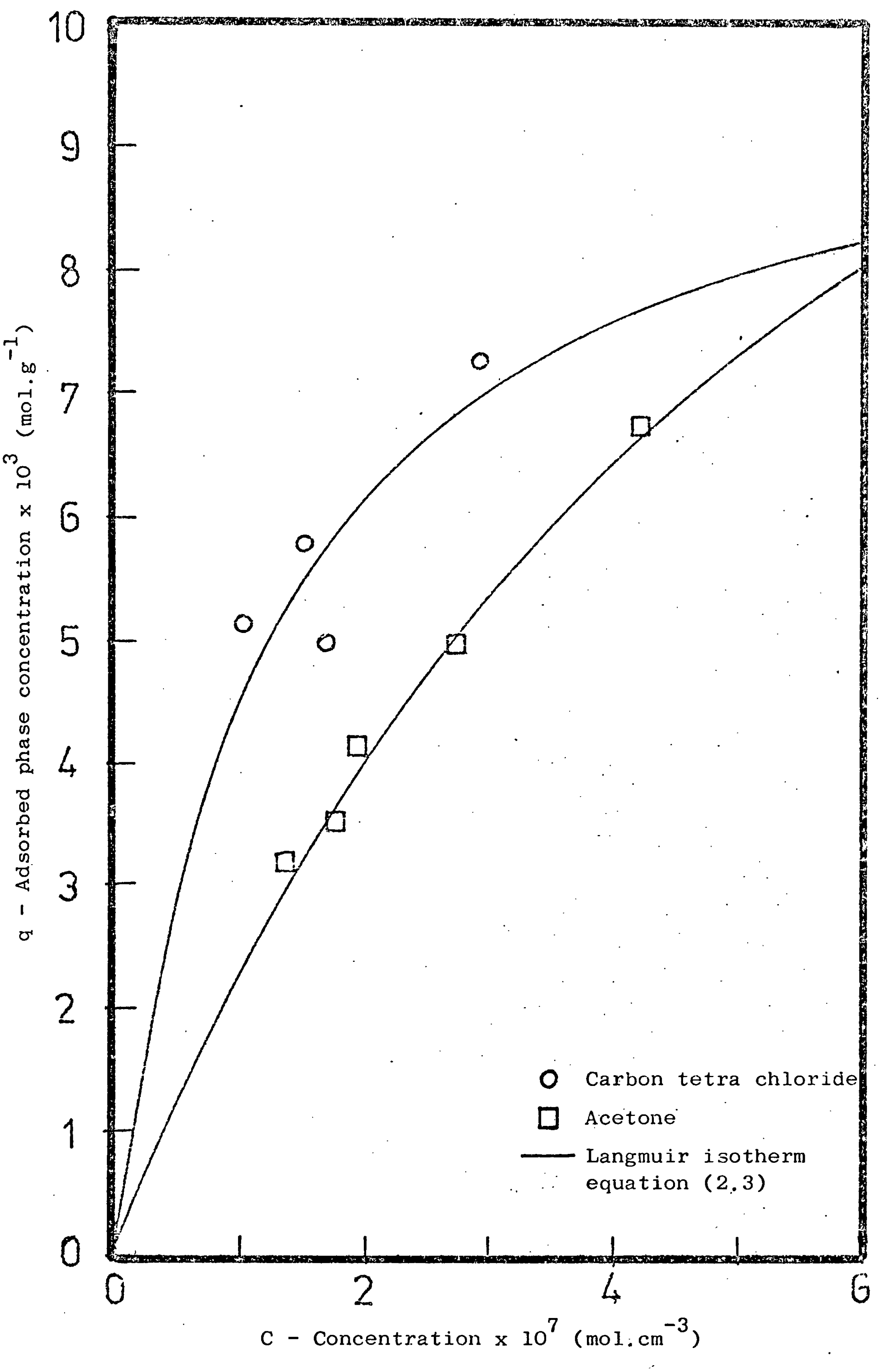

Figure 89: Langmuir isotherms of acetone and carbon tetra chloride on Anthrasorb CC818M at 25^{o}C.

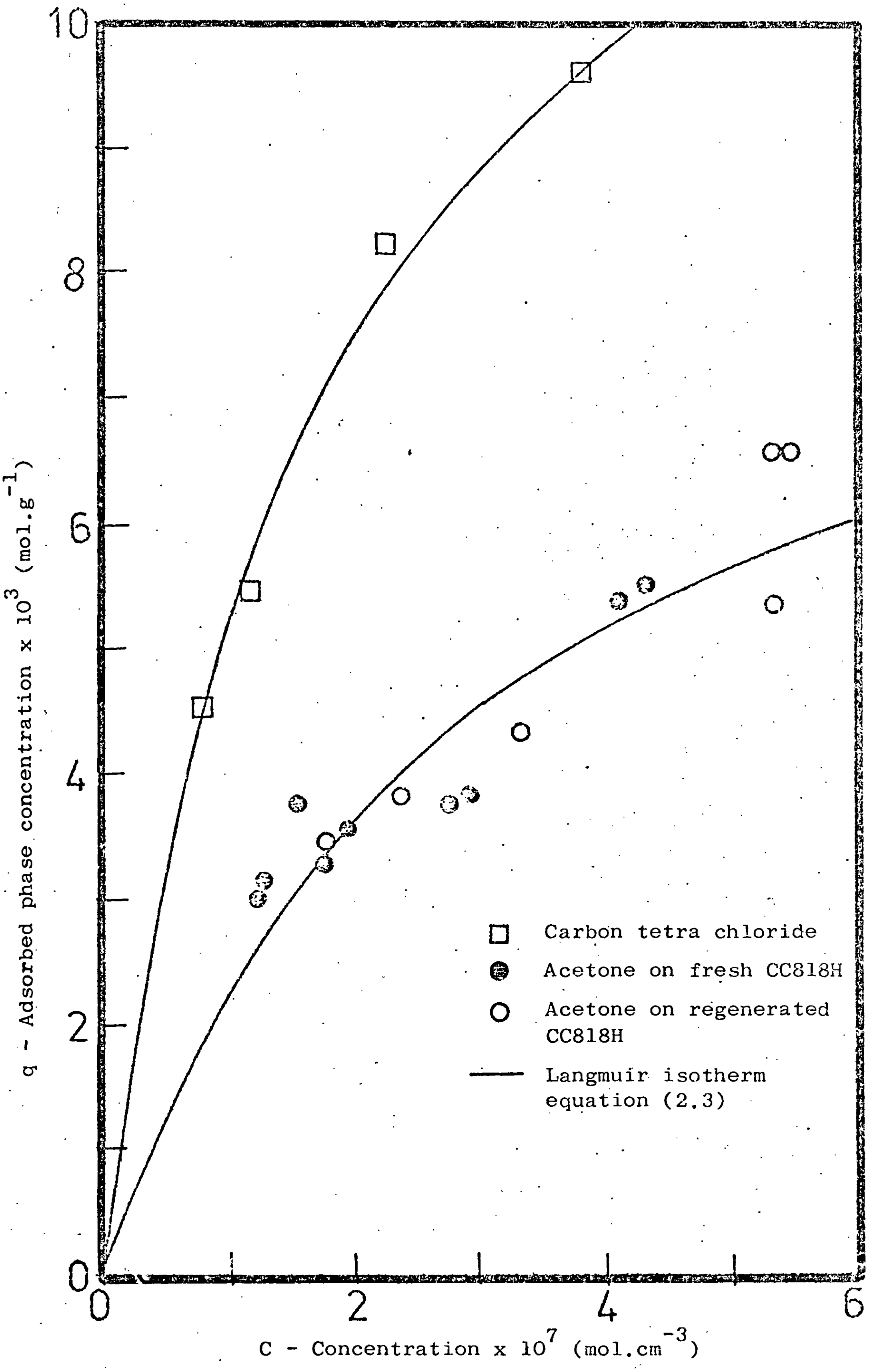

Figure 90: Langmuir isotherms of acetone and carbon tetra chlroide on Anthrasorb CC818H at 25°C

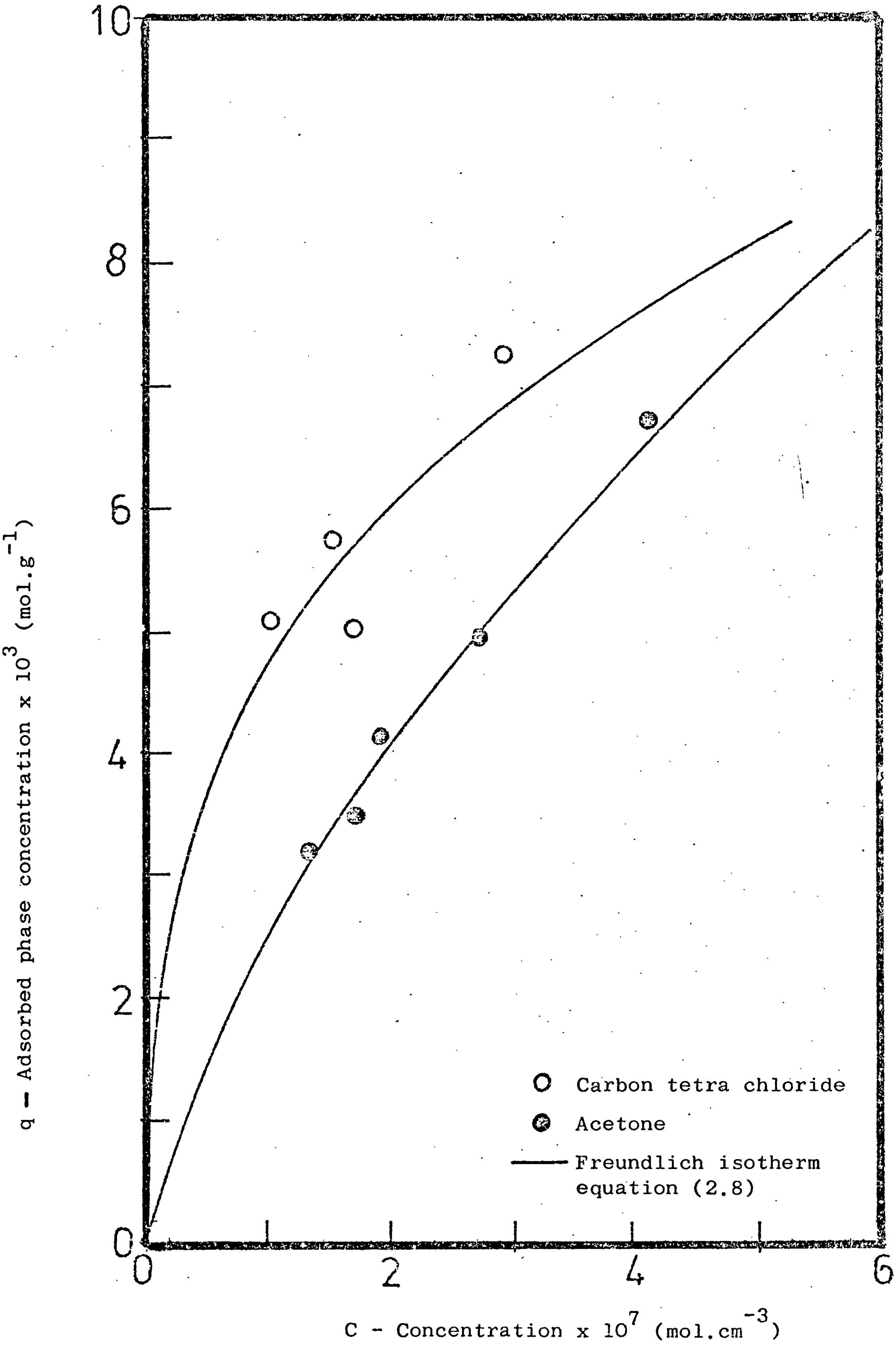

Figure 91: Freundlich isotherms of acetone and carbon tetra chloride on Anthrasorb CC818M at 25°C.

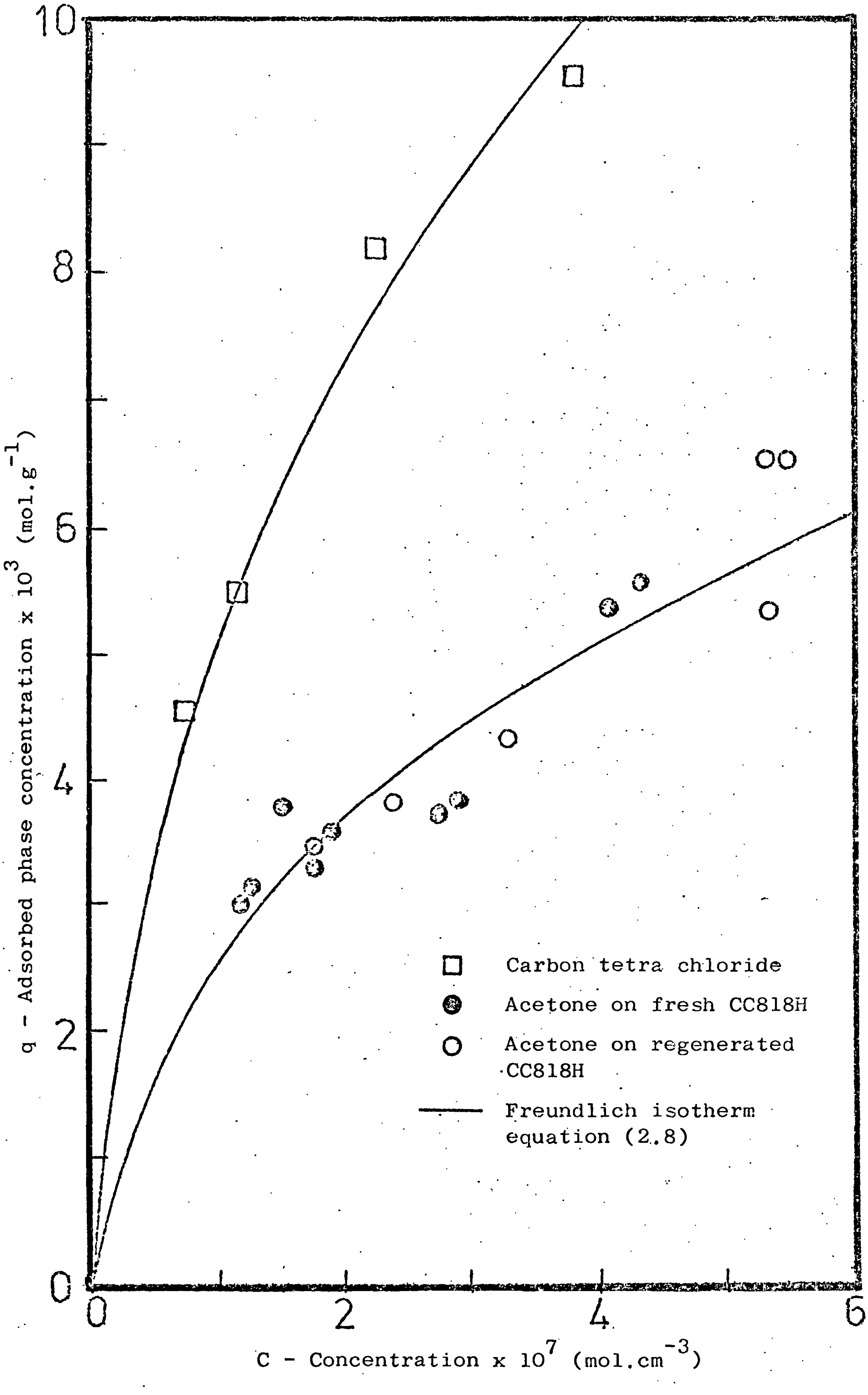

Figure 92: Freundlich isotherms of acetone and carbon tetra chloride on Anthrasorb CC818H at 25°C.

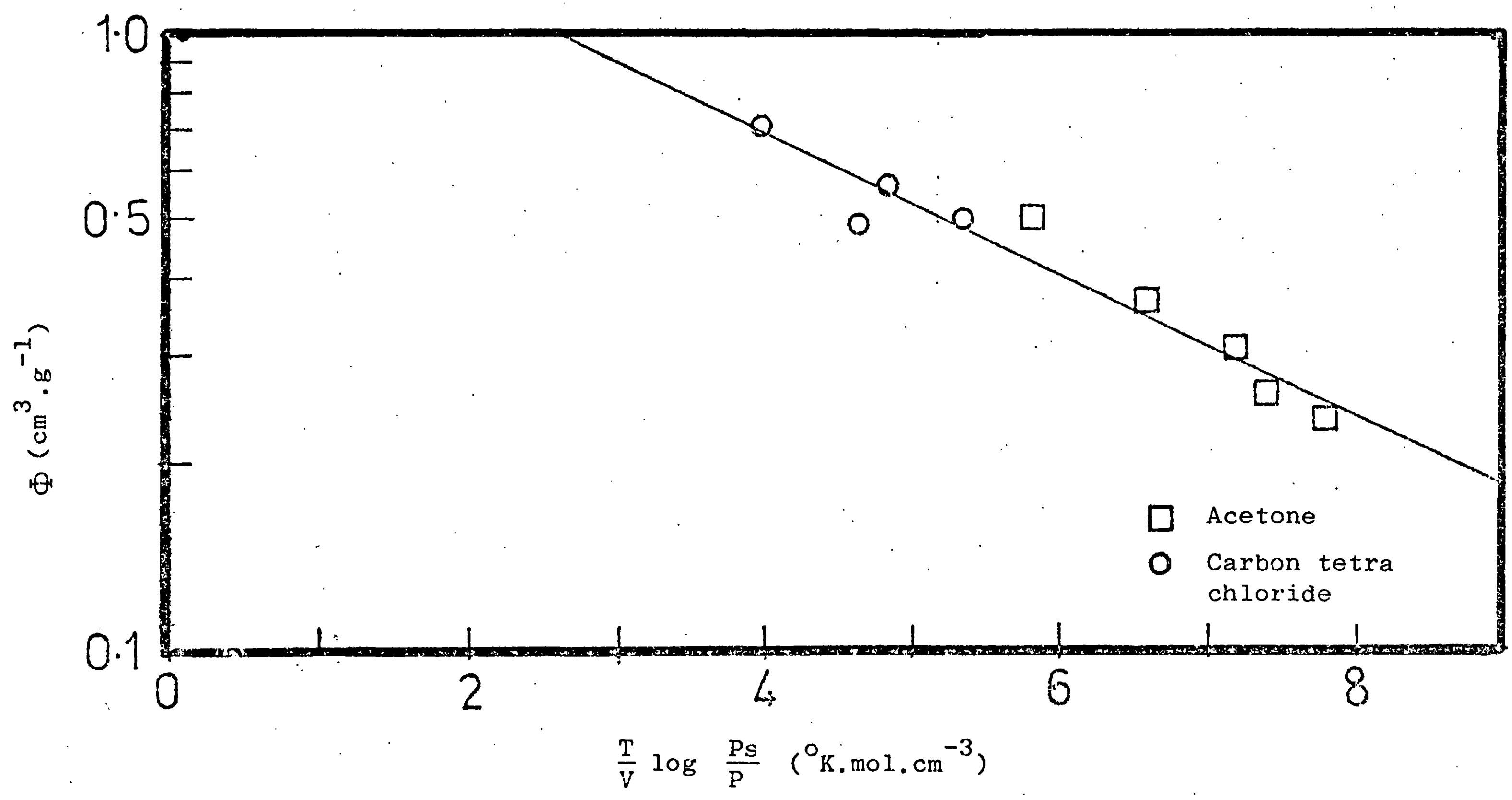

Figure 93: Correlation curve for acetone and carbon tetra chloride on Anthrasorb CC818M at 25°C.

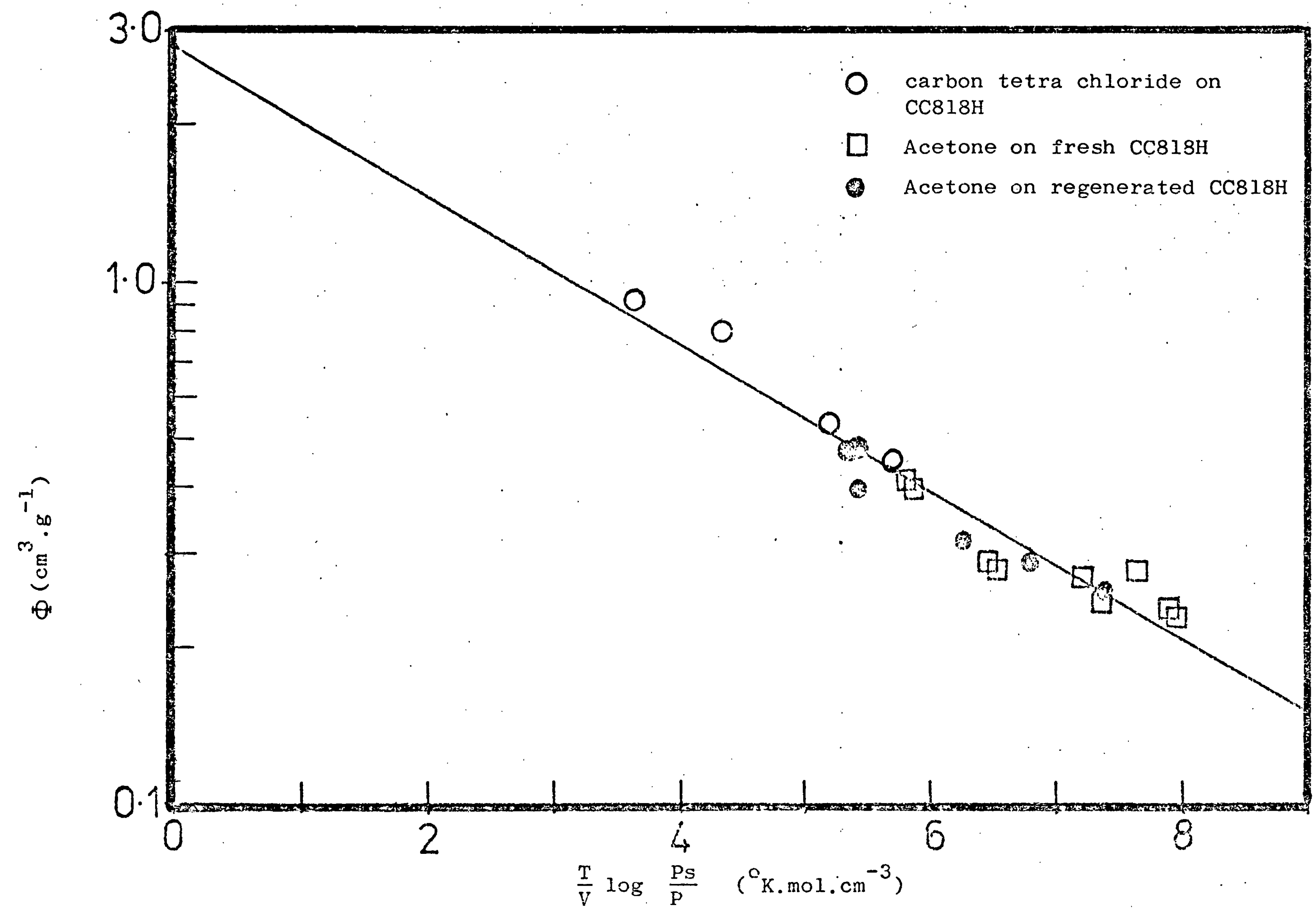

Figure 94: Correlation curve for acetone and carbon tetra chloride on Anthrasorb CC818H at 25^{o}C.

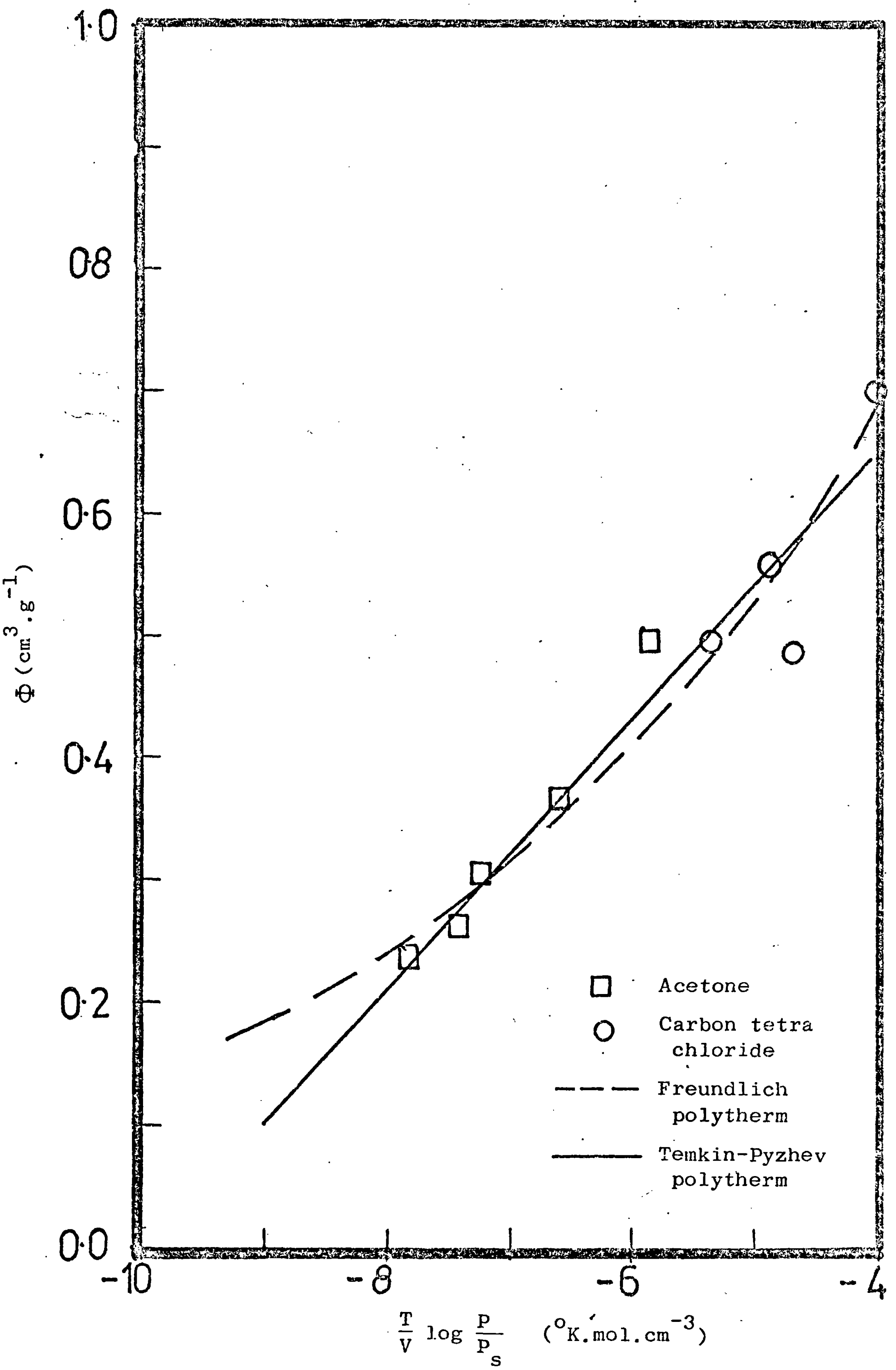

Figure 95: Freundlich and Temkin-Pyzhev polytherms on Anthrasorb CC818M at 25°C.

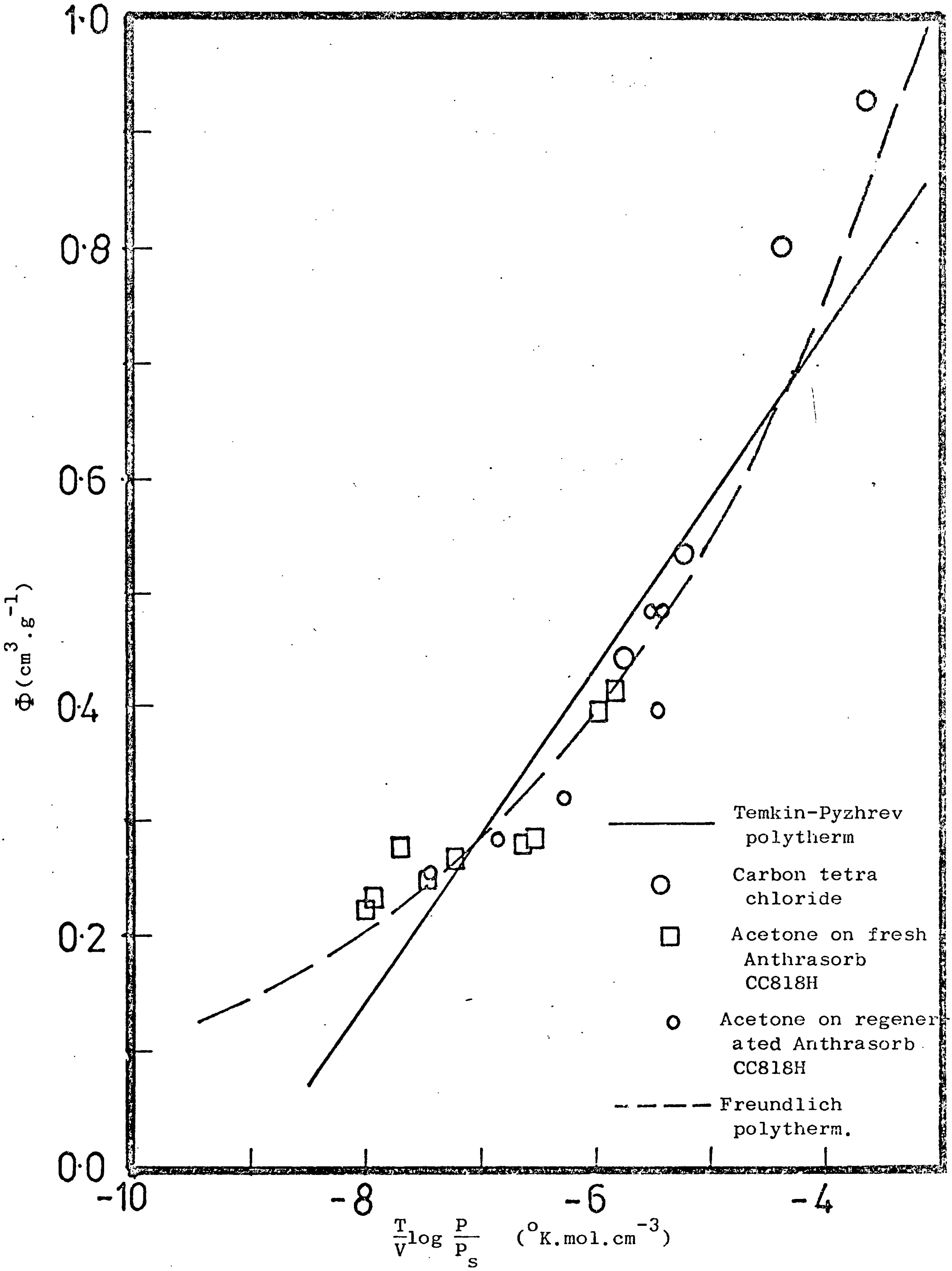

Figure 96: Freundlich and Temkin-Pyzhev polytherms on Anthrasorb CC818H at 25°C.

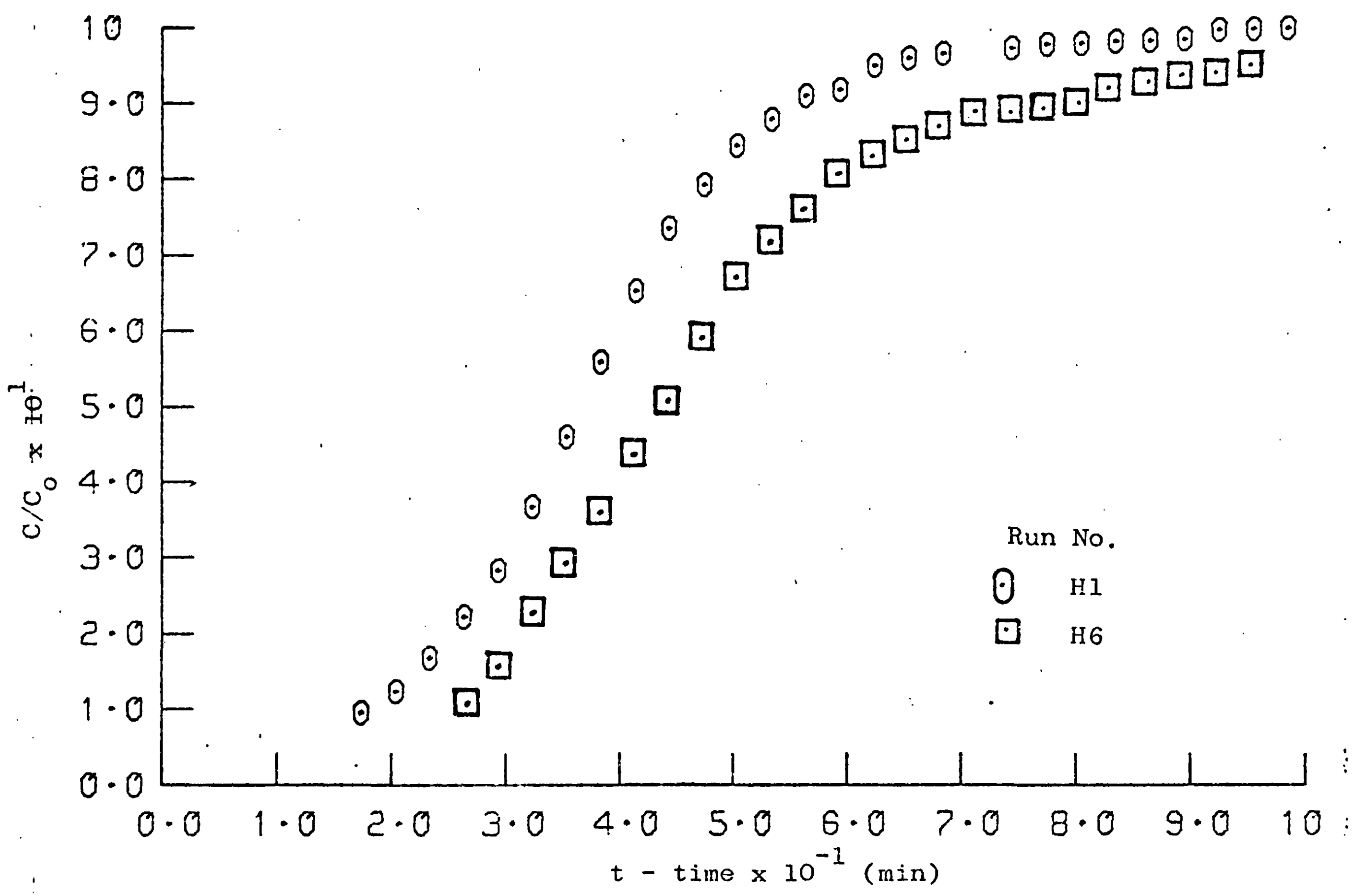

Figure 97: Experimental breakthrough curves for acetone on Anthrasorb CC818H at 25°C.

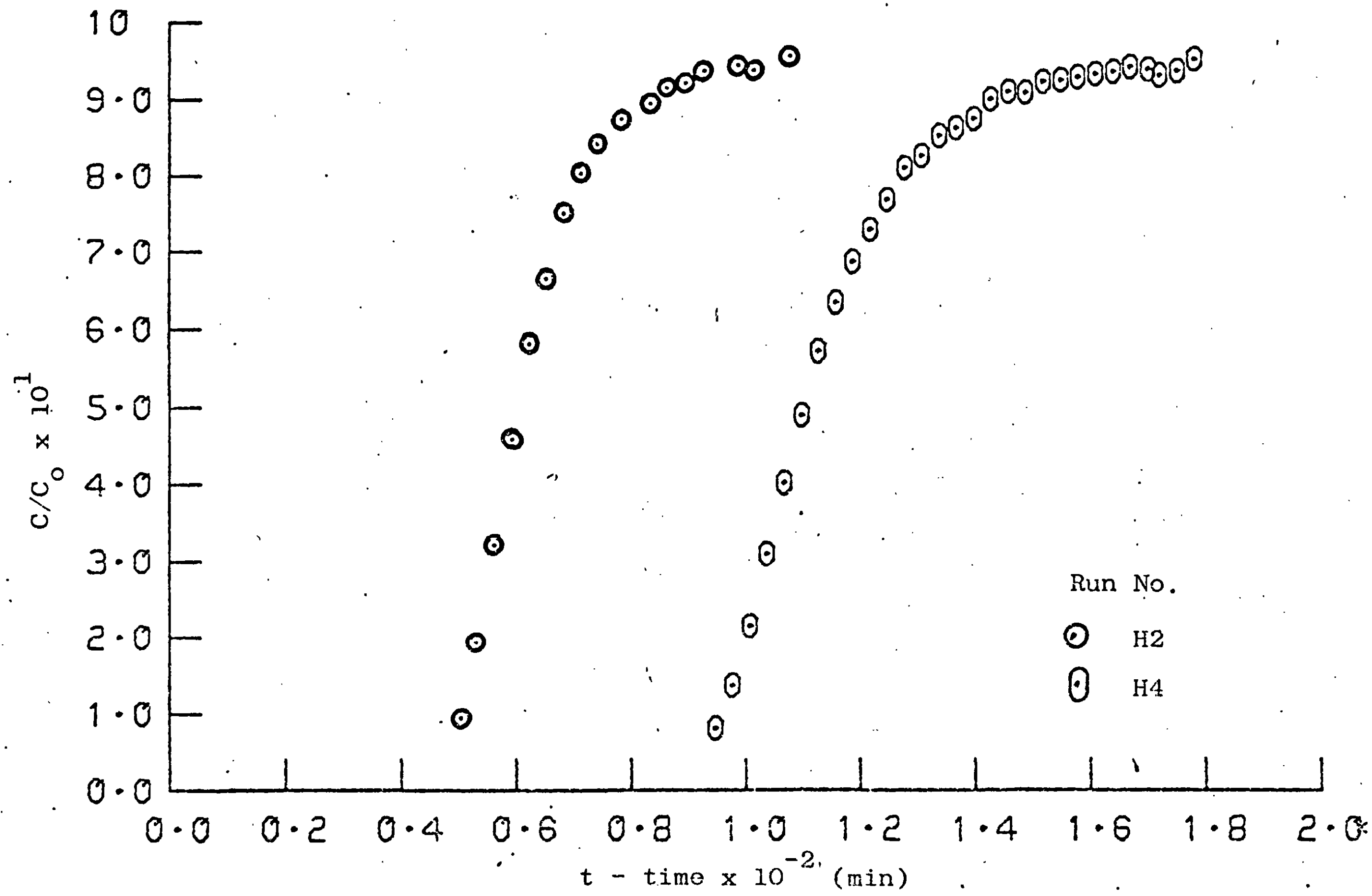

Figure 98: Experimental breakthrough curves for acetone on Anthrasorb CC818H at 25°C.

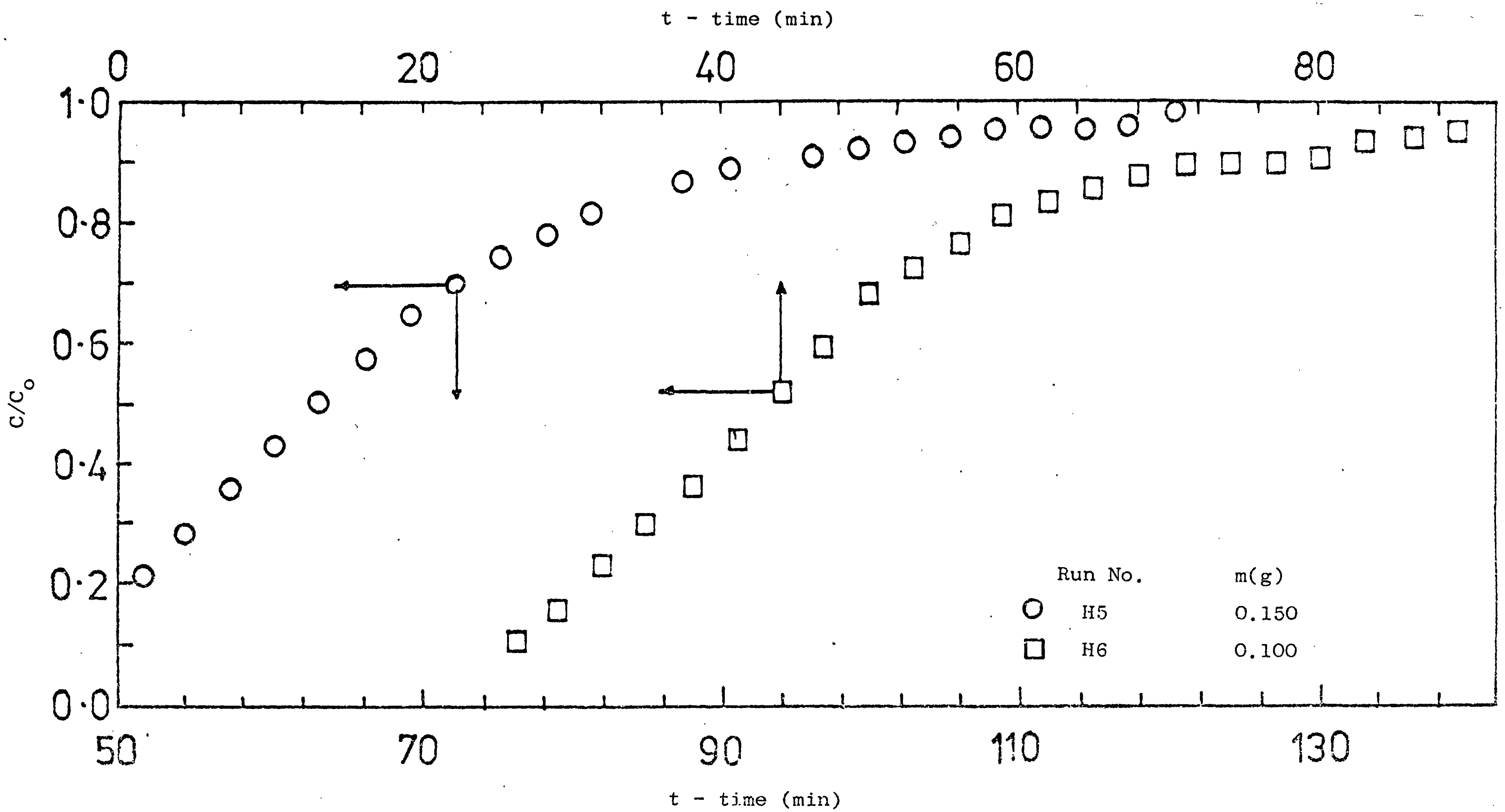

Figure 99: Constant pattern behaviour for acetone on Anthrasorb CC818H

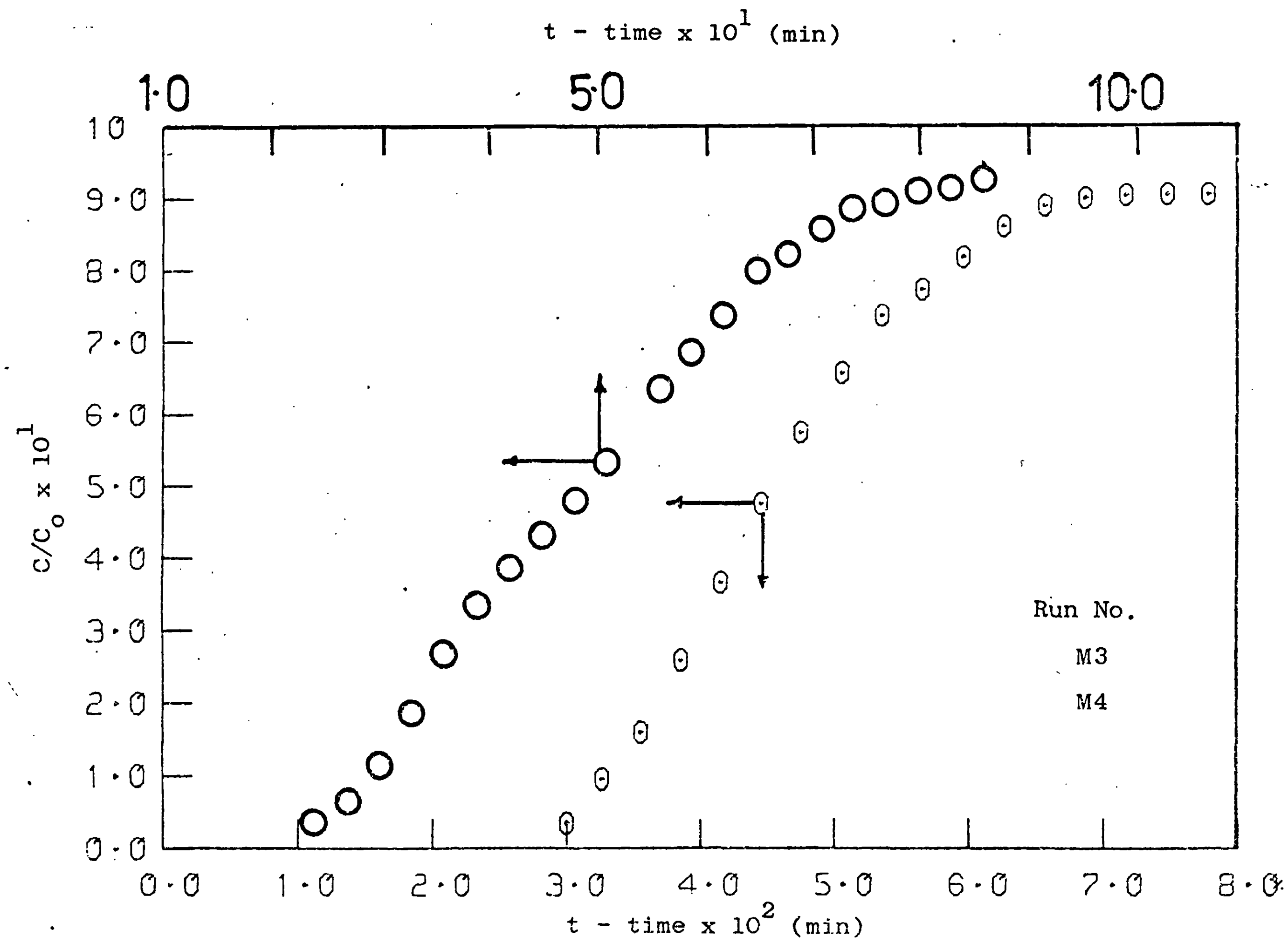

Figure 100: Experimental breakthrough curves for acetone on Anthrasorb CC818M at 25°C.

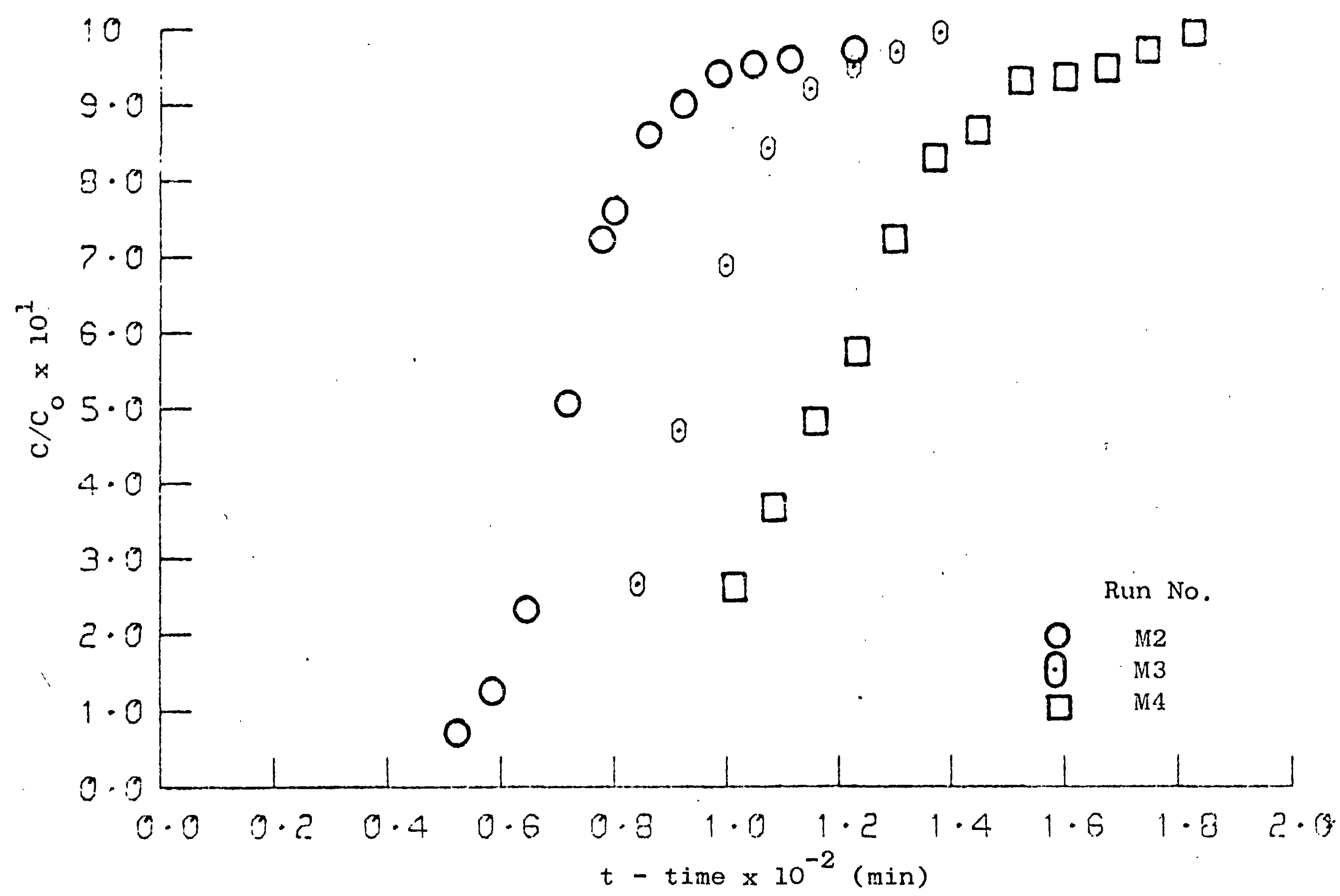

Figure 101: Experimental breakthrough curves for carbon tetra-chloride on Anthrasorb CC818M at 25^{o}C.

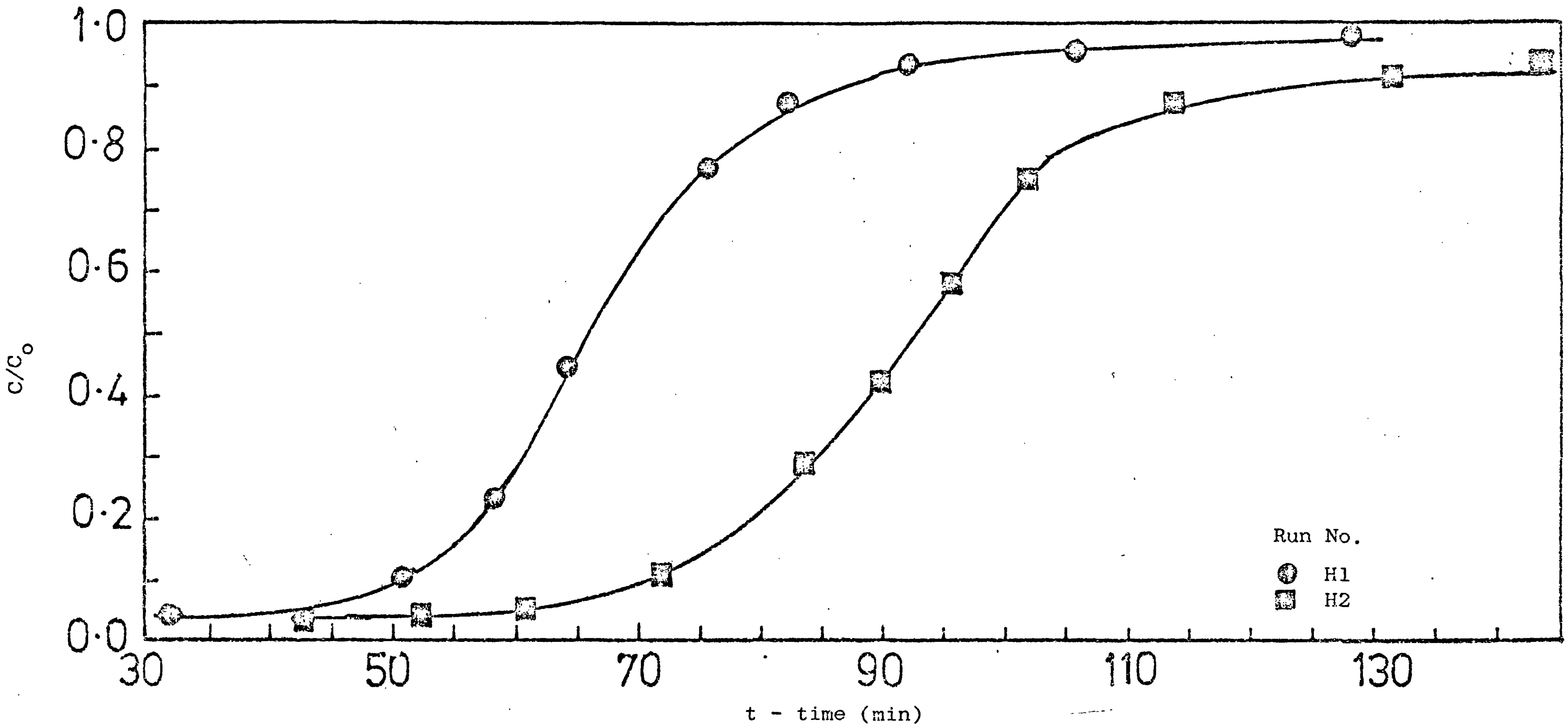

Figure 102: Experimental breakthrough curves for carbon tetra-chloride on Anthrasorb CC818H at 25°C.

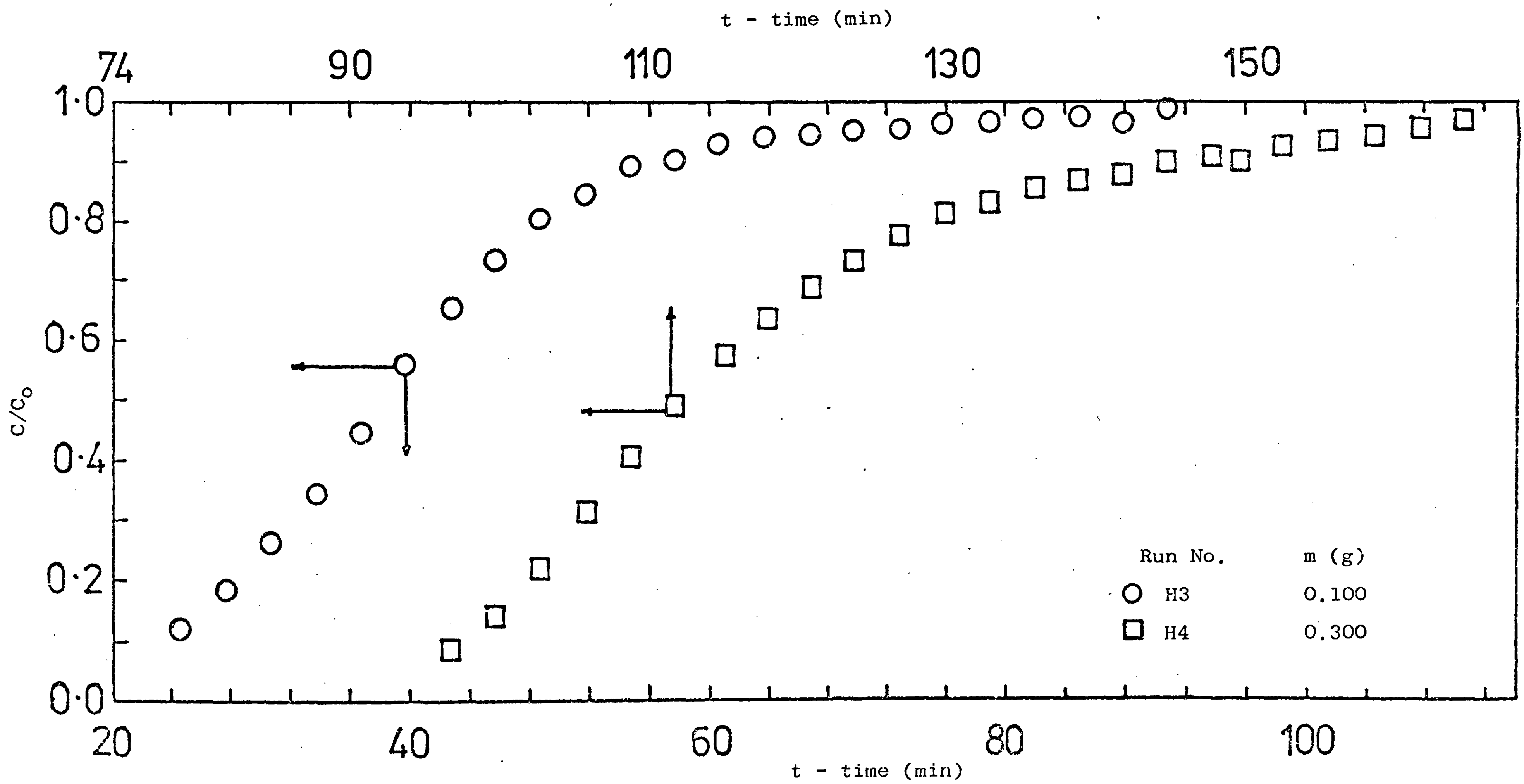

Figure 103: Constant pattern behaviour for acetone on Anthrasorb CC818H

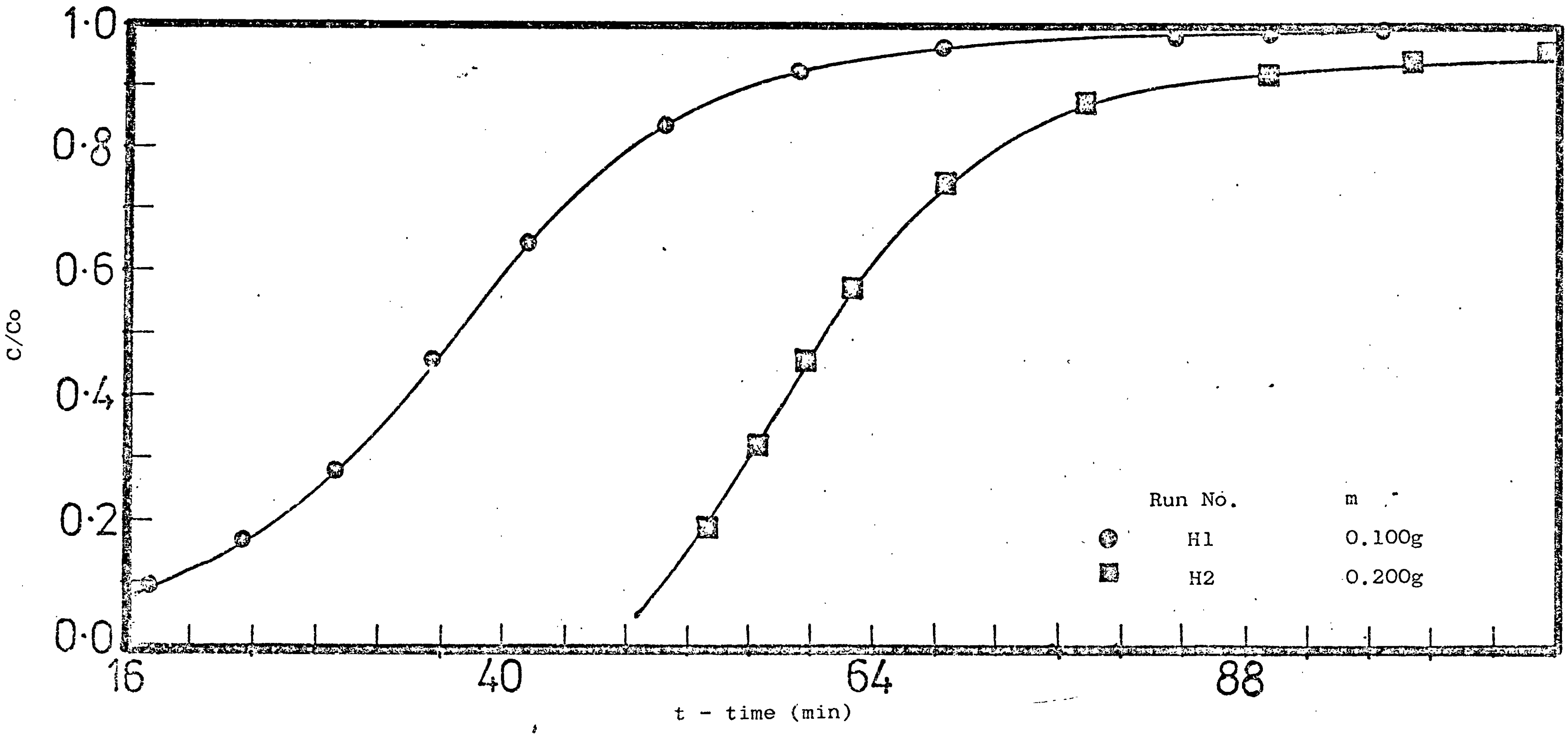

Figure 104: Constant pattern behaviour for acetone.

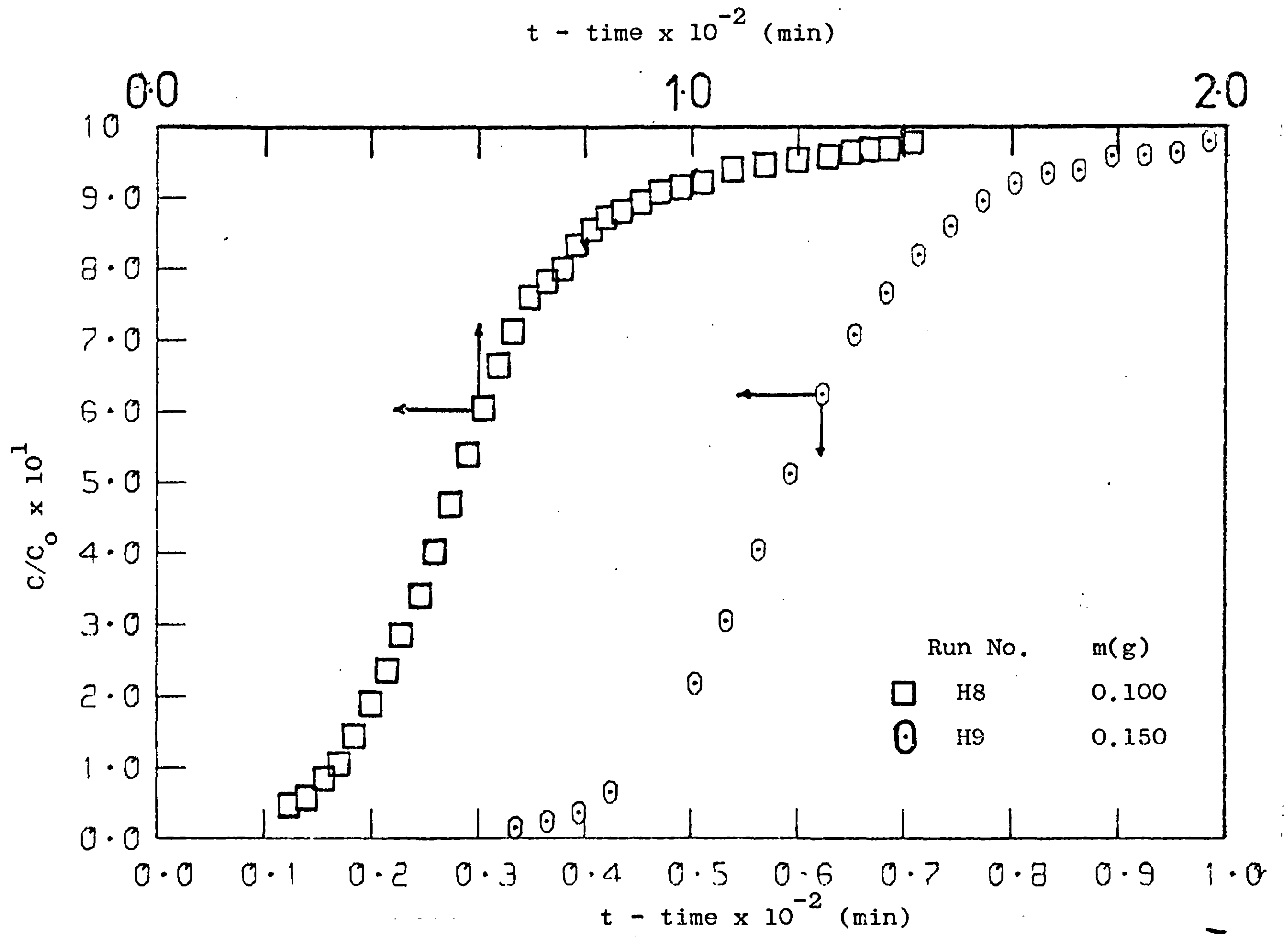

Figure 105: Constant pattern behaviour for acetone on Anthrasorb CC818H at 25°C.

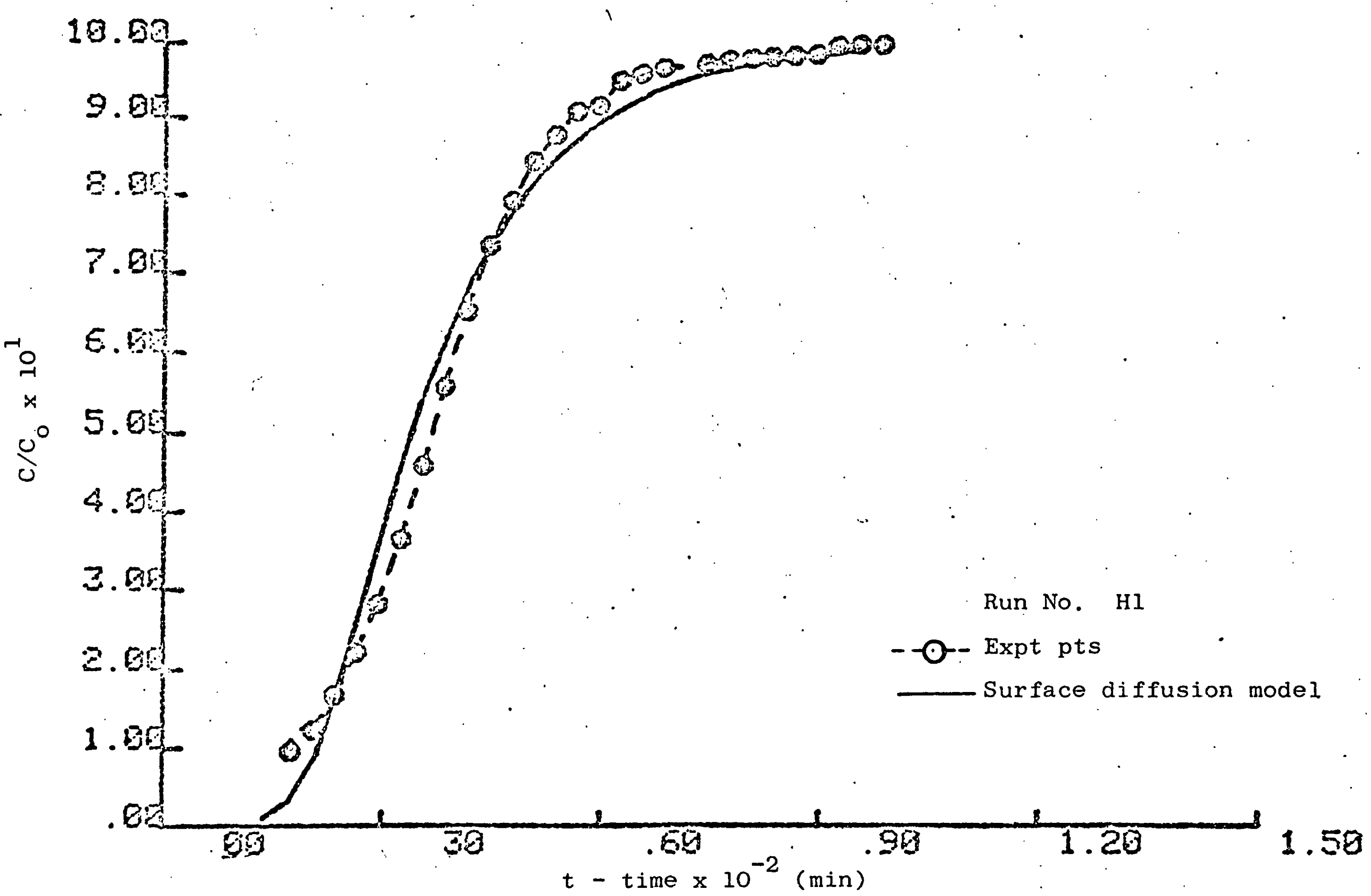

Figure 106: Comparison of experimental and predicted breakthrough curves for acetone on Anthrasorb CC818H at 25°C.

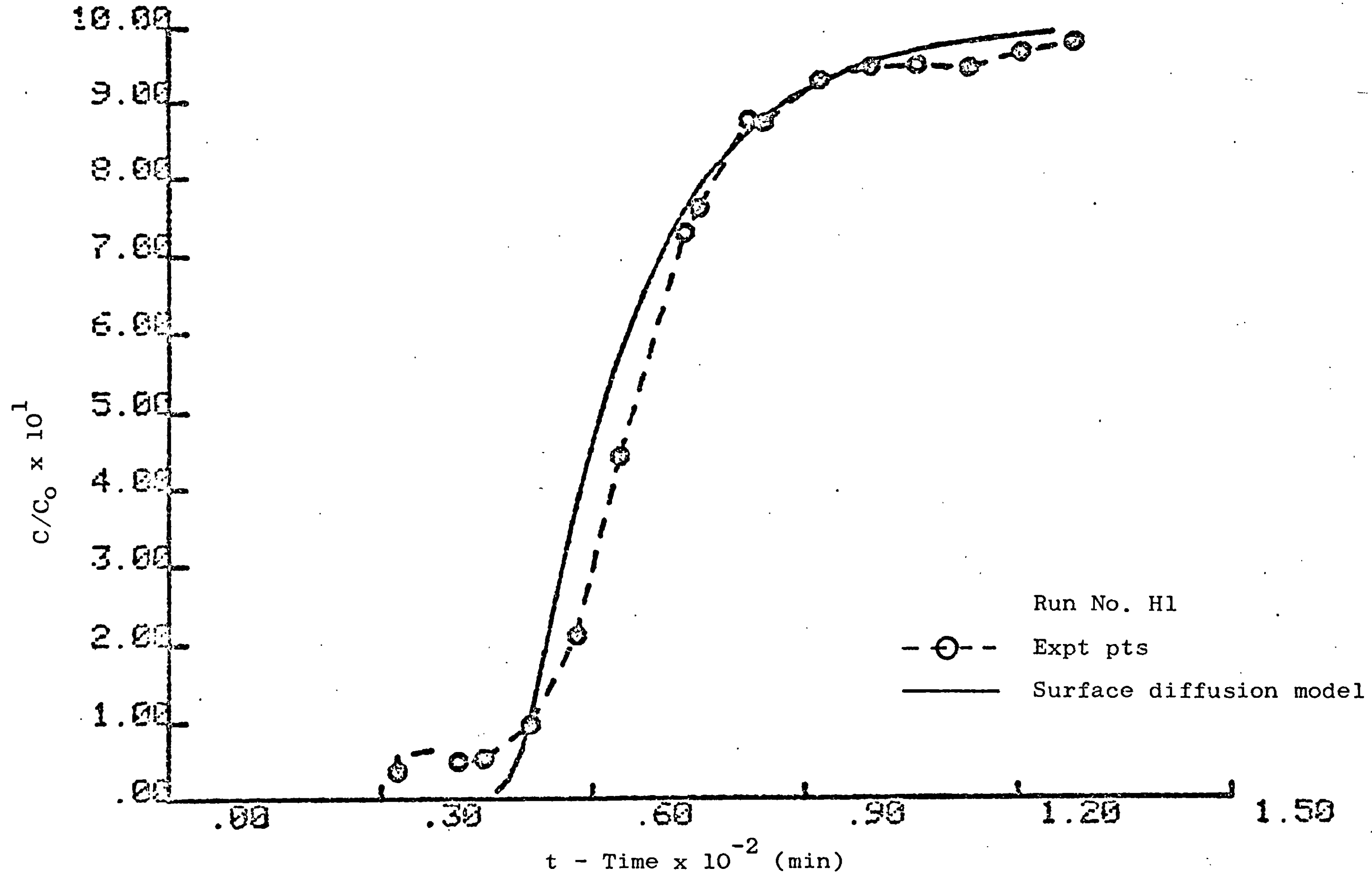

Figure 107: Comparison of experimental and predicted breakthrough curves for carbon tetra-chloride on Anthrasorb CC818H at 25°C.

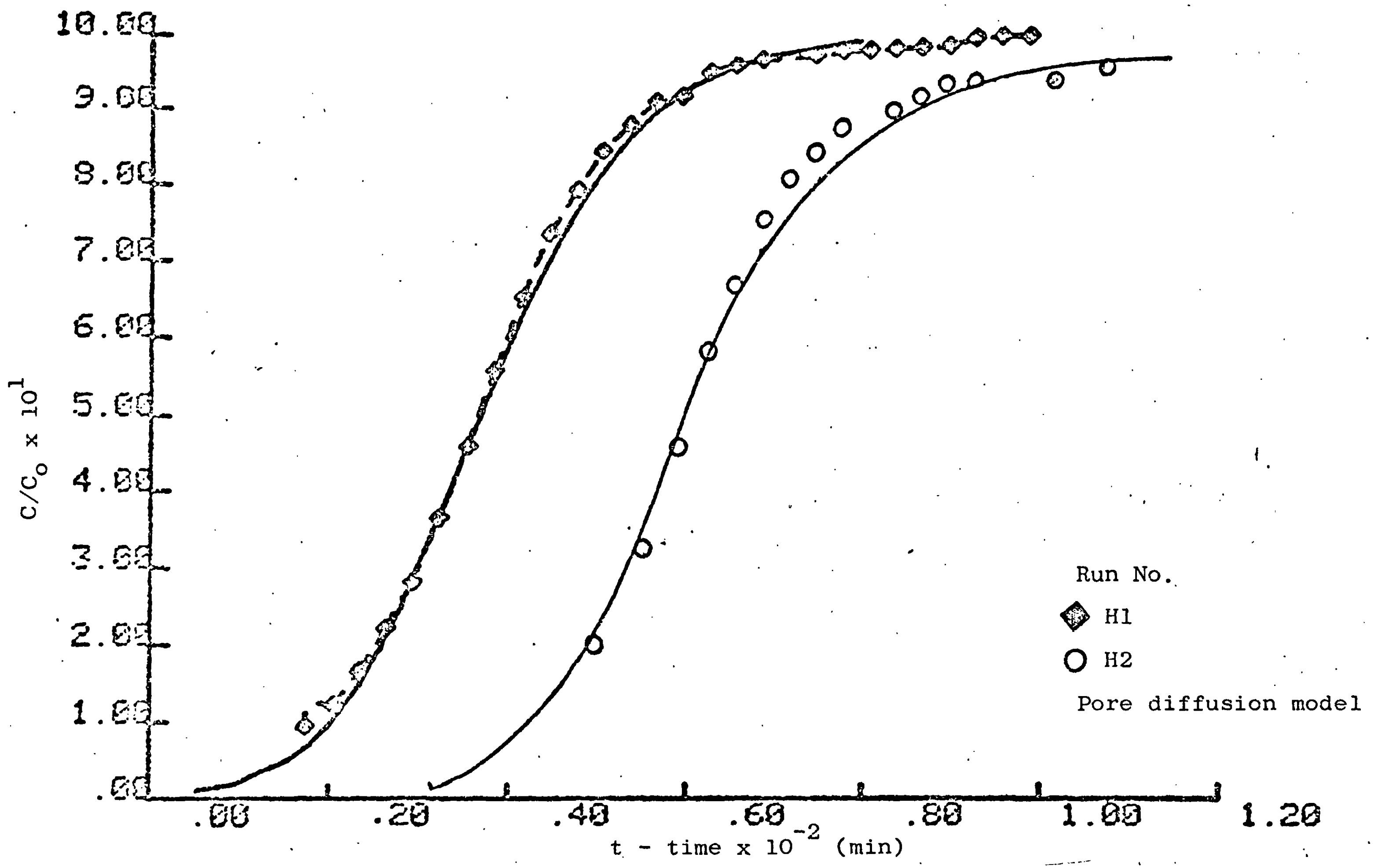

Figure 108: Comparison of experimental and predicted breakthrough curves for acetone on Anthrasorb CC818H at 25°C.

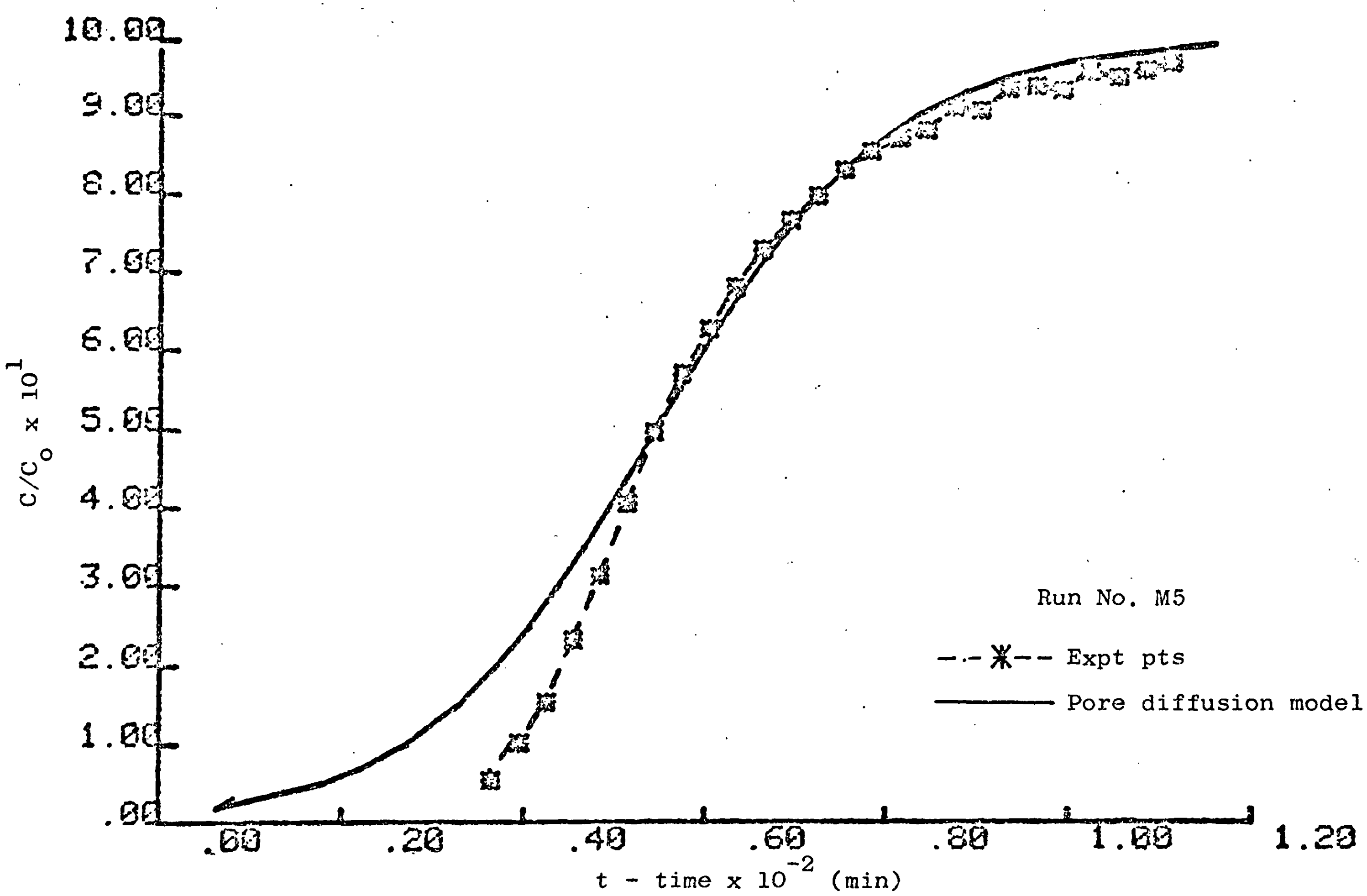

Figure 109: Comparison of experimental and predicted breakthrough curves for acetone on Anthrasorb CC818M at 25°C.

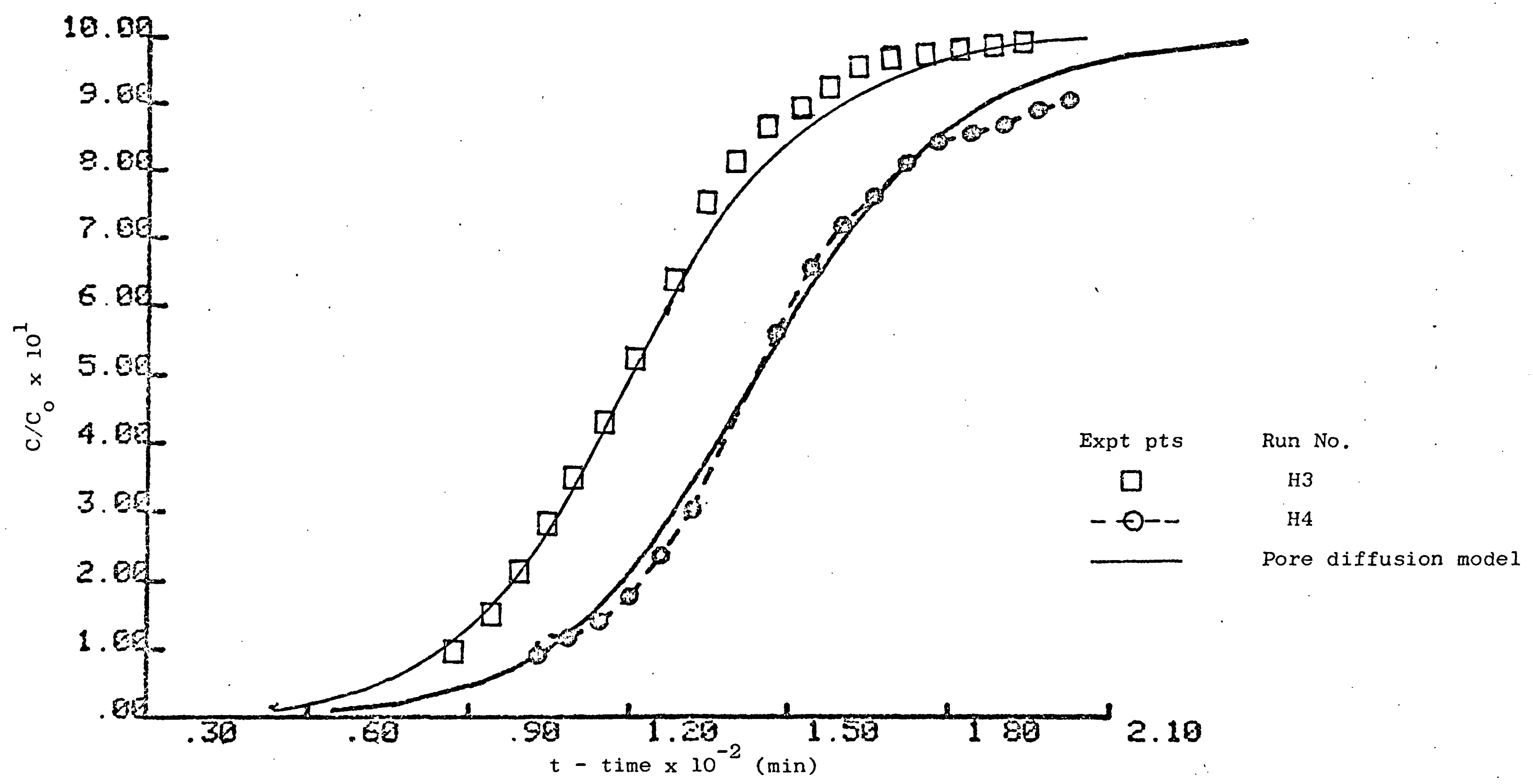

Figure 110: Comparison of experimental and predicted breakthrough curves for carbon tetra chloride on Anthrasorb CC818H at 25°C.

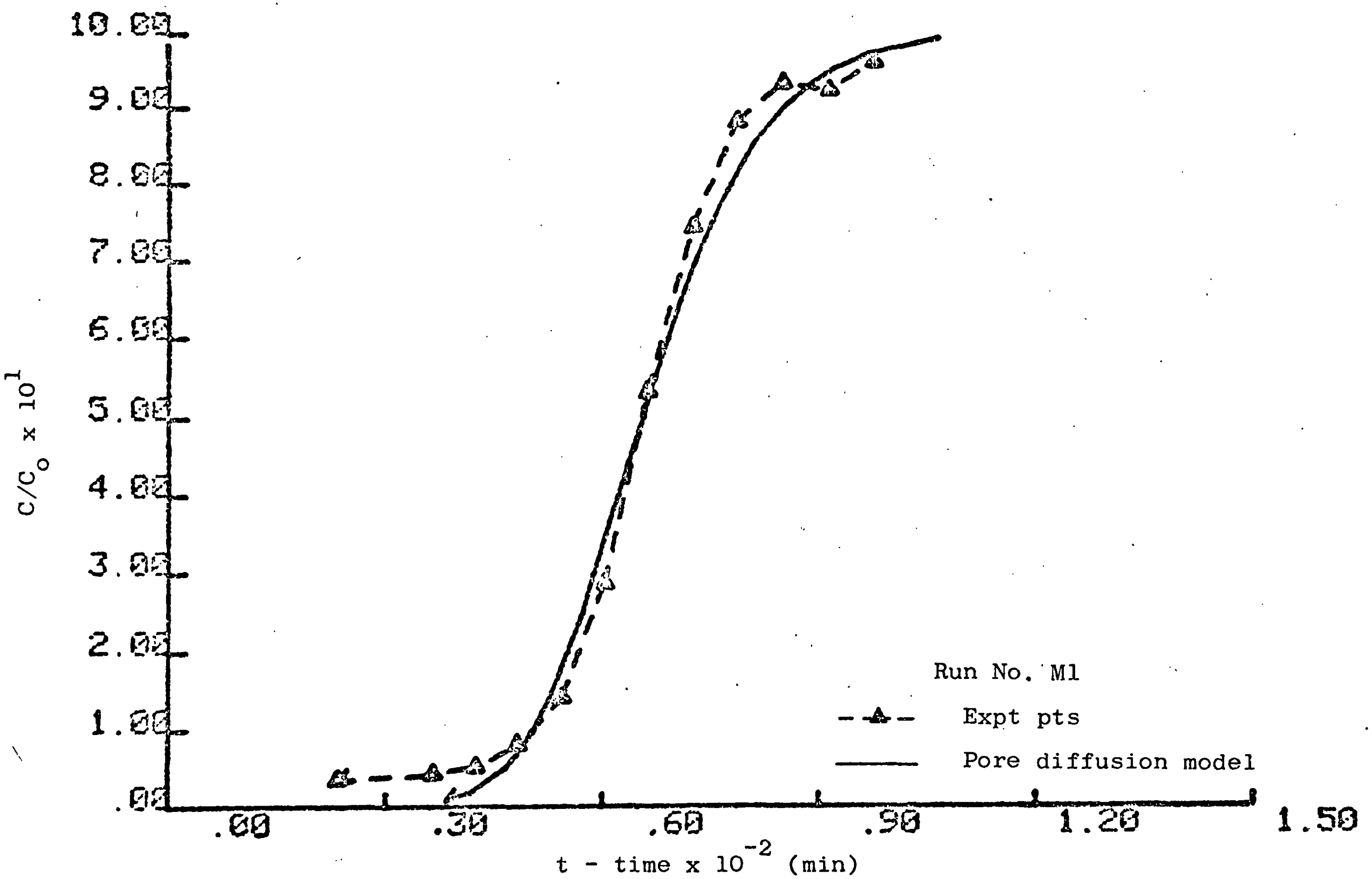

Figure 111: Comparison of experimental and predicted breakthrough curves for carbon tetra chloride on Anthrasorb CC818M at 25°C.

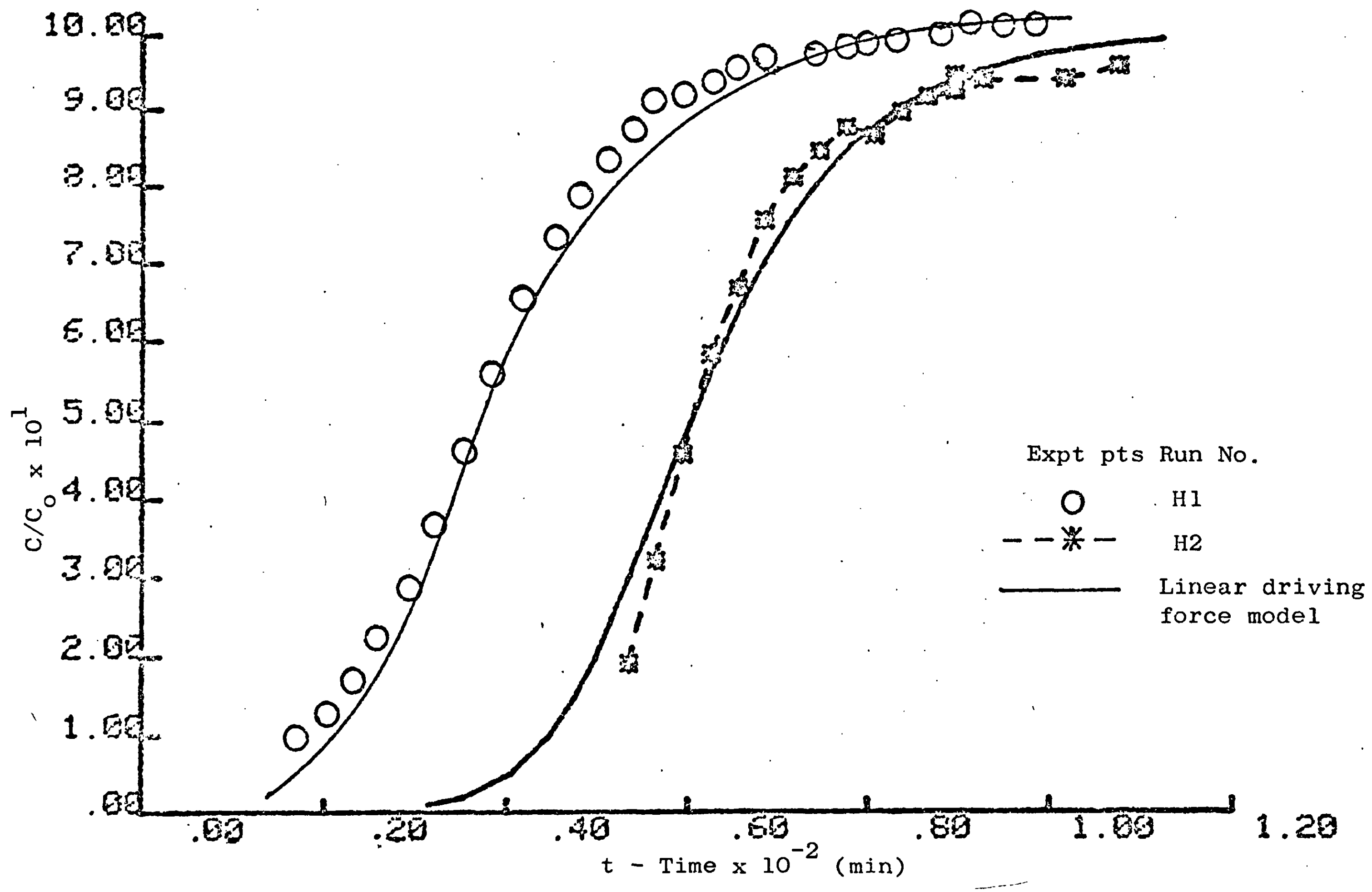

Figure 112: Comparison of experimental and predicted breakthrough curves for acetone on Anthrasorb CC818H at 25°C.

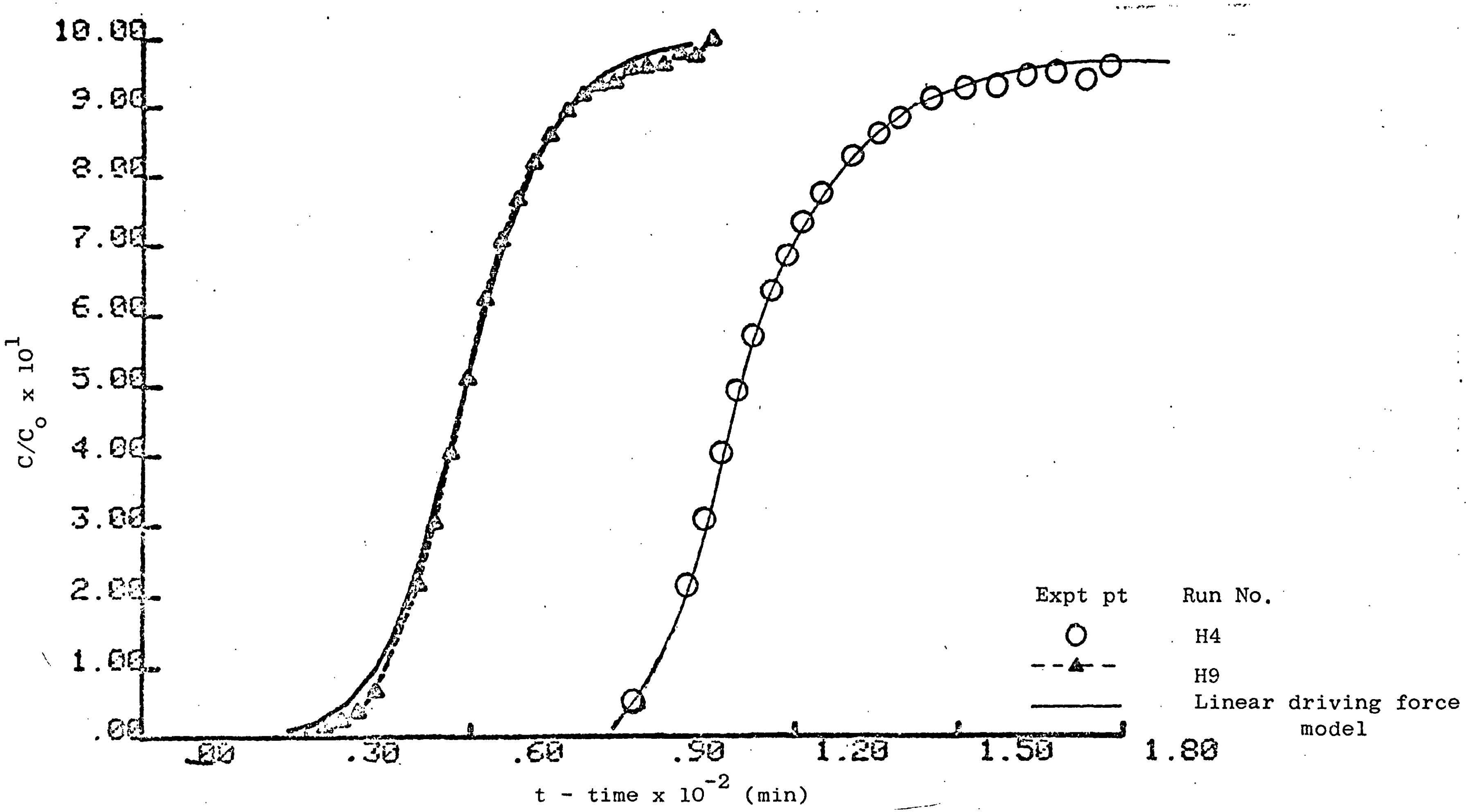

Figure 113: Comparison of experimental and predicted breakthrough curves for acetone on Anthrasorb CC818H at 25°C.

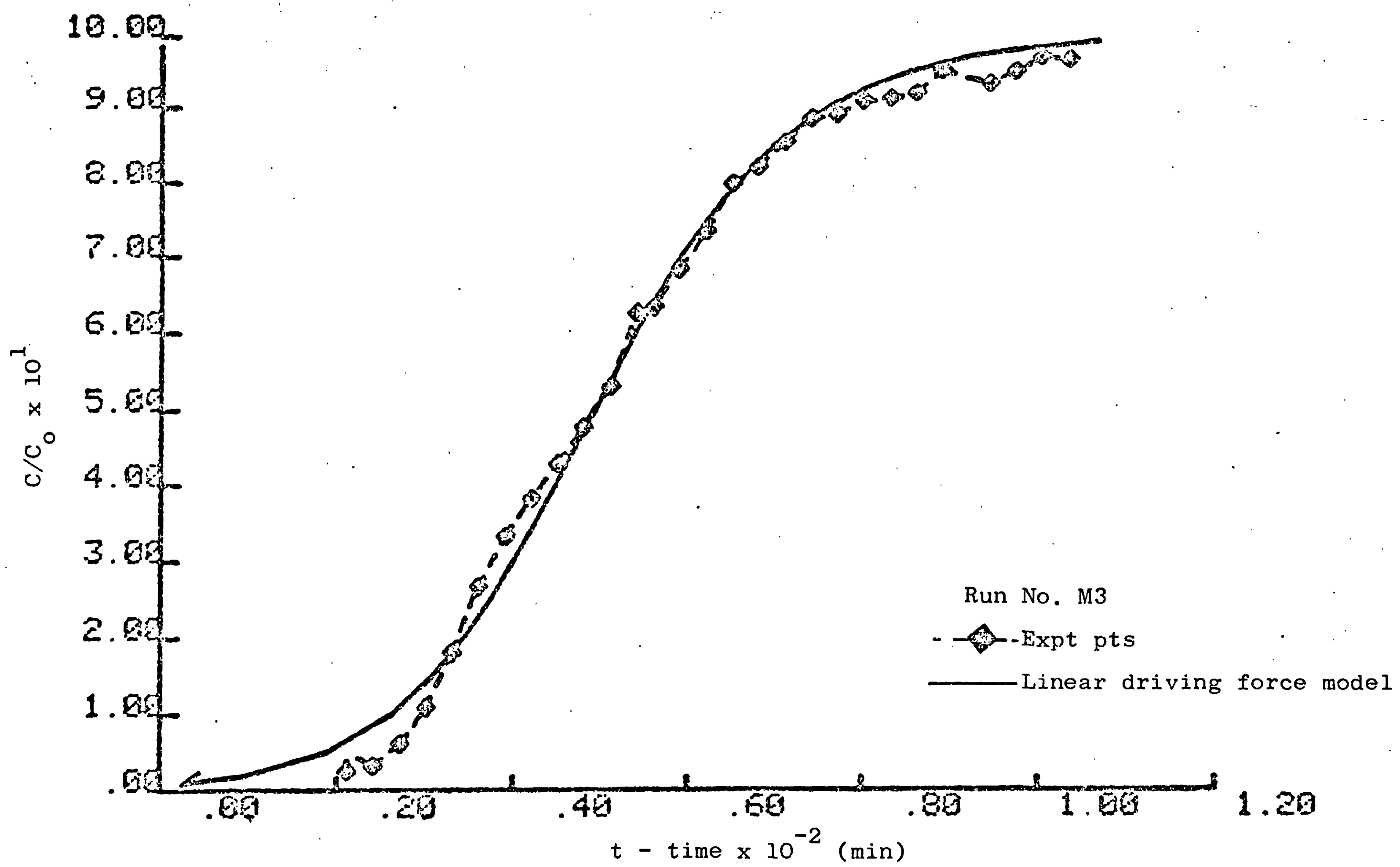

Figure 114: Comparison of experimental and predicted breakthrough curves for acetone on Anthrasorb CC818M at 25^{o}C.

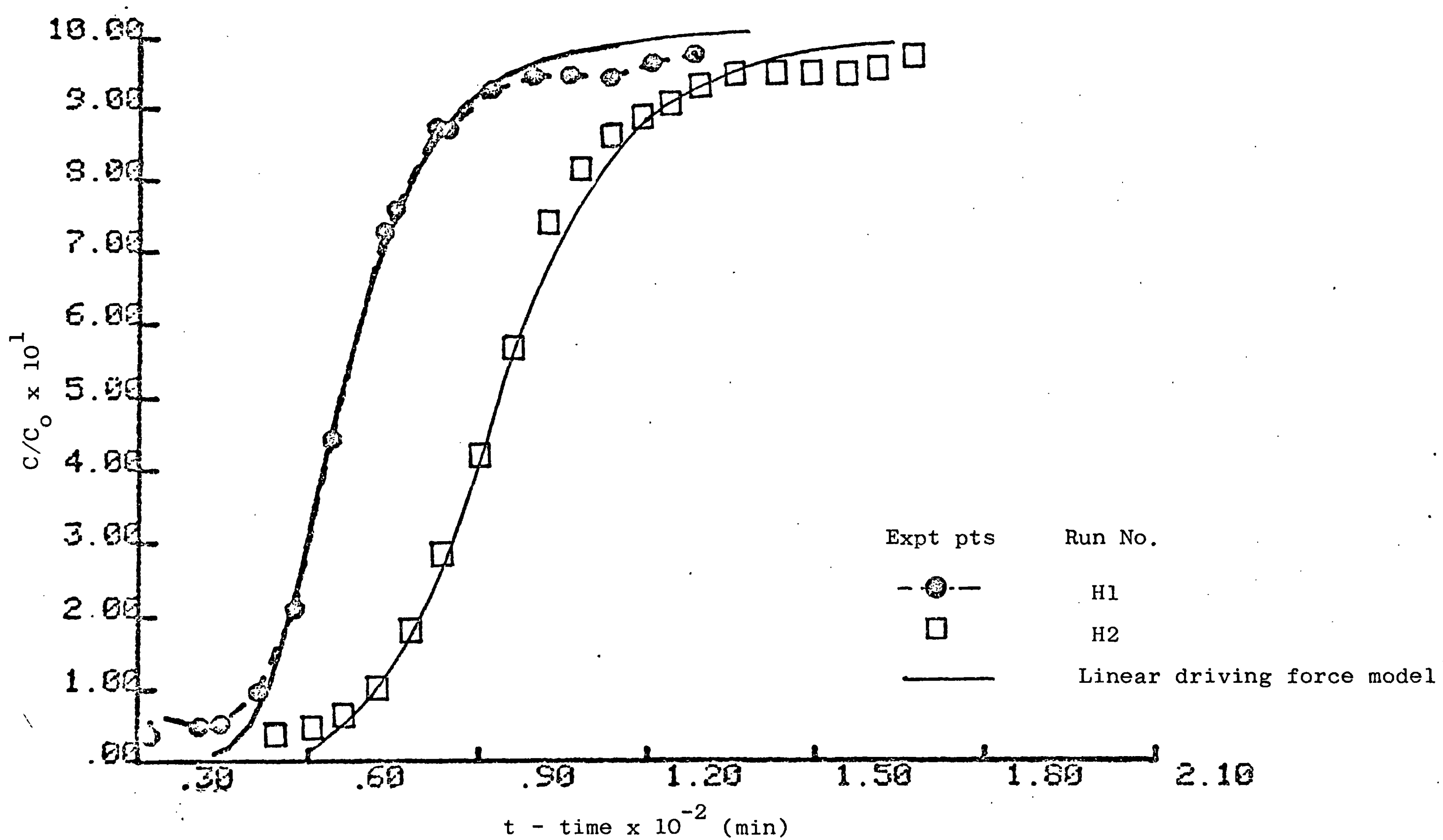

Figure 115: Comparison of experimental and predicted breakthrough curves for carbon tetra-chloride on Anthrasorb CC818H at 25^{o}C.

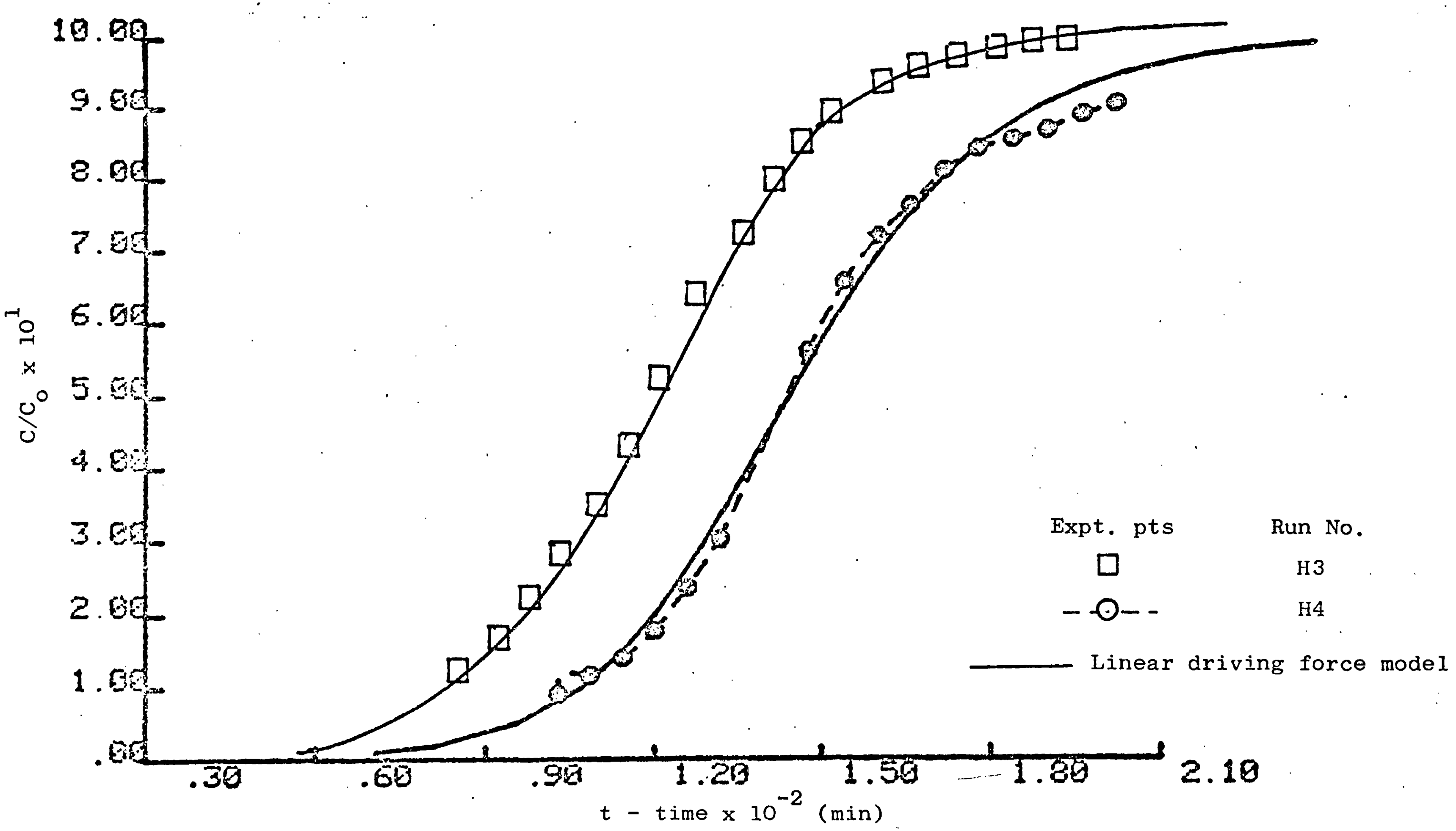

Figure 116: Comparison of experimental and predicted breakthrough curves for carbon tetrachloride on Anthrasorb CC818H at 25°C.

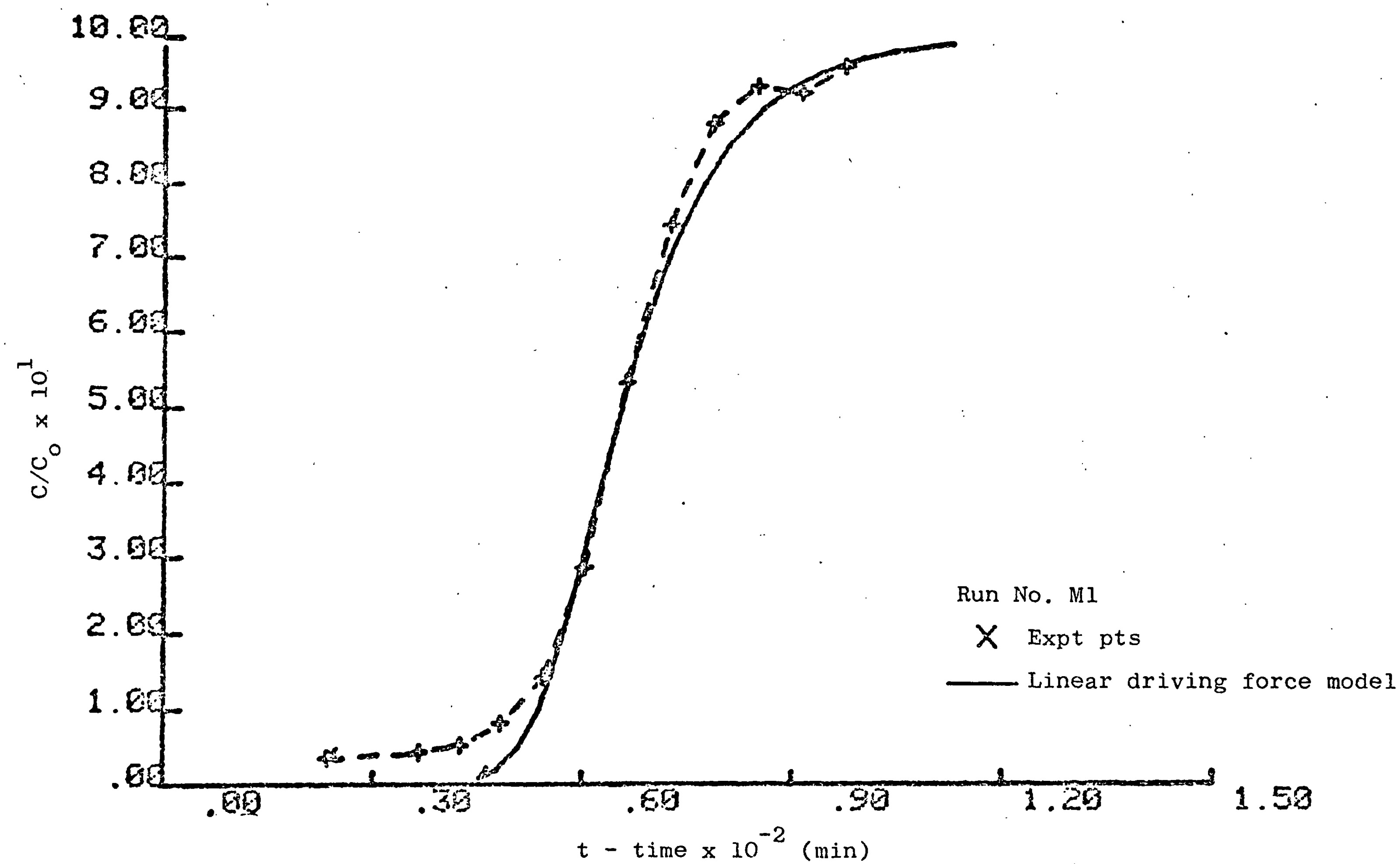

Figure 117: Comparison of experimental and predicted breakthrough curves for carbon tetra-chloride on Anthrasorb CC818M at 25°C.

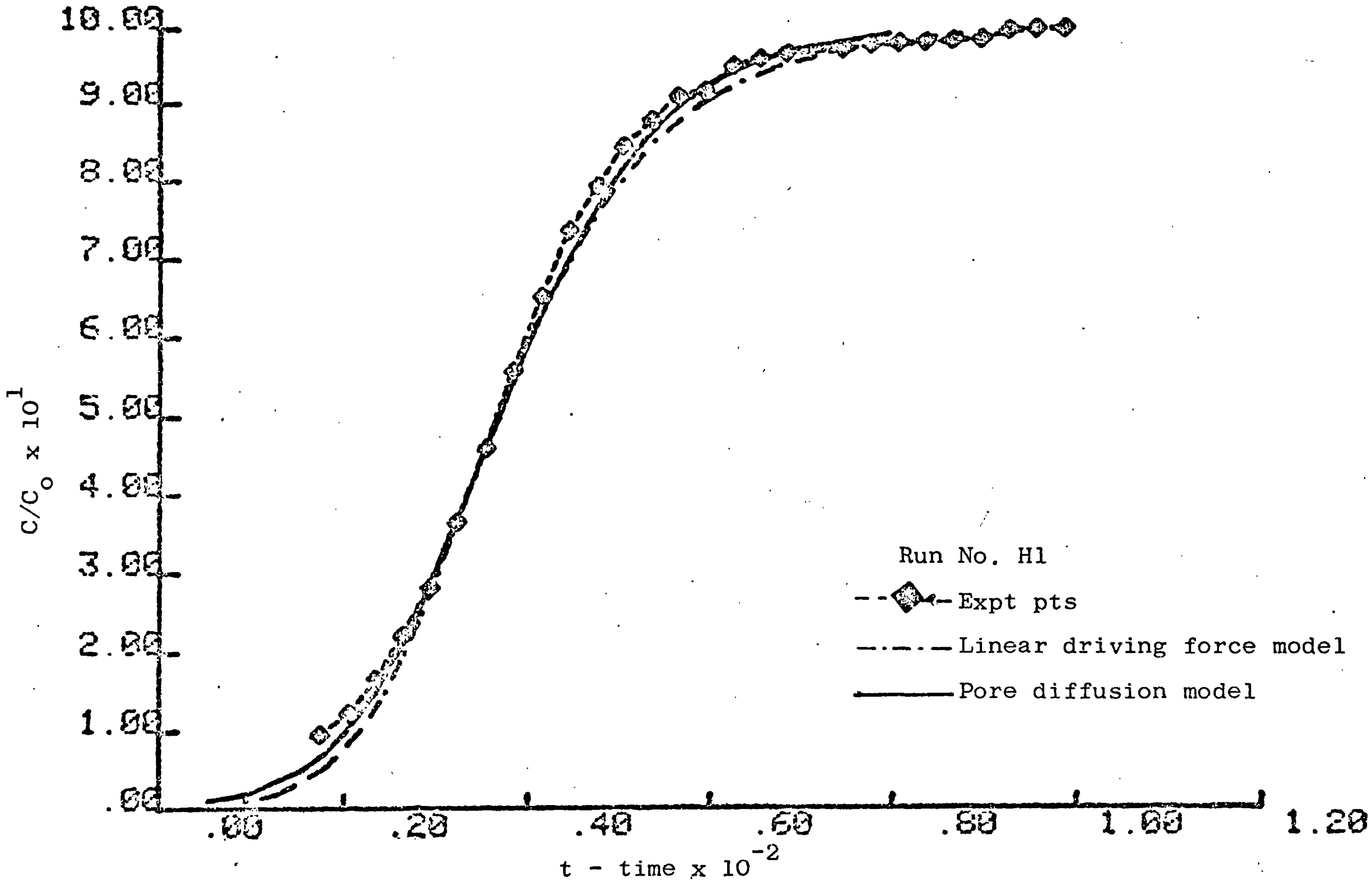

Figure 118: Comparison of experimental and predicted breakthrough curves for acetone on Anthrasorb CC818H at 25°C.

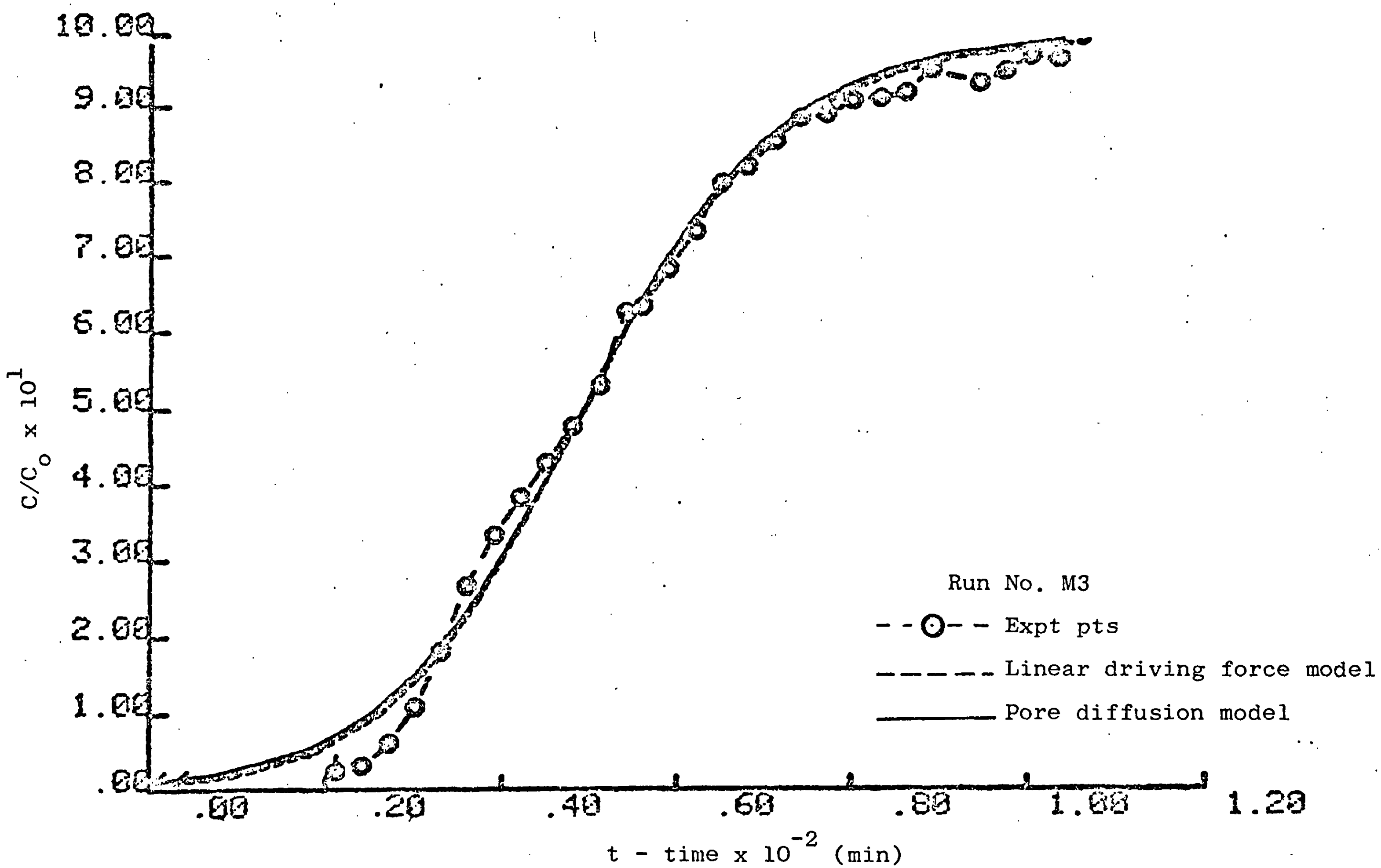

Figure 119: Comparison of experimental and predicted breakthrough curves for acetone on Anthrasorb CC818M at 25°C.

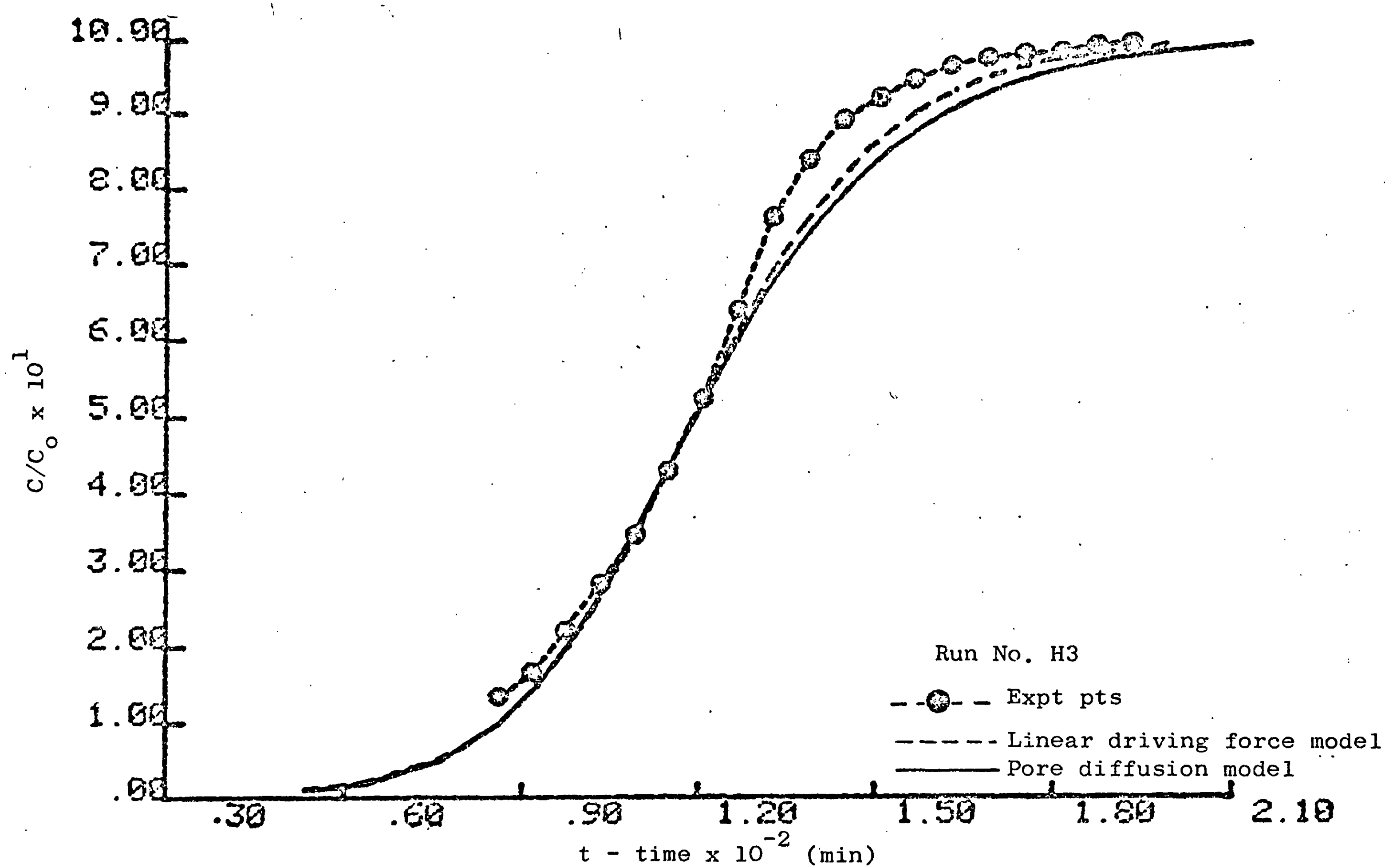

Figure 120: Comparison of experimental and predicted breakthrough curves for carbon tetrachloride on Anthrasorb CC818H at 25°C.

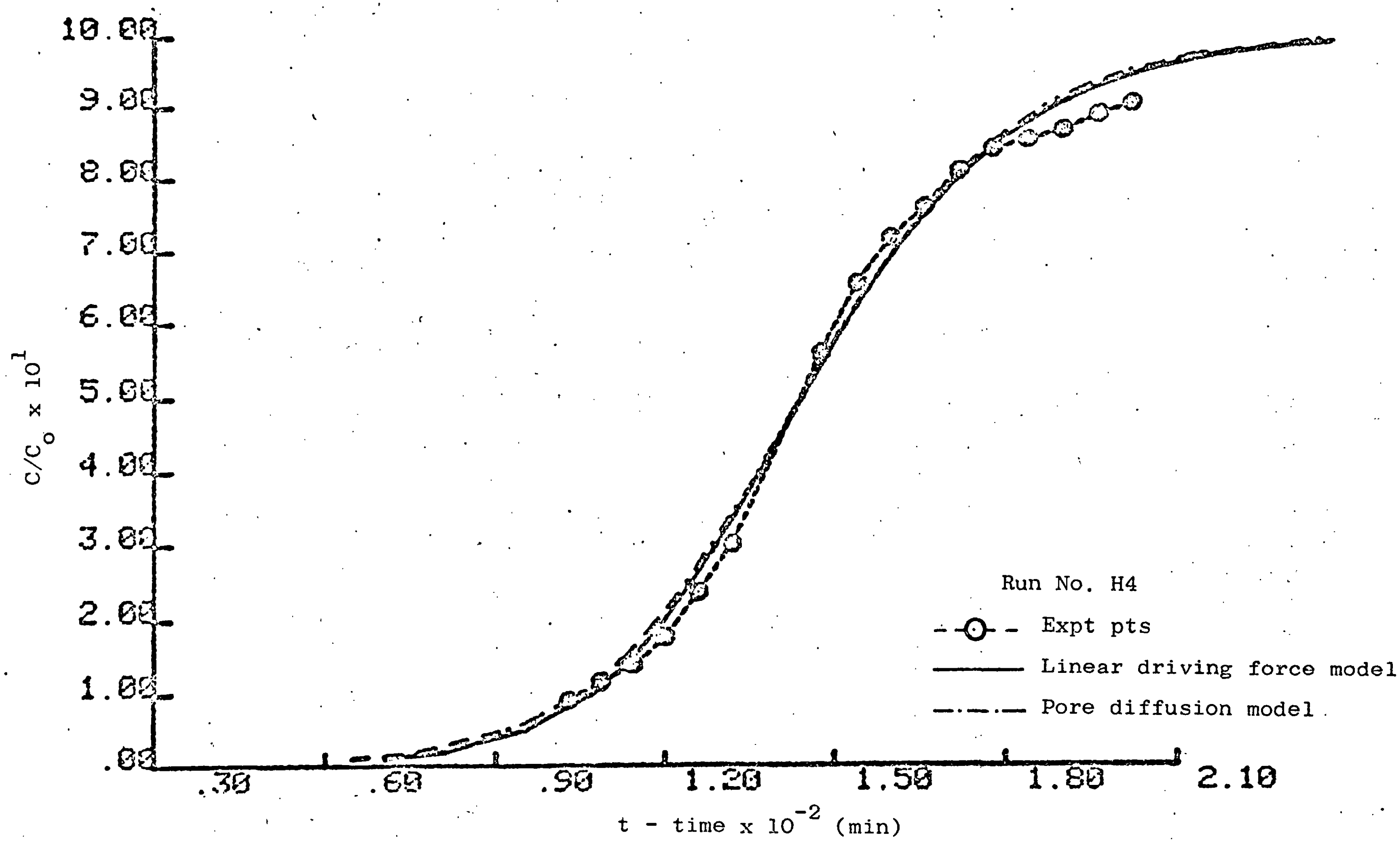

Figure 121: Comparison of experimental and predicted breakthrough curves for carbon tetra-chloride on Anthrasorb CC818H at 25^{o}C.

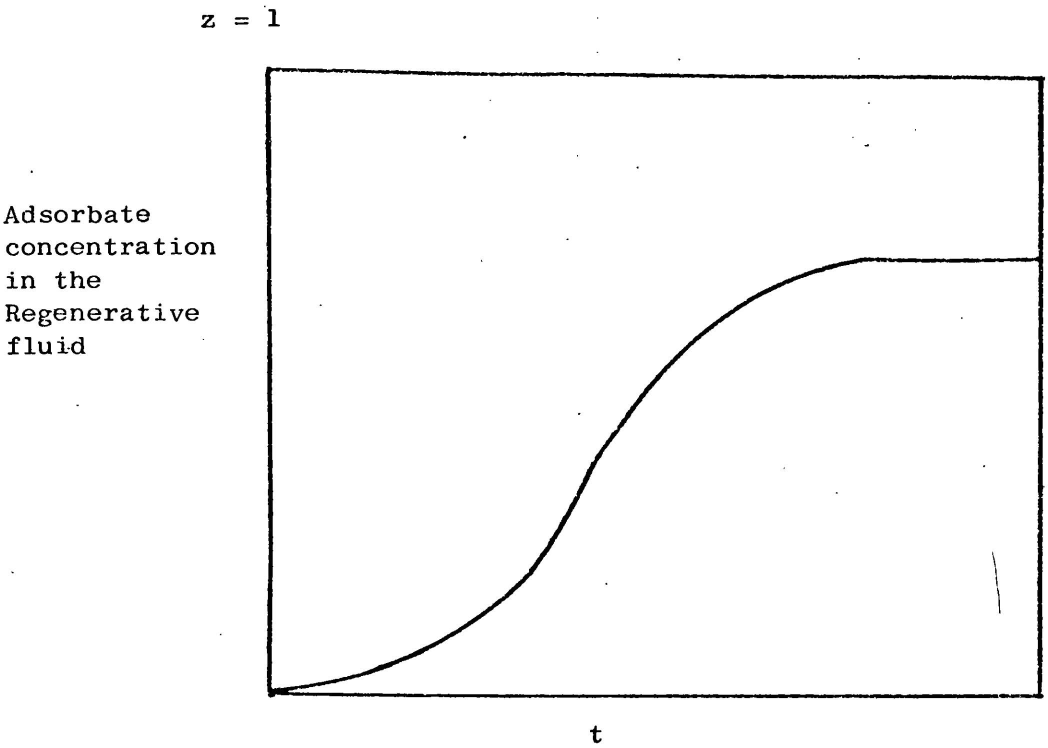

Figure 122: Concentration profile of regenerative fluid for desorption.

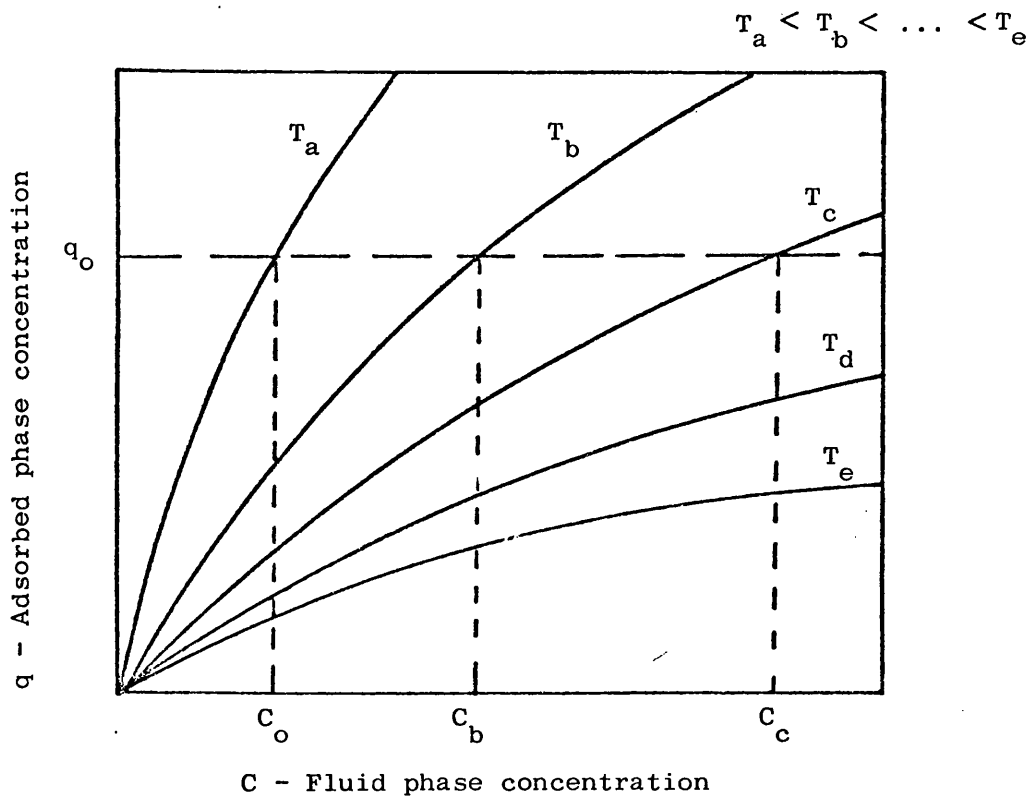

Figure 123: Effect of heated regenerative fluid on desorption.

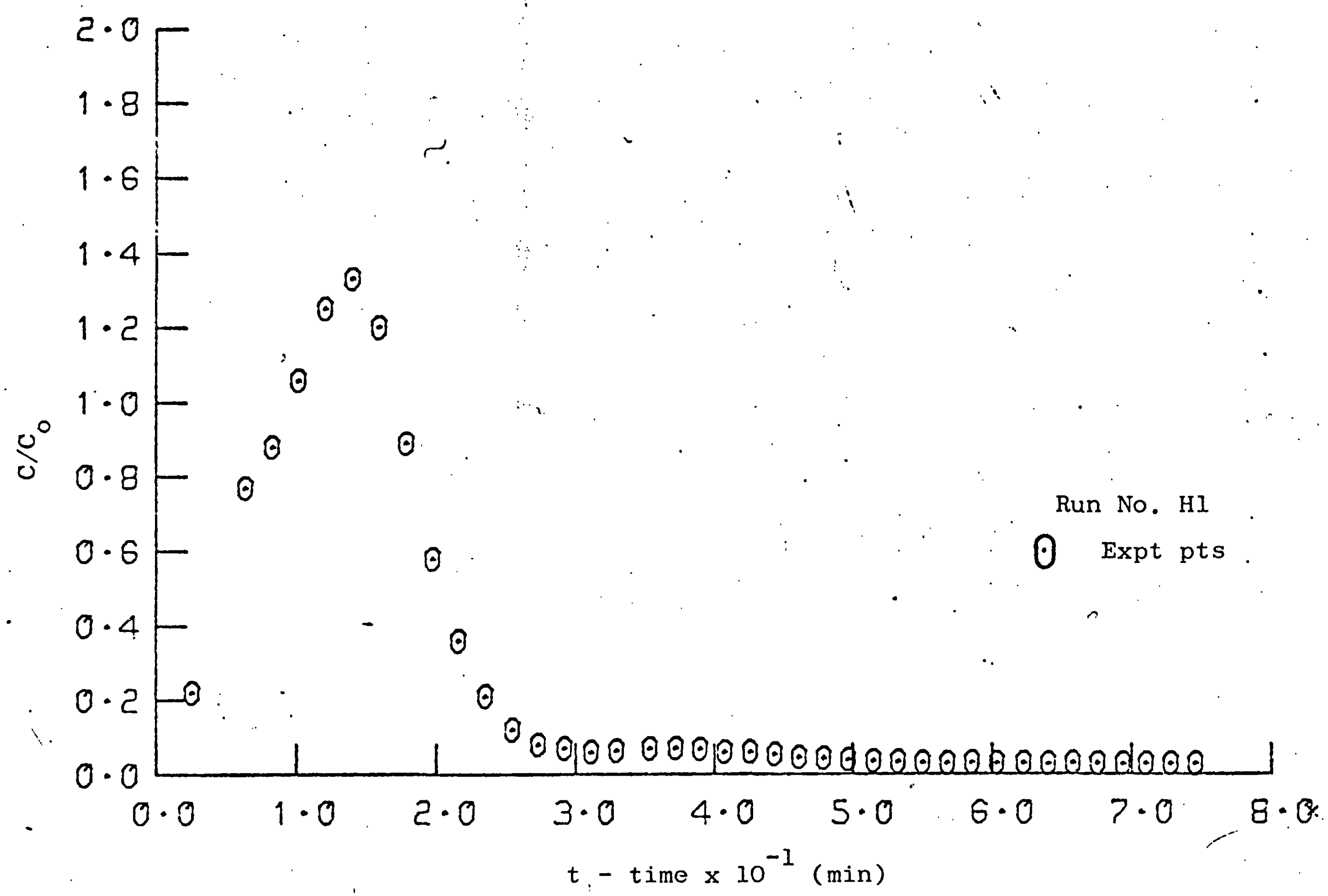

Figure 124: Desorption breakthrough curve for acetone at 200°C.

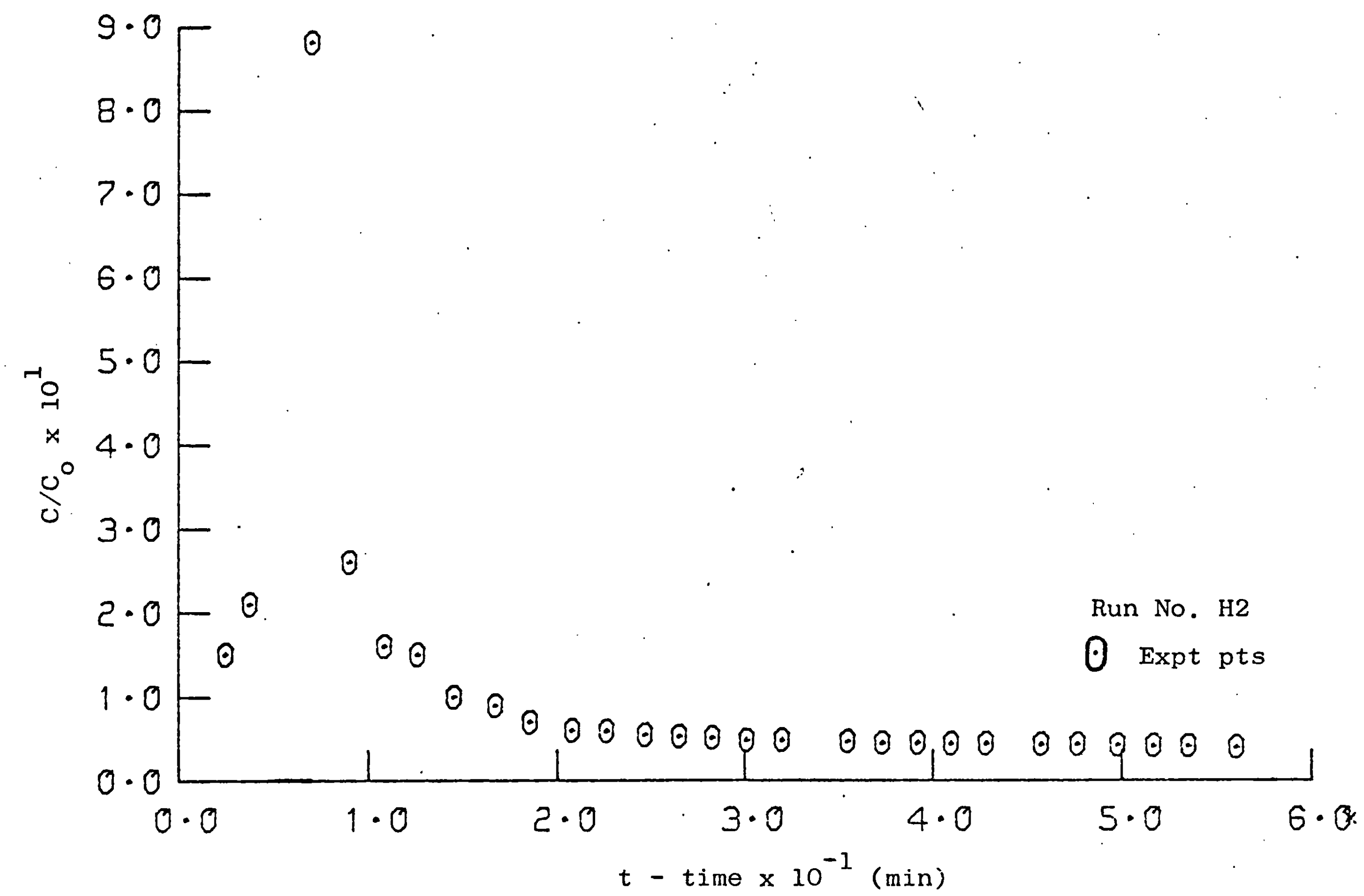

Figure 125: Desorption breakthrough curve for acetone on Anthrasorb CC818H at 150°C

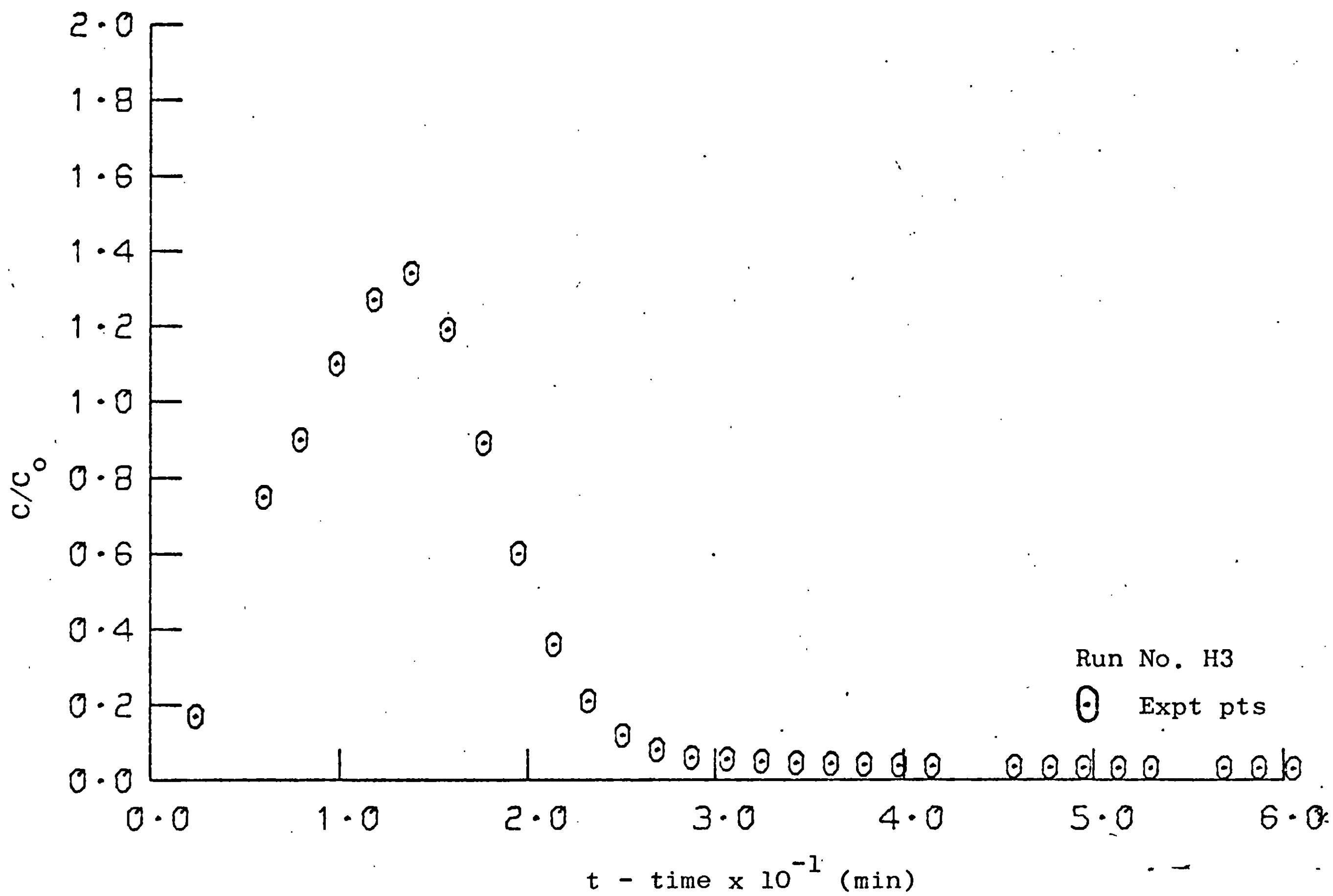

Figure 126: Desorption breakthrough curve for acetone on Anthrasorb CC818H at 200^{o}C

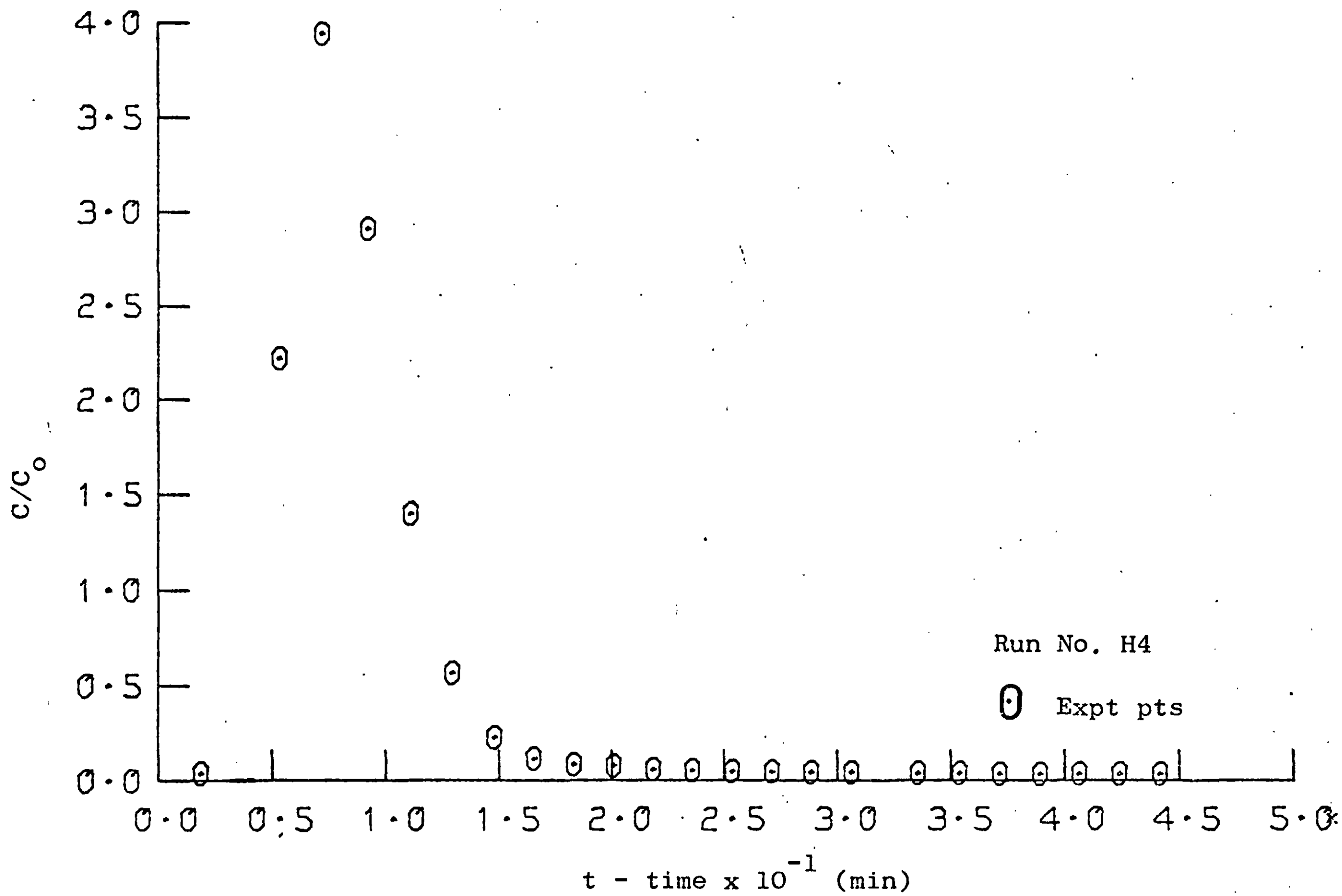

Figure 127: Desorption breakthrough curve for acetone on Anthrasorb CC818H at 250°C.

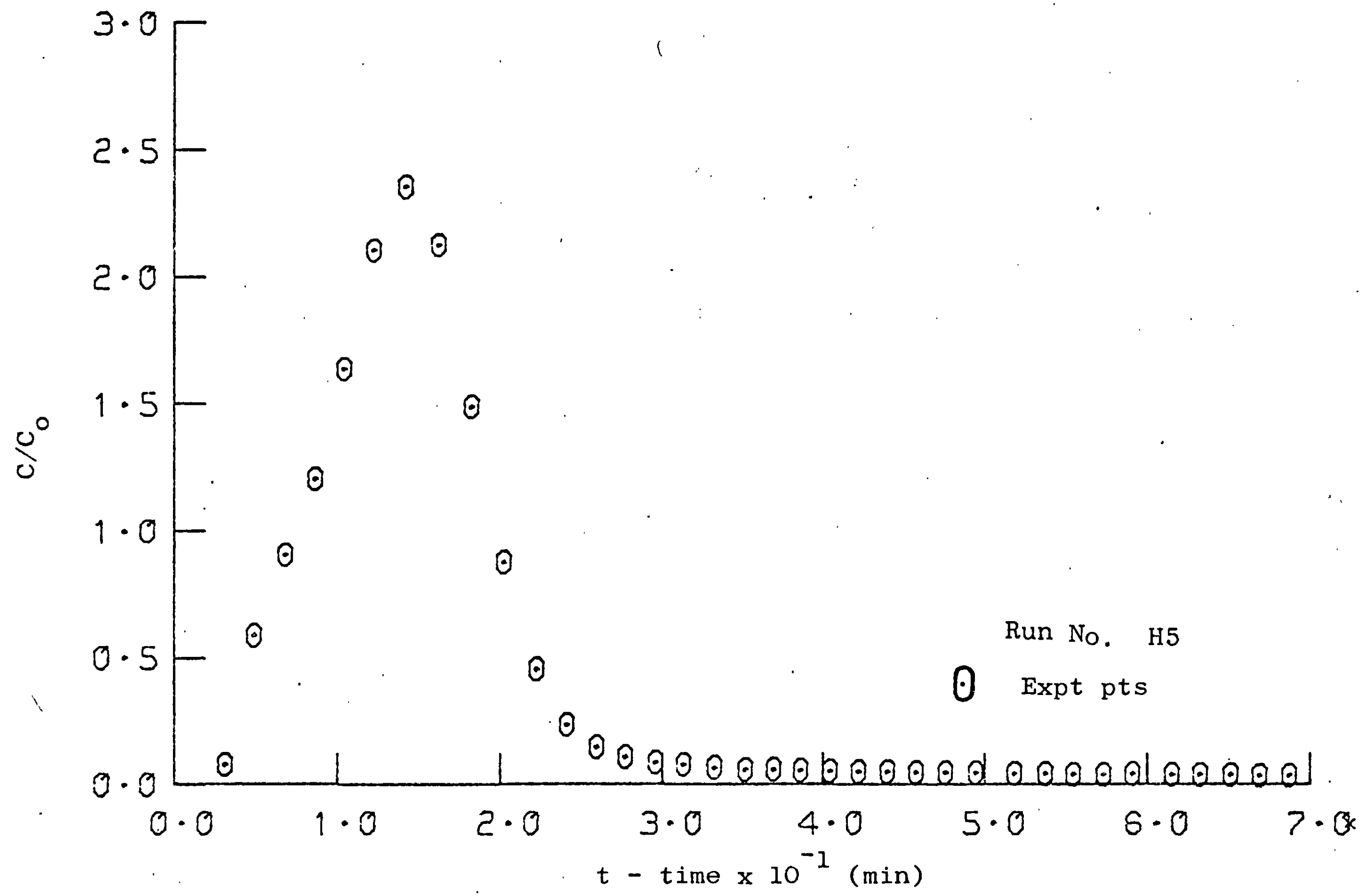

Figure 128: Desorption breakthrough curve for acetone on Anthrasorb CC818H at 200°C.

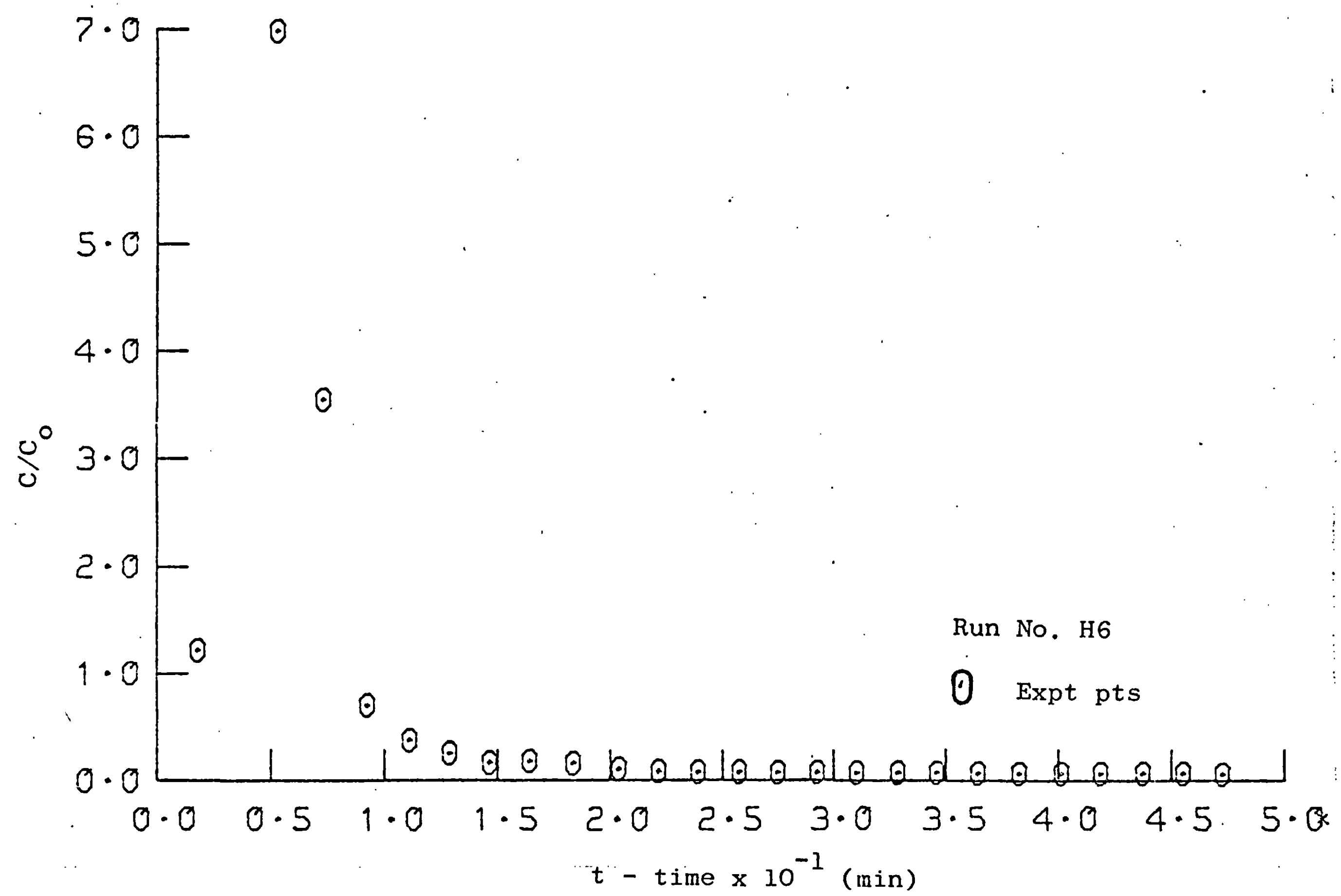

Figure 129: Desorption breakthrough curve for acetone on Anthrasorb CC818H at 250°C.

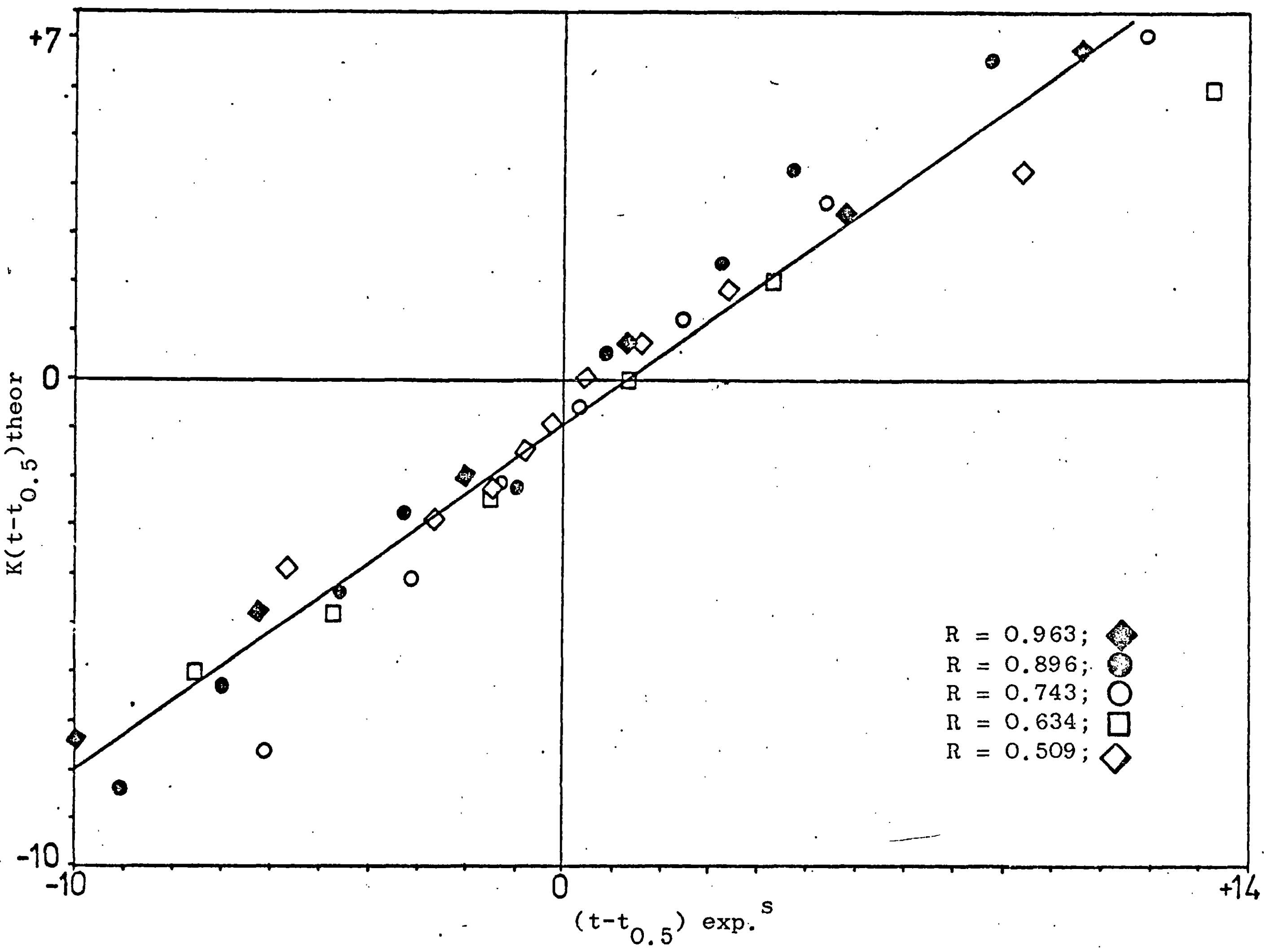

Figure 130: Evaluation of kinetic parameter for surface diffusion model

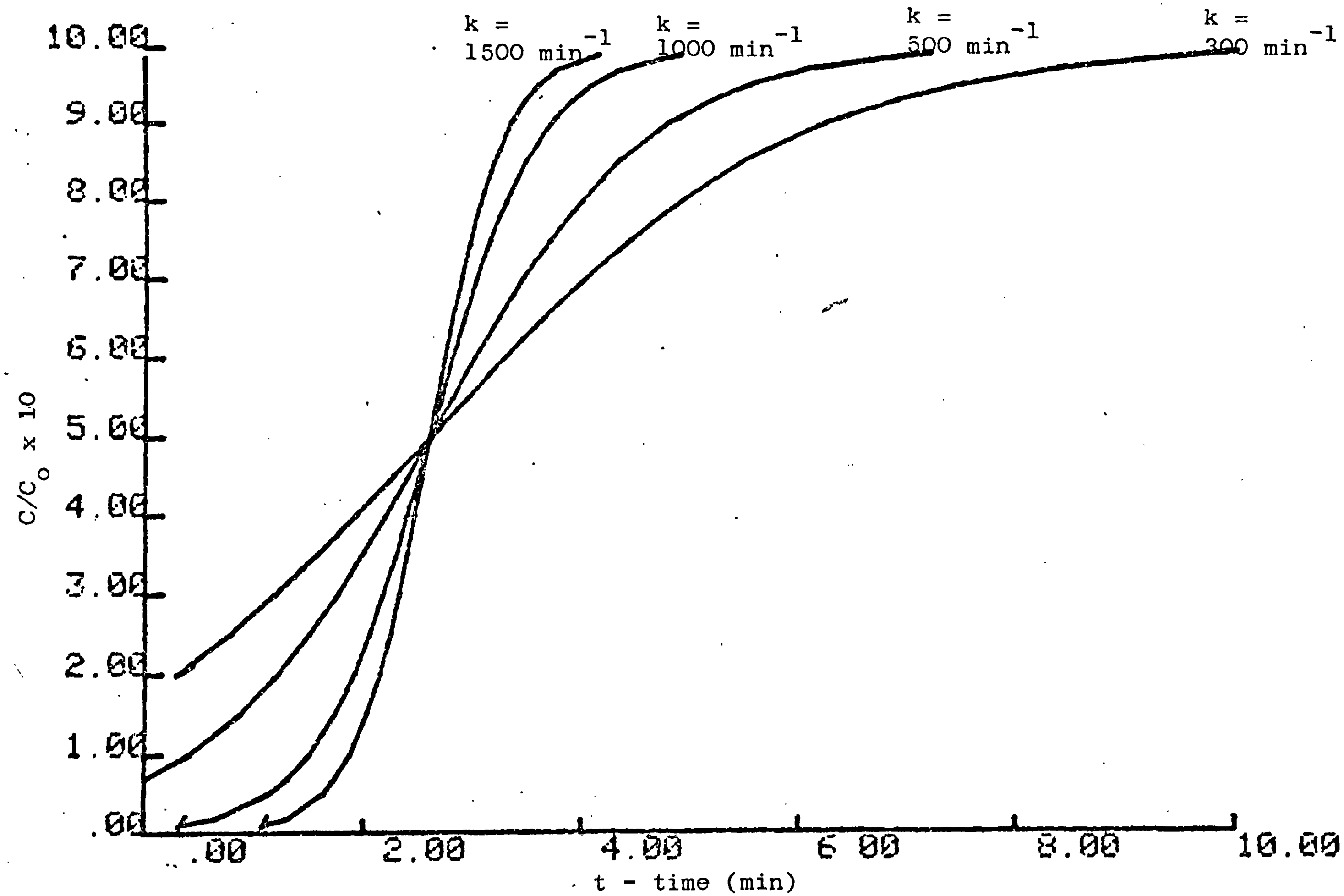

Figure 131: Evaluation of kinetic constant - K, for lumped parameter models.

APPENDIX A

CALIBRATIONS

APPENDIX A

CALIBRATIONS

(a) Direct System

Pre-mixed cylinders of different concentrations were used for methane and ethane systems. The height was then plotted against the concentration, as shown in figures 9 and 10 for methane and ethane respectively. The points fell on straight line which can be expressed by the following equations:

$$\text{mol.cm}^{-3} \text{ of methane} = 6.21 \times 10^{-7} \times (\text{Height of Plateau}) \quad (A1)$$

$$\text{mol.cm}^{-3} \text{ of ethane} = 5.29 \times 10^{-7} \times (\text{Height of Plateau}) \quad (A2)$$

which were obtained by application of the least mean square method. The inlet concentration was evaluated by equations (A1) or (A2), the intermediate values of concentrations were calculated from the following relationship:

$$\frac{C}{C_o} = \frac{(\text{Height of the peak})}{(\text{Height of the peak corresponding to } C_o)} \quad (A3)$$

(b) Chromatographic System:

The Chromatographic system was adopted for the analysis of acetone and carbon tetrachloride. To obtain a reliable calibration, particular care was taken to select an amount of liquid sample so as to produce peaks of similar area; to those obtained for typical gas sample during the experiment. Since the experiments were performed at low-concentration in the range of $1.0 - 4.0 \times 10^{-7}$ mol. cm^{-3}, effluent leaving the saturator was diluted by the carrier gas to the required concentration. The chromatograph was calibrated for two different attenuations. One suitable for the saturated streams prior to the dilution (in order to calculate the efficiency of the saturator), and the other for the concentration range of the experiments.

For acetone, the saturation region was calibrated by injecting acetone by a microlitre syringe, while for experimental range a 1% by volume of acetone-water mixture was used. The sample volume was varied from 0.1 μl to 1 μl, and the calibration data was obtained. The point fell on straight lines, which can be expressed by the following equations:

Saturation region (ATT = 20×10^4)

$$\text{moles of acetone} = 3.803 \times 10^{-10} \times (\text{Area of peak}) \qquad (A4)$$

Experimental region (ATT = 1×10^4)

$$\text{moles of acetone} = 1.866 \times 10^{-11} \times (\text{Area of peak}) \qquad (A5)$$

which were obtained by application of the least mean square method.

Similarly for carbon-tetrachloride following equations were obtained:

Saturation region (ATT = 20×10^2)

$$\text{moles of carbon-tetrachloride} = 4.674 \times 10^{-11} \times (\text{area of peak}) \qquad (A6)$$

Experimental region (ATT x 2×10^2)

$$\text{moles of carbon-tetrachloride} = 6.963 \times 10^{-12} \times (\text{area of peak}) \qquad (A7)$$

Figures 11 and 12 show the calibration for acetone and carbon-tetrachloride respectively. For gas sample, the following relationship is given as:

$$\begin{array}{l} \text{hydrocarbon} \\ \text{concentration} \\ \text{is gas sample} \\ \text{at experiment} \end{array} = \frac{\text{moles of hydrocarbon from equation (A5) or (A7)}}{\text{gas sample volume (always 0.5 cm}^3\text{)}} \qquad \text{(A8)}$$

Inlet concentration was evaluated through equation (A8), the intermediate values of concentrations were calculated from the following relationship.

$$\frac{C}{C_o} = \frac{\text{Area of the peak}}{\text{(Area of the peak corresponding to } C_o\text{)}} \qquad \text{(A9)}$$

It should be mentioned that the data illustrated in figures 9 to 12 inclusive are spread over the whole range of experiments, and they show, therefore, that the system has fairly good stability.

APPENDIX B

EFFICIENCY OF SATURATION AND MIXING OPERATION

APPENDIX B

Efficiency of Saturation and Mixing

The saturator efficiency was estimated by comparing the actual measured effluent carbon tetra-chloride vapour concentration with values calculated from published vapour pressure data and the known carrier gas flowrate.

(a) Case I

Temperature of liquid surface in saturator assumed	=	$0^{\circ}C$
Carrier gas	=	Nitrogen
Vapour pressure of CCl_4 @ $0^{\circ}C$	=	33.12 mm Hg
Total pressure	=	915.10 mm Hg

Nitrogen gas metered at $20^{\circ}C$ and 760 mm Hg

Hence 22.4 litres at N.T.P. = 24 litres under experimental conditions.

Mole fraction $= \dfrac{33.12}{915.10} = 0.036$

Calculated vapour phase concentration $= \dfrac{0.036}{24 \times 10^{3}}$

$= 1.51 \times 10^{-6}\ \text{mol.cm}^{-3}$

Actual concentration obtained by chromatograph $= 2.21 \times 10^{-6}\ \text{mol.cm}^{-3}$

'Efficiency' of saturation $= \dfrac{2.21 \times 10^{-6}}{1.51 \times 10^{-6}}$

$> 100\%$

(b) Case II

Assumed temperature of liquid surface in saturator $= 5^{o}C$

Vapour pressure of CCl_4 @ $5^{o}C$ $= 41.75$ mm Hg

Mole fraction $= \frac{41.75}{915.10} = 0.046$

Calculated vapour phase concentration $= \frac{0.046}{24 \times 10^{3}}$

$= 1.90 \times 10^{-6}$ mol.cm^{-3}

'Efficiency' of saturation $= \frac{2.21 \times 10^{-6}}{1.90 \times 10^{-6}}$

$> 100\%$

(c) Case III

Assumed temperature of liquid surface in saturator $= 10^{o}C$

Vapour pressure of CCl_4 @ $10^{o}C$ $= 54.25$ mm Hg

Mole fraction $= \frac{54.25}{915.10} = 0.059$

Calculated vapour phase concentration $= \frac{0.059}{24 \times 10^{3}} = 2.46 \times 10^{-6}$ mol.cm^{-3}

'Efficiency' of saturation $= \frac{2.21 \times 10^{-6}}{2.46 \times 10^{-6}}$

$= 89.84\%$

From the above calculations it is obvious that the true temperature of the liquid in equilibrium with the vapour is somewhere between $0^{o}C$ and $10^{o}C$. The efficiency of saturation is therefore high.

APPENDIX C

PACKED AND APPARENT DENSITIES AND VOID FRACTION OF BED

APPENDIX C

Packed and apparent densities and void fraction of Bed:

Anthrasorb CC818M was put in a small cylinder and the cylinder tapped gently to fill it to 5 cm^3 mark.

(i) weight of carbon to fill 5 cm^3 cylinder = 2.853 g

hence the bed density = 0.57 $g.cm^{-3}$

(ii) volume toluene to fill the cylinder packed as above

= 3.4 cm^3

(This is the total volume of voids in the packed bed and pores in the particle, and the pore volume of Anthrasorb CC818M is 0.40 $cm.g^{-1}$).

hence the volume of voids = 3.4 - (2.853 x 0.40)

= 2.259 cm^3

and the void fraction $= \dfrac{2.259}{5.0} = 0.45$

(iii) apparent density $= \dfrac{2.853}{5.0 - 2.259}$

= 1.04 $g.cm^{-3}$

APPENDIX D

ESTIMATION OF DIFFUSION TIME FOR BINARY GAS MIXTURES

APPENDIX D

Estimation of diffusion time for binary gas mixtures

For the mixing of two gases in a cylinder where diffusion is in a longitudinal direction only, concentration is a function of distance, z, and time, t, and is given by:

$$\frac{\partial x}{\partial t} = D \frac{\partial^2 x}{\partial z^2} \tag{D1}$$

where x is the mole fraction of the diffusing component. Equation (D1) can be solved with the following boundary conditions which assume that initially the component in question is in one half of the cylinder only.

$$\begin{aligned} \text{At} \quad & t = 0, \quad x = 1 \quad \text{for } 0 \leq z < L/2 \\ & \text{and} \quad x = 0, \quad \text{for } L/2 < z \leq L \end{aligned} \tag{D2}$$

$$\text{At} \quad z = 0 \text{ and } z = L, \quad \frac{dx}{dz} = 0$$

The complete solution is given by Crank (22) as:

For upper half of cylinder $0 < z < L/2$,

$$\bar{x}_u = \frac{\int_0^{L/2} x_u \, dz}{L/2} = \frac{1}{2} + \sum_1^{\infty} \left\{ \frac{4}{n^2 \Pi^2} \left(\sin^2 \frac{n\Pi}{2}\right).\exp\left[-Dt\left(\frac{n\Pi}{L}\right)^2\right] \right\} \tag{D3}$$

while for the lower half $L/2 \leq z \leq L$

$$\bar{x}_L = \frac{\int_{L/2}^{L} x_L \, dz}{L/2} = \frac{1}{2} - \sum_1^{\infty} \left\{ \frac{4}{n^2 \Pi^2} \left(\sin^2 \frac{n\Pi}{2}\right).\exp\left[-Dt\left(\frac{n\Pi}{L}\right)^2\right] \right\} \tag{D4}$$

Equations (D3) and (D4) were applied for the following conditions:-

$L = 91.4$ cm

$D = 0.264\ cm^2.s^{-1}$ (Calculated for methane-nitrogen mixture from Sherwood and Pigford (103)).

For equilibrium, the concentration in both halves should be equal and hence one obtains

For $t = 1$ hour, $\bar{x}_u - \bar{x}_L = 0.263$

For $t = 10$ hours, $\bar{x}_u - \bar{x}_L = 0.00$

The above calculations demonstrate that for a mixing time greater than 10 hours complete mixing will have occurred by diffusion.

APPENDIX E

ALLOWABLE GAS FLOWRATE

APPENDIX E

Allowable gas flowrate

The maximum allowable gas flowrate in a packed bed was calculated using the correlation given by Ledoux (70).

$$\frac{G^2}{d_g d_a D.g.} = 0.0167 \qquad \text{(E1)}$$

where G = mass velocity of gas, $g.cm^{-2}.S^{-1}$

dg = gas density (flow conditions) $g.cm^{-3}$

da = adsorbent bed density, $g.cm^{-3}$

D = average particle diameter. cm

g = acceleration due to gravity, $cm.S^{-2}$

The calculations were carried out for the carrier gas nitrogen to determine a gas velocity that might cause attrition and carrying over the particles.

Following are the values used in equation (E1):

$$\begin{aligned} dg &= 0.00116\ g.cm^{-3} \\ da &= 0.53\ g.cm^{-3} \\ D &= 0.169\ cm \\ g &= 980.66\ cm.S^{-2} \\ A &= 0.712\ cm^2 \end{aligned} \qquad \text{(E2)}$$

Using the values in equation (E2), (E1) yields:

$$G = 0.0412\ g.cm^{-2}.S^{-1}$$

and

$$Fmax = \frac{0.0412 \times 0.712 \times 60}{0.00116} = 1.518 \times 10^3\ cm^3.min^{-1}$$

The flowrate was chosen (40 - 100 $cm^3.min^{-1}$) considerably less than the maximum allowable value during the experiments.

APPENDIX F

NUMERICAL SOLUTION OF A FIXED BED ADSORPTION COLUMN WITH EXTERNAL MASS TRANSFER CONTROL

APPENDIX F

Digital simulation of a fixed-bed adsorption column without axial dispersion (External Mass Transfer Control Model)

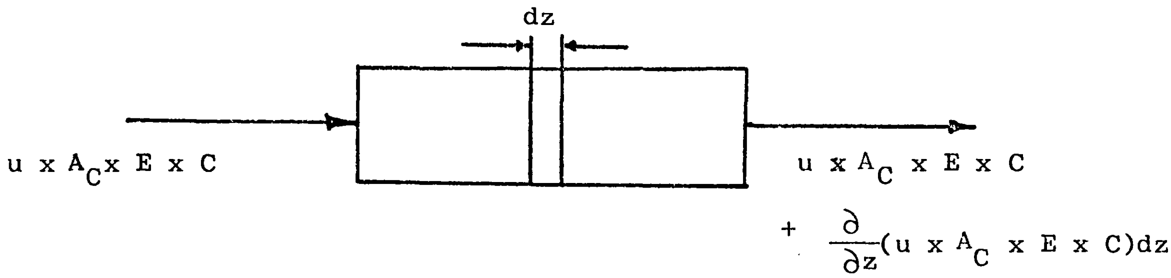

A local mass-balance, undergoing adsorption in an infinitismally thin slice of a bed is described mathematically as:

$$D\frac{\partial^2 C}{\partial Z^2} - u\frac{\partial C}{\partial Z} = \frac{\partial C}{\partial t} + \frac{\rho(1-E)}{E}\frac{\partial q}{\partial t} \qquad \text{(F1)}$$

The first and second term of equation (F1) represent the inlet input of Dispersion and Convection respectively in the axial direction. The third and fourth terms represent the rate of accumulation in the fluid phase and in the adsorbed phase respectively. It is assumed that there is a radial symmetry and that the concentration of adsorbate in the gas phase is sufficiently low to make negligible changes in the total flow rate of the fluid phase.

When the axial dispersion is deleted from the basic mass balance, the partial differential equation is no longer parabolic, and is written as:

$$U\frac{\partial C}{\partial Z} + \frac{\partial C}{\partial t} + \frac{\rho(1-E)}{E}\frac{\partial q}{\partial t} = 0 \qquad \text{(F2)}$$

The mass transport equation and the equilibrium relationship are given by

$$\frac{\partial q}{\partial t} = K(C - C^*) \qquad (F3)$$

$$C^* = \frac{q}{m} \qquad (F4)$$

where m = slope of the isotherm.

<u>Boundary Conditions</u>

The input function was a step change in concentration:

$$C(Z = o, t) = Co \qquad (F5)$$

<u>Finite difference scheme</u>

A finite difference scheme is used to integrate the equation (F2), which is hyperbolic. The finite difference analogue are centred in both space and time with respect to the grid points at which the values of the dependent variables are determined. Spatial and time positions are denoted by the indices i and j respectively. The point about which the finite difference analogues are to be written is located at $Z_{i-\frac{1}{2}}$, $t_{i+\frac{1}{2}}$, on the space-time grid. The analogues are given as:

$$\left(\frac{\partial C}{\partial Z}\right)_{i-\frac{1}{2},j+\frac{1}{2}} = \frac{1}{2h}\Big[C(i,j+1)-C(i-1,j+1)+C(i,j)-C(i-1,j)\Big] \qquad (F6)$$

$$\left(\frac{\partial C}{\partial t}\right)_{i-\frac{1}{2},j+\frac{1}{2}} = \frac{1}{2k}\Big[C(i,j+1)-C(i,j)+C(i-1,j+1)-C(i-1,j)\Big] \qquad (F7)$$

$$\left(\frac{\partial q}{\partial t}\right)_{i-\frac{1}{2},j+\frac{1}{2}} = \frac{1}{2k}\Big[q(i,j+1)-q(i,j)+q(i-1,j+1)-q(i-1,j)\Big] \qquad (F8)$$

$$\left(\frac{\partial q}{\partial t}\right)_{i-\frac{1}{2},j+\frac{1}{2}} = k\left[C(i-\tfrac{1}{2},j+\tfrac{1}{2}) - \frac{1}{m}\left(q(i-\tfrac{1}{2},j+\tfrac{1}{2})\right)\right] \qquad \text{(F9)}$$

The terms $C(i-\frac{1}{2},j+\frac{1}{2})$ and $q(i-\frac{1}{2},j+\frac{1}{2})$ can be evaluated in either of the two ways. The first way is to average the values of the four adjacent points. The alternate way is by diagonally averaging across the time grid. The latter was chosen for its simplicity and is given as:

$$C(i-\tfrac{1}{2},j+\tfrac{1}{2}) = \tfrac{1}{2}\left[C(i,j+1) + C(i-1,j)\right] \qquad \text{(F10)}$$

$$q(i-\tfrac{1}{2},j+\tfrac{1}{2}) = \tfrac{1}{2}\left[q(i,j+1)+q(i-1,j)\right] \qquad \text{(F11)}$$

utilizing equations (F8), (F9), (F10) and (F11) and solving for $q(i,j+1)$

$$\begin{aligned} q(i,j+1) = {} & \left(\frac{m}{m+KEK}\right)\left[q(i,j)-q(i-1,j+1)\right] \\ & + \left(\frac{m-KEK}{m+KEK}\right)\left[q(i-1,j)\right] \\ & \div \left(\frac{mKEK}{m+KEK}\right)\left[C(i,j+1)+C(i-1,j)\right] \end{aligned} \qquad \text{(F12)}$$

substituting equation (F6), (F7), (F8) and (F12) into equation (F2), yield :-

$$\begin{aligned} & A_1C(i,j+1) + A_2C(i-1,j+1) + A_3C(i,j) + A_4C(i-1,j) = \\ & A_5\left[q(i,j) - q(i-1,j+1)\right] + A_6q(i-1,j) \end{aligned} \qquad \text{(F13)}$$

where:

$$A_1 = -(u/2h) - (1/2k) - mk/(2m + 2KEK) \qquad \text{(F14)}$$

$$A_2 = (u/2h) - (1/2k) \tag{F15}$$

$$A_3 = -(u/2h) + (1/2k) \tag{F16}$$

$$A_4 = (u/2h) + (1/2k) - mK/\left(2m + \frac{2KEK}{\rho(1-E)}\right) \tag{F17}$$

$$A_5 = -k/\left(2m + \frac{2KEK}{\rho(1-E)}\right) \tag{F18}$$

$$A_6 = -k/\left(m + \frac{KEK}{\rho(1-E)}\right) \tag{F19}$$

Solving equation (F13) for c(i,j+1)

$$C(i,j+1) = -B_2C(i-1,j+1) - B_3C(i,j) - B_4C(i-1,j)$$

$$+ B_5\left[q(i,j) - q(i-1,j+1)\right] + B_6q(i-1,j) \tag{F20}$$

where $Bi = Ai/A_1$ for i = 2 to 6 (F21)

equation (F20) is an explicit solution to equations (F2), (F3) and (F4).

In the computer solution given in appendix (M), there was an inherent oscillation about the base line until the calculated break-point was reached. In order to reduce the above oscillation to a negligible amount, the values of the spatial and time integration increments had to be quite low. It was necessary to reduce the time increment to 0.01 s and the ratio of spatial increment to bed length to approximately 0.02.

APPENDIX G

NUMERICAL SOLUTION OF A FIXED BED ADSORPTION COLUMN WITH SURFACE DIFFUSION CONTROL

APPENDIX G

Numerical Solution of Surface Diffusion Model

The rate of diffusion into a uniformly porous spherical particle is written as: (y is the dimensionless adsorbed phase concentration (q/q_o))

$$\frac{\partial y}{\partial t} = \frac{D_s}{r^2}\frac{\partial}{\partial r}\left[r^2 \frac{\partial y}{\partial r}\right] \tag{G1}$$

The mean solid concentration value Y, averaged over the particle is:

$$Y = \frac{3}{r_s^3}\int_o^{r_s} y\, r^2\, dr \tag{G2}$$

Differentiation with respect to time gives:

$$\frac{\partial Y}{\partial t} = \frac{3}{r_s^3}\int_o^{y_p}\left(\frac{\partial y}{\partial t}\right)_r r^2 dr \tag{G3}$$

combination of equation (G3) with (G1) yields:

$$\frac{\partial Y}{\partial t} = \frac{3D_s}{r_s}\left(\frac{\partial y}{\partial r}\right)_{r=r_s} \tag{G4}$$

For a constant pattern condition, the material balance equation is given by:

$$Y = X \tag{G5}$$

Now, the simple parameters N , T_δ R_o is defined by the following equations:

$$N = \frac{15D_s K_o \rho_b Z_o}{r_p^2\, u} \tag{G6}$$

$$T_o = \frac{t - VEF}{D_oV/F} \tag{G7}$$

$$R_o = r / r_s \tag{G8}$$

Where D_o is the distribution coefficient $(q_o^* \rho_b / C_o)$ and r_s is the outer radius of the particle.
Combining equations (G4), (G6), (G7) and (G8) leads to:

$$15 \left(\frac{\partial y}{\partial N \; T_o} \right) = \frac{\partial^2 y}{\partial R_o^2} + \frac{2}{R_o} \frac{\partial y}{\partial R_o} \tag{G9}$$

Boundary conditions:

The boundary conditions are:

$$5 \left(\frac{\partial Y}{\partial N \; T_o} \right) = \left(\frac{\partial y}{\partial R_o} \right)_{R_o = 1} \tag{G10}$$

$$\text{At} \quad R_o = 0, \quad \frac{\partial y}{\partial R_o} = 0 \tag{G11}$$

$$\text{For all } R_o, \text{ at } N \; T_o = 0, \; Y = X = 0 \tag{G12}$$

$$\text{At } N \; T_o = \infty, \quad Y = X = 1 \tag{G13}$$

Finite difference scheme

The "parabolic" form of the equation (G9) suggested the use of the four point forward difference integration method. Spatial and time positions are denoted by the indices i and j respectively. λ and μ are the computational interval on R_o and NT_o respectively. The numerical scheme is shown on grid of R_o and NT_o to solve for the Y value of each (R_o, NT_o) intersection; diagrammatically, in figure G1, the three known values (X) are used to determine the unknown value (O).

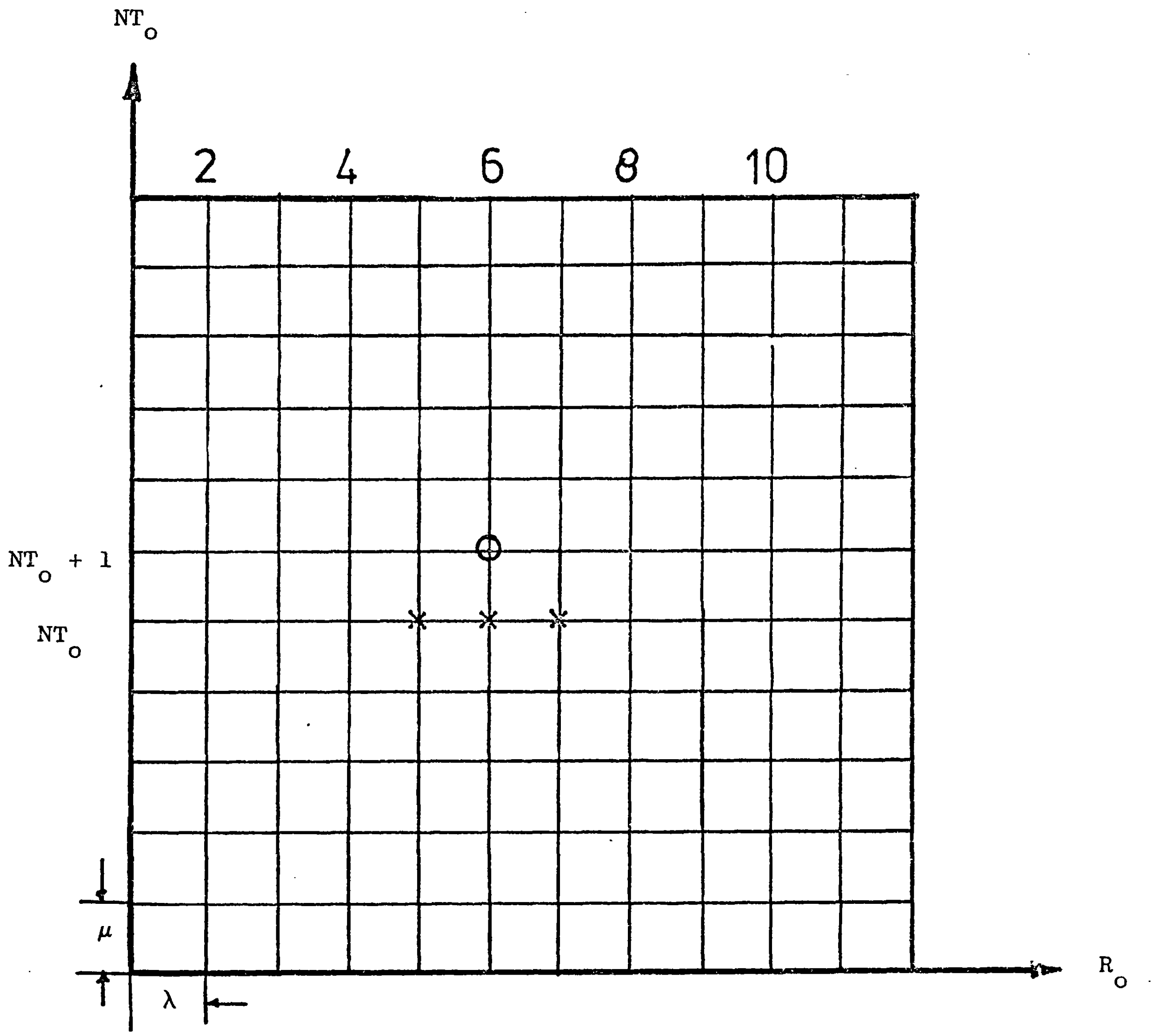

Figure G1

In this method of analysis the elements of equation (G9) become:

$$\frac{\partial y}{\partial NT_o} = \frac{1}{\mu}\left[y(i,j+1) - y(i,j)\right] \tag{G14}$$

$$\frac{\partial y}{\partial R_o} = \frac{1}{2\lambda}\left[y(i+1,j) - y(i-1,j)\right] \tag{G15}$$

$$\frac{\partial^2 y}{\partial R_o^2} = \frac{1}{\lambda^2}\left[y(i+1,j) - 2y(i,j) + y(i-1,j)\right] \tag{G16}$$

combination of equations (G14), (G15) and (G16) with (G1) yields:

$$y(i,j+1) = \left(\frac{\mu}{15\lambda}\right)\left\{\frac{1}{\lambda}\left[y(i+1,j)-2y(i,j)+y(i-1,j)\right]\right.$$

$$\left. + \frac{1}{R_o}\left[\, y(i+1,j) - y(i-1,j) \,\right] + y(i,j)\right\} \qquad \text{(G17)}$$

For boundary conditions, at $R_o = 0$, the equation (G17) combines with equation (G11) to yield:

$$y(i,j+1) = \frac{2\mu}{15\lambda}\left\{\frac{1}{\lambda}\left[y(i+1,j) - y(i,j)\right] + y(i,j)\right\} \qquad \text{(G18)}$$

For $R_o = 1$, combining the boundary condition equation (G10) with equation (G17) gives, after some algebraic manipulation:

$$y(i,j+1) = \left(\frac{15\lambda R_o}{15\lambda R_o + 10R_o + 10\lambda}\right)\left\{\left(\frac{15\lambda^2 R_o + 10\lambda R_o - 2\mu R_o + 10\lambda^2}{15\lambda^2 R_o}\right) \times\right.$$

$$\left.\left[y(i,j)\right] + \left(\frac{2\mu}{15\lambda^2}\right)\left[y(i-1,j)\right]\right\} \qquad \text{(G19)}$$

The choice of values for λ and μ is important in determining the speed, accuracy, and convergence of the computation. After some trials, a value of $\lambda = 0.1$ gave sufficient accuracy, while for μ, it was necessary to start with one value and to reduce it progressively until the solution conveyed.

To start the programme, Hall's (52) empirical concentration distribution was used, which is given as:

$$y = y_I \exp\left[\, - \gamma\,(1-R_o)\right] \qquad \text{(G20)}$$

The values of y_I and γ are given in (52). Computer programme of this model is given in Appendix (P).

APPENDIX H

EVALUATION OF RATE CONSTANT K'

APPENDIX H

EVALUATION OF RATE CONSTANT

(a) For surface diffusion model

In order to select the most suitable value of D_s, to use in the numerical solution of the surface diffusion model, the following procedure, as suggested by Hall et al (52), was employed.

Hall et al presented their theoretical model as tables of the dimensionless outlet concentration (C/C_o) against $N(T_o-1)$, where N is the number of surface transfer units and T_o is a dimensionless time parameter, given by the following relations

$$N = \frac{15\ Dp\ v}{r^2\ F} \quad \frac{q_o^*\ \rho_b}{C_o} \tag{H1}$$

and

$$T_o = \frac{t - (vE/F)}{\rho_b q_o^*\ v/F\ C_o} \tag{H2}$$

By using the graphs of Hall et al in combination with the experimental results reported in this thesis, it is possible to determine D_s. The experimental results are converted into graphs of C/C_o versus $(t - t_{0.5})$, $t_{0.5}$ being the time corresponding to $C/C_o = 0.5$. On the other hand, for each value of C/C_o, at a given R, one can determine a theoretical value of the kinetic parameter from either the tables or graphs. When the experimental values of $(t - t_{0.5})$ are plotted against those predicted, the points should fall on a straight line from which slope a value of the corresponding effective diffusivity, D_s, may be extracted.

Since the difference, $(t - t_{0.5})$ is a constant (i.e. independent of R) plotting the experimental parameter, $(t - t_{0.5})_{exp}$ versus theoretical $K(t - t_{0.5})_{theor}$ is equivalent to the method proposed by Hall et al (52). The model fitted the experimental points well as can be seen from Figure 130. However, scatter in the data indicates there is possibly some variation in K with the parameter R. The data were subjected to a least squares regression analysis and the best straight line drawn through the data yielded a value of $K = 0.711\ s^{-1}$.

(b) For lumped parameter models

For evaluation of the kinetic constant, K, for the lumped parameter models (viz. pore diffusion approximation and linear driving force models) the interactive computing facilities of the Prime computer* (linked with a Tektronix 4011 terminal and coupled with a graph plotter) were utilized. The theoretical breakthrough curves were generated by varying the values of K, until the required breakthrough curve fits the experimental data. It can be seen from Figure 131 that, as the value of K increases, the theoretical breakthrough curve becomes steeper.

* The Prime 400 is part of the Interactive facility of the SRC and as such, is used as an interactive machine supporting a variety of terminals, with an emphasis on graphics. The machine runs a general purpose time-sharing operating system PRIMOS, which gives full multiuser interactive facilities with an on-line filestore.

APPENDIX I

TABULATED EXPERIMENTAL RESULTS FOR METHANE AND ETHANE

APPENDIX I

Tabulated Experimental Results for Methane and Ethane

(a) Adsorption experiments for methane on Anthrasorb CC818M (in isolation)

Run No.	Temperature ^{o}C	C_{Mo} $mol.cm^{-3}$ $\times 10^{6}$	m g	F $cm^{3}.min^{-1}$	t_{Mo} min	q_{Mo} $mol.g^{-1}$ $\times 10^{4}$
M-1	25	1.39	3.0	35.0	2.17	0.34
M-2	25	1.39	3.0	35.0	1.78	0.28
M-3	25	4.21	2.0	35.0	1.43	1.02
M-4	25	4.21	3.0	39.0	1.92	1.02
M-5	25	4.21	2.0	35.0	1.91	1.37
M-6	50	4.21	3.0	37.0	1.47	0.73
M-7	0	4.21	3.0	37.0	3.71	1.89
M-8	25	12.50	3.0	35.0	1.37	1.90
M-9	50	12.50	3.0	35.0	1.15	1.58
M-10	0	12.50	3.0	35.0	1.81	2.54
M-11	25	20.83	3.0	35.0	1.31	3.03
M-12	50	20.83	3.0	33.0	1.13	2.42
M-13	0	20.83	3.0	33.0	1.74	3.83
M-14	25	34.72	3.0	33.0	1.28	4.62
M-15	50	34.72	3.0	33.0	0.99	3.54
M-16	0	34.72	3.0	33.0	1.40	5.08

(b) Adsorption experiments for methane on Anthrasorb CC818H at 25^{o}C (in isolation)

Run No.	C_{Mo} mol.cm^{-3} x10^{6}	m g	F cm^{3}.min^{-1}	t_{Mo} min	q_{Mo} mol.g^{-1} x 10^{4}
H-1	4.18	3.0	11.74	8.19	1.30
H-2	4.17	3.0	54.05	2.28	1.68
H-3	4.17	3.0	53.33	2.35	1.71
H-4	4.17	2.0	54.03	3.78	4.22
H-5	1.38	3.0	51.64	2.68	0.62
H-6	4.16	1.0	52.04	1.39	2.97
H-7	4.16	4.0	84.42	2.66	2.30
H-8	8.25	3.0	94.89	2.69	6.95
H-9	13.73	3.0	38.16	2.62	4.46
H-10	22.01	3.0	34.63	3.39	8.43
H-11	24.74	3.0	24.08	5.01	9.74

(c) Adsorption experiments for ethane on Anthrasorb CC818M (in isolation)

Run No.	Temperature ^oC	C_{Eo} $mol.cm^{-3}$ $x\ 10^6$	m g	F $cm^3.min^{-1}$	t_{Eo} min	q_{Eo} $mol.g^{-1}$ $x\ 10^4$
M-1	25	1.23	3.0	53.44	22.59	4.94
M-2	50	1.23	3.0	52.35	13.61	2.91
M-3	-6	1.24	3.0	50.76	43.14	9.04
M-4	25	4.13	3.0	51.80	12.71	9.03
M-5	50	4.10	3.0	51.80	8.23	5.79
M-6	-6	4.12	3.0	55.10	20.73	15.65
M-7	25	8.29	3.0	54.16	9.78	10.86
M-8	50	8.24	3.0	54.32	8.27	12.27
M-9	-6	8.27	3.0	55.84	16.74	25.70
M-10	25	12.40	3.0	59.29	8.18	19.95
M-11	50	12.40	3.0	30.93	10.09	12.80
M-12	-6	12.40	3.0	41.02	17.21	29.08
M-13	25	20.70	3.0	30.93	8.07	17.06
M-14	50	20.60	3.0	33.73	5.78	13.23
M-15	-6	20.80	3.0	34.83	10.17	24.40
M-16	25	24.84	3.0	40.20	7.41	24.43
M-17	50	24.85	3.0	32.68	6.82	15.27
M-18	-6	24.85	3.0	32.95	12.24	33.15

(d) Adsorption experiments for ethane on Anthrasorb CC818H (in isolation)

Run No.	Temperature ^{o}C	C_{Eo} $mol.cm^{-3}$ $\times 10^{6}$	m g	F $cm^{3}.min^{-1}$	t_{Eo} min	q_{Eo} $mol.g^{-1}$ $\times 10^{4}$
H-1	25	1.23	3.0	54.06	23.19	5.24
H-2	25	1.23	2.0	30.85	26.12	4.94
H-3	50	1.23	3.0	43.71	16.63	2.97
H-4	-6	1.24	3.0	52.28	32.03	6.91
H-5	25	4.13	3.0	52.45	13.45	9.68
H-6	25	4.14	4.0	96.60	10.36	10.32
H-7	50	4.13	3.0	53.03	8.97	6.51
H-8	-6	4.13	3.0	53.04	22.53	16.42
H-9	25	8.27	3.0	64.90	9.34	16.64
H-10	50	8.24	3.0	55.46	7.69	11.64
H-11	-6	8.27	3.0	55.98	18.66	28.73
H-12	25	12.30	3.0	43.15	11.71	21.12
H-13	50	12.40	3.0	40.60	12.65	21.12
H-14	-6	12.40	3.0	41.95	19.04	32.91
H-15	50	20.70	1.0	16.55	6.73	22.88
H-16	25	20.60	2.0	19.69	10.30	20.72
H-17	25	20.70	3.0	30.46	8.71	18.13
H-18	25	20.60	4.0	36.02	9.23	16.95
H-19	50	20.70	3.0	33.44	6.36	14.50
H-20	50	20.60	2.0	34.37	4.92	17.25
H-21	-6	20.70	3.0	34.42	11.10	26.19
H-22	25	24.80	3.0	39.89	8.07	26.40
H-23	50	24.80	3.0	31.90	9.68	25.32
H-24	-6	24.80	3.0	32.76	13.30	35.81

(e) Mixed adsorption experiments on Anthrasorb CC818M at 25°C

Run No.	C_{Mo} mol.cm^{-3} x 10^6	C_{Eo} mol.cm^{-3} x 10^6	F cm^3.min^{-1}	m g	C_{M1} mol.cm^{-3} x 10^6	t_{M1} min	t_{Mo} min	t_{Eo} min	q_{M1} mol.g^{-1} x 10^4	q_{Mo} mol.g^{-1} x 10^4	q_{Eo} mol.g^{-1} x 10^4
M-1	1.36	2.76	39.93	3.0	1.47	5.75	23.26	24.26	1.11	0.77	8.93
M-2	1.36	2.76	40.05	3.0	1.47	5.90	23.45	25.68	1.15	0.80	9.44
M-3	2.06	2.06	40.06	3.0	2.14	5.94	27.78	30.56	1.68	1.38	8.39
M-4	2.76	1.36	40.36	3.0	2.84	6.23	31.48	35.02	2.36	2.02	6.39
M-5	2.74	5.56	39.89	3.0	2.99	5.79	18.06	19.55	2.28	1.68	14.41
M-6	4.12	4.12	40.55	3.0	4.41	6.01	20.15	22.82	3.55	2.76	12.68
M-7	5.53	2.73	31.74	2.0	5.75	6.35	21.70	23.65	5.75	4.99	10.22
M-8	5.53	2.73	40.54	3.0	5.81	5.88	24.69	26.76	4.57	3.64	9.85
M-9	6.81	13.84	39.37	3.0	8.10	5.49	11.78	14.03	5.77	3.79	25.37
M-10	10.32	10.32	40.90	3.0	11.76	5.15	12.82	14.20	8.16	5.66	19.89
M-11	10.32	10.32	50.18	4.0	11.66	5.09	13.32	15.20	7.35	5.13	19.59

(f) Mixed adsorption experiments on Anthrasorb CC818H at 25°C

Run No.	C_{Mo} mol.cm^{-3} x 10^6	C_{Eo} mol.cm^{-3} x 10^6	F cm^3.min^{-1}	m g	C_{M1} mol.cm^{-3} x 10^6	t_{M1} min	t_{Mo} min	t_{Eo} min	q_{M1} mol.g^{-1} x 10^4	q_{Mo} mol.g^{-1} x 10^4	q_{Eo} mol.g^{-1} x 10^4
H-1	1.36	2.76	40.0	3.0	1.50	5.82	23.32	25.51	1.15	0.717	9.36
H-2	1.36	2.76	40.45	3.0	1.43	6.37	25.59	27.42	1.22	0.975	10.18
H-3	2.06	2.06	40.35	3.0	2.14	6.12	30.53	32.68	1.74	1.42	9.04
H-4	2.76	1.36	40.47	3.0	2.84	6.25	33.67	37.15	2.37	2.01	6.80
H-5	2.76	1.36	40.27	4.0	2.84	6.88	40.69	46.95	1.94	1.62	6.42
H-6	2.73	5.55	40.43	3.0	3.00	5.58	18.84	20.72	2.23	1.55	15.45
H-7	4.14	4.14	32.29	2.0	4.35	6.47	19.54	20.93	4.51	3.85	13.96
H-8	4.13	4.13	40.36	3.0	4.42	5.47	22.37	24.20	3.22	2.35	13.44
H-9	5.55	2.73	41.15	3.0	5.83	5.93	26.15	28.15	4.69	3.69	10.52
H-10	6.81	1.38	40.33	3.0	8.10	5.45	12.52	14.30	5.87	3.71	2.64
H-11	6.81	1.38	53.11	4.0	8.10	4.90	13.41	14.40	5.20	2.92	2.63
H-12	10.35	10.35	40.27	3.0	11.69	5.15	13.93	15.06	7.98	5.49	20.84
H-13	13.84	6.81	40.07	3.0	14.95	5.47	16.96	18.93	10.80	8.29	17.16

APPENDIX J

TABULATED EXPERIMENTAL RESULTS FOR ACETONE AND CARBON TETRACHLORIDE

APPENDIX J

TABULATED EXPERIMENTAL RESULTS FOR ACETONE AND CARBON TETRA-CHLORIDE

(a) Adsorption experiments for acetone on Anthrasorb CC818M at 25^{o}C.

Run No.	C_{Ao} mol.cm^{-3} x 10^{7}	m g	F cm^{3}.min^{-1}	t_{Ao} min	q_{Ao} mol.g^{-1} x 10^{3}
M-1	4.26	0.100	37.64	41.92	6.72
M-2	2.75	0.100	39.36	45.75	4.95
M-3	1.93	0.100	41.53	51.60	4.14
M-4	1.76	0.100	41.10	48.22	3.49
M-5	1.39	0.100	38.28	59.55	3.17

(b) Adsorption experiments for acetone on Anthrasorb CC818H at 25°C

Run No.	C_{Ao} $mol.cm^{-3}$ $x\ 10^{7}$	m g	F $cm^{3}.min^{-1}$	t_{Ao} min	q_{Ao} $mol.g^{-1}$ $x\ 10^{3}$
H-1	4.34	0.100	33.75	37.91	5.55
H-2	4.08	0.200	40.48	64.91	5.36
H-3	2.80	0.100	32.93	40.57	3.74
H-4	2.91	0.300	33.75	116.30	3.81
H-5	1.91	0.150	41.06	68.19	3.57
H-6	1.77	0.100	39.33	47.25	3.28
H-7	1.52	0.050	19.79	62.77	3.77
H-8	1.24	0.100	40.00	60.66	3.01
H-9	1.29	0.150	60.00	60.70	3.13

(c) Desorption experiments for acetone on Anthrasorb CC818H

Run No.	C_{Ao} mol.cm^{-3} x 10^7	m g	F cm^3.min^{-1}	t_{Ao} min	q_{Ao} mol.g^{-1} x 10^3
H-1	5.47	0.100	40.46	29.40	6.51
H-2	5.36	0.100	42.24	26.75	6.51
H-3	5.35	0.100	41.37	24.03	5.32
H-4	3.30	0.100	43.29	30.13	4.30
H-5	2.42	0.100	44.40	35.72	3.81
H-6	1.76	0.100	43.00	45.46	3.44

(d) Adsorption experiments for carbon tetra-chloride on Anthrasorb CC818M at 25°C

Run No.	C_{Co} mol.cm^{-3} x 10^{7}	m g	F cm^{3}.min^{-1}	t_{Co} min	q_{Co} mol.g^{-1} x 10^{3}
M-1	2.94	0.100	37.62	65.57	7.25
M-2	1.73	0.100	39.02	73.97	4.99
M-3	1.51	0.100	39.80	95.86	5.76
M-4	1.02	0.100	39.14	128.10	5.11

(e) Adsorption experiments for carbon tetra-chloride on Anthrasorb CC818H at 25°C

Run No.	C_{Co} mol.cm^{-3} x 10^{7}	m g	F cm^{3}.min^{-1}	t_{Co} min	q_{Co} mol.g^{-1} x 10
H-1	3.83	0.100	36.58	68.20	9.55
H-2	2.26	0.100	37.93	95.89	8.22
H-3	1.17	0.100	39.50	118.80	5.49
H-4	0.78	0.100	39.56	147.10	4.54

APPENDIX K

CONSTANT PATTERN BEHAVIOUR

APPENDIX K

CONSTANT PATTERN BEHAVIOUR

The continuity equation for adsorption of a single component in a fixed-bed is described mathematically by

$$D\,\frac{\partial^2 C}{\partial z^2} = u\frac{\partial C}{\partial z} + \frac{\partial C}{\partial t} + \frac{\rho(1-E)}{E}\,\frac{\partial q}{\partial t} \qquad \text{(K1)}$$

where D is the longitudinal dispersion coefficient for a solute in the moving phase ($cm^2.s^{-1}$), and u is the linear interstitial fluid velocity ($cm.s^{-1}$)(different from $\bar{u}$). In the absence of axial dispersion, equation K1 reduces to the equation given in Section 2.3.2., as

$$u\,\frac{\partial C}{\partial z} + \frac{\partial C}{\partial t} + \frac{\rho(1-E)}{E}\,\frac{\partial q}{\partial t} = 0 \qquad (2.36)$$

In order to calculate wave velocity through the bed of a given component (say A), the following mathematical identity is utilized:

$$\left(\frac{\partial C_A}{\partial z}\right)_t \cdot \left(\frac{\partial t}{\partial C_A}\right)_z \cdot \left(\frac{\partial z}{\partial t}\right)_{C_A} = -1 \qquad \text{(K2)}$$

Combining equations K2 and 2.36 yields

$$\left(\frac{\partial z}{\partial t}\right)_{C_A} = \bar{u}_A = \frac{u}{1 + \rho(1-E)(\partial q_A/\partial t)/E(\partial C_A/\partial t)} \qquad \text{(K3)}$$

where $\bar{u}_A$ is the wave velocity of component A through the bed ($cm.s^{-1}$). Equation K3 describeds the velocity of motion of component A through a transfer zone. For sufficiently long beds, the concentration profile is self-sharpening in nature (i.e. a sharp S-shaped front) and which, after a short development period near the bed entrance, remains constant throughout the transfer zone (18). Therefore the velocities of each component must be equal

$$\bar{u}_A = \bar{u}_B = \bar{u}_C = \dots = \text{constant} = \bar{u} \qquad \text{(K4)}$$

Cooney and Lightfoot (18) also proposed a distance co-ordinate z*, whose origin moves with the concentration front, and is defined by

$$z^* = z - \bar{u}t \qquad \text{(K5)}$$

By assuming a constant-pattern concentration profile, the concentration, C_A, becomes a function of z* only and the derivatives with respect to time are eliminated. Calculating the derivatives in the continuity equation K1 in terms of z*, yield

$$\left(\frac{\partial C_A}{\partial t}\right)_z = -\bar{u}\left(\frac{dC_A}{dz^*}\right) \qquad \text{(K6)}$$

$$\left(\frac{\partial C_A}{\partial z}\right)_t = \left(\frac{dC_A}{dz^*}\right) \qquad \text{(K7)}$$

$$\left(\frac{\partial^2 C_A}{\partial z^2}\right)_t = \left(\frac{d^2 C_A}{d\, z^{*2}}\right) \qquad \text{(K8)}$$

$$\left(\frac{\partial q_A}{\partial t}\right)_z = -\bar{u}\left(\frac{dq_A}{dz^*}\right) \qquad \text{(K9)}$$

The constant velocity, $\bar{u}$, can also be obtained in terms of z*, by making use of equations K3, K4, K6 and K9.

$$\bar{u} = \frac{u}{1 + \frac{\rho(1-E)}{E}\left(\frac{dq_A}{dC_A}\right)} \qquad \text{(K10)}$$

Integrating equation K10 for the following boundary conditions

$$C = C_{A1}; \quad q = q_{A1} \qquad \text{(K11)}$$

$$C = C_{A2}; \quad q = q_{A2}$$

where C_{A1} and q_{A1} are concentrations in the plateau-zone downstream of the transfer zone, and C_{A2} and q_{A2} are concentrations on the upstream side of the platueau zone. The resulting relation is

$$\bar{u} = \frac{u}{1 + \frac{\rho(1-E)}{E}\left(\frac{q_{A1} - q_{A2}}{C_{A1} - C_{A2}}\right)} \qquad \text{(K12)}$$

Substituting equations K5, K6, K7, K8, K9, K12 into euqtions K1 and rearranging, the result gives

$$D \frac{d^2\left(\frac{C_A - C_{A2}}{C_{A1} - C_{A2}}\right)}{d\, z^{*2}} =$$

$$= \left[\frac{u\,\rho(1-E)\left(\frac{q_{A1} - q_{A2}}{C_{A1} - C_{A2}}\right)}{E + \rho(1-E)\left(\frac{q_{A1}-q_{A2}}{C_{A1}-C_{A2}}\right)}\right] \cdot \frac{d\left[\left(\frac{C_A-C_{A2}}{C_{A1}-C_{A2}}\right) - \left(\frac{q_A - q_{A2}}{q_{A1} - q_{A2}}\right)\right]}{d\, z^*} \qquad \text{(K13)}$$

Cooney and Lightfoot (18) integrate equation K13 for large beds under the following conditions.

$$\text{Limit} \quad \frac{d\left(\dfrac{C_A - C_{A2}}{C_{A1} - C_{A2}}\right)}{d\ z^*} \longrightarrow 0$$

$$\text{when} \quad \left(\frac{C_A - C_{A2}}{C_{A1} - C_{A2}}\right) \longrightarrow \left(\frac{q_A - q_{A2}}{q_{A1} - q_{A2}}\right) \qquad \text{(K14)}$$

which yields

$$D\ \frac{d\left(\dfrac{C_A - C_{A2}}{C_{A1} - C_{A2}}\right)}{d\ z^*} =$$

$$= \frac{u\ \rho(1-E)\left(\dfrac{q_{A1} - q_{A2}}{C_{A1} - C_{A2}}\right)}{E + \rho(1-E)\left(\dfrac{q_{A1} - q_{A2}}{C_{A1} - C_{A2}}\right)} \left[\left(\frac{C_A - C_{A2}}{C_{A1} - C_{A2}}\right) - \left(\frac{q_A - q_{A2}}{q_{A1} - q_{A2}}\right)\right] \qquad \text{(K15)}$$

For constant pattern conditions, and where axial dispersion is negligible (D = 0), the continuity equation K15 becomes:

$$\frac{C_A - C_{A2}}{C_{A1} - C_{A2}} = \frac{q_A - q_{A2}}{q_{A1} - q_{A2}} \qquad \text{(K16)}$$

Cooney and Lightfoot consider the problem for the following three cases:

Case I $\quad D = 0$ and finite mass-transfer resistance

Case II $\quad$ Negligible mass-transfer resistance and $D > 0$

Case III $\quad$ Finite mass-transfer and $D > 0$

For all three cases, they conclude that when the adsorption isotherm is of a favourable type (i.e. $d^2q^*/d^2C < 0$), the concentration profile shows a self-sharpening behaviour and approaches asymptotically a constant shape. When the adsorption isotherm is of the linear or unfavourable type (i.e. $d^2q^*/dc^2 > 0$) the concentration profile shows no tendency to sharpen but instead spreads out continuously along the bed. For elution processes the asymptotic solution is reached only for a concave isotherm (i.e. $d^2q^*/d^2C > 0$).

For multicomponent systems, in which the concentration profile developed in the bed are of self-sharpening type, the asymptotic solution consists of n constant single solute concentration profiles, each moving with a constant velocity, $\bar{u}$. Thus the solution of single solute system may be used directly, as:

$$\frac{q_{A1} - q_{A2}}{C_{A1} - C_{A2}} = \frac{q_{B1} - q_{B2}}{C_{B1} - C_{B2}} = \frac{q_{C1} - q_{C2}}{C_{C1} - C_{C2}} \tag{K17}$$

Equation K17 is a simple and useful relation for the prediction of plateau zone compositions for a multi-component system.

APPENDIX L

COMPUTER PROGRAMME FOR THE CALCULATIONS OF STOICHIOMETRIC TIME AND ADSORBED PHASE CONCENTRATION AT EQUILIBRIUM

```
C     STOICHIOMETRIC TIME AND ADSORBED PHASE CONCENTRATION CALCULATIONS
C     FOR ADSORPTION EXPERIMENTS WITH UNEQUAL INTERVALS
C
C
C
C     C = INITIAL FLUID PHASE CONCENTRATION (MOL/CC)
C     E = VOID FRACTION
C     F = VOLUMETRIC FLOWRATE (CC/MIN)
C     J = RUN NO
C     JJ= TOTAL NO OF EXPERIMENTS
C     N = NO OF EXPERIMENTAL POINTS
C     P = TOTAL VOIDAGE (E*V)
C     STOUT = ADSORBED PHASE CONCENTRATION (MOL/G)
C     TOUT  = STOICHIOMETRIC TIME (MIN)
C     T = TIME (MIN)
C     V = VOLUME OF THE BED (CC)
C     X = DIMENSIONLESS CONCENTRATION (C/CO)
C     Z = MASS OF THE BED (G)
C
C
C
C     READ DATA
C
      READ (5,4) (V,P,C,Z)
C
C     WRITE EXPERIMENTAL CONDITIONS
      WRITE(6,500)(V,P,C,Z)
C
C
      FINT=0.0
      K=N-1
      DO 200 I=1,K
      DELT=T(I+1)-T(I)
C
C     SUMMATION OF STIOCHIOMETRIC TIME IN TRAPEZOIDAL RULE CALCULATION
```

```
C
      FINT=FINT+DELT*(F(I)+F(I+1))/2.
      TOUT=T(N)-FINT
C
C     ADSORBED PHASE CONCENTRATION CALCULATION
C
      STOUT =(V*TOUT-P)*C/Z
  200 CONTINUE
      WRITE (6,300)J,TOUT,STOUT
  100 CONTINUE
C
    4 FORMAT(F10.3,5X,F10.3,5X,E10.4,5X,F10.3)
  300 FORMAT(5X,I2,30X,E10.4,30X,E10.4)
  500 FORMAT(112H0STOICHIOMETRIC TIME OF ADSORPTION RUN FOR ACETONE ADSO
     1RPTION-DESORPTION EXPERIMENTS ON ANTHRASORB CC813H AT 25C/1H0,6HAD
     2SORB/3H0V=F10.3,3X,2HP=F10.3,3X,2HC=E10.4,3X,2HZ=F10.3/1H0,4X,7HEX
     2P NO=,20X,20HSTOICHIOMETRIC TIME=,20X,20HADSORBED PHASE CONC=)
C
      STOP
      END
```

APPENDIX M

<u>COMPUTER PROGRAMME FOR THE EXTERNAL MASS TRANSFER CONTROL MODEL</u>

```
C     PROGRAMME TO MODEL FIXED BED SINGLE COMPONENT ADSORPTION ON
C     ANTHRASORB BY EXTERNAL MASS TRANSFER MODEL
C
C
C
C     B = SLOPE OF ISOTHERM
C     C(I) = FLUID PHASE CONCENTRATION IN (J+1) TIME LIVEL, (MOL/CC)
C     CSA(I) = FLUID PHASE CONCENTRATION IN J TIME LEVEL, (MOL/CC)
C     DELX = SPATIAL INCREMENT (CM)
C     DELT = TIME INCREMENT (SEC)
C     EPS = BED POROSITY
C     N = NO OF SPATIAL INCREMENTS
C     Q = VOLUMETRIC FLOW RATE (CC/MIN)
C     TMAX = MAXIMUM TIME ALLOWED FOR CONVERGENCE (SEC)
C     V = INTERSITIAL VELOCITY (CM/SEC)
C     W(I) = ADSORBED PHASE CONCENTRATION IN (J+1) TIME LEVEL (MOL/G)
C     WSA(I) = ADSORBED PHASE CONCENTRATION IN J TIME LEVEL (MOL/G)
C     XKMA = MASS TRANSFER COEFFICIENT (MIN**-1)
C     XL = LENGTH OF PACKED BED (CM)
C
C
C
      IMPLICIT REAL*8(A-H,O-Z)
      DIMENSION RUN(10),TOUT(4),COUT(4)
      DIMENSION C(51),CSA(51),W(51),WSA(51)
      DATA ONE,TWO/1.0D0,2.0D0/
C
C
C     READ DATA
    1 READ(5,2,END=99)Q,EPS,XKMA,B,XL
      READ(5,2)DELT,TMAX
      READ(5,3) RUN
C
C
C     WRITE EXPERIMENTAL CONDITIONS
```

```
C
C
      WRITE(6,10) RUN
      WRITE(6,11)Q,EPS,XKHA,B,XL
C
C
C
      NP=0
      N=50
      DELX=XL/50.0D0
      WRITE(6,12)DELT,TMAX
      Q=Q/60.0D0
      XKHA=XKHA/60.0D0
      AREA=0.1765D0
      V=Q/(AREA*EPS)
      D1=V/(TWO*DELX)
      D2=ONE/(TWO*DELT)
      D3=B*XKHA/(TWO*B+TWO*XKHA*DELT*EPS)
      A1=-D1-D2-D3
      A2=D1-D2
      A3=-D1+D2
      A4=D1+D2-D3
      A5=-XKHA/(TWO*B+TWO*XKHA*DELT*EPS)
      A6=-XKHA/(B+XKHA*EPS*DELT)
      C0=ONE
      C(1)=C0
      U(1)=0.0D0
      CSA(1)=C0
      USA(1)=0.0D0
      NOUT=0
```

```fortran
      M1=M+1
      DO 100 I=2,M1
      C(I)=0.0D0
      CSA(I)=0.0D0
      W(I)=0.0D0
  100 WSA(I)=0.0D0
      B2=A2/A1
      B3=A3/A1
      B4=A4/A1
      B5=A5/A1
      B6=A6/A1
      DUM1=(B-XKMA*EPS*DELT)/(B+XKMA*EPS*DELT)
      DUM2=(B*XKMA*EPS*DELT)/(B+XKMA*EPS*DELT)
      DUM3=B/(B+XKMA*EPS*DELT)
      TIME=0.0D0
   20 DO 101 I=2,M1
      C(I)=-B2*C(I-1)-B3*CSA(I)-B4*CSA(I-1)+B5*(WSA(I)-W(I-1))+
     1B6*WSA(I-1)
      W(I)=DUM3*(WSA(I)-W(I-1))+DUM1*WSA(I-1)+DUM2*(C(I)+CSA(I-1))
  101 CONTINUE
      DO 102 I=2,M1
      CSA(I)=C(I)
      WSA(I)=W(I)
  102 CONTINUE
      TIME=TIME+DELT
      TIMIN=TIME/60.0D0
      NP=NP+1
      IF(NP.GT.100)GOTO 103
      TIMES(NP)=TIMIN
      CONCS(NP,1)=C(M1)
```

```
 103  NOUT=NOUT+1
      TOUT(NOUT)=TIMIN
      COUT(NOUT)=C(N1)
      IF((TIMIN-TMAX).GT.1.0D-5) GOTO 117
      IF(NOUT.NE.4) GOTO 20
      WRITE(6,19)(TOUT(N),COUT(N),N=1,4)
      NOUT=0
      GOTO 20
 117  NOUT=NOUT-1
      NP=NP-1
      IF(NP.GT.100)NP=100
      IF(NOUT.LE.0) GOTO 118
      WRITE(6,19)(TOUT(N),COUT(N),N=1,NOUT)
C
C
C
C     CALL SUBROUTINE PBPLT1 FOR PLOTTING PREDICTED BREAK-THROUGH CURVES
C
C
C
 118  CALL PBPLT1('LINZ','LINZ',6,4,TIMES,CONCS,100,1,NP,1,4,11.0,
     1'TIME(MIN)','RELATIVE EFFLUENT CONCENTRATION (C/CO)','CALCULATED
     2BREAKTHROUGH CURVE FOR METHANE ON ANTHRASORB CC818N AT 25C','KHALI
     3D SIDDIQI')
C
      GOTO 1
    2 FORMAT(5F10.3)
    3 FORMAT(10A8)
   10 FORMAT(/////' DIGITAL SIMULATION OF A FIXED BED ADSORPTION COLUMN
     1WITHOUT AXIAL DISPERSION'//' ',10A8)
   11 FORMAT('0',8X,'Q',11X,'EPS',12X,'XKNA',12X,'B',13X,'XL'/
     +' ',5D15.7)
   12 FORMAT('0',6X,'DELT',11X,'TMAX'/' ',2D15.7//)
   19 FORMAT(4(4X,'TIME =',F8.4,2X,'C/C0=',F7.4))
   99 STOP
      END
```

APPENDIX N

COMPUTER PROGRAMME FOR THE PORE DIFFUSION MODEL

```
C     PROGRAMME TO MODEL FIXED BED SINGLE COMPONENT ADSORPTION ON
C     ANTHRASORB BY PORE DIFFUSION MODEL
C
C
C
C     A = CONSTANT
C     B(I),C(I),D(I) = DUMMY VARIABLES
C     E = CONSTANT
C     F(I) = DUMMY VARIABLE
C     N = NO OF EXPERIMENTAL POINTS
C     R = EQUILIBRIUM PARAMETER
C     SR = RATE CONSTANT (MIN**-1)
C     TA = TIME (MIN) AT C/CO = 0.5
C     TN(I) = DUMMY VARIABLE
C     X = DIMENSIONLESS CONCENTRATION (C/CO)
C     Y = INTERGRATION CONSTANT
C
C
C
      DIMENSION B(50),C(50),D(50),TN(50),X(50),F(50),T(50)
C
C     READ DATA
C
      READ(5,500) N
      READ(5,510)(X(K),K=1,N)
      READ(5,501)R,TA,SR
C
C     WRITE EXPERIMENTAL CONDITIONS
C
      WRITE(6,800)N
      WRITE(6,600)R,TA,SR
C
C
      A = (R**2.0)+(1.83*(1.0-R)**0.92)
      Y = 2.44-(2.15*R)
```

```
      E = R/(1.0-R)
      DO 100 I=1,N
      F(I) = SQRT(1.0-X(I)+(R*X(I)))
      B(I) = 2.0*F(I)
      C(I) = E*ALOG((1.0+F(I))/(1.0-F(I)))
      D(I) = ALOG((F(I)+SQRT(R))/(F(I)-SQRT(R)))
      D(I) = D(I)*(SQRT(R)/(1.0-R))
      TN(I) =A*(-B(I)-C(I)+D(I))+Y
      T(I) = (TN(I)/SR)+TA
      WRITE(6,700)TN(I),X(I),T(I)
  100 CONTINUE
      WRITE(6,900)N
      DO 150 I=1,N
      WRITE(6,950)T(I),X(I)
  150 CONTINUE
C
  500 FORMAT(1X,I2)
  501 FORMAT(1X,F6.4,F10.4,F10.4)
  510 FORMAT(10F5.2)
  600 FORMAT(21H1PORE DIFFUSION MODEL/3H0R=F6.4,2X,3HTA=F10.4,2X,3HSR=F1
     10.4/1H0,4X,2HTN,4X,1HX,4X,1HT)
  700 FORMAT(3X,F10.4,2X,F6.4,2X,F10.4)
  900 FORMAT(1X,I2)
  950 FORMAT(2X,F6.4,1X,F6.4)
      STOP
      END
```

APPENDIX P

COMPUTER PROGRAMME FOR THE SURFACE DIFFUSION MODEL

```
C     PROGRAMME TO MODEL FIXED BED SINGLE COMPONENT ADSORPTION ON
C     ANTHRASORB BY SURFACE DIFFUSION MODEL
C
C
C
C     MAIN PROGRAMME
C
C     ANR = FLOATING POINT VALUE OF COUNTER NR
C     ARG = DUMMY VARIABLE FOR EXPONENT ARGUMENT
C     C = CONSTANT IN INPUT FUNCTION TO MAKE Y=0.01
C     CHK = TEST VARIABLE
C     G = DIMENSIONLESS TIME INTERVAL
C     H = DIMENSIONLESS RADIUS INTERVAL
C     KON = DUMMY VARIABLE
C     L = COUNTER
C     LINE, M, MAX, ME = COUNTERS FOR PRINT OUT
C     NEQ = COUNTER ON NUMBER OF TIME INTERVALS
C     NIN = COUNTER FOR PRINT OUT
C     NOD = COUNTER FOR PRINT OUT OF EVERY (N)TH LINE
C     NR = COUNTER ALONG RADIUS GRID
C     NG = NUMBER OF RADIUS GRID POINTS + 1
C     NN = NUMBER OF RADIUS GRID POINTS
C     NO = NUMBER OF RADIUS GRID POINTS + 2
C     NV = COUNTER LIMIT NUMERICALLY EQUAL TO NN
C     NY = NUMBER OF RADIUS GRID POINTS - 1
C     R = DIMENSIONLESS RADIUS
C     RSQ = FLOATING POINT VALUE OF RADIUS SQUARED
C     SR = EQUILIBRIUM PARAMETER
C     Y = DIMENSIONLESS ADSORBED PHASE CONCENTRATION
C     YBAR = MEAN ADSORBED PHASE CONCENTRATION (DIMENSIONLESS)
C     YENDS = BOUNDARY CONDITIONS SUBROUTINE
C     YEV = DUMMY SUMMATION VARIABLE
C     YEVEN = SUMMATION OF EVEN NUMBERED Y'S IN SIMPSON RULE
C     YINPUT = INPUT FUNCTION SUBROUTINE
C     YLIM = SUMMATION OF LIMIT Y'S IN SIMPSON'S RULE
```

```
C     YMID = VALUE OF Y IN GRID SUBROUTINE
C     YP = VALUE OF Y IN EQUILIBRIUM WITH THE MEAN FLUID PHASE CONCENTRA
C     TION (DIMENSIONLESS)
C
C     YOD = DUMMY SUMMATION VARIABLE
C     YODD = SUMMATION OF ODD NUMBERED Y'S IN SIMPSON RULE
C     YP0 = CALCULATED VALUE OF X IN EQUILIBRIUM WITH THE MEAN ADSORBED
C     PHASE CONCENTRATION
C
C     YP1 = VALUE OF X IN EQUILIBRIUM WITH THE MEAN ADSORBED PHASE CONCE
C     NTRATION
C
C     X = FLUID PHASE CONCENTRATION (DIMENSIONLESS)
C
C
C
      DIMENSION Y(101,2),YBAR(20000),YR2(20)
      COMMON H,G,HG,NV,NH,NY,C,YP,SR,YBAR,YP0,NEQ,Y
C
C     READ DATA
C
      READ(5,50) NDSET
    1 READ (5,2) SR,C,H,G,YP
C
      NDSCNT = 0
      NEQ=0
      NH=1./H+1.
      NG=NH+1
      NV=NG-1
      NY=NV-1
```

```
      WRITE(6,60)NDSET
   10 WRITE(6,3)C,H,G,YP,NH,NG,NV,NY
      LINE=0
      L=0
      MOD=1./(10.*G)
      CALL YINPUT
   15 CALL YMID
      CALL YENDS
  601 DO 999 MR=1,NG
      AMR=MR
      RSQ=H*(AMR-1.)
      YR2(MR)=(RSQ**2)*Y(MR,2)
  999 CONTINUE
      YOD=0.
      YEV=0.
      DO 998 MR=2,NY,2
      YOD=YOD+YR2(MR)
  998 CONTINUE
      YODD=4.*YOD
      DO 997 MR=3,NY,2
      YEV=YEV+YR2(MR)
  997 CONTINUE
C     SUMMATION OF EVEN NUMBERED Y IN SIMPSON RULE
      YEVEN=2.*YEV
      L=L+1
      IF(L.GT.20000)GO TO 9999
C     SUMMATION OF LIMIT Y IN SIMPSON RULE
  996 YLIM=YPO
C     MEAN SOLID PHASE CONCENTRATION (DIMENSIONLESS)
      YBAR(L)=H*(YLIM+YODD+YEVEN)
```

```
C     VALUE OF X IN EQUILIBRIUM WITH THE MEAN SOLID PHASE CONS
      YP1=YBAR(L)/(SR+(1.-SR)*YBAR(L))
      CHK=ABS (YP1-YP0)
      IF (.0005-CHK)400,401,401
  400 YP0=YP1
      GO TO 996
  401 Y(NG,2)=YP1
      LINE=LINE+1
      IF (MOD(LINE,MOD)-1)936,937,936
  937 WRITE (6,4) (Y(NR,1),NR=1,NG)
  936 DO 20 NR=1,NG
      Y(NR,1)=Y(NR,2)
      Y(NR,2)=0.
   20 CONTINUE
      IF (.990-YBAR(L))500,500,15
  500 WRITE (6,4) (Y(NR,1),NR=1,NG)
      WRITE (6,8)
      N=L/(10*MOD)
      NE=10*N*MOD
      IF (NE-L)17,18,18
   17 IF (NE-L+MOD)934,18,18
  934 N=N+1
   18 DO 23 I=1,N
      MIN=(10*I-9)*MOD
      MAX=MIN+9*MOD
      IF (MAX-L)23,23,25
   25 MAX=L
   23 WRITE (6,9) (I,(YBAR(K),K=MIN,MAX,MOD))
      WRITE (6,9)(NEQ,YBAR(L))
      NDSCNT = NDSCNT + 1
```

```
      IF(NDSCNT.LT.NDSET) GO TO 1
 9999 WRITE(6,6998)
      WRITE(6,6999)(YBAR(LL),LL=19901,20000)
      NDSCNT=NDSCNT+1
      IF(NDSCNT.LT.NDSET)GO TO 1
    2 FORMAT(F5.3,F6.2,F5.3,F6.4,F7.5)
    3 FORMAT(49H1SOLID DIFFUSION KINETICS IN FIXED BED ADSORPTION/1H0,
     16HKNALID/4H0SR=F5.3,3X,2HC=F6.3,3X,2HH=F5.3,3X,2HG=F6.4,3X,
     23HYP=F7.5,3X,3HNH=I3,3X,3HNG=I3,3X,3HNV=I3,3X,3HNY=I3
     3          /1H0,4X,2HY0,8X,2HY1,8X,2HY2,8X,2HY3,8X,2HY4,8X,2HY5,8X,
     42HY6,8X,2HY7,8X,2HY8,8X,2HY9,8X,3HY10)
    4 FORMAT(1X,2X,F6.4,4X,F6.4,4X,F6.4,4X,F6.4,4X,F6.4,4X,F6.4,4X,F6.4,
     14X,F6.4,4X,F6.4,4X,F6.4,4X,F6.4)
    8 FORMAT(5H1YBAR//3X,1HI,11X,1H1,8X,1H2,8X,1H3,8X,1H4,8X,1H5,8X,1H6,
     18X,1H7,8X,1H8,8X,1H9,7X,2H10)
    9 FORMAT(1X,I6,2X,10F9.4)
   50 FORMAT(1X,I1)
   60 FORMAT(6HNDSET=I1)
 6998 FORMAT('0L > 20000. NO YBAR(L) > .99 LAST 100 YBAR ARE;')
 6999 FORMAT(1X,10E13.4)
      STOP
      END
C
C
      SUBROUTINE YINPUT
C     INPUT FUNCTION SUBROUTINE
      DIMENSION Y(101,2),YBAR(20000)
      COMMON H,G,NG,NV,NH,NY,C,YP,SR,YBAR,YPO,NEQ,Y
      NO=NG+1
      R=0.
```

```
      DO 100 MR=1,NG
C     DUMMY VARIABLE FOR EXPONENT ARGUMENT
      ARG=C*R-C
      IF(50.+ARG)110,110,120
  110 Y(MR,1)=0.
      GO TO 130
C     EMPIRICAL CONCENTRATION-DISTRIBUTION CALCULATION
  120 Y(MR,1)=YP*EXP(ARG)
  130 R=R+H
  100 CONTINUE
      Y(NG,1)=2.*H*C*YP+Y(NV,1)
      RETURN
      END
C
C
C
      SUBROUTINE YNID
C     ESTIMATION OF VALUE OF Y IN GRID SUBROUTINE
      DIMENSION Y(101,2),YBAR(20000)
      COMMON H,G,NG,NV,NN,NY,C,YP,SR,YBAR,YPO,NEQ,Y
      NEQ=NEQ+1
      R=H
      DO 300 MR=2,NV
      Y(MR,2)=(G/(15.*H))*((1./H)*(Y(MR+1,1)-2.*Y(MR,1)+Y(MR-1,1))+(1./
     1R)*(Y(MR+1,1)-Y(MR-1,1)))+Y(MR,1)
      R=R+H
      IF(Y(MR,2))306,300,307
```

```
  306 Y(NR,2)=0.
      GO TO 300
  307 IF(1.-Y(NR,2))308,300,300
  308 Y(NR,2)=1.
  300 CONTINUE
      RETURN
      END
C
C
C
      SUBROUTINE YENDS
C     BOUNDARY CONDITIONS SUBROUTINE
      DIMENSION Y(101,2),YBAR(20000)
      COMMON N,G,NG,NV,NN,NY,C,YP,SR,YBAR,YPO,NEQ,Y
      R=1.-N
C     CALCULATED VALUE OF X IN EQUILIBRIUM WITH THE MEAN SOLID PHASE
C    1CONCENTRATION
      YPO=(R*N/(R+N))*((30.*N/G)*(Y(NV,2)-Y(NV,1))-(1./N)*(Y(NY,2)+Y(NG,
     11)+Y(NY,1)-2.*(Y(NV,2)+Y(NV,1)))-Y(NG,1)+Y(NY,2)+Y(NY,1))
      IF(YPO)613,619,614
  613 YPO=0.
      GO TO 619
  614 IF(1.-YPO)615,619,619
  615 YPO=1.
  619 Y(1,2)=1.5*Y(2,2)-.5*Y(3,2)
      IF(Y(1,2))620,621,621
  620 Y(1,2)=0.
  621 RETURN
      END
```

APPENDIX Q

COMPUTER PROGRAMME FOR THE LINEAR DRIVING FORCE MODEL

```
C     PROGRAMME TO MODEL FIXED BED SINGLE COMPONENT ADSORPTION ON
C     ANTHRASORB BY LINEAR DRIVING FORCE MODEL
C
C
C
C     N=NO OF EXPERIMENTAL POINTS
C     A=CONSTANT
C     B(I)=DUMMY VARIABLE
C     CA=FLUID PHASE CONCENTRATION AT C/CO=0.5(MOL/CC)
C     CBAR=INTERMEDIATE FLUID PHASE CONCENTRATION(MOL/CC)
C     CO=INITIAL FLUID PHASE CONCENTRATION (MOL/CC)
C     D(I)=DUMMY VARIABLE
C     Q(I)=DUMMY VARIABLE
C     R=EQUILIBRIUM PARAMETER (DIMENSIONLESS)
C     SR=RATE CONSTANT(MIN**-1)
C     TA=TIME AT C/CO=0.5
C     Y=DIMENSIONLESS CONCENTRATION (C/CO)
C     Y(I)=DIMENSIONLESS CONCENTRATION (C/CO)
C     YA=DIMENSIONLESS CONCENTRATION (C/CO)=0.5
C
C
C
      DIMENSION CBAR(100),B(100),D(100),Q(100),T(100),Y(100)
C
C     READ DATA
C
      READ(5,510) N
      READ(5,500)(Y(K),K=1,N)
      READ(5,550)YA,R,TA,SR,CO
C
C     WRITE EXPERIMENTAL CONDITIONS
C
      WRITE(6,810)N
      WRITE(6,601)YA,R,TA,SR,CO
C
```

```
      A=R/(1.0-R)
      CA=YA*CO
      DO 100 I=1,N
      CBAR(I)=Y(I)*CO
      B(I)=(CA*(CO-CBAR(I)))/((CO-CA)*(CBAR(I)))
      D(I)=(CO-CBAR(I))/(CO-CA)
      Q(I)=ALOG(B(I))
      Q(I)=A*Q(I)
      Q(I)=Q(I)+ALOG(D(I))
      T(I)=TA-(Q(I)/SS)
      WRITE(6,600)T(I),Y(I),Q(I)
  100 CONTINUE
      DO 150 I=1,N
      WRITE(6,750)T(I),Y(I)
  150 CONTINUE
C
  500 FORMAT(10F5.2)
  510 FORMAT(1X,I2)
  550 FORMAT(4F10.4,E10.3)
  600 FORMAT(1X,2X,F10.4,2X,F6.4,2X,F10.4)
  601 FORMAT(27H1LINEAR DRIVING FORCE MODEL/1H0,6HKHALID/4H0YA=F10.4,3X,
     12HR=F10.4,3X,3HTA=F10.4,3X,3HSR=F10.4,3X,3HCO=E10.4/1H0,4X,1HT,4X,
     21HY,4X,1HQ)
  750 FORMAT(2X,F8.4,1X,F6.4)
  810 FORMAT(1X,1H1,2HN=I2)
C
      STOP
      END
```

APPENDIX R

BINARY ADSORPTION BREAKTHROUGH MODELLING PROGRAMME

```
C     PROGRAMME TO MODEL FIXED BED BINARY COMPONENT (METHANE-ETHANE)
C     ADSORPTION ON ANTHRASORB
C
C
C
C
C     AD = DUMMY CONSTANT
C     AE = LANGMUIR CONSTANT FOR ETHANE (MOL/G)
C     AM = LANGMUIR CONSTANT FOR METHANE (MOL/G)
C     BB = DUMMY CONSTANT
C     BE = LANGMUIR CONSTANT FOR ETHANE (CC/MOL)
C     BE1 = EXTENDED LANGMUIR EMPIRICAL CONSTANT FOR ETHANE IN BINARY
C     MIXTURE (CC/MOL)
C
C     BM = LANGMUIR CONSTANT FOR METHANE (CC/MOL)
C     CA=FLUID PHASE CONCENTRATION (MOL/CC) AT (C/C0)=0.5
C     CEO=INITIAL FLUID PHASE CONCENTRATION FOR ETHANE (MOL/CC)
C     CMO=INITIAL FLUID PHASE CONCENTRATION FOR METHANE (MOL/CC)
C     CM1=METHANE CONCENTRATION IN ZONE-3(PLATEAU ZONE) (MOL/CC)
C     CONCS=DIMENSIONLESS CONCENTRATION OF METHANE IN ZONE-4 (TRANSFER-
C     ZONE)
C
C     CONCS1=DIMENSIONLESS CONCENTRATION OF ETHANE IN ZONE-2 (TRANSFER-
C     ZONE)
C
C     CONCS2=DIMENSIONLESS CONCENTRATION OF METHANE IN ZONE-2 (TRANSFER-
C     ZONE)
C
C     DD=DUMMY CONSTANT
C     DELTAX=TIME RANGE FOR INTEGRATION
C     E=DUMMY CONSTANT
C     F(1)=RATE EQUATION FOR ETHANE
C     F(2)=RATE EQUATION FOR METHANE
C     H=STEP LENGTH IN KUTHER SUB-ROUTINE
C     K=NO OF INTEGRATION STEPS
```

```
C     BM1=EXTENDED LANGMUIR EMPIRICAL CONSTANT FOR METHANE IN BINARY-
C     MIXTURES (CC/MOL)
C
C     QE0=ADSORBED PHASE CONCENTRATION FOR ETHANE (MOL/G), IN
C     EQUILIBRIUM WITH INTIAL CONCENTRATION
C
C     QM0=ADSORBED PHASE CONCENTRATION IN EQUILIBRIUM WITH INITIAL
C     CONCENTRATION OF METHANE (MOL/G)
C
C     QM1=ADSORBED PHASE CONCENTRATION IN ZONE-3 (PLATEAU ZONE) (MOL/G)
C     R=EQUILIBRIUM PARAMETER (DIMENSIONLESS)
C     SE=RATE CONSTANT FOR ETHANE (MIN**-1)
C     SM=RATE CONSTANT FOR METHANE (MIN**-1)
C     TA=TIME AT(C/C0)=0.5
C     TOL=TOLERANCE
C     T=TIME(MIN)
C     X=ETHANE BREAK-POINT (MIN)
C     Y(1)=ETHANE CONCENTRATION(MOL/CC)
C     Y(2)=METHANE CONCENTRATION (MOL/CC)
C     YY=DIMENSIONLESS CONCENTRATION (C/C0)=0.5
C
C
C
      IMPLICIT REAL*8(A-H,O-Z)
      DIMENSION B(100),CBAR(100),D(100),Q(100),T(100),Y(10),TOL(10)
      DIMENSION CONCS(100)
      COMMON/XXX/AE,BE,AM,BM,BM1,QE0,CE0
      COMMON/YYY/QM0,CM0,CM1,QM1,BE1,SE,SM
C
```

```
C
C     READ DATA
C
      READ(5,500)N
      READ(5,501)(CONCS(K),K=1,N)
      READ(5,502) (YY,R,TA)
      READ(5,503)AE,BE,AH,BH,BH1,QE0,CE0
      READ(5,504)QH0,CH0,CH1,QH1,DE1,SE,SH
      READ(5,505)TOL(1)
C
C     WRITE EXPERIMENTAL CONDITIONS
C
      WRITE(6,600)N
      WRITE(6,601)(YY,R,TA)
      WRITE(6,602)AE,BE,AH,BH
      WRITE(6,603)BH1,QE0,CE0
      WRITE(6,604)QH0,CH0,CH1,QH1
      WRITE(6,605)DE1,SE,SH
      WRITE(6,606)TOL(1)
C
C
C
C     METHANE CONCENTRATION IN ZONE-1 (PLATEAU ZONE) EQUAL TO INITIAL
C     CONCENTRATION (CH0)
C
C
C
C     ETHANE CONCENTRATION IN ZONE-1 (PLATEAU ZONE) IS EQUAL TO INITIAL
C     CONCENTRATION (CE0)
C
C
```

```
C
C     CALCULATION OF METHANE AND ETHANE CONCENTRATIONS IN ZONE-2 (TRANSF
C     ER ZONE) USING RUNGA_KUTTA_MERSON (KUTMER) METHOD
      TOL(2)=TOL(1)
      X=11.25D0
      Y(1)=10.320D-08
      Y(2)=CM1
      HEST=0.2D0
      K=0
   10 CONCS1=Y(1)/CE0
      CONCS2=Y(1)/CM0
      WRITE(6,609)X,CONCS1,CONCS2,K
      IF (X.GT.20.0D0)GOTO 15
      CALL KUTMER(2,X,Y,0.5D0,HEST,TOL,K)
      GO TO 10
C
C
C
C     CALCULATION OF METHANE CONCENTRATION IN ZONE-3 (PLATEAU ZONE)
C
C
C
   15 DD=QE0/CE0
      AB=(QM0-(DD*CM0))
      BB=(AM*BM)
      E=DD+(BM*AM)-BB
      CM1=-E+SQRT((E**2.0D0)-(4.0D0*BM*DD*AB))/(2.0D0*BM*DD)
      WRITE(6,607)CM1
C
```

```
C
C     CALCULATION OF METHANE CONCENTRATION IN ZONE-4 (TRANSFER ZONE)
      A=R/(1.0-R)
      CA=YY*CM1
      DO 100 I=1,N
      CBAR(I)=CONCS(I)*CM1
      B(I)=(CA*(CM1-CBAR(I)))/((CM1-CA)*(CBAR(I)))
      D(I)=(CM1-CBAR(I))/(CM1-CA)
      Q(I)=DLOG(B(I))
      Q(I)=A*Q(I)
      Q(I)=Q(I)+DLOG(D(I))
      T(I)=TA-(Q(I)/SM)
      WRITE(6,603)T(I),CONCS(I)
  100 CONTINUE
C
C
  500 FORMAT(1X,I2)
  501 FORMAT(10F5.2)
  502 FORMAT(3F10.4)
  503 FORMAT(7E10.3)
  504 FORMAT(5E10.3,2F10.4)
  505 FORMAT(E10.3)
  600 FORMAT(82H1PREDICTION OF ADSORPTION BREAKTHROUGH CURVES FOR BINARY
     1 MIXTURES (METHANE-ETHANE)/1H0,6HKNALID/3H0N=I2)
  601 FORMAT(4H0YA=F10.4,3X,2HR=F10.4,3X,3HTA=F10.4)
  602 FORMAT(4H0AE=E10.3,3X,3HBE=E10.3,3X,3HAM=E10.3,3X,3HBM=E10.3)
  603 FORMAT(1H0,4HBM1=E10.3,3X,4HQE0=E10.3,3X,4HCE0=E10.3)
  604 FORMAT(5H0QM0=E10.3,3X,4HCM0=E10.3,3X,4HCM1=E10.3,3X,4HQM1=E10.3)
  605 FORMAT(1H0,4HBE1=E10.3,3X,3HSE=F10.4,3X,3HSM=F10.4)
  606 FORMAT(1H0,2X,10HTOLERANCE=E10.3)
  607 FORMAT(47H1METHANE CONCENTRATION IN ZONE-3 (PLATEAU ZONE)/1H0,4HCM
```

```
     11=E10.3)
 600 FORMAT(62H1METHANE CONCENTRATION IN ZONE-4 (TRANSFER ZONE) USING
    1LINEAR DRIVING FORCE MODEL/1H0,4X,1HT,4X,5HCONCS/1H0,1X,2X,F10.4,
    22X,F6.4)
 609 FORMAT(83H1METHANE AND ETHANE CONCENTRATIONS IN ZONE-2(TRANSFER-ZO
    1NE) USING KUTNER SUBROUTINE/1H0,4X,4HTIME,8X,12HETHANE CONCS,8X,13
    2HMETHANE CONCS,8X,1HR/1H0,2X,F8.4,8X,F8.4,8X,F10.4,12X,I3)
      STOP
      END
C
C
C
C     AUXILARY SUBROUTINE
      SUBROUTINE DERIVS(X,Y,F)
      IMPLICIT REAL*8(A-H,O-Z)
      DIMENSION Y(2),TOL(2),F(2)
      COMMON/XXX/AE,BE,AM,BM,BM1,QE0,CE0
      COMMON/YYY/QM0,CM0,CM1,QM1,BE1,SE,SM
C
      DD=QE0/CE0
      DE=SE/DD
      DB=AM*BM
      DC=AE*BE
      BD=(QM1-QM0)/(CM1-CM0)
      F(1)=DE*(((DC*Y(1))/(0.674D0+(BE*Y(1))-(BM1*Y(2))))-(DD*Y(1)))
      F(2)=(SM/DD)*(((DB*Y(2))/(0.447D0+(BM*Y(2))-(BE1*Y(1)))))-(BD*(Y(2)
     1-CM0))-QM0)
      RETURN
      END
C
```

```
C
C
C
C     SUBROUTINE KUTHER
      SUBROUTINE KUTHER(EQ,X,Y,DELTAX,HEST,TOL,K)
      INTEGER EQ
      DOUBLE PRECISION X,Y(EQ),DELTAX,HEST,TOL(EQ)
      DOUBLE PRECISION DABS
      LOGICAL B1,B2
      DOUBLE PRECISION Y0(50),YA(50),YB(50),YC(50),YD(50),Y1(50),F0(50),
     1FA(50),FB(50),FC(50),FD(50),E(50),EX,H,TEST,HOUT,X0
      EQUIVALENCE(YA,YB,YC,YD)
      X0=X
      K=0
      H=HEST
      DO 200 I=1,EQ
  200 Y0(I)=Y(I)
  102 B1=.FALSE.
      B2=.FALSE.
      HOUT=H
      TEST=(X+DELTAX-X0-H)/DELTAX
      IF(TEST.GT.1.0D-6) GOTO 101
      IF(TEST.LT.-1.0D-6) GO TO 104
      B2=.TRUE.
  101 CALL DERIVS(X0,Y0,F0)
      DO 201 I=1,EQ
  201 YA(I)=Y0(I)+H*F0(I)/3.0D0
      EX=X0+H/3.0D0
      CALL DERIVS(EX,YA,FA)
      DO 202 I=1,EQ
```

```fortran
  202 YD(I)=Y0(I)+H*(F0(I)+FA(I))/6.0D0
      CALL DERIVS(EX,YD,FD)
      DO 203 I=1,EQ
  203 YC(I)=Y0(I)+H*(F0(I)+3.0D0*FD(I))/8.0D0
      EX=X0+0.5D0*H
      CALL DERIVS(EX,YC,FC)
      DO 204 I=1,EQ
  204 YD(I)=Y0(I)+0.5D0*H*F0(I)-1.5D0*H*FD(I)+2.0D0*H*FC(I)
      EX=X0+H
      CALL DERIVS(EX,YD,FD)
      DO 205 I=1,EQ
  205 Y1(I)=Y0(I)+H*(F0(I)+4.0D0*FC(I)+FD(I))/6.0D0
      DO 206 I=1,EQ
      E(I)=DABS(0.2D0*(YD(I)-Y1(I)))
      IF(E(I).GT.TOL(I)) GOTO 105
  206 CONTINUE
      K=K+1
      IF(B1.OR.B2) GOTO 103
      X0=X0+H
      DO 209 I=1,EQ
  209 Y0(I)=Y1(I)
      DO 210 I=1,EQ
      IF(E(I).GT.(TOL(I)/64.0D0)) GOTO 102
  210 CONTINUE
      H=2.0D0*H
      GOTO 102
  103 HEST=HOUT
      X=X0+H
      DO 211 I=1,EQ
  211 Y(I)=Y1(I)
      RETURN
  104 B1=.TRUE.
      H=DELTAX-X0+X
      GOTO 101
  105 H=0.5D0*H
      GOTO 102
      END
```

CHROMATOGRAPHIC BREAKTHROUGH CURVE

FOR BINARY ADSORPTION

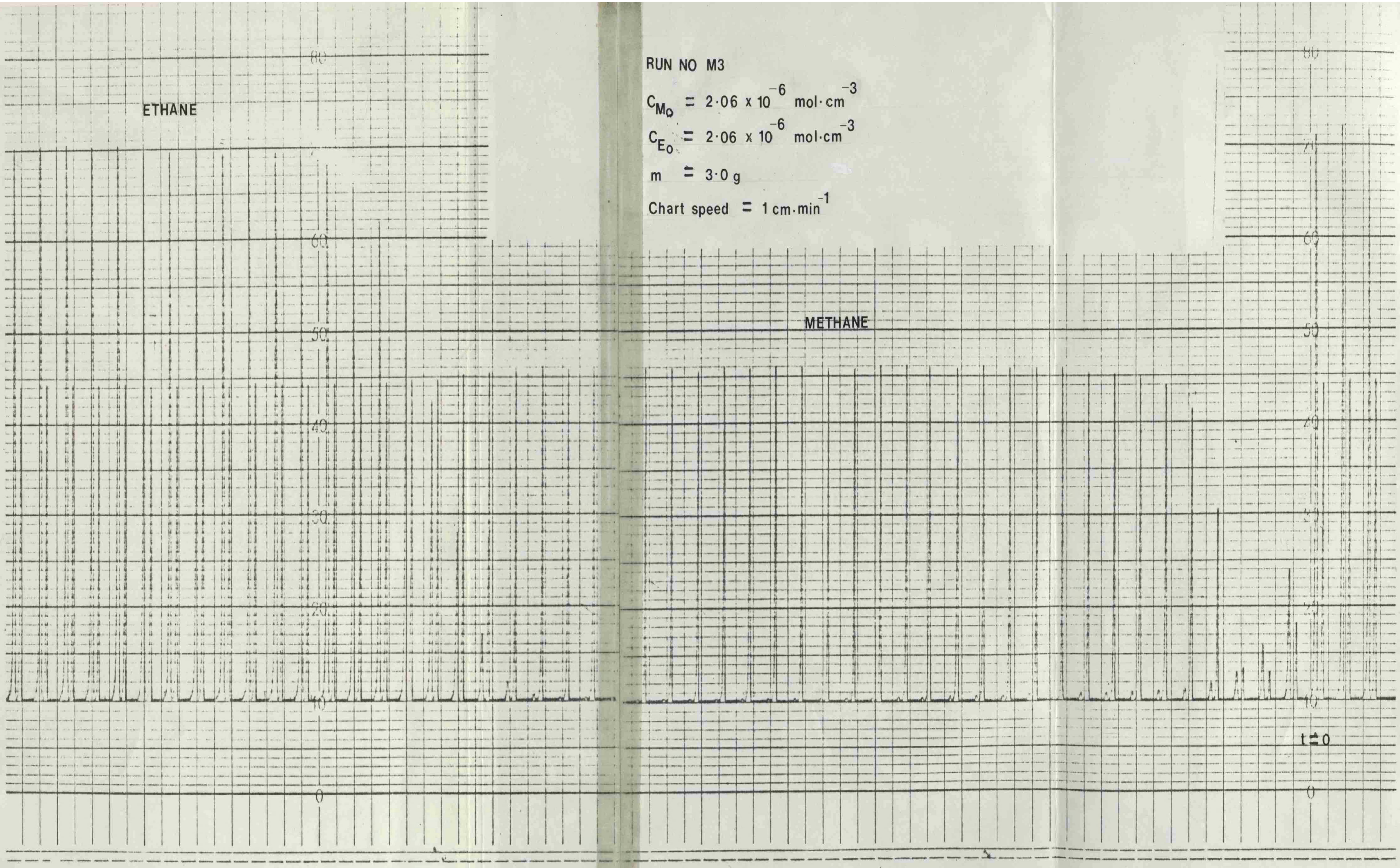

Chromatographic breakthrough curve for binary adsorption (supplement to Figure 8)